Charles University in Prague
Faculty of Science

Department of Cell Biology

Regulation of cell cycle and DNA damage response in mouse oocytes

Alexandra Mayer, MSc.

PhD thesis

Supervisors: RNDr. Petr Šolc, Ph.D.
Prof. Jan Motlík, Vet. MD., PhD., DSc.

Institute of Animal Physiology and Genetics, ASCR v. v. i.

Prague, 2015

I hereby declare that I wrote this thesis independently, using the cited literature. This work or a substantial part of it has not been submitted elsewhere to obtain any other academic degree.

Prague, 2015 Alexandra Mayer

First of all, I am deeply grateful to my supervisors: Jan Motlik, who gave me the opportunity to join the lab and supported me throughout my research, and Petr Solc for his guidance, helpful ideas and considerable time spent discussing my project. I would like to thank Vladimir Baran for giving me hints about immunohistochemistry, Adela Brzakova and Ivana Ferencova, who were willing to stay overtime in order to help me with the experiments. Many thanks belong to previous and recent members of our department for creating a friendly working environment, and to our foreign colleagues – Tomoya S Kitajima, Richard M Schultz and Jan Ellenberg for their contribution to the research papers. Finally, I would like to thank my family members and close friends for encouragement and patience.

This study was supported by grant LH12057 (Czech-US scientific program, Ministry of 498 Education, Youth and Sports), European Regional Development Fund project ExAM - CZ.1.05/2.1.00/03.0124**,** Grant Agency of the Czech Republic (P502/11/0593), grant ME08030 (Czech-US scientific program).

Contents

Abstract

A specific feature of mammalian oocytes is a long prophase I arrest, which can be maintained for many years in humans. The oocytes must ensure robust mechanisms, which can keep them in prophase I, but effectively trigger meiotic resumption when required. Consequently, throughout the maturation of an oocyte, non-erroneous chromosome segregation is a prerequisite for the generation of healthy offspring.

In this study we aimed to investigate the new roles of Aurora A (AURKA) and polo-like kinase 1 (PLK1) in the regulation of the cell cycle progression. For this purpose, we used transgenic mice that specifically overexpress wild type (WT-) or kinase-dead (KD-) AURKA in oocytes only, and to study PLK1 we treated oocytes with BI2536, a small molecule inhibitor known to specifically inhibit PLK1 in somatic cells. Our data show, that both AURKA and PLK1 are not essential for meiotic resumption, however they participate in this process. Active AURKA regualtes the increase in microtubule organizing centers (MTOC) in prophase I, which is the first visible marker of resumption of meiosis in oocytes. AURKA activation is biphasic, and the initial increase in MTOC is transient, while full AURKA activation needed for the stability of MTOC requires the activity of Cyclin-dependent kinase 1 (CDK1). We show that PLK1 participates in meiotic resumption by promoting nuclear envelope breakdown. Both AURKA and PLK1 are needed to recruit centrosomal proteins to MTOC in order to promote normal spindle formation. In metaphase I (MI) PLK1 is needed for stable kinetochore-microtubule attachment, and inhibition of PLK1 leads to MI arrest with misaligned chromosomes activating the spindle assembly checkpoint (SAC). We show that PLK1 is required for the full activation of the anaphase promoting complex/cyclosome (APC/C) and is therefore essential for entry into anaphase I. In contrast, overexpression of WT- or KD- AURKA does not interfere with oocyte maturation.

During prophase I arrest and maturation the oocytes may be repeatedly exposed to drugs which induce DNA damage. Alternatively, endogenous DNA lesions may arise from cell's own metabolism (oxygen radicals, DNA replication and trascription), and their timely repair may increase the survival of oocytes and prevent genetic abnormalities in the embryos. We studied the response of oocytes to endogenous DNA double strand breaks (DSBs), and to DSBs induced by low concentration of the radiomimetic drug Neocarzinostatin (NCS). We found that low levels of DSBs induced by NCS in prophase I increase the incidence of chromosome fragments and lagging chromosomes but do not lead to APC/C activation and anaphase onset delay. The number of DSBs, represented by γH2AX foci, significantly decreases between prophase I and metaphase II in both control and NCS-treated oocytes. Besides, prolonged incubation of oocytes arrested in prophase I decreases the number of NCS-induced DSBs. Meiotic recombination 11 homologue (MRE11), but not Ataxia telangiectasia mutated (ATM), is essential for DSBs detection in prophase I and is involved in H2AX phosphorylation during MI. Inhibiting MRE11 by mirin during meiotic maturation results in anaphase bridges and also increases the number of γH2AX foci in metaphase II. Compromised DNA integrity in mirin-treated oocytes indicates a role for MRE11 in the DNA repair during meiotic maturation. Collectively, our data suggest that DNA repair occurs in prophase I arrested oocytes and after resumption of meiosis.

Abstrakt

Buněčný cyklus savčích oocytů je dočasně zastaven v průběhu profáze I. meiotického dělení a v tomto stádiu mohou oocyty přetrvávat až několik desítek let. V oocytech proto musí fungovat účinné mechanismy, které je udržují v profázi I a umožňují znovuzahájení meiózy, když je potřeba. Následně, správná segregace chromozomů během maturace oocytů je podmínkou pro vývoj zdravých potomků.

Naším cílem bylo zjistit nové role AURKA a PLK1 kináz v regulaci buněčného cyklu. Použili jsme transgenní myši, které nadprodukují wild type (WT-) nebo neaktivní (kinase-dead, KD-) AURKA pouze v oocytech, a ke studiu PLK1 kinázy jsme použili specifický inhibitor BI2536, jehož účinnost je ověřená v somatických buňkách. Naše data ukazují, že jak AURKA tak PLK1 nejsou nezbytné pro znovuzahájení meiózy, i když obě kinázy se tohoto procesu účastní. Aktivní AURKA reguluje proces multiplikace mikrotubuly organizujících center (MTOC) v profázi I, což je první viditelná známka znovuzahajení meiózy. Aktivace AURKA je bifázní, proto primární nárůst počtu MTOC je tranzientní. Plná aktivace AURKA, která je potřebná pro stabilitu MTOC, vyžaduje aktivitu Cyklin-dependentní kinázy 1 (CDK1). Ukázali jsme, že PLK1 se účastní rozpadu jaderné membrány během znovuzahájení meiózy. Jak AURKA tak PLK1 se podílí na akumulaci centrozomálních proteinů na MTOC a na výstavbě dělícího vřeténka. V metafázi I (MI) PLK1 reguluje napojení kinetochorů na mikrotubuly a inhibice PLK1 brání správnému seřazení chromozomů do metafázní roviny a vede k aktivaci kontrolního bodu SAC (spindle assembly checkpoint) a zástavě buněčného cyklu v MI. Aktivita PLK1 v oocytech je podmínkou pro plnou aktivaci APC/C (anaphase promoting complex/cyclosome) a proto PLK1 je nezbytná pro vstup do anafáze I. Na rozdíl od PLK1, nadprodukce WT- nebo KD-AURKA nebrání meiotické maturaci.

Během profáze I a meiotického zrání mohou být oocyty opakovaně vystaveny působení chemikálií, které vyvolávají poškození DNA. Také buněčný metabolismus může přispívat k endogennímu poškození DNA (kyslíkové radikály, replikace DNA, transkripce), a jeho včasná oprava může zvýšit míru přežití oocytů a zabránit vzniku abnormálních embryí. Studovali jsme reakci oocytů jak na endogenní dvouvláknové zlomy DNA (double strand breaks, DSBs), tak na DSBs vyvolané nízkou koncentrací radiomimetické drogy Neocarzinostaninu (NCS). Zjistili jsme, že nízké množství DSBs po ošetření NCS v profázi I vede ke vzniku chromozomálních fragmentů a opožděných chromozomů (tzv. lagging chromosomes) ale neaktivuje APC/C a nezpožďuje vstup do anafáze. Počet DSBs, stanovený podle γH2AX- markeru DSBs, se značně snižuje mezi profází I a metafází II v kontrolních i NCS ošetřených oocytech. Navíc, prodloužená kultivace oocytů v profázi I vede ke snížení počtu DSBs indukovaných NCS. Není to ATM, ale MRE11, která je nezbytná pro detekci γH2AX v profázi I a je zapojená do fosforylace H2AX během MI. Inhibice MRE11 pomocí mirinu během maturace vede ke vzniku anafázních můstku a také ke zvýšení množství DSBs v metafázi II. Narušená integrita DNA v oocytech po kultivaci v mirinu svědčí o roli MRE11 v opravě poškození DNA během zrání. V souhrnu naše data naznačují, že oprava DNA probíhá v profázi I a také po znovuzahájení meiózy.

1 Theoretical background

1.1 Development and life span of oocytes

1.1.1 Oogenesis and folliculogenesis

Oogenesis, the process when primordial germ cells (PGCs) give rise to developmentally competent female germ cells capable of generating viable offspring, is iniciated already during embryogenesis in mammals. In fetal ovaries, PGCs develop into oogonia which divide to form a limited number of oocyte precursors. In mice, oogonia undergo mitotic division until embryonic day 13.5 and consequently enter meiosis I resulting in diploid primary oocytes arrested at dictyate stage of prophase I, called germinal vesicle (GV) stage. They are surrounded by flat pregranulosa cells and are enclosed in primordial follicles (McLaren and Southee, 1997).

By the end of fetal development all primary oocytes are formed and arrested at GV stage and at early postnatal age oogonia disappear completely (Byskov et al., 2011). Some primordial follicles are recruited and start growing immediately after their assembly (the process called folliculogenesis) and develop into primary follicles with cuboid granulosa cells (Fig.1) (Hirshfield, 1991). The mechanisms by which follicles are chosen to be activated are still not completely understood. Simultaneously with folliculogenesis and granulosa cell differentiation, oocytes increase their volume, produce mRNA and rRNA and generate essential proteins required for maturation of oocytes and further development of embryos (Gilbert, 2000). At the same period genes for oocyte specific proteins ZP1, ZP2 and ZP3 are actively transcribed and zona pellucida starts to appear (Roller et al., 1989). Granulosa cells further proliferate and assemble into multiple layers, giving rise to secondary follicles. Oocytes are connected to granulosa cells through gap junctions which allow the exchange of small molecules (Anderson and Albertini, 1976). This communication between somatic granulose cells and oocytes is believed to be crucial for the regulation of oocyte growth and meiotic arrest, and consequently for acquisition of full developmental competence (Eppig, 2001). This process is reciprocal, and on the other hand, oocytes promote proliferation and differentiation of granulosa cells though gap junctions (Buccione et al., 1990). The final steps of oocyte development are controlled by gonadotropins –follicle stimulating hormone (FSH) and luteinizing hormone (LH). FSH stimulates formation of cavity filled with fluid and

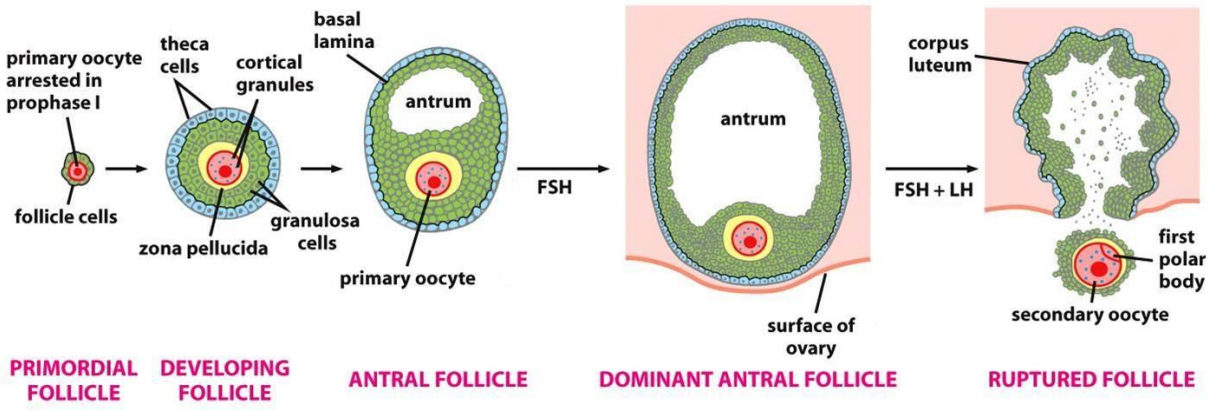

Fig.1. Folliculogenesis. Primordial follicle starts to grow and transforms into developing (secondary) follicle. FSH stimulates formation of cavity (antrum) and after the surge of LH resumption of meiosis occurs.

development of early antral follicle from secondary follicle. Finally, preovulatory Graafian follicle with cumular cells surrounding the oocytes and mural granulosa cells at the inner layers of follicular wall is formed. After the surge of LH the resumption of meiosis in fully grown oocyte occurs, and following the first meiotic division oocyte becomes arrested in meiosis II.

1.1.2 Aging

It is not surprising, that oocytes decline in number and quality with age (Broekmans et al., 2007). The loss of germ cell starts already during embryonic development by apoptosis and during follicle recruitment before puberty (Coucouvanis et al., 1993; Pesce and De Felici, 1994). Later, throughout the reproductive period of life, more follicles from the ovarian pool are recruited and start the growth (Faddy and Gosden, 1995; Richardson et al., 1987). FSH stimulates selection and dominance of one follicle, which then produces high levels of estrogens and inhibins that lead to atresia of remaining follicles (diZerega and Hodgen, 1981). There is evidence that some oocytes may form de novo in adult ovaries, and germinal stem cells expressing genes related to primordial germ cells were found originating in ovarian tissue, however the impact of such oogenesis on reproduction capacity remains questionable (Oatley and Hunt, 2012; Virant-Klun et al., 2012; Vogel, 2012; White et al., 2012). By the age of 30 years in women only 12% of the maximum pre-birth follicular population is present, which decreases to 3% by the age of 40 years (Wallace and Kelsey, 2010). The decrease culminates in menopause when only approximately 1000 oocytes enclosed the follicles are remained, and the decline of hormonal impulses result in cessation of ovulation (Hsueh et al., 1994; Velde et al., 1998).

Delaying reproduction beyond 35 years in humans may result in infertility, aneuploidy and miscarriage, or birth defects (Munné et al., 1994). Particularly, the quality of an oocyte plays a crucial role in embryo development, since the majority of meiotic errors in pregnancies result from female meiosis (Hassold and Hunt, 2001). The risk of trisomy (e.g trisomy 21, Down's syndrom) highly correlates with the age and 95% of Down syndrome children inherit the extra chromosome from their mother most frequently due to nondisjunction in Meiosis I (Gaulden, 1992). One source of aneuploidy is the loss of centromeric cohesion due to reduction of meiosis specific cohesin subunits Rec8 and Smc1β during female aging (Chiang et al., 2010; Kudo et al., 2009; Liu and Keefe, 2008; Tsutsumi et al., 2014). Rec8 protects centromeric cohesion from separase during anaphase I while Smc1β stabilizes the chiasmata sites and prevents premature separation of sister centrosomes before anaphase I (Hodges et al., 2005; Katis et al., 2010).

Further, unlike in spermatogenesis, which lasts for few weeks, oocytes arrest in diplotene for ages and may be repeatedly exposed to a number of exogenous DNA damaging agents. In aging mouse and human oocytes an increase in DSBs is associated with a physiologically declined expression of DSB repair genes. Inhibition of major genes involved in DSBs detection at prophase I arrested oocytes leads to higher levels of DNA damage in the presence of genotoxic stress, activates apoptotic pathways and reduces oocytes survival rates (Titus et al., 2013). Similarly to oocytes, the advancing age is associated with the

accumulation of double strand breaks (DSBs) in granulosa cells and the declined ability to repair them (Zhang et al., 2015).

1.2 Regulation of the cell cycle of the oocytes

While in somatic cells the mistakes in cell cycle regulation may lead to malignant transformation or may be associated with neurodegenerative diseases, the regulation of meiotic progression in oocytes is important for generation of viable offspring. Unlike mitosis, the purpose of meiosis is to produce haploid cells suitable for reproduction. It consists of two sequential rounds of chromosome segregation: a reductive division (Meiosis I) when homologous chromosomes segregate, and an equational division (Meiosis II) which resembles mitosis and enables sister chromatids segregation thus generating a haploid cell (Marston and Amon, 2004). Isolation of oocytes from the follicles iniciates a spontaneous meiosis resumtion, but in *in vivo* condition LH controls this process (Sato and Koide, 1984). Meiosis resumption starts with nuclear envelope breakdown (NEBD), followed by prometaphase I onset and spindle formation; when bivalents are arranged at metaphase plate and correctly attached to meiotic spindle, anaphase I is triggered, I. polar body is extruded and oocytes are consequently arrested in metaphase II (Fig.2). Fertilization stimulates meiosis II resumption and Ca^{2+} influx, needed for II. polar body emission (Miao et al., 2012).

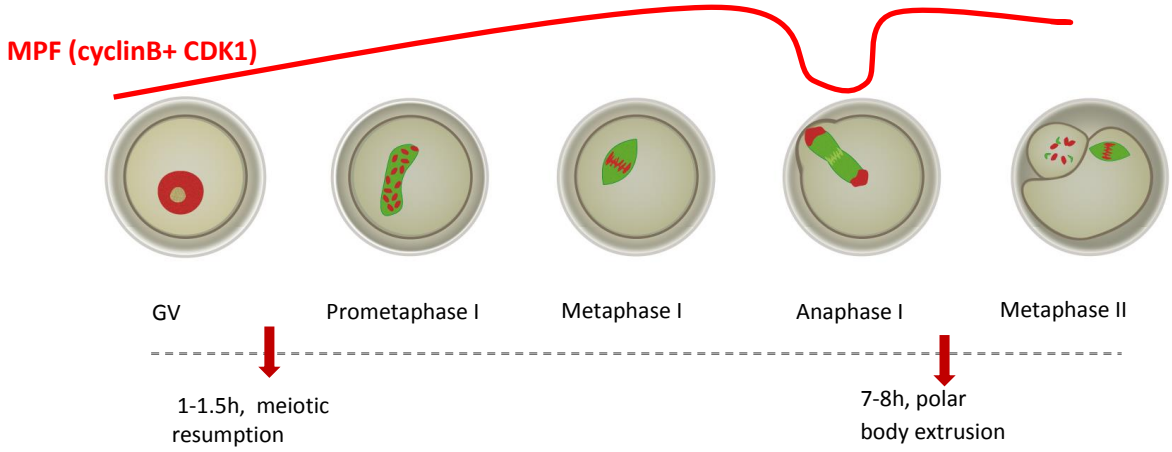

Fig.2. Maturation of an oocyte. After hormonal stimulation or spontaneously in *in vitro* conditions meiotic resumption occurs: after germinal vesicle breakdown the spindle is formed (green), the oocyte reaches metaphase I and proceeds to anaphase I, the bivalents are separated and 1st polar body is extruded. MPF activity (cyclinB +CDK1) grows and is maintained high until anaphase I, when the drop in cyclin B/CDK1 levels enable MI exit.

All cellular events during meiotic maturation must be timely synchronized and precisely coordinated. Cyclins and cyclin-dependent kinases (CDKs) are the main regulators of oocyte cell cycle. CDK1 activity is stimulated by binding of cyclin B, which starts to accumulate already in S phase prior to meiosis, and its concentration reaches the threshold level needed to trigger meiosis resumption in late G2 (Lindqvist et al., 2009; Solomon et al., 1990). This complex of CDK1 and cyclin B together with recently identified Greatwall kinase form M-phase promoting factor (MPF)(Hara et al., 2012). On the other hand, the destruction of cyclin B enables CDK1 inactivation, needed for M-phase exit (Fig.2). Thus, oscillation of cyclin B-CDK1 level is a critical step in ensuring cell cycle progression.

1.2.1 Prophase I

1.2.1.1 Prophase I arrest

A specific feature of oocytes is a long prophase arrest, which can be maintained for many years in humans. The oocyte must ensure robust mechanisms, which can keep oocytes in prophase I, but effectively trigger meiotic resumption when required. CDK1/CyclinB remains inactive during prophase arrest due to high levels of cAMP and activity of protein kinase A (PKA) (Schmitt and Nebreda, 2002; Vaccari et al., 2008). PKA phosphorylates and activates oocyte-specific Wee1B kinase, a part of WEE1B/MYT kinases family, which mediates CDK1 inhibition through phosphorylation of Thr14 and Tyr15 residues located within ATP-binding loop (Han et al., 2005; Nurse, 1997) (Fig.3). On the other hand, Cdc25 phosphatases ensure dephosphorylation of these residues and promote meiotic resumption (Pines, 1999). The family of CDC25 phosphatases consists of CDC25A, B and C, and among them, CDC25B is the most potent activator of CDK1 in mouse oocytes (Lincoln et al., 2002). During prophase I arrest PKA-mediated phosphorylation of CDC25B at Ser 321 causes its association with 14-3-3 protein and retention in cytoplasm, while physiologically it becomes translocated into nucleus shortly before meiotic resumption (Pirino et al., 2009; Solc et al., 2008; Zhang et al., 2008).

The other important player in prophase I arrest maintenance, cAMP, is produced by adenylate cyclase 3 in mouse oocytes (ADCY3). Oocytes lacking ADCY3 spontaneously resume meiosis at the stage of early antral follicles, however low cAMP levels are not critical for meiotic resumption in incompetent oocytes, which do not have enough of essential proteins (Horner et al., 2003; Mehlmann et al., 2002). Further, cAMP acts via PKA pathway, as PKA inhibition in the presence of high cAMP still induces meiotic resumption (Bornslaeger et al., 1986). At the time of meiotic resumption, cAMP is cleaved by phosphodiesterase 3A (PD3A), but during prophase I arrest high levels of cAMP are also ensured by competitive cleavage of another PD3A substrate, cGMP, produced by cumulus cells (Norris et al., 2009).

Degradation of cyclin B through ubiquitine ligase APC/C ^{CDH1} (anaphase promoting complex/cyclosome) is the next mechanism of CDK1 activity regulation (Holt et al., 2010). During meiotic resumption APC/C ^{CDH1} activity is regulated negatively by CDK1 itself allowing cyclin B accumulation (Fig.3). On the other hand, CDC14 phosphatase precedes premature meiotic resumption by removing CDK1-mediated inhibitory phosphorylation of APC/C ^{CDH1} (Solc et al., 2010).

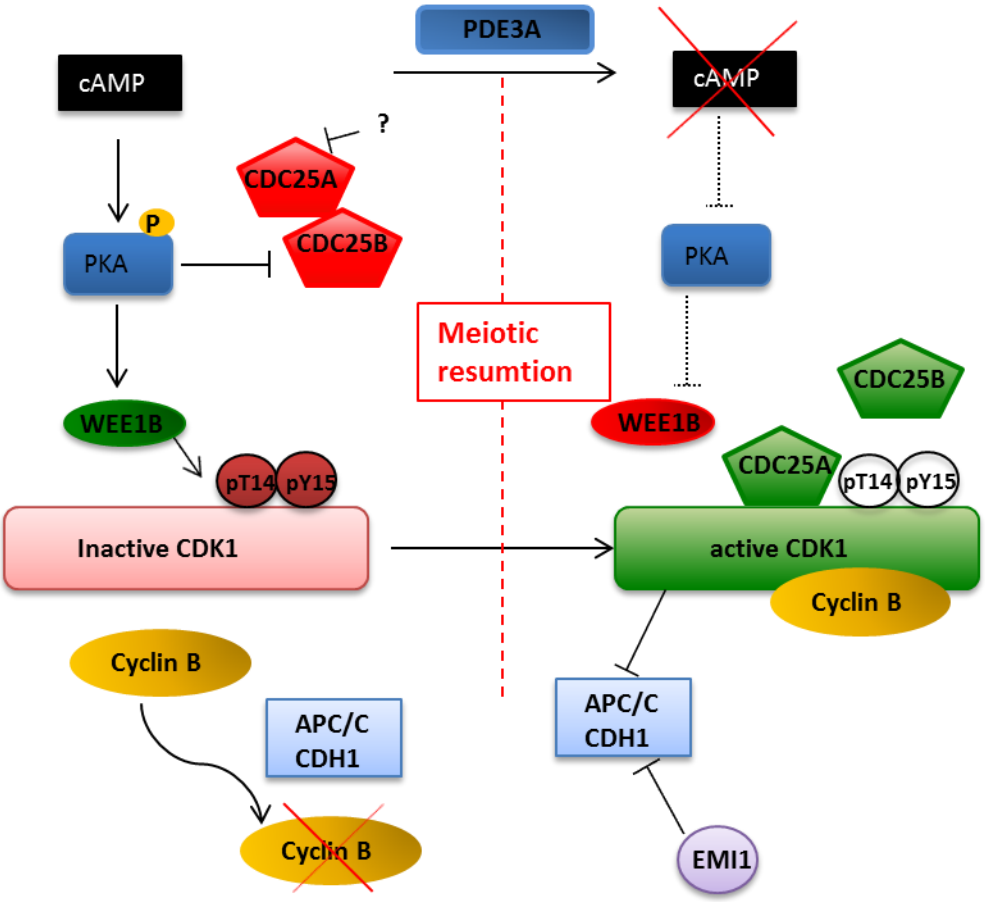

Fig.3. Prophase I arrest and resumption of meiosis. Mechanisms that keep oocytes arrested in prophase I (left part of the image) include cAMP-mediated activation of PKA which inhibits CDC25B and activates WEE1. WEE1 mediates negative phosphorylation of CDK1. APC/C is involved in cyclin B degradation. Upon resumption of meiosis cAMP is degraded by PDE3A, PKA and WEE1 are inactivated. Active CDC25B and CDC25A remove negative phosphorylations from CDK1. CDK1 inhibits APC/C preventing cyclin B degradation.

1.2.1.2 Meiotic recombination

Meiotic recombination takes place from leptotene to pachytene stage of prophase I. The chromatids of homologous chromosoms start to condence in leptotene, while the pairing of homologous chromosomes along their full length (synapsis and synaptonemal complex formation) occurs in zygotene. Recombination of paired homologous chromosomes (called bivalents) is initiated at double strand breaks (DSBs), which are created naturally in zygotene stage by nuclease SPO11 (Fig. 4). SPO11 also supports the initiation of synapsis formation prior to DSBs induction (Baudat et al., 2000; Boateng et al., 2013; Keeney and Neale, 2006; Neale et al., 2005). MRN complex (MRE11, RAD50, NBS1) was found to be involved in resection of DSBs and removal of SPO11 complexes in budding yeast, and probably it has similar functions in mice: mutations in MRE11 lead to slower meiotic prophase progression and incompletely synapsed bivalents, however meiotic recombination is not defective (Borde, 2007). In pachytene, at the sites of DSBs proteins DMC1 and RAD51 promote the exchange of parts of DNA between homologous non-sister chromatides (Bannister and Schimenti, 2004). Recombination ends with formation of chiasmata, bridges that connect chromsomes

toghether at the spots of recombination and persist throughout MI progression. Chiasmata ensure correct segregation of whole homologous chromosomes instead of chromatids during the I. meiotic division.

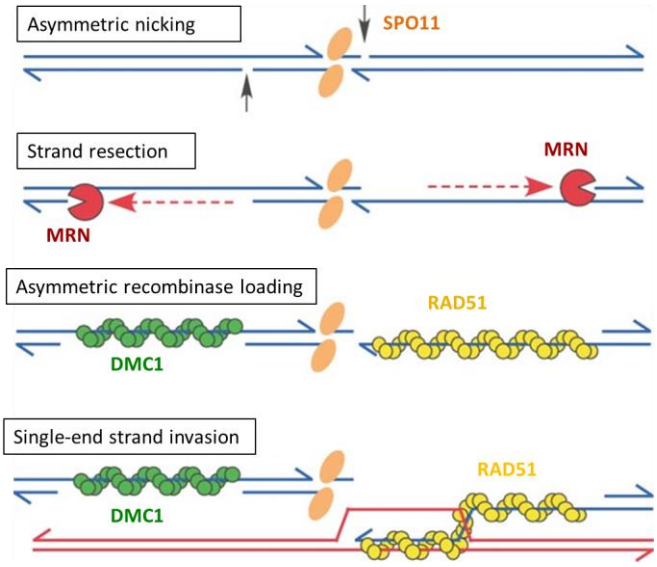

Fig.4. Meiotic recombination. SPO11 promotes DSBs formation. The resection of strands is supported by MRN complex. DMC1 and RAD51 are loaded on the strands and promote recombination. Adapted from Neale et al., 2005.

1.2.1.3 Pachytene checkpoint

Incorrect recombination may lead to generation of aneuploid gametes. Therefore, oocytes possess a pachytene checkpoint, which prevents I. meiotic division in case recombination fails (Roeder and Bailis, 2000) This response is iniciated by two types of events: the problem of unrepaired DSBs and the absence of homologous pairing. The importance of DSBs repair is crucial, as the loss of ATM function during early prophase I, which is involved in the repair process, results in folliculogenesis failure and programmed oocyte death. Interestingly, oogenesis failure in the absence of ATM can be suppressed by the reduction of DSBs formation due to SPO11 mutation (Di Giacomo et al., 2005).

While decreased ability of DSBs repair induces a severe meiotic arrest, faulty DSBs formation leads to defects in folliculogenesis (Di Giacomo et al., 2005). Disruption of recombination proteins in mice (for example, DMC1) causes the arrest of gametogenesis (Baudat et al., 2000; Pittman et al., 1998).

1.2.2 Meiotic resumption

Meiotic resumption depends on the decline in cAMP levels and inhibition of PKA kinase in order to ensure activity of CDK1/cycline B complex (Fig.3) (Duncan et al., 2006; Schultz et al., 1983). cAMP levels drop due to LH surge and PKA is inactivated, which is essential for meiotic entry (Fig.3). LH receptor is expressed only in mural granulosa cells, whereas it was not detected neither in cumulus cells nor in the oocytes (Peng et al., 1991).

LH induces expression of epidermal growth like factors (EGF) amphiregulin AREG, epiregulin EREG and betacellulin (BTC) in mural granulosa cells (Park et al., 2004). They are expressed as transmembrane precursors and cleaved into a soluble diffusive form which reaches tyrosine-kinase epidermal growth factor receptor (EGFR) in the cumulus cells (Schneider and Wolf, 2009). Further, LH reduces cGMP transfer from granulosa cells to oocytes via gap junctions closure, and the decline in cGMP results in increased PDE3A activity towards cAMP (Norris et al., 2009; Sela-Abramovich et al., 2006). Also PKB/AKT kinase is responsible for PDE3A activation in mouse oocytes (Han et al., 2005; Kalous et al., 2006). PDE3A is the main phosphodiesterase responsible for cAMP degradation, as pde3A mice are not able to resume meiosis neither after LH stimulation, nor spontaneusly in *in vitro* conditions (Masciarelli et al., 2004). The decrease of cAMP concentration allows accumulation of CDC25B, which translocates to the nucleus from cytoplasm shortly before NEBD (Solc et al., 2010). While CDC25C is dispensable for meiotic resumption (Chen et al., 2001), cdc25b -/- oocytes remain in prophase and are sterile because of permanent meiotic arrest (Lincoln et al., 2002). The role of CDC25A is not completely understood in meiotic resumtion, as cdc25a-/- mice show embryonic lethality, but downregulation of CDC25A decreases the number of oocytes resuming meiosis (Solc et al., 2008).

The nuclear localization of factors promoting meiotic resumption is crucial. Not only CDC25B, which is sequestered in cytoplasm by PKA, translocates to the nucleus prior to meiotic resumption, but also cyclin B and CDK1 (Fig.5) (Marangos and Carroll, 2004; Mitra and Schultz, 1996; Zhang et al., 2008). While WEE1B is excluded from the nucleus before NEBD, inhibitory kinase MYT1 is found in the cytoplasm and is not affected prior meiotic resumption(Oh et al., 2010).

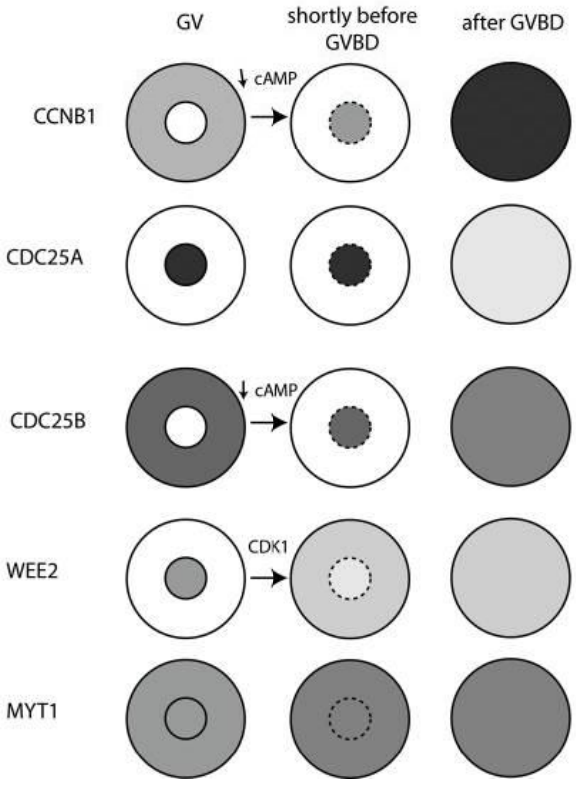

The other pathway supressing CDK1 activation through APC/C^{CDH1} activity is regulated at the time of meiotic resumption by increasing CDK1 activity itself (Fig.3). Besides that, EMI1 expressed in oocytes suppresses APC/C^{CDH1} activity thereby promoting CDK1 phosphorylation, and microinjection of EMI1 into oocytes accelerates meiotic resumption (Marangos et al., 2007)

Fig.5. Localization of factors regulating meiotic resumption. Cyclin B (CCNB1), CDC25A/B localize into the nucleus, while WEE1B (also known as WEE2) and MYT1 are diffused in cytoplasm. Adapted from Solc et al., 2010.

1.2.2.1 Aurka and PLK1 involvement in meiotic resumption

Mitotic entry is also regulated by AURKA and PLK1 kinases. In somatic cells, AURKA expression peaks at G2/M transition (Honda et al., 2000), and AURKA activates PLK1. PLK1 then promotes mitotic entry by phosphorylating MYT1 and WEE1, which leads to their inhibition and SCF-dependent degradation, respectively (Macůrek et al., 2008; Nakajima et al., 2003; Watanabe et al., 2005). PLK1 takes part in translocation of CDC25B or C to the nucleus prior mitotic entry (Lobjois et al., 2009; Toyoshima-Morimoto et al., 2002) Additionally, PLK1 phosphorylates cyclin B, but chemical inhibition of PLK1 does not prevent import of CDK1/CyclinB to the nucleus (Lénárt et al., 2007). More likely, PLK1-mediated phosphorylation of cyclin B contributes to mitotic entry by regulation of the activity of CDK1 on centrosomes (Jackman et al., 2003). While PLK1 is dispensable for mitotic entry, it is needed for G2 checkpoint recovery in case of DNA damage, which resembles meiotic resumption (Macůrek et al., 2008; Solc et al., 2010; van Vugt et al., 2010).

Similarly, PLK1 and AURKA are dispensable for resumption of meiosis, but they both enhance the process. Downregulation of AURKA in oocytes decreases the rates of meiotic resumption and delays NEBD onset, however, AURKA overexpression does not overcome cAMP-mediated prophase I arrest- AURKA induces phosphorylation and recruitement of CDC25B to MTOC (Saskova et al., 2008).

Inhibition of PLK1 delays NEBD in oocytes with the same kinetics as AURKA alone and is not involved in CDC25B nuclear translocation (Solc et al., 2010). It is known that PLK1 is inhibited via PKA-dependent pathway during prophase I arrest, and is also involved in meiotic arrest of pde3A-/- oocytes (Shen et al., 2010). Interestingly, other member from the family of Polo-like kinases, PLK4, is essential for meiotic resumption: depletion of PLK4 causes meiotic arrest at GV stage and suppresses CDK1/CyclinB (Luo and Kim, 2015). Moreover, PLK4 depletion cannot be rescued by PLK1 overexpression.

1.2.3 Chromatin condensation and NEBD

While arrested at the prophase I, the chromatin of GV-stage oocytes undergoes several levels of chromatin modifications and large scale remodelling in order to control gene expression. Mouse and human oocytes show size-dependent changes in chromatin configuration (Miyara et al., 2003). In pre-antral follicles the configuration of chromatin is called NSN (nucleolus is non-surrounded by chromatin), while in fully grown oocytes it is called SN (nucleolus surrounded by chromatin) (Debey et al., 1993). Active polymerase I– and II- dependent transcription takes place in NSN oocytes, while SN oocytes are transcriptionally silent (La Fuente and Eppig, 2001). However, SN configuration is not strictly required for global transcription repression (Tan et al., 2009).

Meiotic resumption is characterized by tightly coupled events: chromatin condensation and nuclear envelope breakdown (NEBD, or germinal vesicle breakdown- GVBD). Chromatin condensation helps the cells to keep genetic information intact during M-phase progression. The condensation process starts before NEBD and continues throughout prophase I. In somatic cells, condensation is regulated by histones, topoisomerase II, cohesins and condensins, and guarded by CDK1 activity (Belmont, 2006; Vagnarelli, 2012;

Woodcock and Ghosh, 2010). The factors that play a role in chromatin condensation have not been properly described in oocytes yet. Inhibition of topoisomerase II (TOP2) in oocytes leads to severe defects in chromatin condensation (Li et al., 2013). TOP2 resolves topological configuration of DNA through introduction of DNA breaks, which are later repaired. However, inhibition of ATPase activity downregulates TOP2 before formation of DSBs and therefore is independent of breaks repair. Under these conditions, chromatin fails to condense, and thin chromatin strands are formed. Interestingly, after meiotic resumption chromatin condensation problems lead to an impaired localization of centromeric proteins to centromere regions (eg. BUB3), microtubules cannot form attachments, and spindle formation fails (Li et al., 2013).

During mitosis, nuclear envelope proteins (lamins) become phosphorylated by MPF, which leads to disruption of interactions among nuclear proteins. NEBD is characterized by formation of small holes in the membrane, which is dependent on microtubules and molecular motors in somatic cells (Beaudouin et al., 2002) The holes increase in size and facilitate NEBD. In oocytes, molecular motors move microtubule organizing centers (MTOC) toward the nucleus and push against nuclear envelope, causing invaginations (Schuh and Ellenberg, 2007).

1.2.4 Spindle formation

Spindle formation and correct kinetochore-microtubule attachments are crucial steps for error-free separation of bivalents in meiosis I. In oocytes, MI spindle formation abnormalities may be linked to aneuploidy which increases with maternal age (Hunt and Hassold, 2008). Traditional centrosomes containing two centriols are in mouse oocytes eliminated during pachytehe and substituted by microtubule organizing centers (MTOC)(Calarco-Gillam et al., 1983; Szollosi et al., 1972). Acentriolar MTOC contain γ -tubulin and pericentrin and before NEBD are located in the cytoplasm or on nuclear envelope, later promoting generation of bipolar spindles (Carabatsos et al., 2000; Gueth-Hallonet et al., 1993; Schuh and Ellenberg, 2007). In early prophase there can be found a dense interfase-like microtubule network with 1-3 MTOC, but in late prophase MTOC split reaching the amount of about 80, and after NEBD they also can be formed *de novo* (Calarco, 2000). After NEBD, the number of microtubules increases and they assemble in a multipolar ball-like structure in close proximity to chromosomes (Fig.6) (Schuh and Ellenberg, 2007). Individualization of bivalents occurs after first microtubule-chromatin contact, and the bivalents become located on the surface of the microtubule ball. Multiple poles are ejected from the microtubule ball, and later they cluster in two dominant poles directing spindle elongation (Dumont et al., 2007a; Schuh and Ellenberg, 2007). Interestingly, there are differences between spindle formation *in vitro* and *in vivo*: the first mentioned are bigger, and γ-tubulin localizes on MTOC and proximal microtubules, while *in vivo* matured oocytes contain γ-tubulin only on spindle poles and are smaller in size (Sanfins et al., 2003).

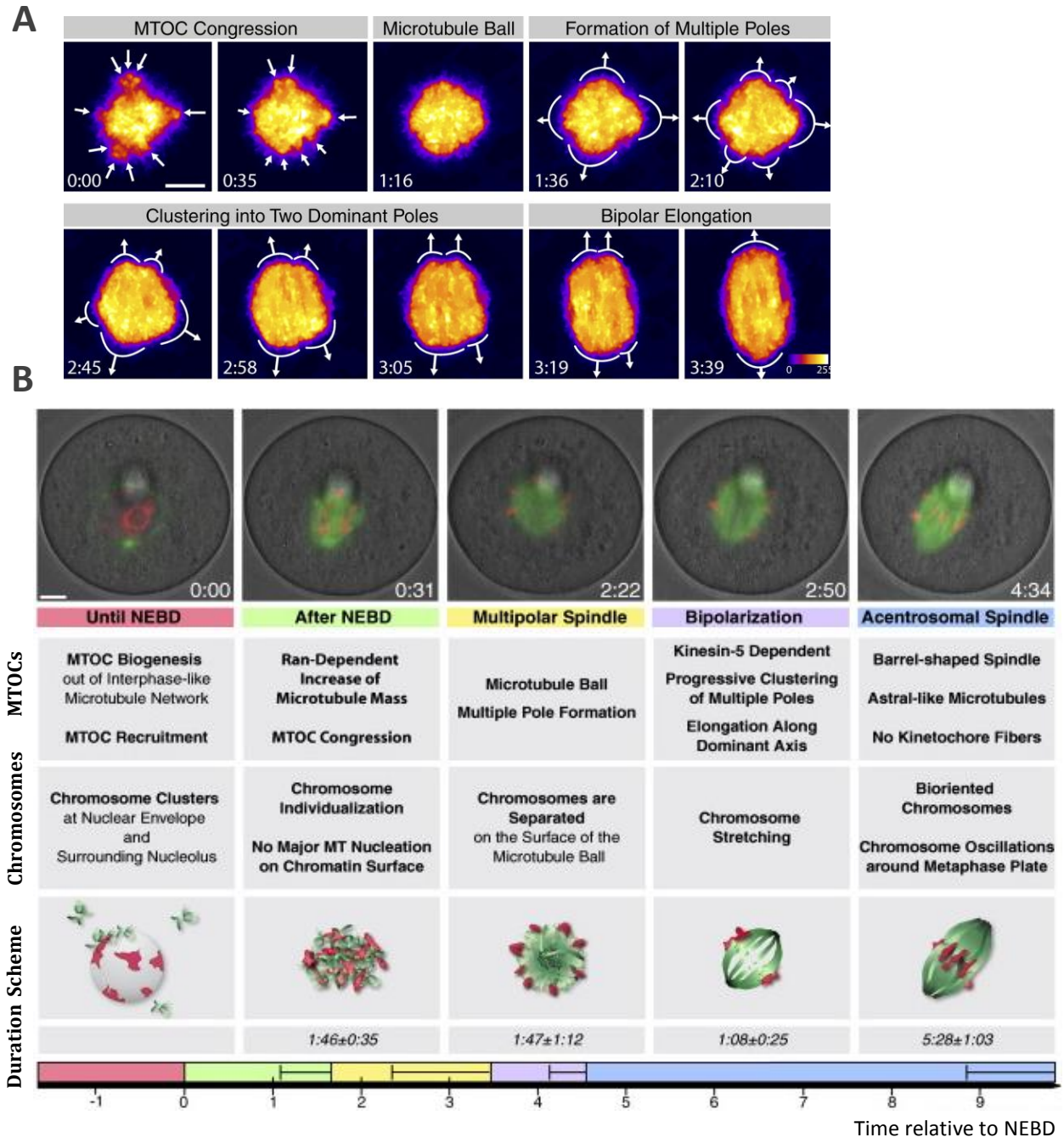

Fig.6. Spindle formation in oocytes. A) Formation of meiotic spindle after NEBD: MTOC congression, microtubule ball formation, formation of bipolar spindle and its elongation. B) The stages of spindle assembly. Adapted from Schuh and Ellenberg, 2007.

The process of spindle formation is promoted by Ran GTPase, whose active GTP-bound state is regulated by RCC1 exchange factor, localized on chromatin (Kalab et al., 1999). The gradient of active Ran is formed around chromosomes, and it promotes activation of spindle assembly factors around chromosomes which ensure microtubule nucleation and molecular motor activities (Clarke and Zhang, 2008). For example, the activity of kinesin 5 family is required for pole ejection and spindle bipolarisation (Schuh and Ellenberg, 2007).

Chromosome congression towards the spindle equator occurs without stably attached microtubules to kinetochores (KT-MT attachments). In prometaphase, micrutubules interact with chromosome arms, and stable interactions are established only in MI shortly before anaphase onset. Chromokinesins interact with microtubules and deliever chromosomes towards the spindle equator (Brunet et al., 1999; Kitajima et al., 2011). Homologous chromosomes attached to spindle from different poles are still held together by chiasmata at the sites of recombination, which generates tension in Metaphase I. Chromosomal passenger complex (CPC) is able to destabilize incorrect KT-MT attachments and register the lack of tension in kinetochores, and consequently promote re-orrientation (Lampson and Cheeseman, 2011). Although CPC is not essential for the I. meiotic division, it is important for the fidelity of the process. CPC includes AURORA B and C kinases, INCENP, Borealin and Survivin. It localizes to centromere region and chromosome arms after NEBD until anaphase onset and then changes localization to the center of the spindle (Sharif et al., 2010; Shuda et al., 2009). Inhibition of AURORA B/C function disrupts spindle formation, and knockdown of INCENP leads to misaligned chromosomes and to a failure of polar body extrusion (Sharif et al., 2010). Functions of AURORA B and C are not identical, as AURORA B localizes at centromeres while AURORA C localizes to interchromatid axes and chiasmata in oocytes. Overexpression of AURORA B leads to unresolved chiasmata, but overexpression of AURORA C rather leads to cytokinesis defect. However, it is also possible that these kinases are able to substitute their functions (Sharif et al., 2010). The third member of AURORA kinase family, AURKA, the most abundantly expressed homolog, also participates in the regulation of spindle formation. It colocalizes with MTOC and can be found at the spindle poles during meiosis I and meiosis II, but during MI-MII transition it transiently localizes to spindle midzone (Shuda et al., 2009). AURKA is activated on MTOC, and is responsible for MTOC amplification. Both depletion and overexpression of AURKA result in MI spindle defects and abnormal chromosome separation (Ding et al., 2011; Saskova et al., 2008; Yao et al., 2004; Zhao et al., 2015). Also the binding partner of AURKA, Bora, is involved in spindle assembly. It associates with α-tubulin in metaphase I, and is physically connected to meiotic spindle. Inhibition or depletion of Bora leads to formation of defective spindles with misaligned chromosomes and inhibits first polar body extrusion (Zhai et al., 2013) Interestingly, Bora does not only associate with AURKA, but is required for PLK1 activation. Injection of PLK1 antibody into mouse oocytes interferes with spindle formation suggesting that PLK1 is also an important regulator of microtubule assembly during meiosis (Tong et al., 2002; Xiong et al., 2008). In somatic cells, it is known that PLK1 inhibition causes the delayed start of microtubule assembly and monopolar spindle formation probably due to inability to separate centrosomes in early M-phase. The inhibition of PLK1 when bipolar spindle is already formed leads to the loss of contact between microtubules and kinetochores, defocusing of spindle poles and microtubules loss (Lénárt et al., 2007; Santamaria et al., 2007; Sumara et al., 2004). In oocytes, PLK1 is enriched in the nucleus at GV stage and its activation takes place before NEBD (Tong et al., 2002; Xiong et al., 2008). At prometaphase PLK1 localizes to spindle poles, while in anaphase it changes localization to the equatorial plate (Otsuki et al., 2009; Pahlavan et al., 2000; Tong et al., 2002). It was also found on kinetochores colocalizing with a member of CPC, Survivin, during meiosis, implying its role

in regulation of MT-KT attachments (Sun et al., 2012). Furthermore, inhibition of PLK1 during anaphase I changed spindle dimentions (Pomerantz et al., 2012).

1.2.5 SAC and anaphase onset

Spindle assembly checkpoint (SAC) represents a surveillance mechanism which keeps cells in M-phase in the presence of unattached chromosomes. The hallmark of meiosis is that while spindle is formed in mid-prophase, stable interactions between kinetochores and microtubules are established in late metaphase I shortly before anaphase I onset, however there still could be non-aligned bivalents which generate aneuploidy (Davydenko et al., 2013; Kitajima et al., 2011; Lane et al., 2012). Earlier in prometaphase microtubules interact with chromosome arms, and erroneous connections may be corrected by the function of CPC as described above (Brunet et al., 1999). The correction of attachments is very common in mouse oocytes – up to three rounds of microtubule error corrections occur for each bivalent (Kitajima et al., 2011). Slow increase in CDK1 activity during meiosis I allows establishment of stable KT-MT attachments only after bipolar spindle is formed, while premature increase in kinase activity stabilizes KT-MT attachments leading to lagging chromosomes in anaphase I (Davydenko et al., 2013). Checkpoint components (MAD1, MAD2, BUB1, BUBR1, BUB3, MPS1) accumulate at incorrectly attached kinetochores and help to eliminate aneuploidy by preventing premature anaphase onset. Depletion of BUB1 accelerates chiasmata resolution resulting in premature chromosome segregation and severe aneuplody in meiosis I (McGuinness et al., 2009). Similar phenotypes are observed upon disruption of BUBR1, BUB3 or MAD2 which cause accelerated meiotic progression with higher percentage of chromosome misalignment (Li et al., 2009; Wassmann et al., 2003; Wei et al., 2010).

In somatic cells, mitotic checkpoint complex (MCC) is formed in prometaphase from MAD2, BUBR1 and BUB3. It sequesters Cdc20 (activator of anaphase promoting complex/cyclosome, APC/C), keeping APC/C inactive and blocking anaphase onset until chromosomes are properly attached to the spindle and are under tension (Fig.7) (Burgess et al., 2014; Lampson and Cheeseman, 2011). APC/C is an E3 ubiquitine ligase, which targets

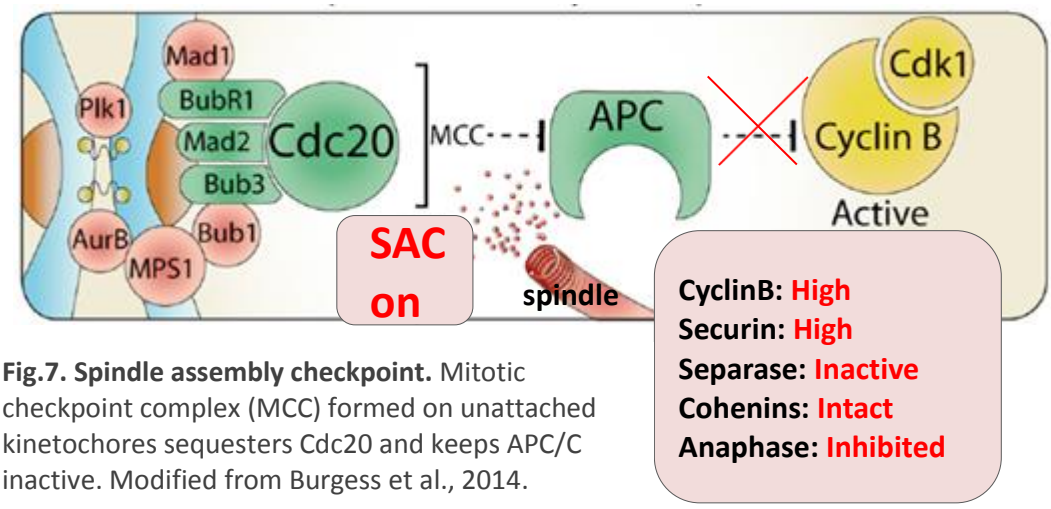

Fig.7. Spindle assembly checkpoint. Mitotic checkpoint complex (MCC) formed on unattached kinetochores sequesters Cdc20 and keeps APC/C inactive. Modified from Burgess et al., 2014.

cyclin B and securin for degradation by proteasome. But prior to MCC, APC/C ^{Cdc20} is in complex with another inhibitor, EMI1 (early mitotic inhibitor I) which is degraded in prometaphase while SAC proteins take over its function (Reimann and Jackson, 2002; Reimann et al., 2001). The activity of APC/C in prometaphase is also supressed by CDK1, allowing the accumulation of above mentioned substrates essential for meiosis progression (Nabti et al., 2014).

The turn off of the checkpoint is accelerated by the removal of SAC proteins from kinetochores, which is dependent on the function of molecular motors (dynein, CENP-E) (Musacchio and Salmon, 2007). In oocytes, however, depletion of CENP-E does not prevent MAD2 removal from kinetochores (Gui and Homer, 2012). When APC/C becomes activated, it degrades cyclin B1 and securin (Herbert et al., 2003). Securin degradation releases protease separase, which cleaves REC8 subunits of cohesin on the arms of chromosomes (but not in centromeric region) and enables separation of bivalents (Kudo et al., 2006; Lee et al., 2003).

Despite the existence of control mechanisms, the oocytes are more susceptible to chromosome missegregation during MI than somatic cells (Vogt et al., 2008). Segregation errors are frequent in meiosis, especially with increasing age. Incorrect segregation and generation of aberrant gametes may severely affect future embryo development. One explanation for segregation errors, already mentioned above, may be weakening of centromeric cohesion with age, because oocytes are not able to replace cohesins during lengthy prophase I arrest (Chiang et al., 2010; Revenkova et al., 2010; Tachibana-Konwalski et al., 2010). Interestingly, APC activation does not require the strict alignment of all chromosomes on equatorial plate: reaching some threshold number of correctly attached chromosomes is sufficient (Lane et al., 2012; Sebestova et al., 2012; Tachibana-Konwalski et al., 2013). Further, MAD2 associatiation with unattached bivalents is rather weak and probably not sufficient to induce SAC-mediated APC/C inhibition (Lane et al., 2012). Therefore, SAC is silenced in late MI despite the presence of misaligned chromosomes (Gui and Homer, 2012; Kolano et al., 2012; Lane et al., 2012). Interestingly, APC/C is activated, however, APC/C activity is submaximal in oocytes due to negative influence of persistent SAC components (Lane and Jones, 2014). Such non-canonical inhibition prolongs MI, because the degradation of the same total amount of cyclin B levels by APC/C takes more time. Experimentally it was proved that increasing APC/C activity by inhibition of residual SAC proteins raises aneuploidy in such case. Altogether, instead of strict inhibition of anaphase onset through APC/C inhibition, the oocytes delay anaphase I by reducing APC/C activation, thus allowing more time for erroneous microtubule-kinetochore attachments to be repaired (Lane and Jones, 2014).

1.2.6 Chromosome segregation

Additionally to established KT-MT attachments, correct chromosome segregation in meiosis I is ensured by timely cohesin removal and chiasmata resolution. This is mediated by separase, which is inhibited by securin before anaphase onset, but also by binding of CDK1-cyclinB (Gorr et al., 2005). During anaphase I onset APC/C ensures both securin degradation and CDK1-cyclinB levels decrease, thus leading to separase activation. While cohesin

removal from chromosome arms and chiasmata resolution is mediated by separase, sister chromatid cohesion must be retained in the region of centromere, which otherwise would lead to premature sister chromatids segregation to opposite poles already at anaphase I. The cohesin complex includes multiple subunits: Smc1, Smc3, Rec8, SA1, SA2 (Lee et al., 2003). Whereas Rec8 is cleaved at chromosome arms, it is specifically protected at the pericentromere during meiosis I, and later cleaved at anaphase II enabling the separation of sister chromatids (Fig. 8) (Kudo et al., 2006; Watanabe and Nurse, 1999). Protection of centromeric cohesin requires Shugoshin (Sgo1 and Sgo2)-dependent recruitment of PP2A phosphatase and involves AURKB kinase activity (Kitajima et al., 2006; Llano et al., 2008; Tanno et al., 2010). Cohesin has to be phosphorylated in order to be processed by separase, but PP2A dephosphorylates Rec8 at the centromere region thus preventing its cleavage (Lee et al., 2003; Wassmann, 2013). In mitosis, cohesin removal from chromosome arms requires the phosphorylation of cohesin subunit SA2 by PLK1 kinase (Wassmann, 2013).

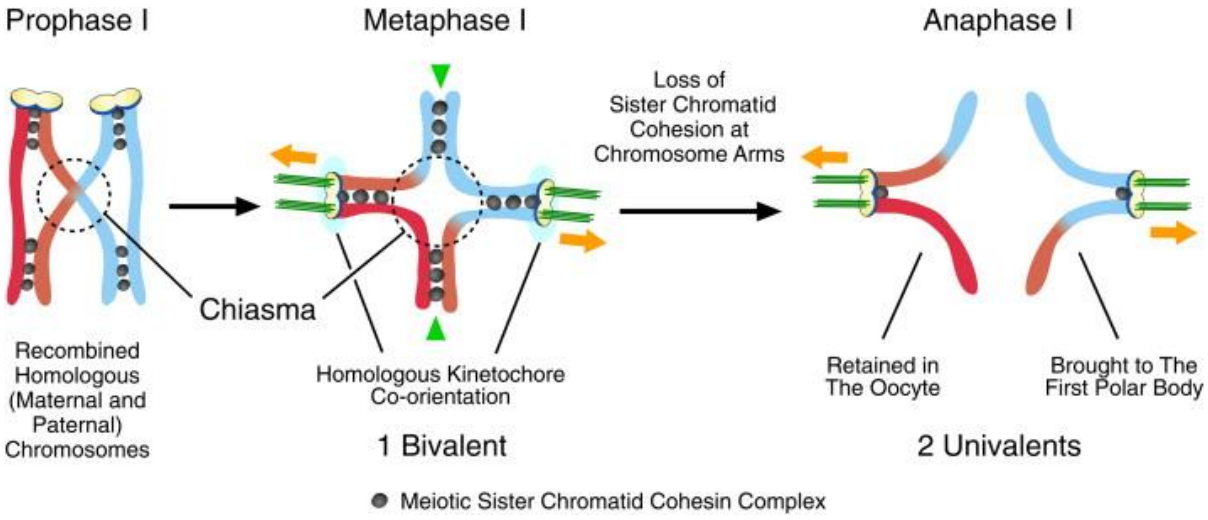

Fig.8. Segregation of bivalents in Anaphase I. Removal of cohesin at chromosome arms enables bivalent separation, while sister chromatid cohesion at centromere region is retained. Adapted from Kudo et al., 2006.

1.2.7 Cytokinesis

Oocyte division is assymetrical, resulting in formation of a small polar body which degenerates, while the majority of cytoplasm containing proteins and RNA stays in oocyte and further supports embryo development. This assymetry is ensured by the process of migration of meiotic spindle to the cortex, which is actin-dependent (Fig.9) (Clift and Schuh, 2013; Longo and Chen, 1985). Depletion of actin nucleator Formin2 in oocytes leads to defects in spindle migration (Dumont et al., 2007b; Leader et al., 2002). Another actin nucleator involved in spindle positioning is ARP2/3 complex: upon its inhibition the spindle does not migrate to the complex which leads to symmetric division (Sun et al., 2011). Besides, ARP2/3 dynamically maintains spindle position in MII oocytes (Yi et al., 2011).

Cytoskeletal regulator proteins are also involved in spindle migration: the movement of the spindle to the cortex is dependent on myosin II (MyoII), which is actin associated molecular motor, localized to the spindle poles and cleavage furrow (Dumont et al., 2007b; Schuh and Ellenberg, 2008) Inhibition of MyoII impairs spindle migration (Schuh and Ellenberg, 2008). In MII, MyoII is required for the rotation of the spindle (Matson et al., 2006).

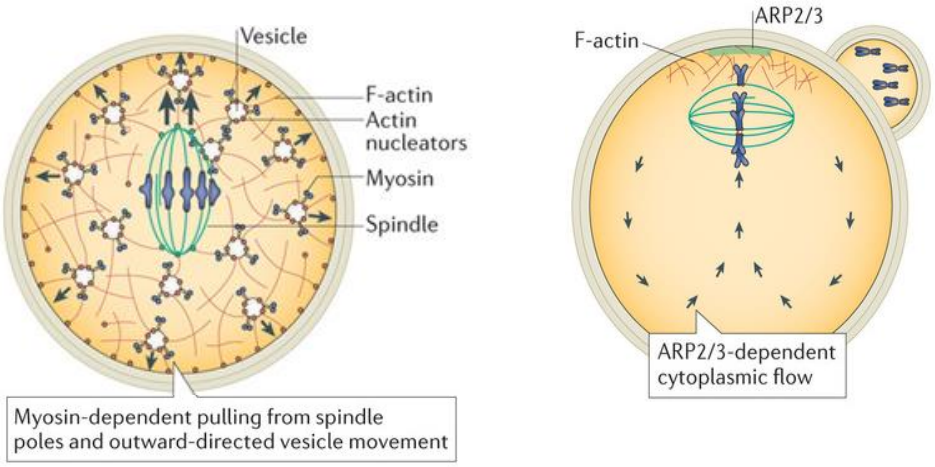

Fig.9. Spindle positioning in the oocyte and in the mature egg. Spindle migration to the cortex is essential for assymetric division of the oocyte and is ensured by actin and actin nucleator proteins (left). In metaphase II oocyte spindle position is dynamically maintained by ARP2/3 complex (right). Adapted from Clift and Schuh, 2013.

As cytokinesis is tightly bound with spindle function, proteins involved in spindle formation or KT-MT attachments may be required for polar body extrusion. AURKA, AURKC and PLK1 were reported to localize to midzone and midbody during anaphase I-telophase I transition (Pahlavan et al., 2000; Shuda et al., 2009; Tong et al., 2002). Inhibition of AURKC results in cytokinesis failure in meiosis I(Yang et al., 2010). Overexpression of AURKC decreases the proportion of oocytes successfully completing maturation, but securin is degraded in both oocytes that failed and succeeded in extruding polar body. Activated separase promotes separation of homologues in meiosis I, but due to cytokinesis failure such oocytes contain twice more univalents (Sharif et al., 2010). Inhibition of PLK1 concomitantly with CDK1 inhibition blocks I polar body extrusion, implying that PLK1 may play a role in cytokinesis (Pomerantz et al., 2012).

1.2.8 MII arrest

After cytokinesis the oocytes do not enter S-phase, but proceed to metaphase II of second meiosis, where they are arrested until fertilization. The arrest is maintained by cytostatic factor (CSF), which ensures high CDK1 activity by preventing APC/C dependent cyclin B destruction (Madgwick and Jones, 2007). In this mechanism, EMI2 mediates cytostatic arrest by preventing CDC20 binding to APC/C and its consequent activation (Fig.10) (Jones, 2005). During the release of the MII arrest Ca^{2+} signal induces degradation of EMI2 and activation of APC/C, thus leading to degradation of cyclin B resulting in decrease of CDK1 activity (Nixon et al., 2002).

As described previously, during prophase I arrest CDK1 function is regulated by phosphorylation of Thr14 and Tyr15, catalyzed by WEE kinases, while dephosphorylation of these residues is ensured by CDC25 phosphatases. Such mechanism is functional in meiosis II, when downregulation of CDC25A inactivates MPF and releases the oocytes from MII (Oh et al., 2013). Interestingly, recent data indicate that cyclin B degradation promotes CDK1 downregulation, but is not essential for the release from MII arrest. On the other hand, WEE1B-mediated phosphorylation of CDK1 is required for MPF inactivation during MII exit (Oh et al., 2011, 2013). These data demonstrate, that CDC25A mediates dephosphorylation of CDK1 and is required for maintenance of MII arrest.

The third mechanism that ensures MII arrest is c-mos mediated pathway, which is responsible for mitogen activated protein kinase (MAPK) activation. The downstream effectors of this pathway are SAC components and therefore the arrest may be partially mediated by BUB1, MAD1 and MAD2 proteins (Madgwick and Jones, 2007). In mouse oocytes the depletion of mos leads to the failure of MII arrest (Colledge et al., 1994; O'Keefe et al., 1989).

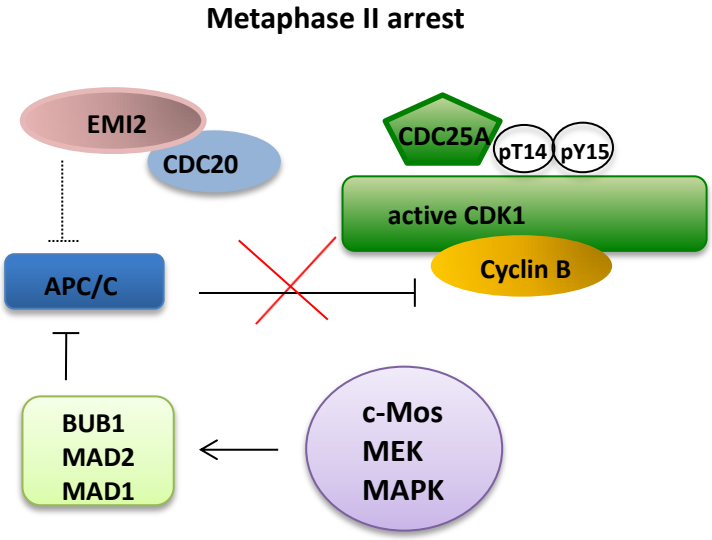

Fig.10. Mechanisms of metaphase II arrest. EMI2 prevents APC/C activation by sequestration of CDC20, while MAPK pathway mediates APC/C inactivation partially through SAC components. Cyclin B is not degraded and CDK1 activity remains high. CDC25A removes inhibitory residues from CDK1 and helps to maintain its high activity.

1.3 DNA-damage mediated response

Prophase I arrest and the resumption of meiosis in oocytes resembles G2 checkpoint in somatic cells, both targeting cyclin B-CDK1 activity (Solc et al., 2010). However, little is known about the DNA damage- induced checkpoint in prophase I in oocytes and about mechanisms which operate in oocytes later during maturation in order to maintain genome integrity. DNA lesions may arise from cell's metabolism (oxygen radicals, DNA replication and trascription) during a lengthy diplotene arrest, or the oocytes may be repeatedly exposed to a number of exogenous DNA damaging agents. Among possible lesions, DSBs are the most serious threat to genomic integrity and when unrepaired, they could have an impact on

maturation of the oocyte or cause fertilization problems (Acilan et al., 2007; Agarwal et al., 2006; Mehta and Haber, 2014).

1.3.1 Overview of DSBs response in somatic cells.

While the response to DSBs in somatic cells has been extensively investigated, surprisingly little is known about the pathways operating in oocytes. The difficulties in studying DNA damage response in oocytes also arise from the fact, that the isolation and culture of oocytes *in vitro* increases the levels of DNA damage (Uppangala et al., 2015), and besides, DSBs response during *in vivo* or *in vitro* maturation of oocytes could be regulated differently (Lin et al., 2014).

Here is a brief overview of DSBs sigaling and repair options in somatic cells, which may be operating in oocytes, but still remain to be discovered.

1.3.1.1 DSBs signaling pathway

In somatic cells, DNA damage response (DDR) pathways are tightly coordinated: the DSBs are recognized by sensors that amplify the signal, while transducers transmit the signal to effector kinases, whose goal is to trigger checkpoint arrest and to iniciate repair pathways. In case of abundant DNA damage when the DNA damage cannot be efficiently repaired, the cells enter senescence or apoptosis (Altmeyer and Lukas, 2013).

H2AX phosphorylation at Ser 139 is the first visible marker of the DNA damage, which appears within minutes (Rogakou et al., 1998, 1999). This phosphorylation is enhanced by ATM (or other PIKK kinases such as DNA-PK or ATR). ATM is activated upon the contact with MRN complex (MRE11, RAD50, NBS1) which is recruited to the sites of DSB among first molecules (An et al., 2010; Burma et al., 2001; Falck et al., 2005; Stiff et al., 2004; Ward and Chen, 2001; Williams and Tainer, 2005). The amplification of the DNA damage signal is triggered by MDC1, which interacts with γH2AX and recruits further MRN-ATM complexes, thus initiating a positive feedback loop (Lee and Paull, 2004; Stucki and Jackson, 2004; Stucki et al., 2005) In fact, γH2AX and MDC1 operate as a docking platform to facilitate accumulation of protein complexes of MRN, ATM, 53BP1, BRCA1(Fig.11) (Bekker-Jensen et al., 2006; Sulli et al., 2012). ATM phosphorylates ubiquitin ligases RNF8 and RNF168 which mediate a protein ubiquitination cascade believed to be important for remodeling of the chromatin flanking DSBs and resulting in accumulation of 53BP1 or BRCA1 (Gatti et al., 2012; Mallette et al., 2012). ATM then targets effector kinase CHK2 to spread the damage signal through the nucleus and phosphorylate proteins involved in checkpoint establishment and DNA repair (Ciccia and Elledge, 2010). As the cells need to react rapidly to DNA damage in order to eliminate possible threat, this pathway is independent of CDK activity. On the other hand, ATR-mediated pathway requires CDK activity and in somatic cells is restricted to S and G2 phases, where single strands of DNA are created through resection. Single strands become coated by RPA, which facilitates recruitment of ATR with its binding partner ATRIP (Zou and Elledge, 2003). ATR-ATRIP complex becomes activated and DNA repair is executed via homologous recombination (Bartek and Lukas, 2007; Jazayeri et al., 2006).

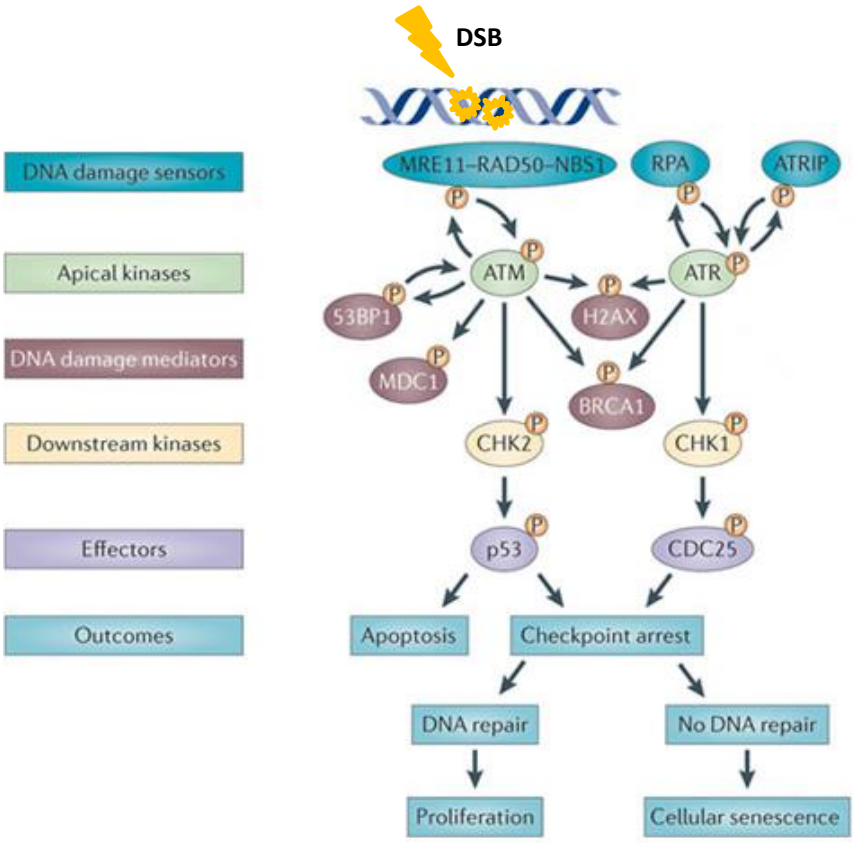

Fig.11. Cellular response to double strand breaks. MRN complex (Mre11, RAD50, NBS1) detects DSBs and activates ATM. ATM together with ATR phosphorylates H2AX and other DNA damage mediators (MDC1, BRCA1, 53PB1). The signaling cascade activates CHK1 and CHK2 kinases which phosphorylate their targets (CDC25 and p53) and induce cell cycle arrest and DNA repair. In case of severe damage apoptosis is triggered. Adapted from Sulli et al., 2012.

1.3.1.2 The MRN complex is a key regulator of DSBs repair

The MRN complex plays a central role in sensing and repairing DSBs. MRN is involved in multiple pathways, regulating DSBs repair through the homology recombination (HR), non-homologous end-joining (NHEJ) and alternative non-homologous end-joining (a-NHEJ) pathways (Stracker and Petrini, 2011). Its inicital recruitment at DSBs is independent of any other proteins and is transient, however sufficient to recruit the ATM kinase (Lukas et al., 2003). While RAD50 subunit recognizes DNA, DNA binding is mediated by MRE11, and ATM recruitment is promoted via NBS1 subunit (Nijmegen breakage syndrome 1) (Moreno-Herrero et al., 2005; You et al., 2005). Besides, NBS1 provides regulatory functions through many protein-protein interactions (e.g. MDC1) (Stucki and Jackson, 2006). Other MRN components exhibit several enzymatic activities including 3´-5´ exonuclease and endonuclease activity of MRE11, required for initiation of HR, and ATPase and adenylate kinase activity of RAD50 (Rein and Stracker, 2014). The switch between sensing of DSBs and end processing is facilitated by MRE11 binding partner CtIP, which undergoes DSBs-

induced phosphorylation and activation (You et al., 2009). Due to nuclease activity, MRN - mediated early end resection of DSBs leads to activation of ATR (Buis et al., 2008; Jazayeri et al., 2006). Interestingly, generation of 3´ ssDNA overhangs by MRE11 possibly inhibits repair of the DNA by NHEJ (Stracker and Petrini, 2011). On the other hand, MRE11 is directly involved in NHEJ and could control end joining through ATM-independent pathway (Rass et al., 2009; Shibata et al., 2014). MRN complex influences DSBs repair not only enzymatically, but also structurally by bridging the gap between broken DNA ends (Mimitou and Symington, 2009; Stracker and Petrini, 2011; Williams et al., 2008).

MRN complex is involved in maintenance of telomerase activity at telomeres. At G2 phase in somatic cells telomeres co-localize with MRN components (MRE11 and NBS1) and ATM and probably are recognized as DSBs. It has been suggested that localized DNA damage response may contribute to the formation of end protection complex by recruiting processing machinery (Verdun et al., 2005). MRN also probably induces resection at telomeres to protect them from NHEJ-mediated „repair“ at G2 (Dimitrova and de Lange, 2009).

It has been published, that malfunction of MRN (mutation, knockdown, degradation or mislocalization of its components) leads to defective ATM signaling (Carson et al., 2003; Stewart et al., 1999; Uziel et al., 2003). Disruption of MRN complex components (MRE11, RAD50, NBS1) results in the failure of proliferation and embryonic lethality in mice (Kang et al., 2002; Xiao and Weaver, 1997). Mutations in mre11 cause chromosomal instability, hypersensitivity to ionizing radiation, radioresistant DNA synthesis, and lower Mre11 expression is associated with ovarian cancer (Stewart et al., 1999; Ye et al., 2014).

1.3.1.3 DSB repair

The major pathways for DSBs repair in somatic cells include HR and NHEJ, but the regulation of pathway choice is not completely understood, and depends on the cell cycle. HR pathway of DNA damage repair is based on sister chromatid homology and therefore is highly precise, while NHEJ promotes potentially inaccurate ligation of DSBs, however it is faster, more efficient and available throughout the cell cycle (Lamarche et al., 2010; Mao et al., 2008; Takata et al., 1998).

During HR the DNA ends are extensively processed in 5’ to 3’ direction promoted by MRN activity. The exonuclease activity of MRE11 operates in the opposite polarity, but MRE11 binding partner CtIP interacts with MRE11 and catalyzes the resections in the right direction (Sartori et al., 2007; You and Bailis, 2010). The generated ssDNA is coated with RPA, which is replaced with RAD51. Single strand DNA with bound RAD51 invades a homologous sequence and RAD51 dissociated from the strand, while the invading strand is paired with the donor strand and is extended by DNA polymerase. The repaired strand anneals with non-invading strand, and single strands are extended and connected through DNA polymerase and ligase activities. BRCA1 and BRCA2 are essential for HR, and promote HR through protein-protein interactions: BRCA1 interacts with CtIP and MRN and BRCA2 interacts with RAD51 facilitating its upload on ssDNA (Huen et al., 2010; Shrivastav et al., 2008).

When precise rejoinment of ends cannot be done, NHEJ involves alignment of few complementary bases (microhomology) to direct repair, which may lead to small deletions or insertions (one or few). During NHEJ, MRN provides limited DSBs processing which is modulated by BRCA1(Durant and Nickoloff, 2005). MRN is an important contributor to this process, because depletion of mre11 reduces the use of microhomology during NHEJ(Xie et al., 2009). Consequently DSBs are bound by KU heterodimer (Ku70 and Ku80), which also has a DNA end processing activity (Mahaney et al., 2009; Roberts et al., 2010). KU activates DNA-PK, which stabilizes DNA ends and together with ARTEMIS protein stimulates processing of DNA ends (Ma et al., 2002; Meek et al., 2008). Loading of DNA-PK leads to XRCC4/DNA ligase 4 recruitment, which promotes ligation of broken ends (Mahaney et al., 2009).

Alternative pathway is probably a backup to classical NHEJ and operates in the absence of conventional NHEJ components DNA-PK, Ku, XRCC4 or DNA ligase 4. Like conventional NHEJ it includes modest deletions and microhomology (<100 nucleotides), but is even more error-prone. Instead of the classical components, poly(ADP-ribose)polymerase 1 (PARP-1) recognises DSBs and promotes ends ligation through ligase 3 (Wang et al., 2006). Additionally, together with classical NHEJ, A-NHEJ is believed to be the pathway responsible for the fusion of deprotected telomeres (Fig.12) (Badie et al., 2015). In this case, BRCA1 and CtIP are involved in processing and fusion of uncapped ends.

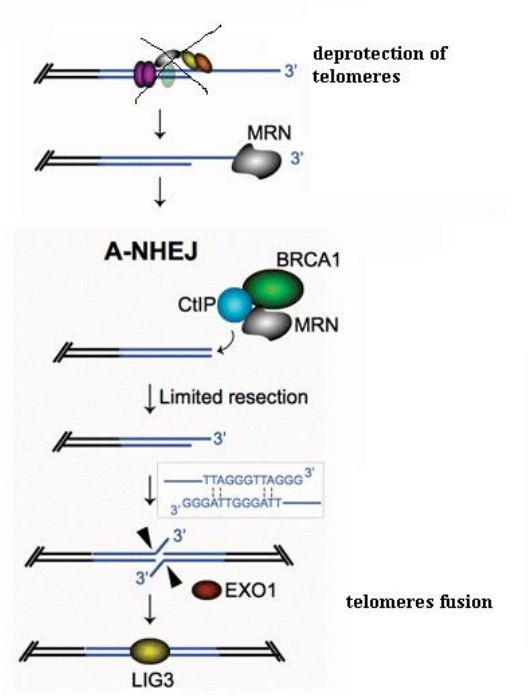

Fig.12. Role of MRN complex in telomere fusion MRN complex together with CtIP and BRCA1 recognizes and processes deprotected telomeres. Ligase 3 is responsible for fusion of telomeres. Modified from Badie et al., 2015.

1.3.1.4 DNA damage response during mitosis

While DSBs are repaired throughout the cell cycle, the suppression of the canonical pathways during mitosis seems to be essential for maintenance of genome integrity. During late prophase the cells are able to respond to DSBs by restricting mitotic entry, however upon reaching a point of no return in mitosis the cells do not react to the presence of chromosome fragments and do not arrest cell cycle (Rieder and Cole, 1998). These data suggest that cells in mitosis regulate the DSBs repair differently, however the full mechanisms of DDR during mitosis are not well understood. While the early components of DSBs response localize to the sites of DSBs, the recruitment of 53BP1 and BRCA1 is suppressed, and RNF8/ RNF168 are

recruited only in late mitosis (Giunta and Jackson, 2011; Giunta et al., 2010; Lee et al., 2014; Nelson et al., 2009; Orthwein et al., 2014; Zhang et al., 2011). The phosphorylation of RNF8 and 53BP1 by CDK1 prevents their binding to MDC1, which results in their sequestration from the sites of DSBs. The other kinase involved in inhibitory phosphorylation of DDR components in mitosis is PLK1 (Fig. 13) (Orthwein et al., 2014; Terasawa et al., 2014a; Zhang et al., 2011).

While the major pathways of DSBs response is suppressed during mitosis, some repair still occurs (Terasawa et al., 2014a). Induction of DSBs during M-phase leads to fragmentation of chromosomes, but also partially activates DSBs repair through C-NHEJ. However, activation of C-NHEJ in mitosis results in dicentric chromosomes originating possibly due to erroneous telomere connection in XRCC4-dependent way, and leads to anaphase bridges formation (Terasawa et al., 2014a). During unperturbed mitosis XRCC4 is negatively phosphorylated to downregulate its function, but in case of DNA damage it seems to promote DNA ends connection, although this process is not precise and induces chromosome instability. Similarly, the artificial restoration of recruitment of late DDR components (53BP1 and RNF8) in mitosis causes defects in chromosome segregation, leads to micronuclei formation and increases telomere fusion, which is most likely also mediated by C-NHEJ (Fig. 14) (Denchi and Li, 2014; Lee et al., 2014; Orthwein et al., 2014).

On the other hand, knockdown of XRCC3, a component of HR pathway, does not influence anaphase bridge formation in mitotic cells. Thus, C-NHEJ is probably the main repair pathway during mitosis, although its efficiency is rather questionable. Interestingly, CtIP which besides HR promotes end resection also in A-NHEJ, may be involved in maintenance of DNA integrity during mitosis, as its downregulation increases the incidence of anaphase bridges (Terasawa et al., 2014a).

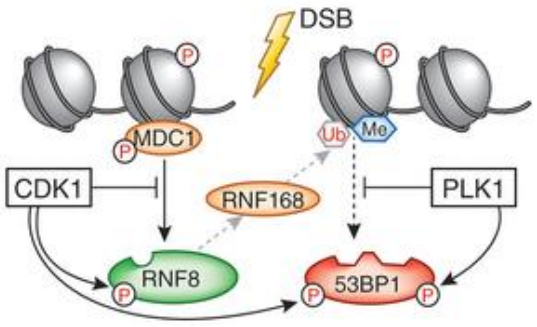

Fig.13. CDK1 and PLK1 inhibit full DNA damage response in mitosis. CDK1 phosphorylates RNF8 and inhibits its recognition by MDC1. Inhibition of RNF8 abrogates the recruitment of to the site of DNA damage. Both CDK1 and PLK1 phosphorylate 53BP1 and suppress its association with DNA. Adapted from Denchi and Li, 2014.

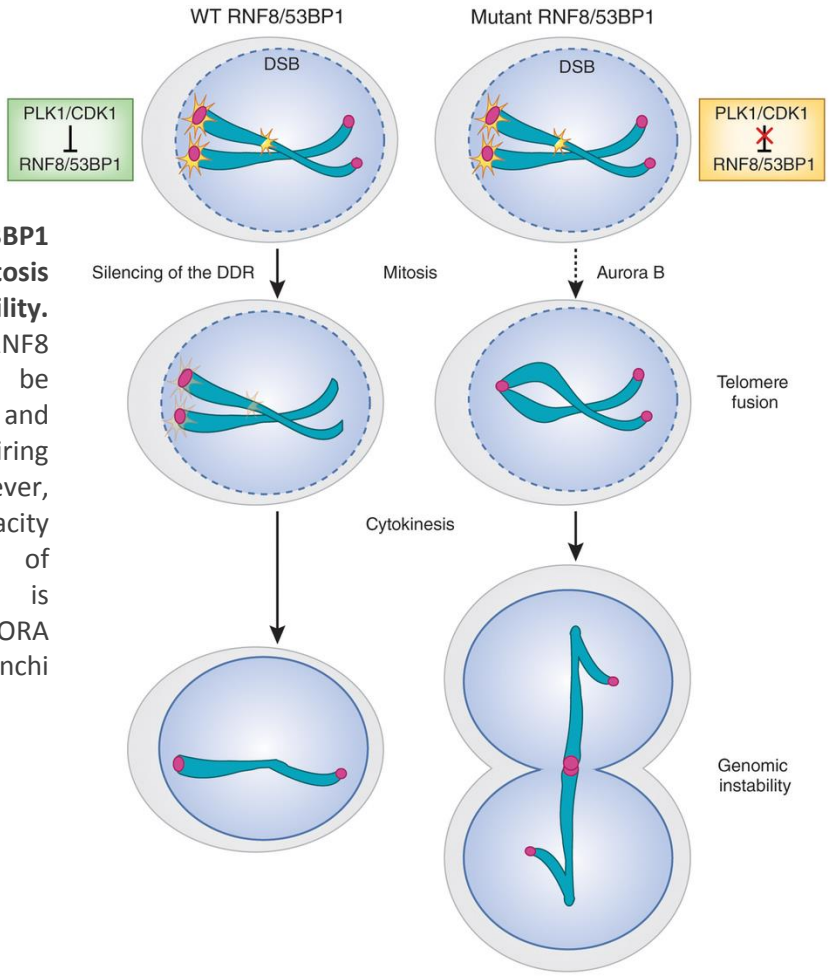

Fig.14. RNF8 and 53BP1 recruitment during mitosis results in genomic instability. Cells expressing mutant RNF8 and 53BP1 that cannot be phosphorylated by CDK1 and PLK1 are capable of repairing DSBs in mitosis. However, restoration of repair capacity leads to high frequency of telomere fusions, which is partially dependent on AURORA B activity. Adapted from Denchi and Li, 2014.

1.3.2 DNA damage response and repair in oocytes

In the oocytes, the DSBs induced physiologically to enable recombination are effectively repaired during early prophase I. Besides, primordial, primary and pre-antral follicles were found to trigger apopotosis through TAp63-dependent expression of proapoptotic factors PUMA and NOXA as a response to exogenous damage induced by ionizing radiation (Suh et al., 2006). Oocytes from primordial follicles with DSBs induced by doxorubicin activate ATM and also undergo apoptosis most likely through TAp63-dependent way. Remarkably, about a third of such oocytes survive and repair the damage (Soleimani et al., 2011).

In contrast, the response of fully grown oocytes to DSB is rather limited and the threshold for DNA damage detection or checkpoint activation is set higher than in somatic cells or immature oocytes. The concentraction of topoisomerase II inhibitor etopside which is sufficient to cause G2 arrest in somatic cells, does not stop oocytes from meiosis I resumption (Mailhes et al., 1994; Marangos and Carroll, 2012). Oocytes become sensitive only to increased concentrations of radiomimetic DSBs inducing drugs (ethopsid, bleomycin, neocarzinostatin) or higher UV-A irradiation, which gradually reduce their ability to resume meiosis I (Lin et al., 2014; Ma et al., 2013; Marangos and Carroll, 2012; Yuen et al., 2012). Once oocytes with DSBs undergo NEBD, spindle formation is not impaired, however, SAC is inactivated despite misaligned chromosomes, and therefore, polar body extrusion rates remain close to normal (Lin et al., 2014; Ma et al., 2013).

The low sensitivity of fully grown oocytes checkpoint is surprising. Checkpoint is a natural mechanism to delay cell cycle progression by inhibition of CDK1/CyclinB in order to prevent genomic instability, and to give opportunity to repair DNA. In somatic cells it is mediated through ATM/ATR dependent phorphorylation of kinases CHK1 and CHK2, which inactivate CDC25 phosphatases (Bartek and Lukas, 2007). CDC25A becomes degraded through ubiquitin mediated SCF-complex-dependent patway (Busino et al., 2003; Mailand et al., 2000), while CDC25B and C are inhibited through phosphorylation (Boutros et al., 2007; Darzynkiewicz et al., 2009). In the oocytes, the checkpoint is also triggered through ATM-mediated pathway. However, the concentration of DSBs inducing drug etopsid, sufficient for ATM activation in blastomeres maintain ATM kinase activity at basal levels: only higher rates of DSBs increase ATM phosphorylation and activate its downstream effector CHK1 in the oocytes (Fig. 15) (Marangos and Carroll, 2012). Interestingly, the phosphorylation of DSBs marker H2AX in blastomeres and oocytes does not show any significant difference, implying that H2AX may be phosphorylated independently of ATM in oocytes.

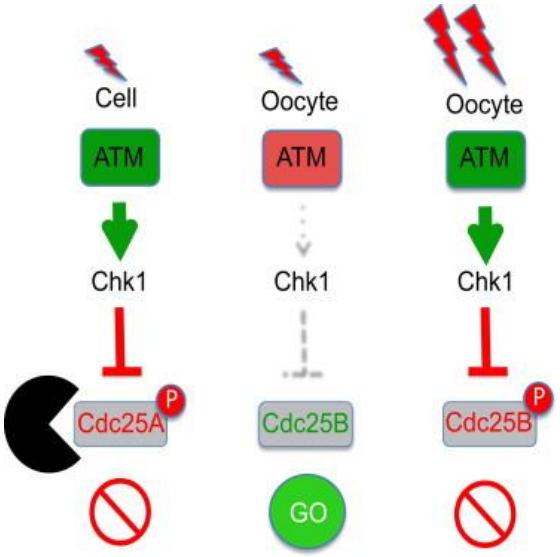

Fig.15. Oocytes respond only to extreme levels of DSBs at prophase I. In contrast to somatic cells, the oocytes do not activate ATM in response to low or medium DNA damage. ATM becomes activated only as a consequence of high DNA damage and mediates CHK1-dependent CDC25B inhibition instead of CDC25A phosphorylation and degradation. Adapted from Marangos and Carroll, 2013.

The other diference from somatic cells is that instead of CDC25A degradation as a response to DSBs, CDC25B is phosphorylated on Ser323 through ATM-CHK1 dependent pathway (Fig. 15) (Marangos and Carroll, 2012). Thus, the oocytes use for DNA damage checkpoint establishment similar mechanism as for physiological prophase I arrest.

Although fully grown oocytes are not able to launch an adequate checkpoint, low levels of DNA damage are still repaired during prophase arrest or M-phase. UV irradiation of prophase I, MI and MII oocytes induced ^{3}H-tymidine incorporation, indicating the ability of oocytes to repair DNA during maturation (Masui and Pedersen, 1975). RNAi inhibition of main DSBs recognition and repair factors MRE11, ATM and RAD51 at prophase I leads to higher levels of γH2AX in the presence of genotoxic stress and activates apoptosis (Titus et al., 2013). Similarly, in oocytes from BRCA1 heterozygous mice there is an increase in γH2AX signal and DNA damage accumulation (Titus et al., 2013). Further, MII oocytes from

young mice significantly reduce internal DNA damage after 6 hours of *in vitro* culture, and RAD51 becomes recruited to MII chromosomes (Kujjo et al., 2010)

Not all DNA damage is repaired during oocyte maturation. Some of the DSBs induced in prophase I persist at a partenogenetically activated 1-cell embryo (Ma et al., 2013). In oocytes carrying interstrand crosslinks, induced by mitomycin C, FANCD2 is not recruited to the sites of DNA damage at GV stage, but forms foci in the embryo (Yuen et al., 2012).

According to these data, active DSB repair is important for survival of oocytes and further embryo development. Given that oocytes regulate some aspects of the repair pathway differently, still little is known about DSB response and other active components of early DDR in MI and MII oocytes.

2 Goals of the project

1. To gain new insights into the roles of PLK1 and AURKA in meiotic maturation of mouse oocytes.
2. To investigate early signaling events of DSBs repair pathway in maturing oocytes and to estimate the capacity of the oocytes to repair DSBs.
3. To explore the involvement of MRE11 in regulation of DNA damage response in oocytes.

3 Materials and methods

3.1 Animal use

The mice used in PLK1 and DNA damage studies were 8-12 weeks old CD1 or H2B-EGFP transgenic mice(Hadjantonakis and Papaioannou, 2004) on CD1 genetic background (CD1-Tg(HIST1H2BB/EGFP)). To obtain CD1-Tg(HIST1H2BB/EGFP) we repeatedly (>10 times) backcrossed transgenic and H2B-EGFP-expressing males with wild-type CD1 females. To generate transgenic mice overexpressing human WT-AURKA or catalytically inactive KD-AURKA, we bred previously described CAG-CAT-Aurka female mice to Zp3-Cre male mice (Lewandoski et al., 1997). The CAT sequence, which contains a polyA signal that is flanked by two loxP sites, can be removed by Cre-mediated recombination. Because Zp3 promotor mediates Cre expression only to oocytes, WT- or KD-Aurka mice express AURKA only in oocytes. Cdc25b-deficient oocytes were obtained from Cdc25b germ line knockout mice (Lincoln et al., 2002). Mice were genotyped using tail DNA by PCR as previously described (Lincoln et al., 2002; Zhang et al., 2004) . In experiments using WT- and KD-Aurka mice, we used CAG-CAT-Aurka and/or Zp3-Cre mice as controls; these mice have normal WT phenotypes. The genetic background of Cdc25b−/− mice is C57BL, therefore we used as controls WT C57BL/6NCrl.

All mice used in experiments were housed in a temperature-controlled room with proper 12/12 darkness-light cycles, fed with a regular ad libitum diet.

3.2 Culture of oocytes

The oocytes were obtained from mice sacrificed by cervical dislocation 46 h after the injection of 5 IU equine serum gonadotropin (eCG). Oocytes were collected in M2 medium and cultured in MEM medium (Sigma-Aldrich) supplemented with 0.22 mM sodium pyruvate, 4 mg/ml BSA (Sigma-Aldrich) and 50 µg/ml Gentamicin (Sigma-Aldrich) in a 5% CO2 atmosphere. The culture medium was supplemented with 2.5 µM milrinone (Sigma-Aldrich) or 200 nM 3-isobutyl-1-metyl-xanthine (IBMX, Sigma-Aldrich) to prevent meiotic maturation (Tsafriri et al., 1996).

For *in vivo* studies, the mice were injected with 5 IU equine serum gonadotropin and 44 h later by 5 IU human chorionic gonadotropin (hCG) to initiate resumption of meiosis. Cumulus cell-enclosed oocytes were isolated in M2 medium (Sigma-Aldrich) at different times after hCG administration; for GV-stage oocytes 0h, for NEBD 3–4 h, for MI 7 h, and for MII 12 h post-hCG administration. The expanded cumulus cells surrounding MII eggs were removed by hyaluronidase (Sigma Aldrich, H4272) treatment.

3.3 In vitro cRNA production and microinjection

Polyadenylated and capped mRNA for microinjection was produced by in vitro transcription using mMESSAGE mMACHINE® T3 Kit (Ambion). To generate the template for transcription the genes of interest were cloned into pBluescript (Addgene) or pGEMHE vector (provided by T.Kitajima, RIKEN, Japan). For *in vitro* transcription, the vectors were linearized with Asc1. After *in vitro* transcription, cRNAs were immediately polyadenylated using the Poly(A) Tailing Kit (Ambion). mRNAs were purified using RNeasy Mini Kit (Qiagen).

Oocytes were microinjected in M2 medium with 5 pl of 80 ng/µl H2B-mCherry , 150 ng/µl 2mEgfp-Cenp-C(Sakakibara et al., 2015), 50 ng/µl Securin-Egfp (Kudo et al., 2006), 125 ng/µl Map4-Egfp (Schuh and Ellenberg, 2007) cRNAs; 2 pl mEgfp-Plk1, 1 pl mEgfp-Emi1cRNAs,4pl 3mCherry-Cenp-C from 1 µg/µl mRNA stocks. The microinjection was performed using a MIS-5000 micromanipulator (Burleigh, Exfo Life Sciences, USA) and PM 2000B4 microinjector (MicroData Instrument, USA). For nuclear envelope permeability measurement, H2B-EGFP oocytes were microinjected with 5 pl of 2 mg/ml 70-kDa dextran conjugated with tetramethylrhodamine (TAMRA) (Sigma Aldrich). Oocytes were cultured for 2 h in MEM medium supplemented with milrinone or IBMX to allow protein expression after mRNAs microinjection.

3.4 Live confocal microscopy

Time-lapse image acquisitions in Fig. 24A, 33A, 34 A, 42E, 43 were performed using Leica TCS SP5 with an HCX PL Apo Lambda Blue 40x 1.25 oil objective; 12 confocal 7.5-µm optical sections were taken with a1024 x 1024 pixel image resolution using 10 min time intervals. For kinetochore imaging in EGFP-CENP-C expressing oocytes (Fig.43) we used the tracking function of the Matrix Screen module in LAS AF software (Leica Microsystems). The area of the chromosomes of individual oocytes expressing H2B-mCHERRY and EGFP-CENP-C was irradiated with 6% of the 488 nm and 3% of the 561 nm lasers and 14 confocal 2-µm optical sections scanned by HyD detectors with 12x zoom in 256 x 256 or 512 x 512 pixel image resolution by 1000Hz speed bi-directional scan were acquired. Time-lapse image acquisitions in Fig. 23A, 26A, 28A, 29A, 30, 33B were performed by Zeiss LSM710 equipped with a 40x C-Apochromat 1.2 W Corr M27 objective lens (Carl Zeiss). Kinetochores imaging in live oocytes in Fig. 33 B was done as described previously (Kitajima et al., 2011; Sakakibara et al., 2015).

3.5 Immunofluorescence confocal microscopy

Oocytes were fixed in 3.7% paraformaldehyde (PFA) in PBS for 30 min, and after washing with PBS, the oocytes were permeabilized for 15 min in 0.5% Triton X-100 in PBS. For stable KT-MT attachment detection, oocytes were cultured in ice-cold M2 medium for 10 minutes before fixation. The oocytes were incubated with 2% normal donkey serum (Jackson ImmunoResearch) in PBS for 2h. Then the oocytes were incubated overnight at 4°C with primary antibodies diluted in PBS/0.2% normal donkey serum, and after washing with PBS incubated 1h at RT with secondary antibodies. γH2AX was detected by rabbit monoclonal anti-phospho-histone H2AX (1:200, Cell Signaling Technology, 9718), MDC1 by mouse monoclonal anti-MDC1 , clone P2B11 (1:200,Millipore, 05-1572), MRE11 by rabbit polyclonal antibody (1:200, Novus Bio, NB100-142), pT210 PLK1 was detected by rabbit polyclonal (1: 100; Santa Cruz Biotechnology), kinetochores by human CREST serum (1:100; Europa Bioproducts), α-tubulin by mouse monoclonal (1:500, Sigma Aldrich), AURKA phosphorylated on T288 was detected by a rabbit polyclonal antibody (1:200,Novus Bio NB100-2371), γ-tubulin by a rabbit polyclonal antibody (1:200, Biolegend, 620901), pericentrin by a mouse monoclonal antibody (BD Biosciences, 611815). Secondary antibodies were anti-mouse conjugated with TRITC or anti-rabbit conjugated with FITC (1:100, Jackson ImmunoResearch). Anti-mouse antibody conjugated with TRITC or anti-rabbit antibody

conjugated with FITC (Jackson ImmunoResearch) were used at a dilution 1:100. After a final wash in PBS/BSA, the oocytes were mounted in Mowiol (with 0.25µg/ml DAPI for DNA staining) between a slide and cover glass using a spacer to preserve the three-dimensional (3D) structure of the oocytes.

Oocytes were scanned using Leica TCS SP5 with HCX Pl Apo Lambda Blue 63x 1.4 oil objective. A sequential scan was applied in the 16-bit image depth (or 12-bit image depth) with 1024 x 1024 pixel image resolution for 4x zoom on the entire oocytes or 512 x 512 pixel image resolution for 8x zoom on the chromosome area. Three-dimensional scanning was performed using 1-µm optical sections through the oocyte volume

3.6 Image analysis

Image analysis was performed using Fiji software (Schindelin et al., 2012). For γH2AX foci number analysis we segmented γH2AX signal by applying an intensity threshold on 3D images previously denoised using PureDenoise plugin (Luisier et al., 2011). γH2AX foci number was measured by 3D Object Counter (Bolte and Cordelières, 2006) on the segmented 3D images (Fig.31B, 32C, Fig. 35D, Fig. 37 D, Fig. 40A,C, Fig. 41A). γH2AX fluorescence associated with chromatin was measured by redirection of 3D mask of intensity-thresholded DNA signal to γH2AX channel (Fig. 35A, Fig. 37E, Fig. 38B, Fig. 40B) .pT288 AURKA (Fig. 21) and p210PLK1(Fig.23) associated with MTOC were measured by redirection of 3D mask of intensity-thresholded pericentrin signal to pAURKA or pPLK1 channel. The same approach was used for quantifying MTOC-associated γ-tubulin and pericentrin (Fig. 25D, Fig. 27B).To measure the total MTOC volume (Fig. 20B, 25E) the γ-tubulin channel was converted by intensity thresholding into the binary channel, individual MTOCs were identified with a 3D Object Counter, and the MTOC volume was measured. Similarly, the spindle volume and chromosome volume were measured from the intensity threshold binary channel of α-tubulin (or EFGP-MAP4 in Fig. 42) and H2B signal, respectively (Fig. 24,25C, 28C). For spindle length measurement x, y, z coordinates of spindle poles stained by γ-tubulin were stored and the spindle length was calculated as the distance between spindle poles (Fig. 25 B). Securin-EGFP intensity was measured on maximum intensity z-projection images of the oocytes (Fig.29, Fig.34). Dextran in the area of the nucleus was measured from the single confocal section through the center of the nucleus, when H2B-EGFP signal was registered by Correct 3D Drift plug-in. Identifications of the onset and end of AF, dextran influx, and chromosome condensation were done using defined thresholds (Fig. 24)

3.7 Western blot

For immunoblotting, 200 oocytes per sample were collected at GV stage (0 h) or MII stage (18 h) for MRE11 and 20 oocytes per sample were used for WT or KD-AURKA. Oocytes were lysed in 10 µl of 1 × Reducing SDS Loading Buffer (Cell Signaling) and heated at 100 °C for 3 min. Proteins were separated by gradient 4-12% SDS–PAGE and transferred to a nitrocellulose membrane using a dry blotting system iBlot (Life Technologies). The membrane was blocked in 5% milk in 0.05% Tris-buffer saline-Tween (TBST), pH 7.4 for 1 h. The membrane was then washed in TBST and incubated at 4 °C overnight in the presence of the MRE11 antibody (Cell Signaling Technology, 4895) at dilution 1:1000 or AURKA

rabbit polyclonal antibody (3092; Cell Signaling) at dilution 1:500. To visualize the proteins an ECL kit (Amersham) was used and films were scanned with a GS-800 densitometer (Bio-Rad).

3.8 Statistical analysis

NCSS2007 software (NCSS, LLC., Kaysville Utah) was used for statistical analysis. Differences in foci number and immunofluorescence intensity were evaluated by the Student t-test. Differences in medians were measured by Mann-Whitney test when the data showed non-normal distribution. Samples with $P<0.05$ were considered as statistically significant.

4 Results

4.1 Roles of AURKA and PLK1 in meiotic resumption

4.1.1 AURKA triggers MTOC multiplication *in vivo* but is dispensable for meiotic resumption

The role of AURKA *in vitro* in mouse oocytes has been studied: it is present in mouse oocytes at GV stage and progressively accumulates at MTOC controlling their amplification prior to meiotic resumption. Inhibition of AURKA using RNAi approach delays meiotic resumption (Saskova et al., 2008). However, the mechanisms that trigger meiotic resumption *in vitro* and *in vivo* differ: while removing the oocytes from follicles *in vitro* leads to spontaneous resumption of meiosis via PDE3A-mediated decrease in cAMP, this process is triggered *in vivo* by LH-mediated decrease of cGMP and activation of PDE3A (Conti et al., 2012). Such differences may result in different regulation of upstream components involved in CDK1/cyclinB activation, especially AURKA.

Our data demonstrate, that physiologically AURKA is autophosphorylated at T288 and activated (Littlepage et al., 2002) within 1 hour from the start of maturation *in vivo* (Fig 17), reaching its full activity by 2 hour (Fig 18). Besides, AURKA is localized on MTOC after their amplification (Fig 17).

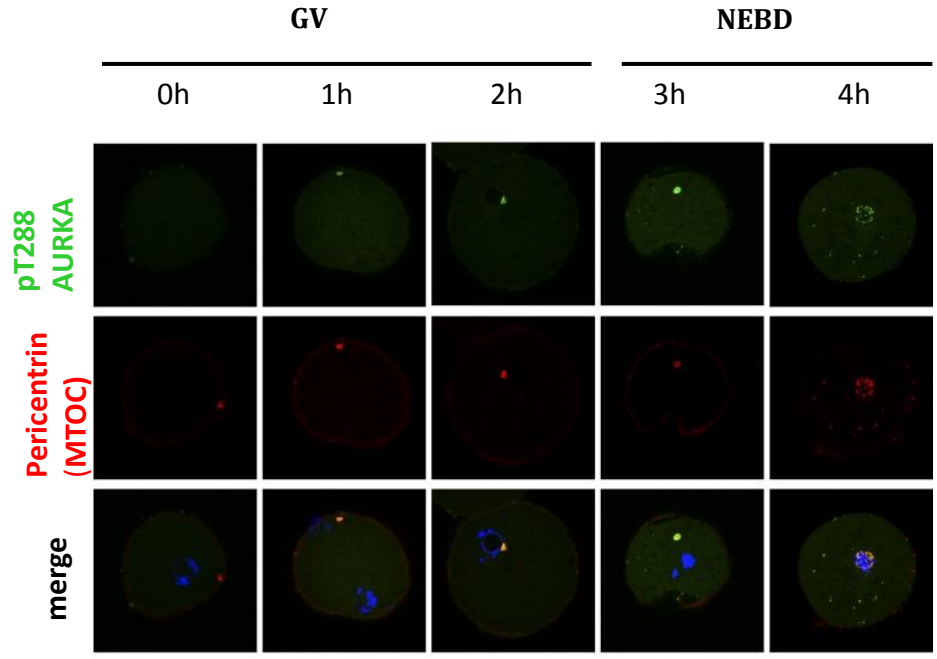

Fig.17. Activation of AURKA during resumption of meiosis. Resumption of meiosis was induced by hCG at 0h. We observed AURKA activation on MTOC in 0-4h intervals. AURKA phosphorylated on T288 colocalizes with pericentrin at GV stage, 1h after the start of meiotic resumption. At 4h MTOC become multiplied and AURKA colocalizes with all of them. At 0h, 1h, 2h intervals the images of pT288 AURKA and pericentrin represent single confocal sections whereas at the 3h and 4h intervals the images are maximum projections; DNA is presented as maximum projection.

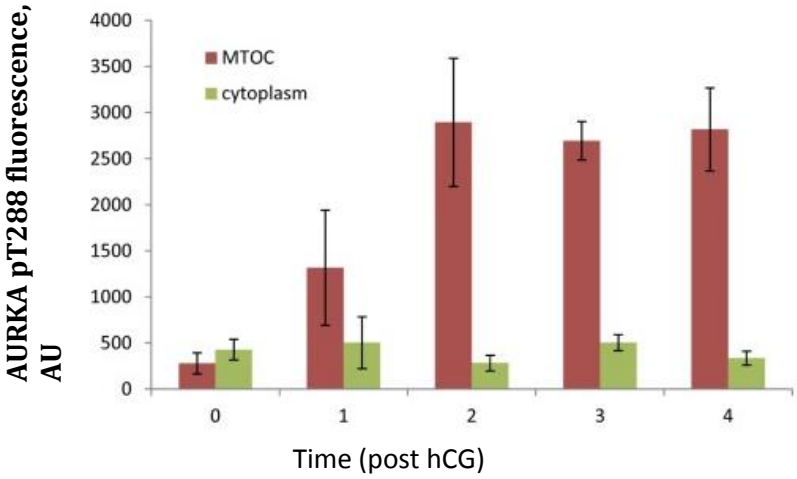

Fig. 18. Quantification of AURKA activation on MTOC. The data represent relative fluorescence of pT288 AURKA on MTOC during meiotic resumption. Data are means with 95% confidence intervals in arbitrary units.

To investigate AURKA role in meiotic resumption *in vivo* we used transgenic mice carrying human wild type (WT)- or kinase dead (KD-) AURKA transgenes under the control of constitutive CAG promoter (Zhang et al., 2004). Breeding such mice with *Zp3-Cre* mice mediated the excision of inhibitory sequence and allowed to overexpress WT-AURKA or KD-AURKA only in oocytes. While in control oocytes the detection threshold on Western blot for AURKA is 200 oocytes (data not shown and Saskova et al., 2008), we used 20 oocytes per lane (Fig 19, A) and observed the overexpression of WT and KD in such experimental conditions. It means that the expression of AURKA transgenes was at least 10 times greater than endogenously expressed AURKA, and higher amounts of KD-AURKA were detected compared to WT-AURKA (Fig. 19, A). The increase in activated WT-AURKA was also observed by immunofluorescence analysis, and MTOC in WT-AURKA were already amplified and associated with activated AURKA (Fig. 19, B).

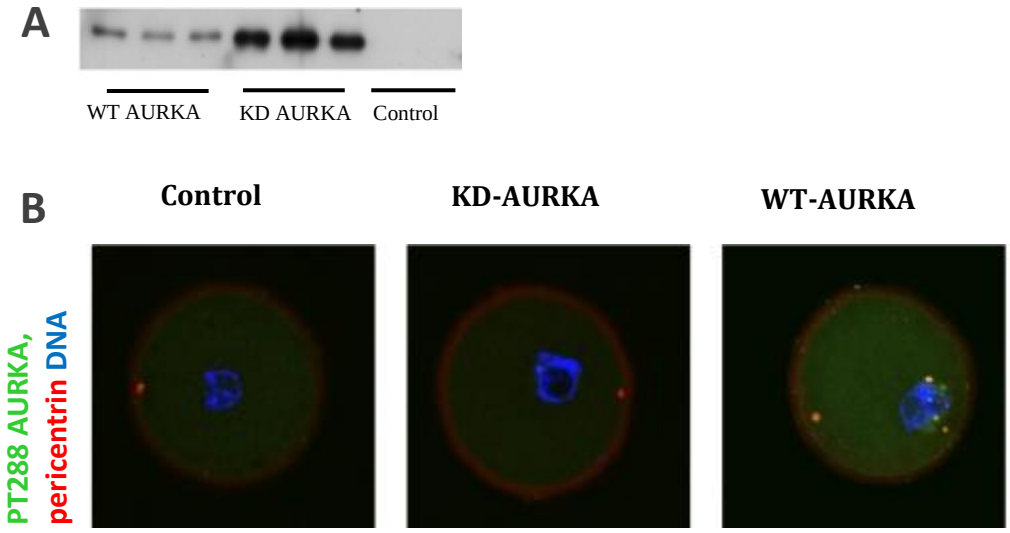

Fig. 19. Conditional overexpression of WT and KD AURKA transgenes in mouse oocytes. A)Western blot of 20 oocytes isolated from mice conditionally expressing KD- or WT-AURKA. To detect endogenous AURKA (control) around 200 oocytes are required. B) Immunofluorescence analysis of GV-stage arrested oocytes revealed premature AURKA activation (pT288) on MTOC (pericentrin) in WT-AURKA expressing oocytes. The images are single confocal sections for KD and control group; maximum z-projection of confocal sections for WT-AURKA is shown.

In contrast, 1-3 MTOC could be found in control oocytes arrested within follicles, which persisted up to 3-4 hours after the induction of maturation by hCG and the increase in MTOC (more than 3 MTOC) occured only after NEBD. While the increase of MTOC in WT-AURKA occured already at t=0 in GV-intact oocytes, we found this increase to be transient, and the second wave of MTOC increase occured synchronously with control oocytes and KD-AURKA oocytes (Fig. 20, A). Remarkably, the transient increase of MTOC number was also associated with increase in their volume, which suggests that MTOC were multiplified rather than fragmented (Fig.20, B).

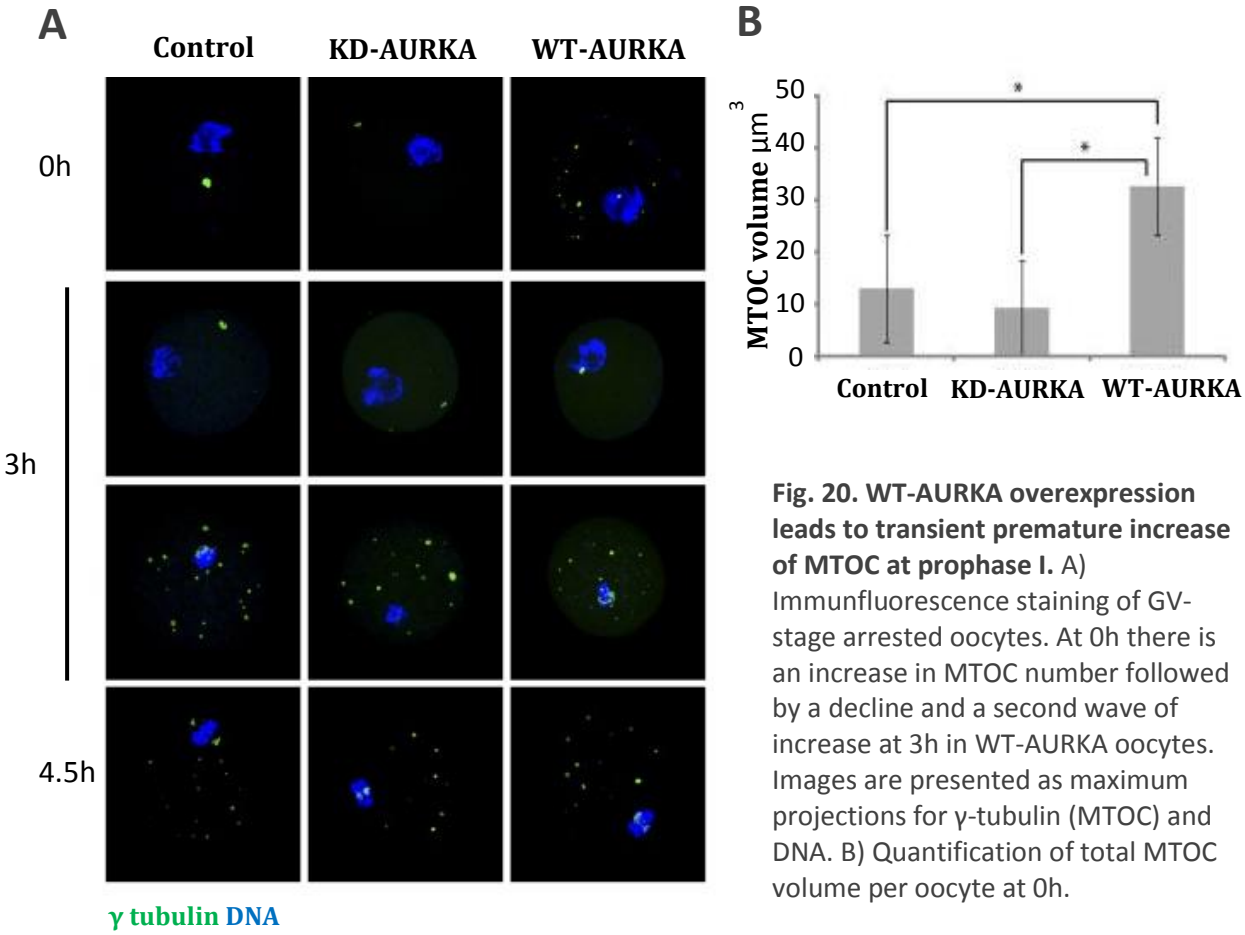

Fig. 20. WT-AURKA overexpression leads to transient premature increase of MTOC at prophase I. A) Immunfluorescence staining of GV-stage arrested oocytes. At 0h there is an increase in MTOC number followed by a decline and a second wave of increase at 3h in WT-AURKA oocytes. Images are presented as maximum projections for γ-tubulin (MTOC) and DNA. B) Quantification of total MTOC volume per oocyte at 0h.

Next we raised the question whether CDK1 is involved in AURKA –dependent process of MTOC multiplication. For this purpose we used *Cdc25b*-/- oocytes, in which CDK1 activity is too low to induce resumption of meiosis (Lincoln et al., 2002) The increase in MTOC number did not occure in *Cdc25b*-/- oocytes and AURKA was only partially activated at 4h or 7h post hCG (Fig. 21, A, B, C). These data imply that CDC25B-dependent activation of CDK1 is essential for full AURKA activation. The microinjection of GFP-AURKA cRNA into oocytes deficient for *Cdc25b* restored MTOC amplification, however the oocytes remained arrested in prophase I (Fig. 21, D).

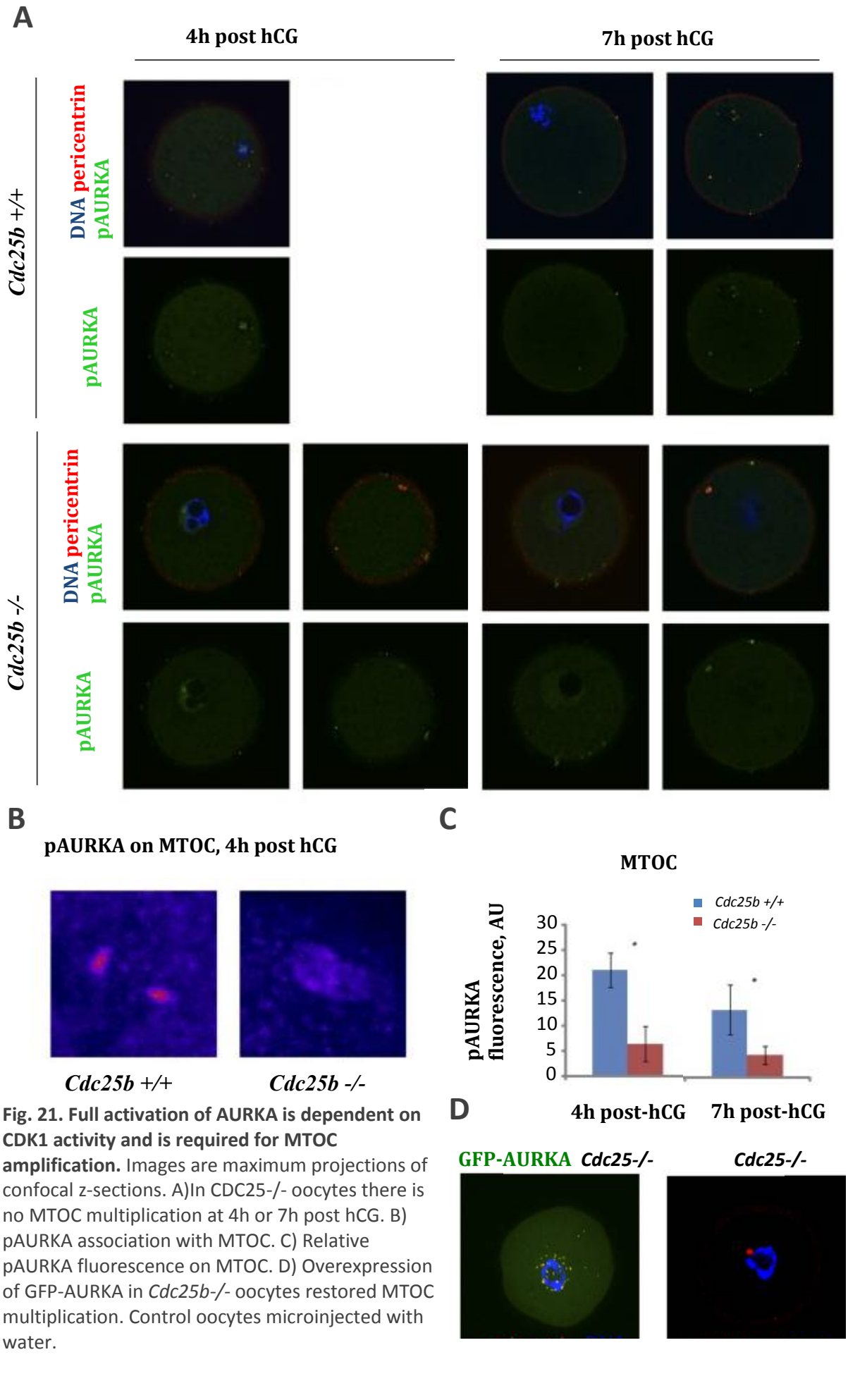

Fig. 21. Full activation of AURKA is dependent on CDK1 activity and is required for MTOC amplification. Images are maximum projections of confocal z-sections. A)In CDC25-/- oocytes there is no MTOC multiplication at 4h or 7h post hCG. B) pAURKA association with MTOC. C) Relative pAURKA fluorescence on MTOC. D) Overexpression of GFP-AURKA in *Cdc25b-/-* oocytes restored MTOC multiplication. Control oocytes microinjected with water.

Apart from MTOC amplification our data demontrate, that AURKA is dispensable for meiotic resumption. Conditional overexpression of both *WT*- and *KD- AURKA* in wild type oocytes did not accelerate the resumption of meiosis (Fig. 22). The meiotic maturation rates were not changed either, and upon fertilization of metaphase II oocytes the amount of pups was comparable to control from female mice up to 6 months old (data not shown).

Altogether, AURKA is not required for meiotic resumption, but is involved in MTOC amplification, which occurs *in vivo* shortly after NEBD, while *in vitro* this proces occures before NEBD(Can et al., 2003). Overexpression of AURKA *in vivo* causes a transient premature increase in MTOC before NEBD, whereas full AURKA activation required for permanent MTOC multiplication is dependent on CDC25B-mediated activation of CDK1. Therefore, the oocytes possess the mechanism that tightly control the timing of MTOC amplification.

Fig. 22. AURKA overexpression does not accelerate the resumption of meiosis. Resumption of meiosis (NEBD) at 3 and 7 h after hCG administration. The number of oocytes examined was 262 for controls (CTRL), 195 for WT-AURKA, and 136 for KD-AURKA. The differences among groups are not significant.

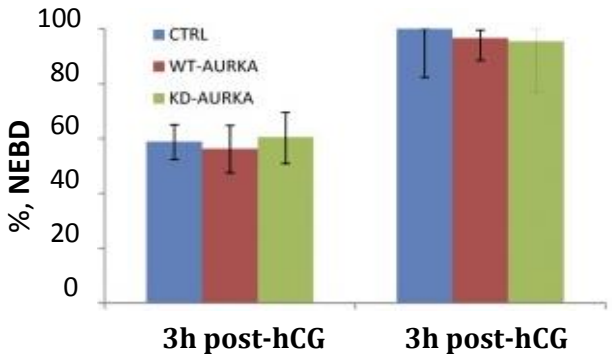

4.1.2 PLK1 is activated on MTOC during the resumption of meiosis and promotes nuclear envelope breakdown

Although the localization of PLK1 in the cytoplasm at GV stage and at MTOC and kinetochores after meiotic resumption was confirmed earlier (Pahlavan et al., 2000; Tong et al., 2002), we quantitatively analyzed the changes in PLK1 localization. The microinjected Egfp-Plk1 cRNA localized into cytoplasm at GV stage and during meiotic resumption PLK1exhibited punctate signals throughout cytoplasm (Fig. 23 A). Further we immunostained and quantitatively analyzed the oocytes for presence of the specific phosphorylation of endogenous PLK1 on T210 (pPLK) associated with PLK1 activation. The active PLK1 was detected 20 minutes before the time of NEBD and it also colocalized with pericentrin, the marker of MTOC (Fig. 23 B, C). pPLK1 reached its maximum level on MTOC at the time of NEBD and its association with MTOC marker was detected also after NEBD (Fig.23. C). The high activity of PLK1 during meiotic resumption implies that PLK1 is involved in the regulation of this process. In the oocytes the resumption of meiosis includes both NEBD and chromosome condensation. To explore the role of PLK1 in these processes we treated H2B-EGFP expressing oocytes with BI2536, a small molecule inhibitor of PLK1 immediately after induction of meiotic resumption. To precisely detect NEBD we injected 70kDa dextran into the cytoplasm of the oocytes and measured its entry into the nucleus when the membrane started to disassemble (Fig. 24 A). We also analyzed chromosome volume by reconstruction of H2B-EGFP chromosome signals in 3D (Fig. 24 B). In oocytes treated with BI2536 both the

permeabilization of nuclear membranes and chromosome condensation were significantly delayed, and the NEBD onset was more affected, as evaluated by the presence of condensed chromosomes inside the intact nucleus (Fig. 24 A, B).

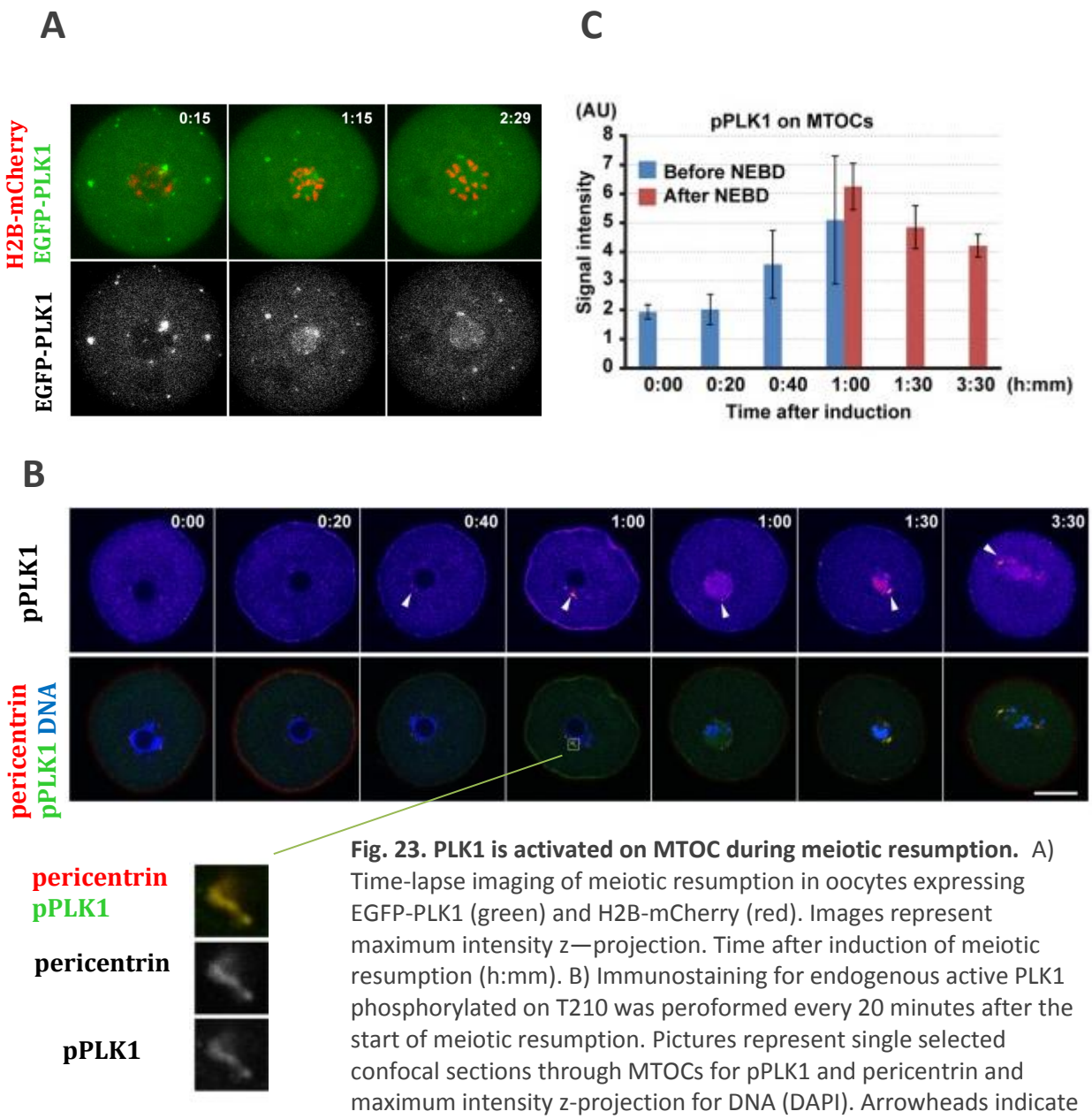

Fig. 23. PLK1 is activated on MTOC during meiotic resumption. A) Time-lapse imaging of meiotic resumption in oocytes expressing EGFP-PLK1 (green) and H2B-mCherry (red). Images represent maximum intensity z—projection. Time after induction of meiotic resumption (h:mm). B) Immunostaining for endogenous active PLK1 phosphorylated on T210 was peroformed every 20 minutes after the start of meiotic resumption. Pictures represent single selected confocal sections through MTOCs for pPLK1 and pericentrin and maximum intensity z-projection for DNA (DAPI). Arrowheads indicate pPLK1 signals on MTOCs. Time after induction of meiotic resumption (h:mm). Insets show magnified images of MTOC and pPLK1 C) Quantification of MTOC-associated pPLK1 signals, n (oocytes) = 11, 5, 7, 5, 5, 9, 17.

As PLK1 is involved in an autoamplification loop and activates CDK1(Lobjois et al., 2009), the effects on NEBD timing and chromosome condensation could reflect impaired CDK1 activity. We therefore partially inhibited CDK1 by 1µM flavopiridol to address this possibility (Fig. 24 B). In contrast to PLK1 inhibition, flavopiridol inhibited chromosome

condensation much more, than NEBD. Further we microinjected *lamin B1-Egfp* cRNA into oocytes and followed nuclear membrane breakdown by live-cell imaging. Lamin disassembly, a process that accompanies NEBD and is controlled by CDK1 activity, was significantly delayed after flavopiridol treatment as expected. However the length of lamin disassembly process was not affected in oocytes treated with BI2536, suggesting that downregulation of CDK1 activity in oocytes after PLK1 inhibition is not the mechanism responsible for NEBD delay (Fig. 24 C). Collectively, our data demonstrate that PLK1 is involved in NEBD and chromosome condensation and probably controls these processes not only through PLK1-dependent CDK1 activation pathway.

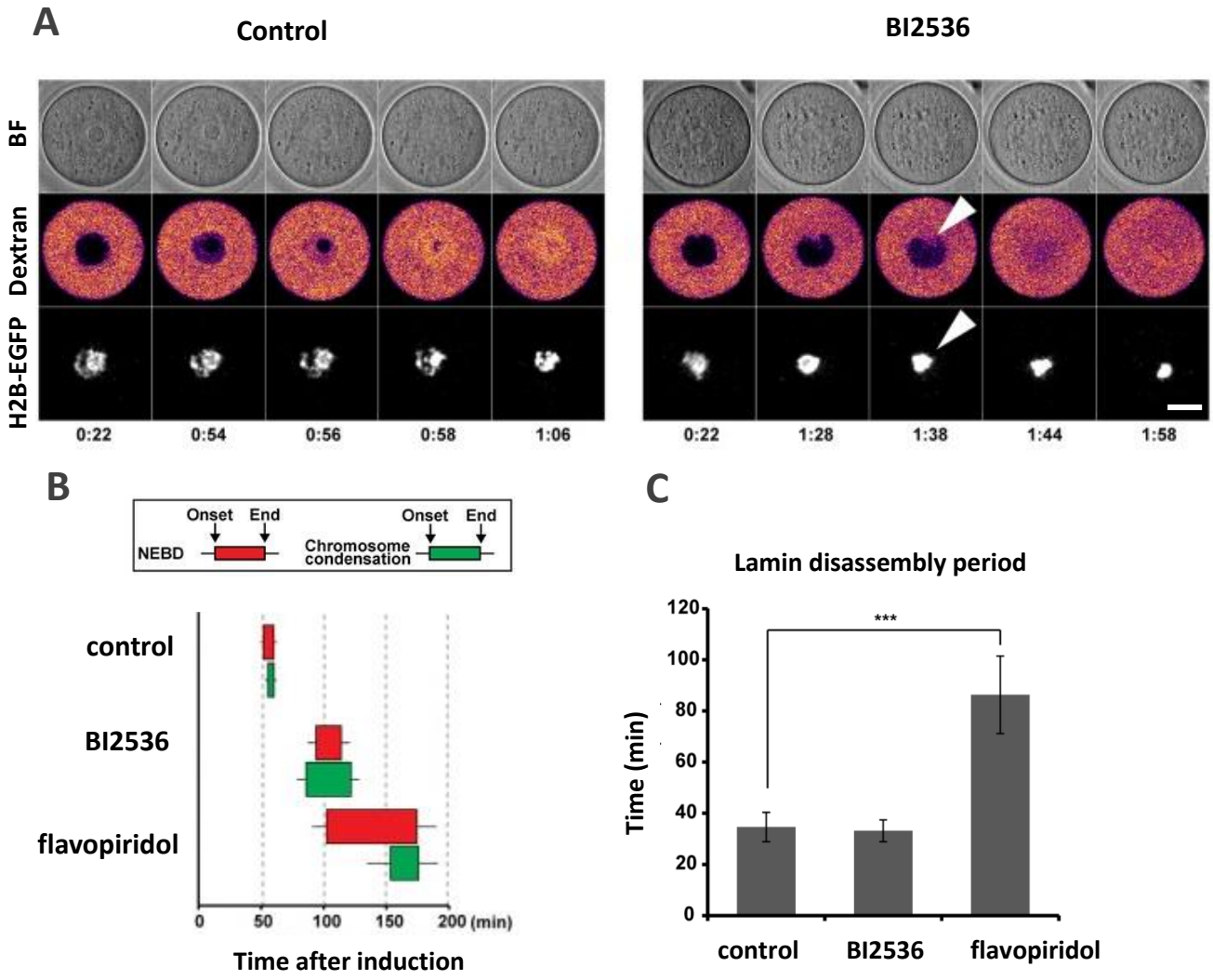

Fig. 24. PLK1 promotes NEBD during meiotic resumption. Time-lapse imaging of H2B-EGFP expressing oocytes microinjected with 70kDa-dextran-TAMRA in control, 100 nM BI2536 and 1 µM flavopiridol medium. Pictures represent single section from bright field (BF), single confocal section of 70kDa-dextran-TAMRA signals and maximum intensity z-projection for H2B-EGFP. Arrowheads indicate condensed chromosomes in the intact nucleus, observed in BI2536-treated oocytes. Time after induction of meiotic resumption (h:mm). Scale bar = 20 µm. B)The timing and length of NEBD and chromosome condensation periods – onsets and ends (minutes) in control, BI2536 and flavopiridol treated oocytes. The precise timing was identified by measuring dextran-TAMRA nuclear entry and chromosome volume. The left and right sides of the box indicate the mean timings of the onset and end of the process, respectively, with the 95% confidence intervals (n = 16, 17, 15). C) The length of laminB1-EGFP disassembly period. Means with 95% confidence intervals are presented (n = 16, 21, 12; ***$p < 0.0001$).

4.2 PLK1 and AURKA in M-phase

4.2.1 AURKA influences spindle length and regulates MTOC-associated γ-tubulin.

Previously it was published, that overexpression of AURKA *in vitro* leads to defects in Metaphase I spindle formation: the spindles were formed as multipolar or their length was increased (Saskova et al., 2008). Such oocytes did not enter anaphase I and were arrested in Metaphase I. We did not observe MI arrest in oocytes overexpressing WT- or KD-AURKA and maturing *in vivo*. Moreover, upon fertilization of these oocytes the embryonic development was not altered (data not shown). We therefore asked whether AURKA overexpression has any effect on spindle formation *in vivo*. We found that the spindles from WT- AURKA expressing oocytes were normally bipolar, however elongated (Fig.25 A).

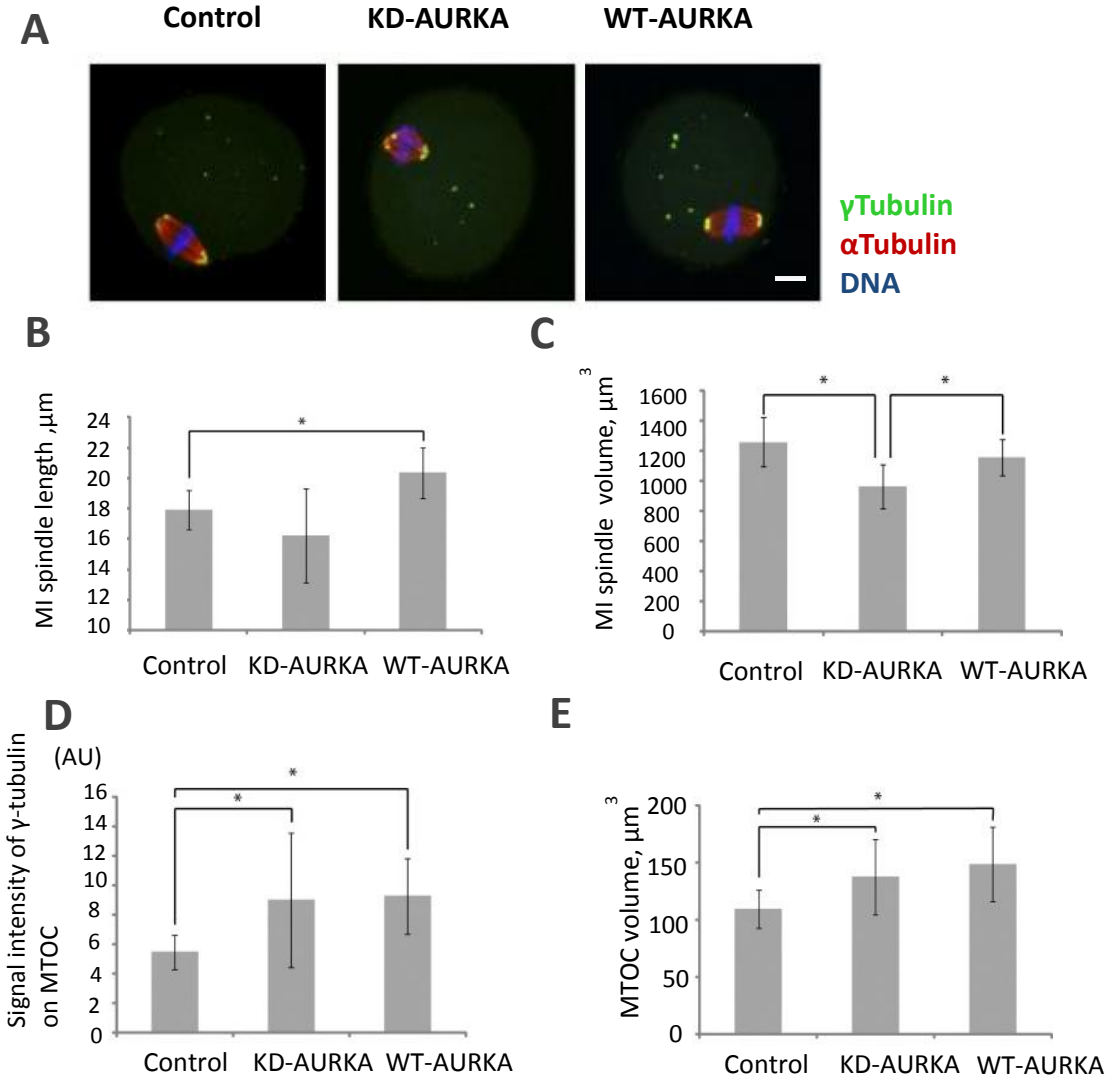

Fig. 25. AURKA regulates MI spindle length and MTOC formation. A) Immunostaining of control, WT-AURKA and KD-AURKA oocytes at MI stage for γ- and α-tubulin and DNA. Scale bar 10µm. DNA staining (blue) and γ-tubulin staining (green) are shown as maximum intensity z-projection, γ-tubulin staining is shown as a maximum intensity z-projection of confocal sections only throughout the spindle. B, C) Quantification of the effect of AURKA on spindle length and volume (n= 19, 11, 13 for controls, WT-AURKA and KD-AURKA respectively). D, E) Quantification of total γ-tubulin associated with MTOC and total MTOC volume. n= 10, 7, 10 for controls, WT-AURKA and KD-AURKA respectively.

The elongation was dependent on protein kinase activity, because spindle length was not affected in KD-AURKA expressing oocytes (Fig. 25, B). Elongated spindles from WT-AURKA oocytes had the same volume compared to control (Fig. 25 C), but spindles from KD-AURKA oocytes had a decreased spindle volume and were smaller in size, suggesting that KD-AURKA exhibited a dominant negative effect. In both cases the number of MTOC on spindle poles and in cytoplasm was similar to control oocytes, but the total volume of MTOC and the amount of γ-tubulin associated with MTOC was higher in oocytes overexpressing KD- or WT- AURKA (Fig. 25 D, E), suggesting that AURKA regulates the turnover of γ-tubulin independently of its protein kinase activity. Collectively, our data demonstrate an involvement of AURKA both in spindle formation, where AURKA regulates the length of MI spindle, and in regulation of γ-tubulin associated with MTOC.

4.2.2 PLK1 promotes the recruitment of γ-tubulin and pericentrin to MTOC, regulates bipolar spindle formation and kinetochore-microtubule attachments, and is required for APC/C activation

After meiotic resumption active pPLK1 (T210) was highly concentrated on MTOC and kinetochores, and this localization was confirmed by monitoring of localization of microinjected EGFP-PLK1 into oocytes (Fig. 26). At anaphase, EGFP-PLK1 disappeared from the spindle poles and kinetochores and relocated to the spindle midzone (Fig. 26 A).

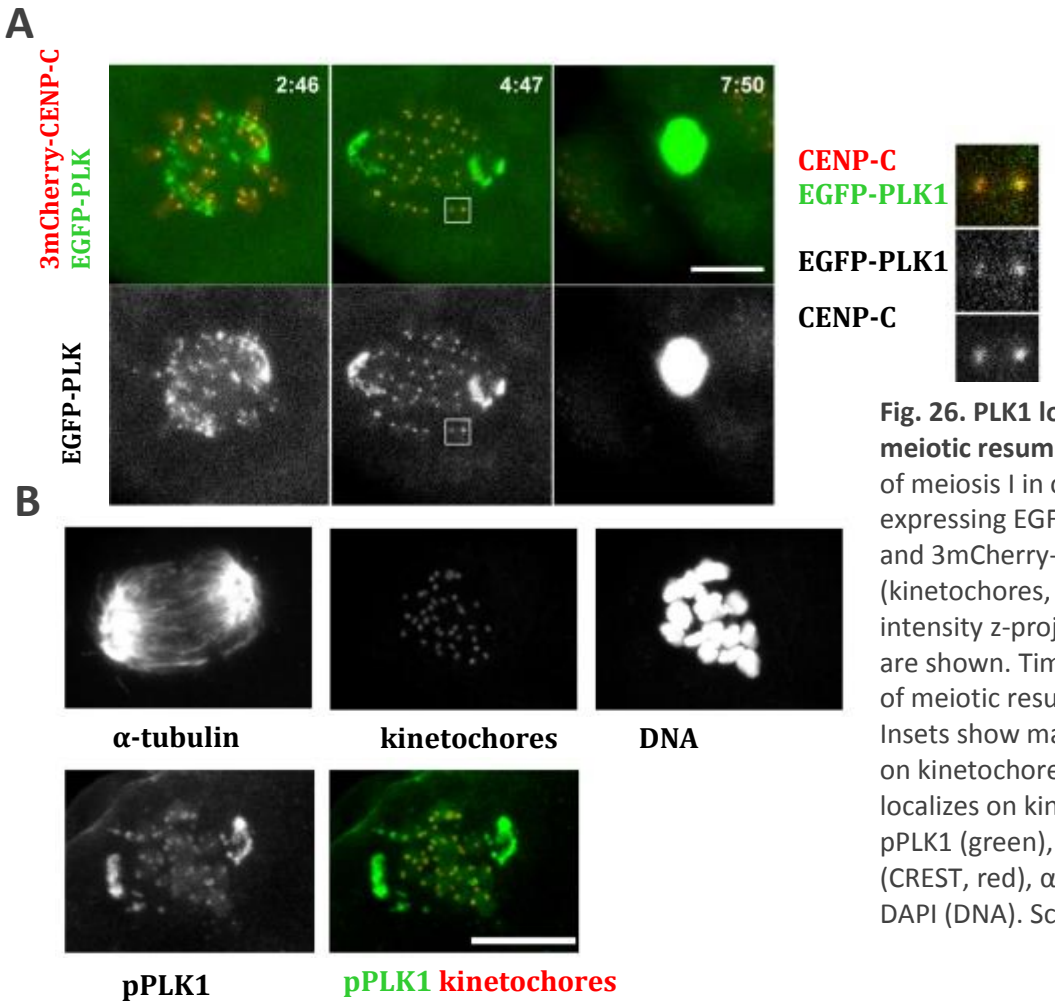

Fig. 26. PLK1 localization after meiotic resumption. A) Imaging of meiosis I in oocytes expressing EGFP-PLK1 (green) and 3mCherry-CENP-C (kinetochores, red). Maximum intensity z-projection images are shown. Time after induction of meiotic resumption (h:mm). Insets show magnified images on kinetochores.B) pPLK1 localizes on kinetochores at MI. pPLK1 (green), kinetochores (CREST, red), α-tubulin, and DAPI (DNA). Scale bars = 10 µm.

After the treatment of oocytes with BI2536 we found, that metaphase I spindle poles contained lower amount of γ-tubulin and pericentrin (Fig.27 A, B). Besides that, BI2536 treated oocytes lacked cytoplasmic MTOC not associated with spindle poles, which were observed in control oocytes (Fig.27 A).

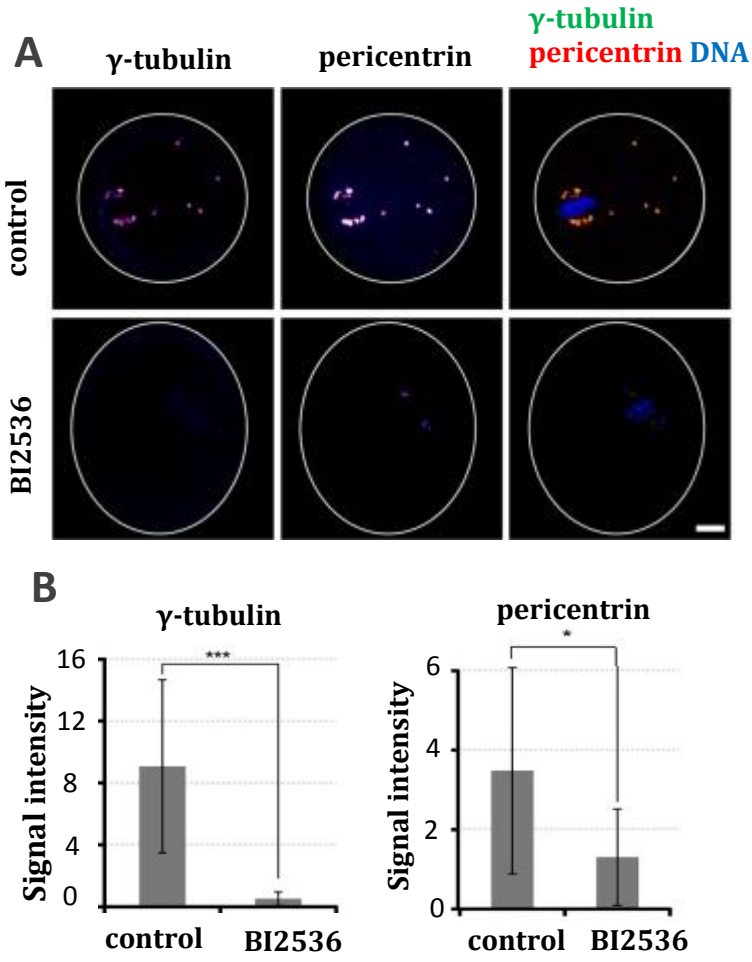

Fig. 27. PLK1 is required for correct MTOC function A) Immunostaining of metaphase I oocytes cultured in BI2536 and control oocyte- γ-tubulin (green), pericentrin (red), DAPI (blue) Maximum z-projections of entire confocal stacks are shown. Scale bar 10 µm. B) Quantifications of the spindle pole-associated integrated signals of γ-tubulin and pericentrin. Averages with the 95% confidence intervals are shown (n = 6, 7, 4, 4. *p<0.05,***p<0.002).

The compromised MTOC may lead to metaphase I spindle formation defects. To explore the consequence of PLK1 inhibition on spindle assembly, we microinjected microtubule marker EGFP-MAP4 into oocytes and monitored meiotic progression by live-cell imaging (Fig.28 A). Control oocytes formed a transient microtubule ball structure in prometaphase, which elongated into a bipolar spindle 2.4±0.4 hours after NEBD, and upon KT-MT attachment the anaphase oocured. In contrast, inhibition of PLK1 with BI2536 led to a delay in spindle elongation, when the apolar microtubule ball persisted for 3.7±0.8 hours (Fig. 28, B). We compared the volume of the spindles between control and BI2536 treated oocytes and discovered a significant reduction in the size of the spindle when PLK1 was inhibited (Fig. 28, C). Thus, inhibition of PLK1 causes impaired MTOC function due to decreased amounts of γ-tubulin and pericentrin and altered metaphase I spindle formation. Although bipolar spindle formed, the chromosomes could not align properly at the metaphase I (Fig. 28 A).

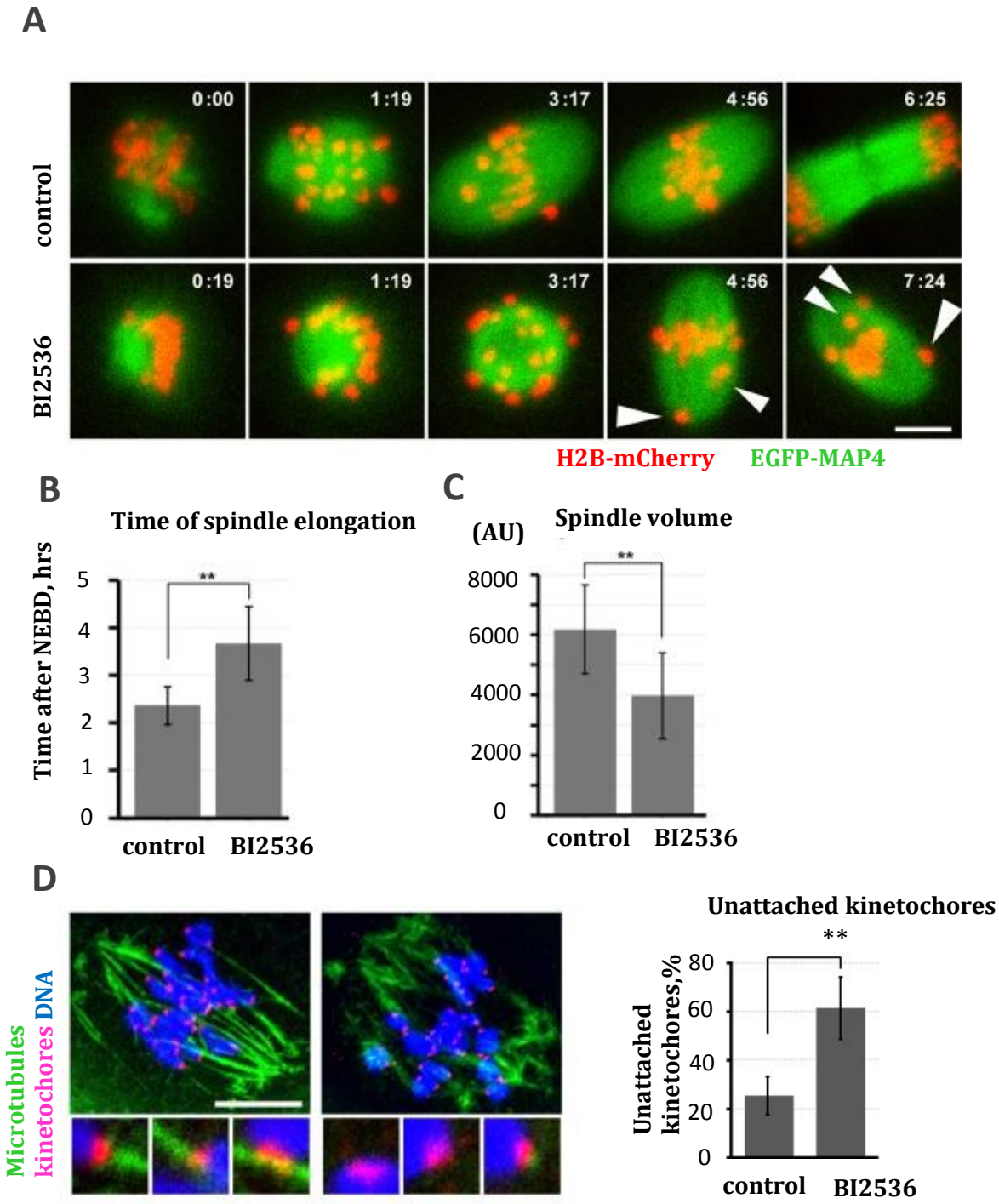

Fig. 28. PLK1 is required for chromosome alignment A) Time lapse imaging of oocytes expressing EGFP-MAP4 (microtubules, green) and H2B-mCherry (chromosomes, red) in cultured in control medium or BI2536. B) The EGFP-MAP4 signals were reconstructed in 3D and the time of spindle elongation was determined. Averages and s.d. are shown (n = 8, 17. **p < 0.01). C) The volume of the spindle at 6 hours after NEBD was measured after 3D reconstruction of EGFP-MAP4 signals. Average and s.d (n = 8, 17. **p < 0.01). D) Oocytes 4 hours after NEBD were briefly treated with a cold buffer and fixed for immunostaining of microtubules (blue) and kinetochores (red). 100 nM BI2536 was added at 2 hours after NEBD. DNA was stained with Hoechst33342 (blue). Insets show magnified images of kinetochore-microtubule attachments. Scale bar 10 µm. Average and s.d. of the population of unattached kinetochores are shown (n = 5, 5. **p < 0.01).

In mitosis PLK1 is required for stable kinetochore-microtubule attachments, and due to visible chromosome misalignment in oocytes we proposed similar function for PLK1. We checked the stability of KT-MT attachments by cold treatment. Incubation of oocytes with BI2536 significantly increased unattached kinetochors, indicating that PLK1 is required for stable KT-MT attachments (Fig. 28 D).

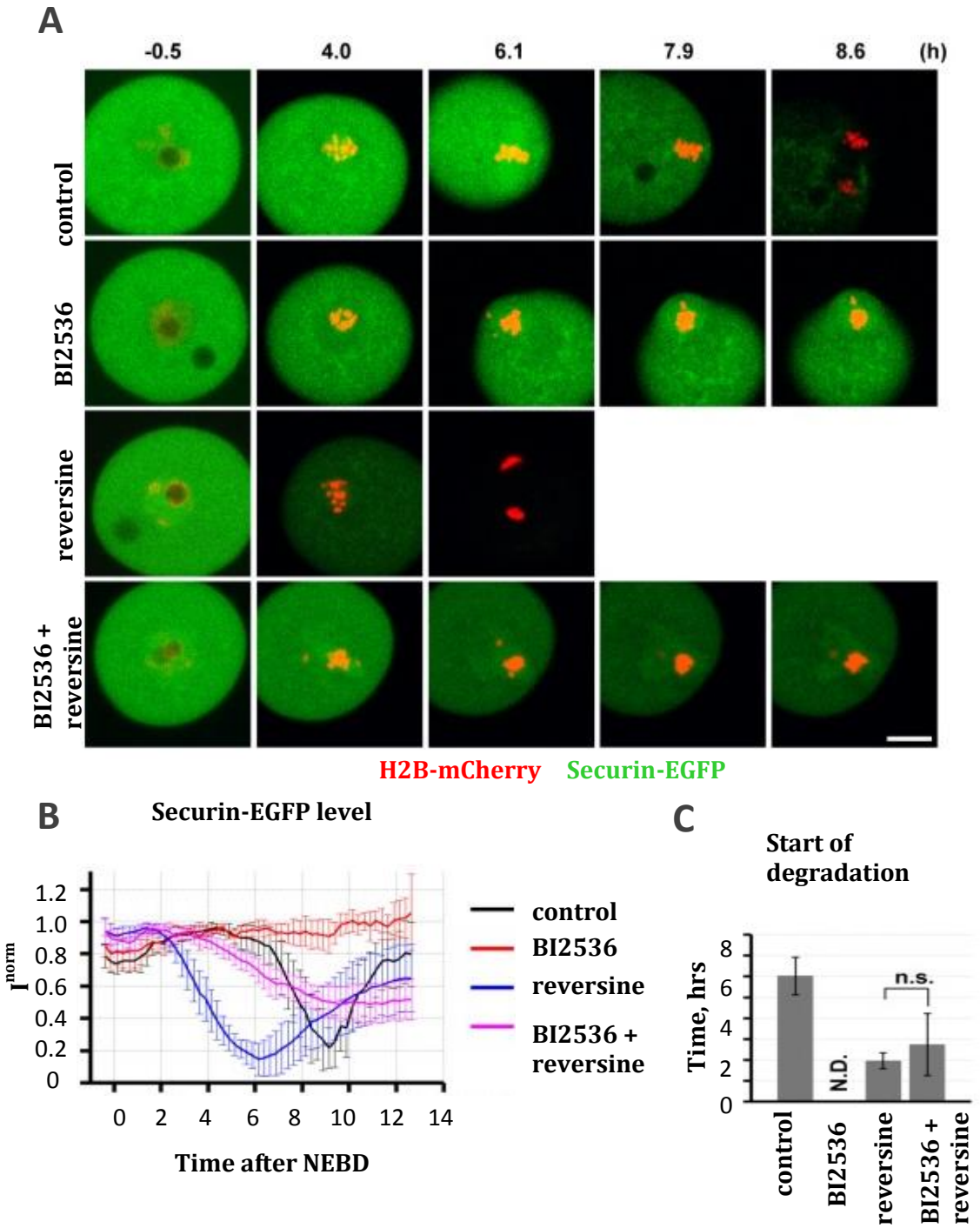

Fig. 29. PLK1 is required for APC/C activation. A)Imaging of oocytes expressing securin-EGFP (green) and H2B-mCherry (chromosomes, red) in the presence of 100 nM BI2536 and/or 1 µM reversine. Maximum intensity z-projection images are shown. Time after NEBD (h). Scale bar 10 µm. B) Normalized intensities of cytoplasmic securin-EGFP signals (Inorm) were plotted. Average and s.d. are shown (n = 6, 4, 12, 15). C) The start of securin degradation was measured from (B) (n = 6, 12, 15. **p < 0.01).

Somatic cells do not to enter anaphase I with misaligned chromosomes due to persistent SAC activity and failure to activate APC/C (Lénárt et al., 2007; Sumara et al., 2004; van Vugt et al., 2004a). As the oocytes are also arrested in MI, we monitored APC/C activity during maturation using the established marker securin-EGFP (Fig. 29 A, B)(Herbert et al., 2003). APC/C became activated around 6 hours after NEBD when securin-EGFP degradation started (Fig.29 C). The levels of securin-EGFP reached minimum approximately 9 hours after NEBD, which marked the anaphase I onset. In contrast, securin-EGFP levels were stable for 12 hours after NEBD when PLK1 was inhibited, and APC/C was not activated. Next we inhibited the component of SAC MPS1 with reversine to estimate whether persistent SAC activity was responsible for metaphase I arrest and failure to activate APC/C. The treatment of control oocytes with reversine induced premature securin-EGFP destruction often accompanied by defective chromosome segregation (data not shown). In case of PLK1 inhibition with BI2536, reversine abolished SAC function and APC/C mediated securin-EGFP degradation. The onset of APC/C activation was comparable in reversine treated oocytes independently of PLK1 inhibition suggesting that SAC function was fully abolished. However, the kinetics of securin-EGFP degradation was significantly slowed when PLK1 was inhibited in the presence of reversine and the level of degradation did not reach the threshold needed for anaphase I onset (approximately 20% and 50% in control oocytes and BI2536 treated oocytes, respectively). While PLK1 is dispensable for anaphase I onset during mitosis, our data and earlier reports demonstrate that PLK1 is essential for this process (Lénárt et al., 2007; Sumara et al., 2004; van Vugt et al., 2004a). Importantly, we discovered another difference from somatic cells: in mouse oocytes PLK1 activity plays a role in full APC/C activation and anaphase onset and operates through a mechanism which is independent of PLK1 role in SAC satisfaction.

We asked whether PLK1 is required for the degradation of APC/C inhibitor EMI1(Marangos et al., 2007). Live-cell imaging of oocytes microinjected with EGFP-EMI1 revealed that in BI2536 the degradation of EMI1 was severely compromised (Fig. 30). As a control we used EGFP-EMI1-2A with substituted PLK1 phosphorylation sites S124A and S128A, which failed to be degraded after NEBD. Altogether, our data suggest that PLK1 mediated phosphorylation of EMI1 is required for APC/C activation in oocytes.

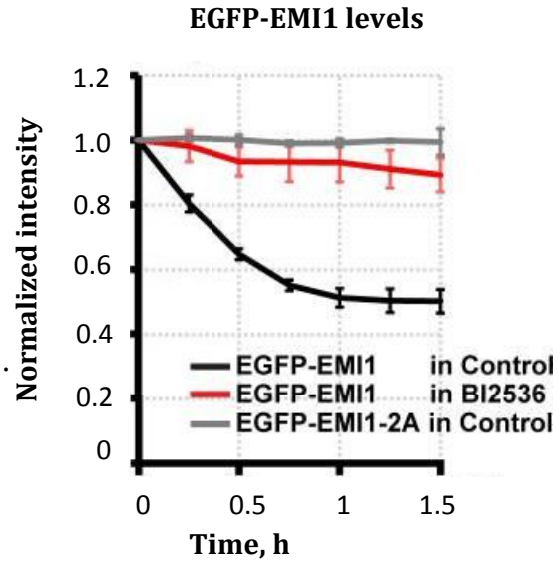

Fig. 30. PLK1 is required for EMI1 destruction. The oocytes were microinjected with EGFP-EMI1 or EGFP-EMI1–2A and H2B-mCherry and their maturation in control medium or in 100 nM BI2536 was analysed by live-cell imaging. Cytoplasmic EGFP-EMI1 signals were measured and normalized. Average and s.d. are shown (n = 7, 5, 3). Time after NEBD (h).

4.3 DNA damage response in oocytes

4.3.1 DNA damage response in oocytes arrested in prophase I

To study DNA damage response in fully grown oocytes we immunostained the oocytes for the presence of γH2AX foci, which is an established sensitive marker of DSBs (Sharma et al., 2012; Valdiglesias et al., 2013). We discovered that normal oocytes isolated at prophase I stage possessed few number of DSBs (Fig.31A).

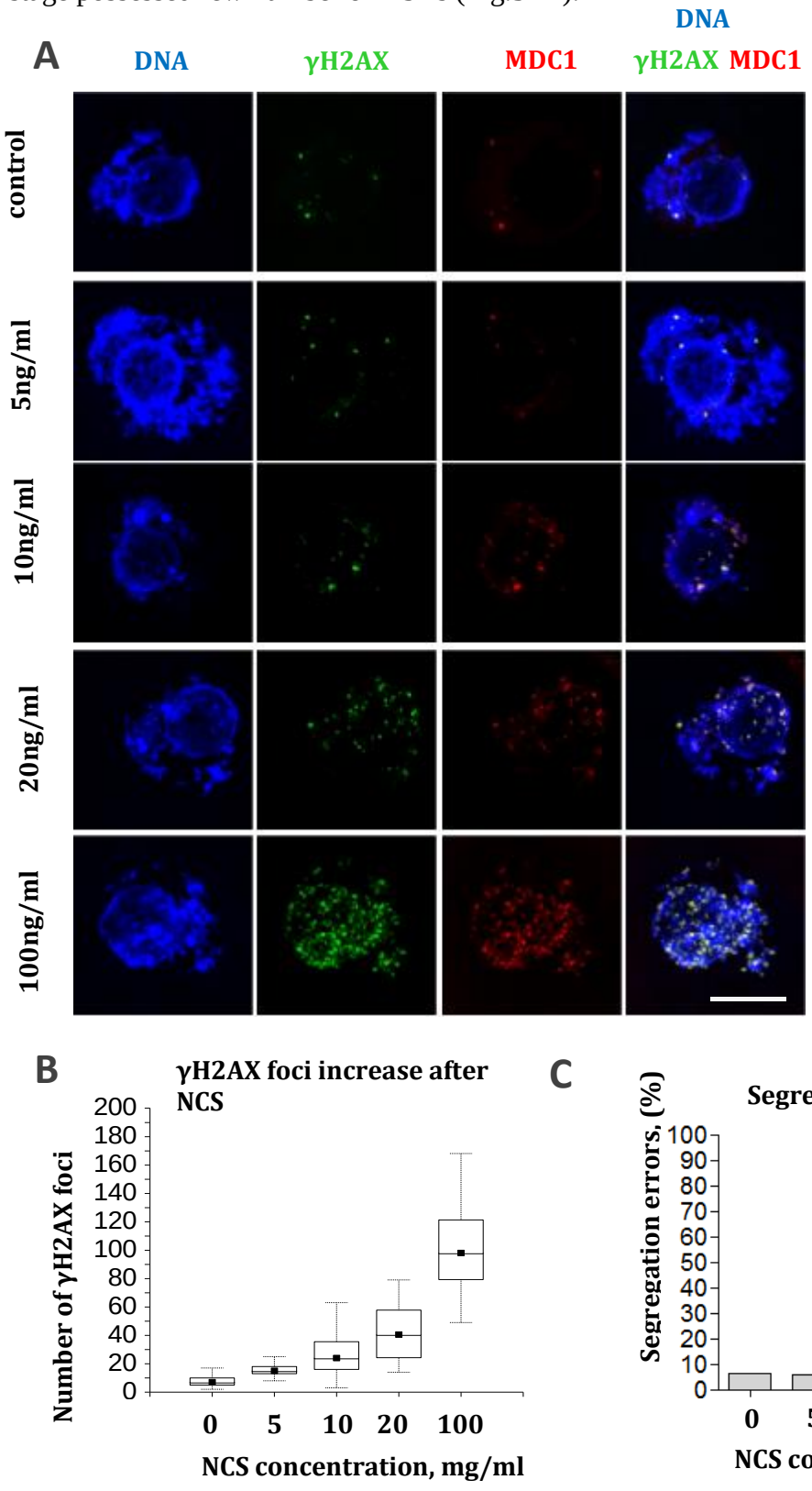

Fig. 31. NCS induces DSBs in oocytes

A) Immunofluorescence of control and NCS treated GV-stage oocytes labeled with pS139 H2AX (γH2AX) and MDC1 antibodies. Maximum z-projection of confocal section across nucleus is shown. Scale bar 10µm
B) Number of γH2AX foci in control and NCS treated GV-stage oocytes (n=137, 22, 118, 29, 21).
C) Percentage of segregation errors in anaphase I (n=98, 17, 20, 56, 47, 113).

To estimate the ability of oocytes to repair DSBs during prophase I arrest we induced exogenous DNA damage with radiomimetic drug Neocarzinosatin, which was proved to be efficient in oocytes (Yuen et al., 2012). We exposed oocytes in GV-stage to increasing concentrations of NCS (5-100ng/ml) for 1 hour and then analyzed γH2AX foci. We identified NCS concentration dependent increase in DSBs, as documented by γH2AX foci (Fig. 31A, B). The specificity of foci was confirmed by colocalization of another DSBs marker, MDC1. Moreover, after Milrinone (inhibitor of PDE3A preventing oocyte maturation) and NCS washout we monitored the maturation of NCS pretreated oocytes by live-cell imaging. We revealed the dose-dependent increase of chromosome segregation problems in anaphase I reflecting the effect of NCS (Fig.31 C). Altogether, these data indicate that we are able to precisely detect endogenous and exogenously induced DSBs in GV-stage arrested oocytes. Even in low concentration of NCS (10ng/ml) there was about 2.5 times increase in γH2AX foci number accompanied by the increase in segregation problems during maturation (Fig. 31 B, C). Therefore, low NCS concentration should allow studying physiologically relevant response to DSBs and may enable DNA repair.

We induced DSBs in GV oocytes by transient 1 hour treatment with low concentration of NCS and monitored the number of γH2AX foci over a period of 18 hours, while the oocytes were maintained arrested in prophase I by Milrinone (Fig.32). Interestingly, there was a transient increase in γH2AX at 6h after NCS treatment however we observed a decrease in γH2AX after 18h (NCS 18h group) (Fig. 32 B). In contrast, in control oocytes there is a slight but significant increase in γH2AX foci number at 6h and 18h probably due to *in vitro* culture conditions and manipulation (Fig. 32 A). Remarkably, while at 0h we observed a significant difference between control and NCS-treated oocytes, at 18h the DNA damage level was comparable in both groups (Fig.32 C).

We washed out NCS and used live-cell imaging to monitor the maturation of oocytes in NCS 18h group and NCS0h (Fig. 32 D). The oocytes maturation therefore occurred in normal medium in order not to induce additional DNA damage during MI phase. We did not observe any decrease in segregation problems in these groups despite a significant decreased in γH2AX foci number at 18h. Moreover, segregation errors in NCS18h group were higher than in control 18h although the number of γH2AX foci was comparable.

Collectively, our data indicate that fully grown prophase I arrested oocytes have the ability to initiate DSBs signaling pathway, however the efficiency of repair is questionable.

4.3.2 DSBs generate chromosome fragments in anaphase I but do not delay APC/C activation and anaphase onset

As mentioned above, we observed chromosome segregations problems which appeared in anaphase I after transient treatment of GV stage oocytes with low concentration of NCS.

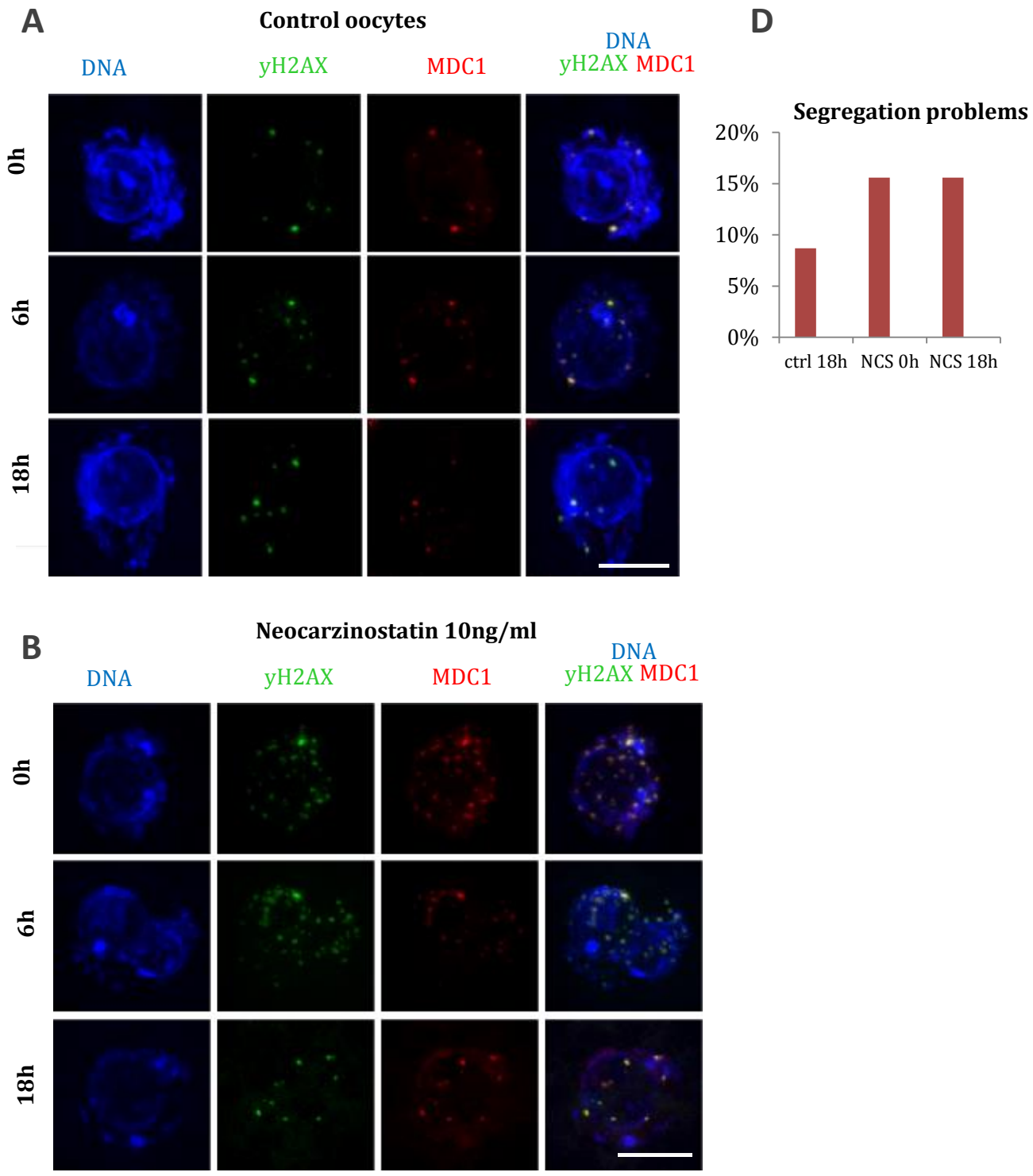

Fig. 32. The response of GV stage arrested oocytes on DSBs. A) Immunofluorescence of control GV-stage oocytes labeled with pS139 H2AX (γH2AX) and MDC1 antibodies. The oocytes were examined at 0h, 6h and 18h. Maximum z-projection of confocal section across nucleus is shown. Scale bar 10µm.B) The oocytes were transiently treated with NCS (10ng/ml) for 1h. After NCS washout, the oocytes were examined as described in (A). C) Quantification of γH2AX foci (n=152, 18, 24, 118, 9, 11). D) Segregation problems (percentage) detected from live-cell imaging of oocytes from the groups control 18h, NCS 0h and NCS 18h.

Live imaging of NCS pretreated oocytes revealed lagging chromosomes, and free diffusion of several chromosomes in the cytoplasm of MII oocytes (Fig.33 A) To understand how these abnormal chromosomes are generated we monitored the dynamics of individual chromosomes throughout meiotic maturation expressing the chromosome marker H2B-mCherry together with kinetochore marker 2mEGFP-CENPC (Fig. 33 B).

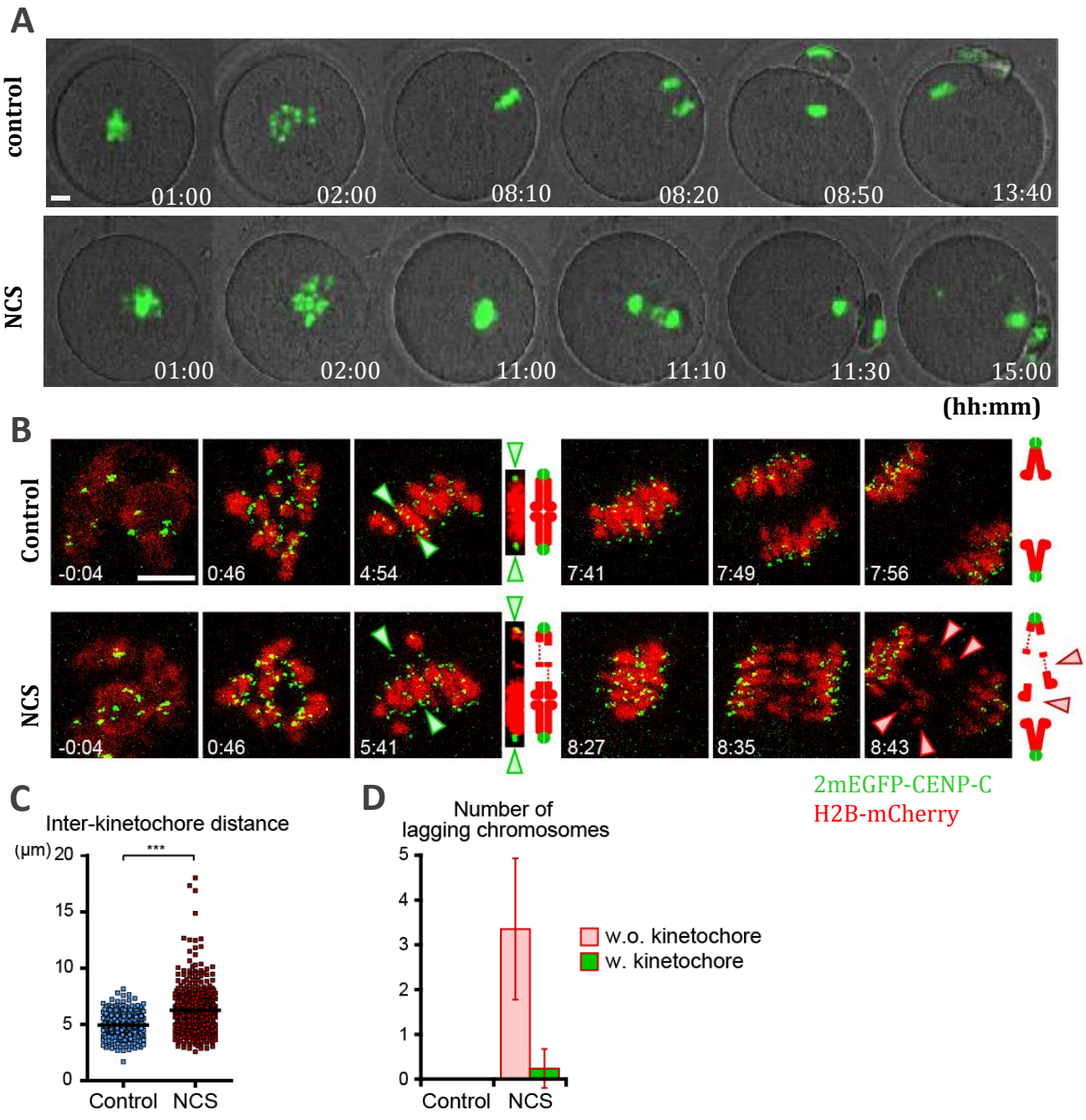

Fig. 33. Chromosomes are fragmented in NCS-treated oocytes. A) Imaging of chromosome dynamics and integrity in live oocytes expressing H2B –EGFP treated with NCS at100ng/ml. Time in hh:mm. Scale bar 10µm.B) High-resolution imaging of control and NCS-treated oocytes expressing H2B-mCHERRY and CENPC-EGFP. Arrowheads indicate the homologous kinetochores(green) of a bivalent and lagging chromosomes (red). Scale bar, 10µm. C) Chromosome hyperstretching in NCS-treated oocytes. The distance between homologous kinetochores was measured in 3D in oocytes 6 hours after NEBD (n=252, 409 bivalents).***p<0.0001. D) The number of lagging chromosomes at anaphase was counted (n=11, 17 oocytes). The lagging chromosomes were categorized.

No differences in chromosome congression and metaphase chromosome alignment between control and NCS-treated oocytes were detected however the chromosomes were abnormally stretched because the distance between homologous kinetochores was longer (Fig.33C). The physical connection between stretched chromosomes was maintained as judged by correct alignment on metaphase plate. In anaphase I NCS treated oocytes exhibited 1- 6 lagging chromosomes without kinetochore signal, indicating that they were chromosome fragments (Fig. 33 D). Taken together, higher number of DSBs leads to the loss of chromosome integrity and results in chromosome fragmentation in anaphase I.

Previously, it was shown that severe DSBs caused by bleomycin or zeocin treatment induced disruption of KT-MT attachments and indirectly activated SAC, reduced APC/C activation and delayed anaphase I onset(Lin et al., 2014; Ma et al., 2013). High doses of NCS (1µg/ml) inhibited 1st polar body emission(Yuen et al., 2012). To estimate the effect of DSBs on anaphase I onset we monitored degradation of securin-EGFP as a marker of APC/C activation (Herbert et al., 2003) in oocytes treated with high and low dose of NCS (10ng/ml or 100ng/ml) (Fig.34 A). In oocytes treated with low dose of NCS both the anaphase I onset and securin-EGFP degradation did not alter from the control group and were not affected by the presence of segregation problems in about 25% of oocytes (Fig.34 B, C). We observed delayed anaphase I onset and securin-EGFP degradation only in oocytes treated with high NCS concentration- in such experimental conditions all tested oocytes exhibited segregation problems.

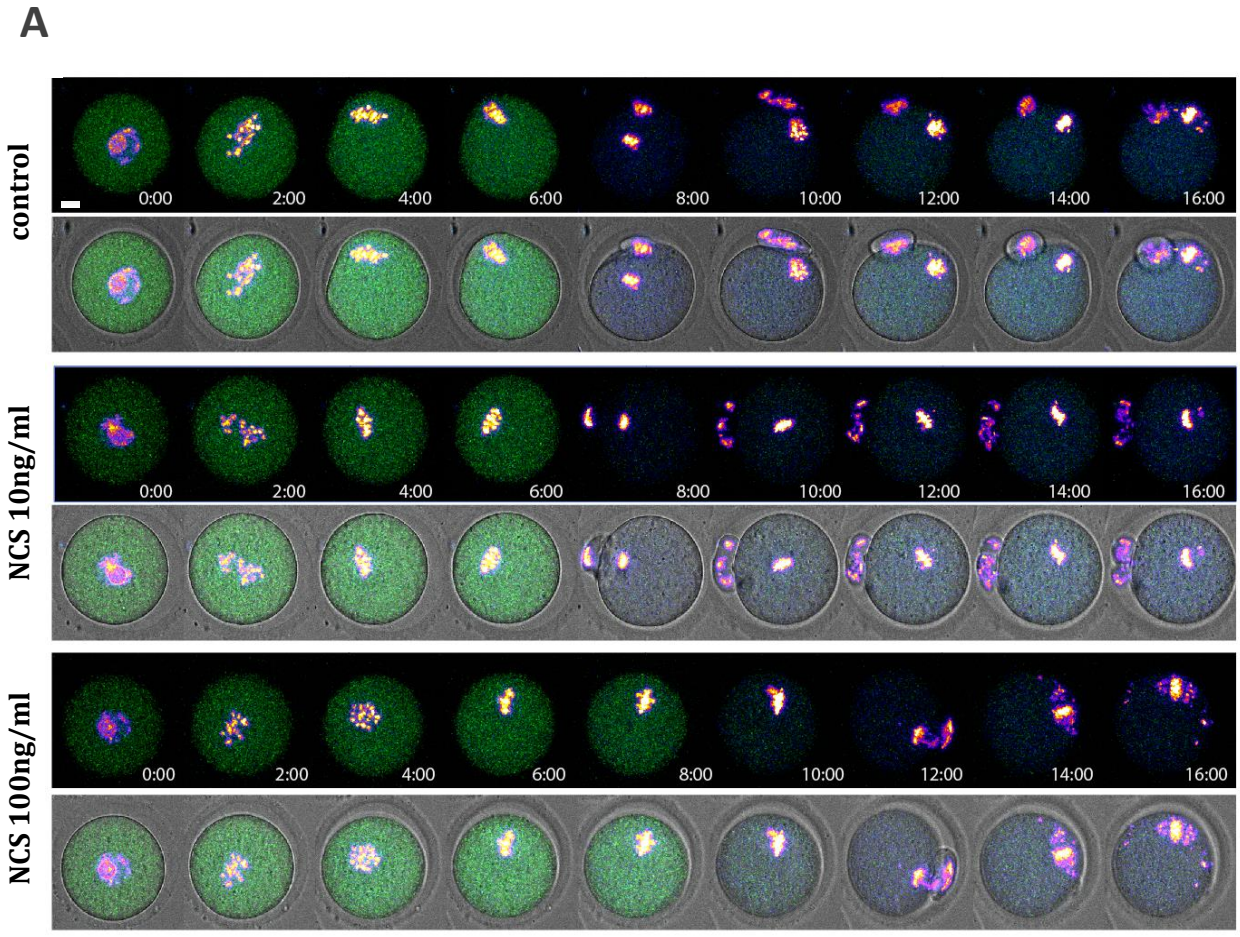

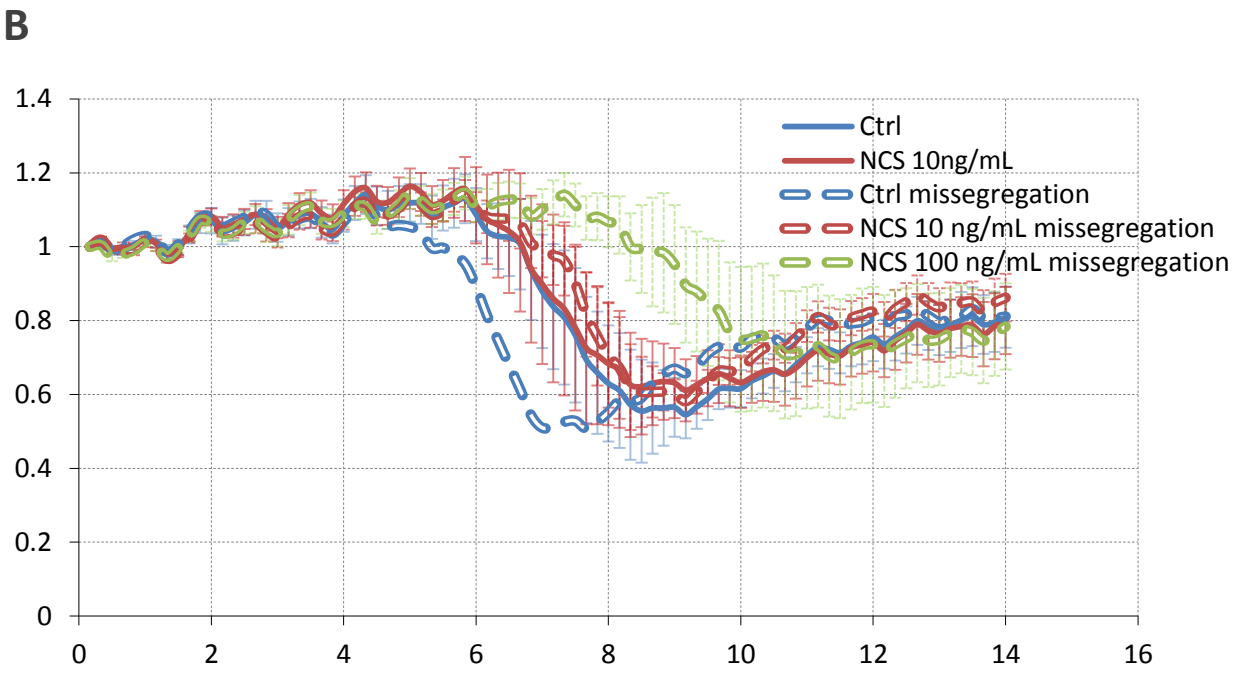

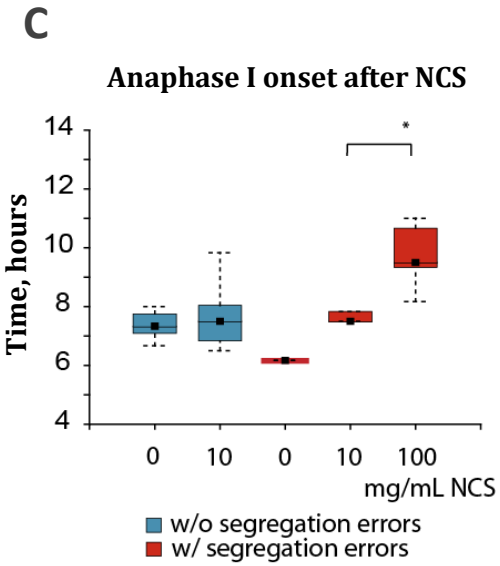

Fig. 34. APC/C activation and anaphase onset is not delayed in oocytes with low level of DNA damage. A) Time lapse imaging of oocytes expressing H2B-mCHERRY and securin-EGFP. Oocytes were treated with 10 or 100 ng/ml NCS in GV stage and then matured in normal medium. Single bright field section and maximum z-projection of EGFP and mCHERRY channels are shown. Time in hh:mm. Scale bar 10µm.B) Quantification of securin-EGFP level during meiotic maturation. Securin-EGFP level was normalized to 1 after NEBD. Means with SE are shown. Time is in hours. Note that only one control oocyte exhibited segregation errors. C) Anaphase onset in oocytes expressing H2B-mCHERRY and securin-EGFP. Untreated (control), NCS treated (10 and 100 ng/ml) groups are subdivided into the subgroups with and without segregation errors. For B) and C) n=10, 9, 1, 6, 10.

Therefore, our data indicate that low level of DSBs which is close to physiological level, does not interfere with APC/C activation or anaphase I onset, although causes segregtion problems.

4.3.3 γH2AX phosphorylation during oocyte maturation in response to DSBs

To estimated DDR response during maturation we analyzed H2AX phosphorylation on Ser139 in control oocytes and oocytes treated with low concentration of NCS. While at the GV stage in control oocytes γH2AX formed nuclear foci, we observed γH2AX spreading on whole chromosomes after meiotic resumption (Fig. 35 A, B). The chromosomal γH2AX reached maximum in Metaphase I and in Metaphase II γH2AX declined.

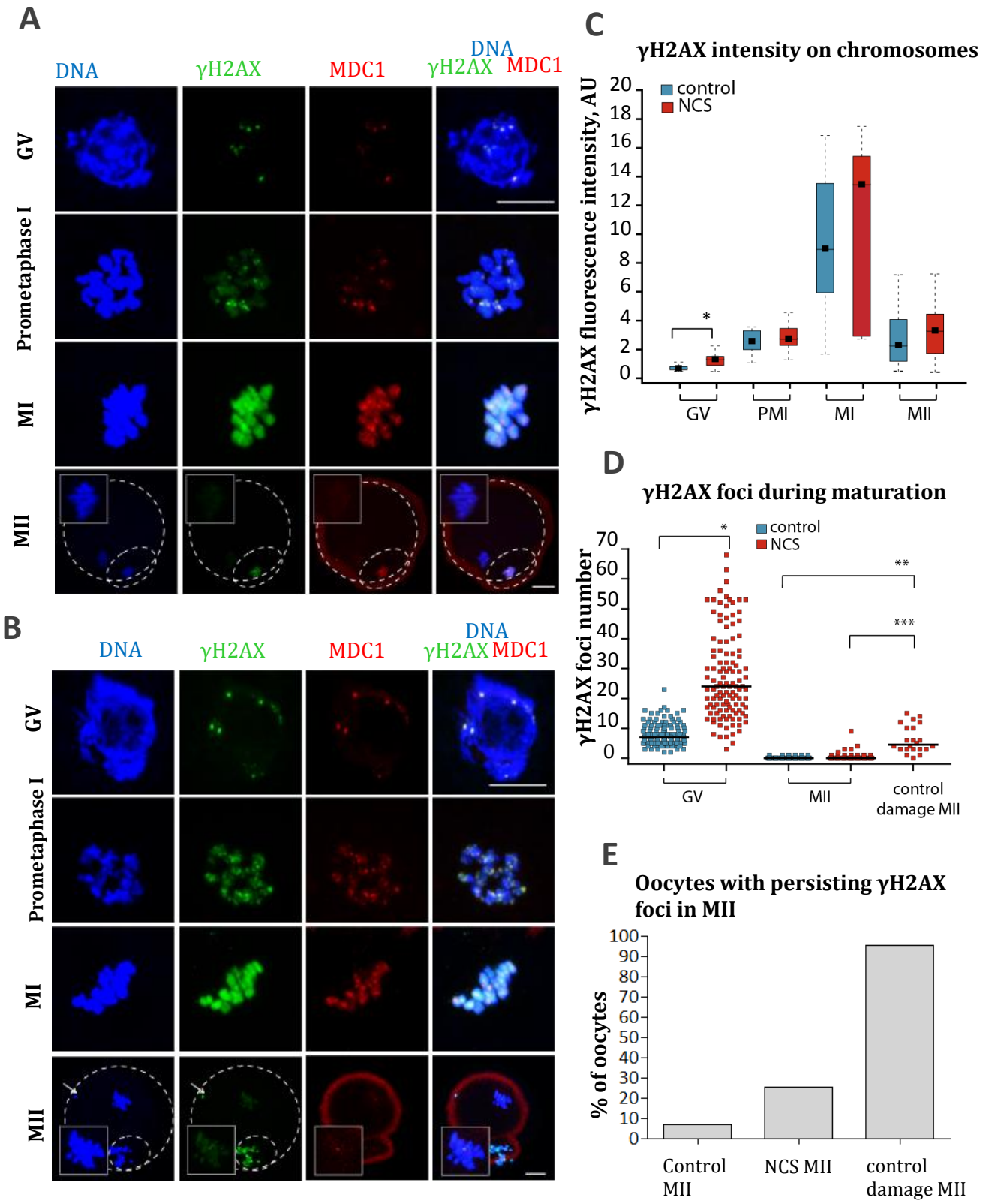

Fig. 35. H2AX phosphorylation changes dynamically during meiotic maturation. Immunofluorescence of control (A) and NCS (B) treated GV-stage, prometaphase I, MI and M II oocytes labeled with γH2AX and MDC1 antibodies. Maximum z-projection of confocal section across chromatin region is shown. In MII oocytes maximum z-projection for DNA and γH2AX but single confocal section for MDC1 is used. Insets show maximum z-projection of metaphase II plate area. C) Quantification of γH2AX during meiotic maturation in control and NCS treated oocytes (n = 26, 28, 26, 27, 43, 8, 28, 23). D) Quantification of γH2AX foci number in GV-stage and MII oocytes treated with NCS in GV stage before meiotic maturation. Acute NCS treatment of metaphase II oocytes (control damage MII) is also shown (n = 137, 118, 98, 84, 24). E) Percentage of oocytes with at least one γH2AX focus (n = 106, 55, 21).

As expected, NCS treatment increased not only the number of γH2AX foci, but also γH2AX intensity on whole chromosomes at the GV stage (Fig. 35C). After meiotic resumption the levels of chromosome associated γH2AX were comparable in control and NCS-treated oocytes. Significant decrease in γH2AX foci number during Metaphase I-Metaphase II transition allowed to analyze γH2AX foci formation. We registered a significant decrease in γH2AX foci number between GV and MII stage both in control and NCS-treated oocytes (Fig. 35 D). At MII stage γH2AX foci number was slightly increased in NCS treated oocytes compared to the control. Then we counted the number of oocytes with at least 1 γH2AX focus. By this analysis, about 30% of NCS-treated oocytes appeared positive for γH2AX compared to about 5% of control oocytes, while 95% of control oocytes did not exhibit any γH2AX focus. The number of oocytes enetring anaphase I with segregation problems after NCS treatment is consistent with the number of oocytes which exhibit at least 1 γH2AX focus in MII (Fig.31C).

To exclude the posibility that the decrease in γH2AX foci number in MII is a consequence of low ability to detect foci on highly condenced chromosomes, we acutely induced DSBs with NCS directly at MII stage oocytes (Fig. 36). Such treatment led to significantly higher amount of γH2AX foci compared to MII oocytes which recieved a dose of NCS at GV stage and then underwent maturation (Fig. 35 D). Besides, treatment with NCS at MII stage also increased the number of oocytes possessing at least 1 γH2AX focus up to 90% (Fig. 35 E). These data indicate that the observed decrease in γH2AX between GV and MII stages is not only due to lower accessibility of NCS to condensed structure of metaphase chromosomes.

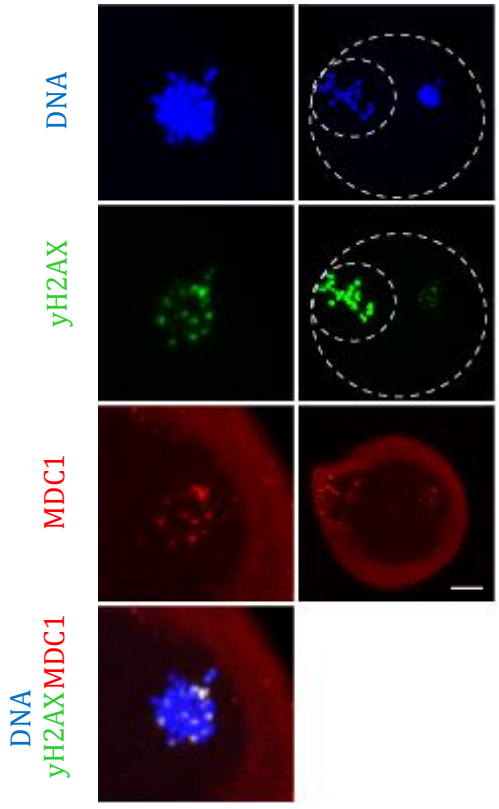

Fig. 36. Acute treatment of MII oocytes with NCS. Immunofluorescence of metaphase II oocytes treated acutely with NCS and labeled with γH2AX and MDC1 antibodies. Maximum z-projection of confocal sections is shown. Error bar, 10μm.

MDC1, another sensor of DSBs,colocalized with γH2AX throughout oocyte maturation. The colocalization was full until metaphase I, but we observed the loss of whole chromosomal MDC1 as well as the reduced association of MDC1 with γH2AX foci in MII (Fig. 35 A, B). In contrast, the induction of DSBs directly at MII stage arrested oocytes led to accumulation of both γH2AX and MDC1 (Fig. 36).

Altogether, we show that γH2AX is constitutively phosphorylated on whole chromosomes during maturation and the phosphorylation at MI is

not affected by DNA damage induction. The more precise measurement of DSBs through γH2AX foci calculation revealed the decrease in both endogenous and exogenously induced foci from GV to MII stage. This decrease may indicate DSBs repair or other DNA transaction associated with maintenance of DNA integrity during maturation such as DSBs tethering.

4.3.4 Kinases regulating DSBs response: MRE11 but not ATM is responsible for H2AX phosphorylation in meiosis I

ATM is the main kinase responsible for H2AX phosphorylation on Ser139 in somatic cells (Burma et al., 2001). ATM was reported to be expressed in GV stage arrested oocytes, but it is activated only in response to severe levels of DSBs (Marangos and Carroll, 2012). To estimate the role of ATM in phosphorylating H2AX during meiotic maturation we used pharmacological inhibitor of ATM KU55933 (Fig.37). As expected, inhibition of ATM had no effect on γH2AX/MDC1 foci number in the oocytes at GV stage (Fig 37A, D). γH2AX/MDC1 association with chromatin at metaphase I was not affected either (Fig. 37 B, E). No significant reduction of γH2AX foci induced by NCS in GV stage was found upon addition of KU55933. Moreover, inhibition of ATM during maturation did not increase segregation problems rate compared to control oocytes (Fig. 37 C).

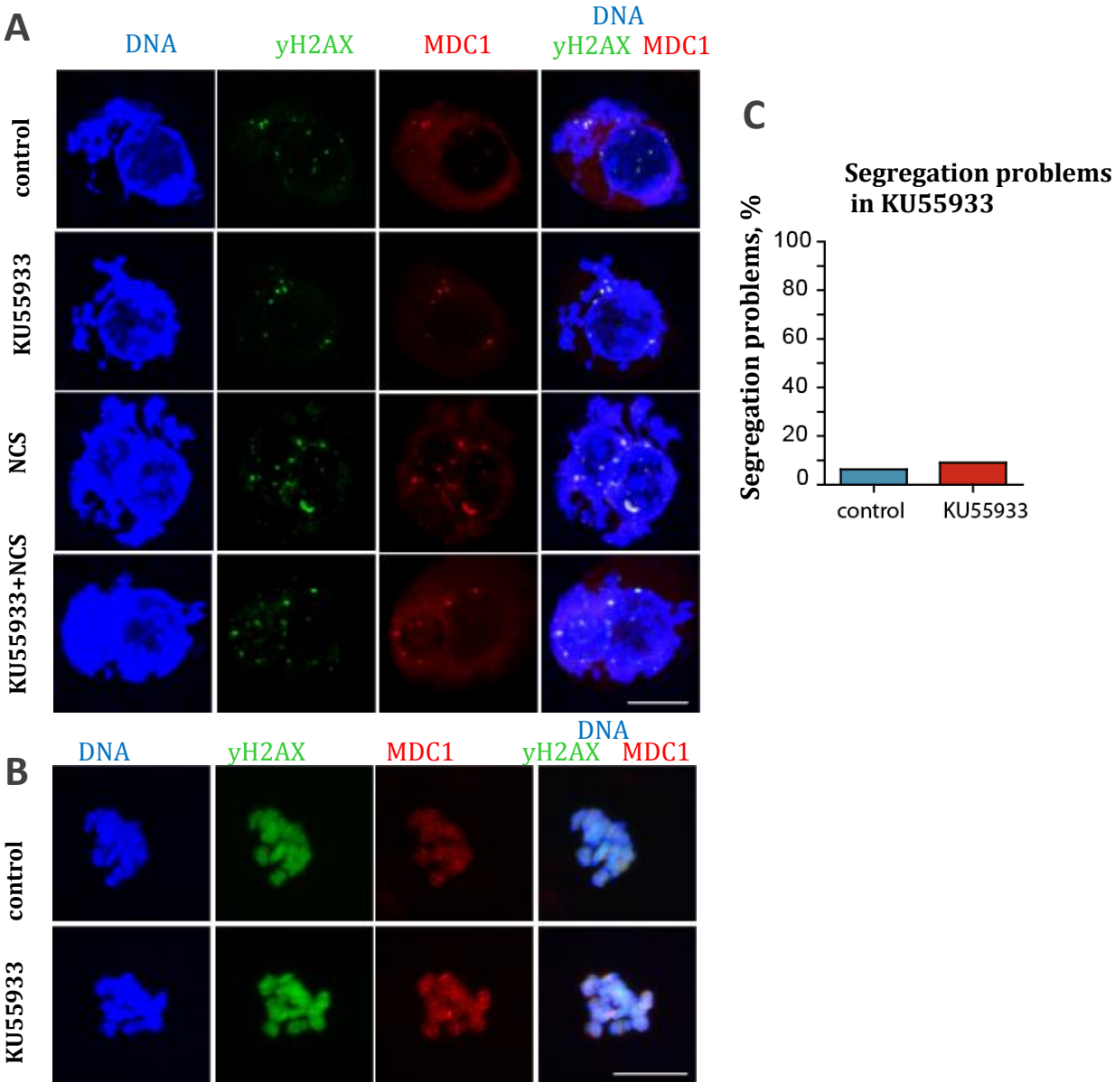

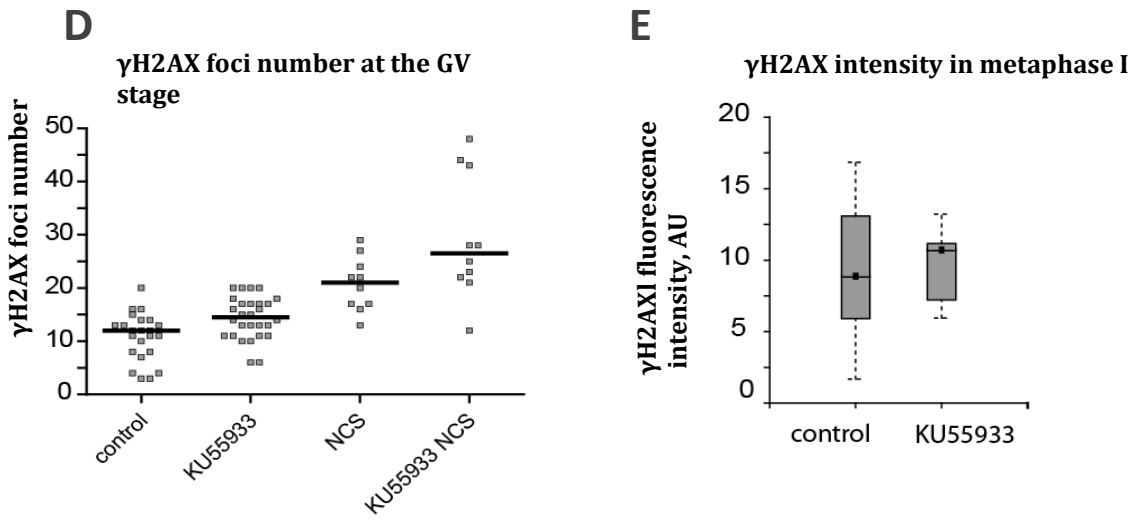

Fig. 37. ATM is not responsible for H2AX phosphorylation during meiotic maturation. A) Immunofluorescence of GV-stage oocytes labeled with γH2AX and MDC1 antibodies. Maximum z-projection of confocal section across chromatin region is shown. KU55933 treated oocytes were preincubated for 1h with 10 μM KU55933 Error bar 10μm. B) The oocytes preincubated for 1h with KU55933 from (A) were cultured for 7 h after Milrinone washout till Metaphase I in the presence of KU55933. C) Quantification of chromosome segregation errors of H2B-EGFP control and KU55933 treated oocytes analysed by live confocal imaging (n= 20, 11). D) Quantification of γH2AX foci number in GV-stage oocytes non-treated or treated with KU55933, NCS or both for 1 h (n= 23, 28, 10, 10). E) Quantification of γH2AX intensity in metaphase I in control oocytes and oocytes cultured for 7h in KU55933 (n = 10, 43).

In contrast, KU55933 efficiently inhibited H2AX phosphorylation in NIH3T3 fibroblasts treated with NCS (Fig. 38). Collectively, our data indicate that ATM does not play a major role in regulation of H2AX phosphorylation during normal oocyte maturation or in the presence of low levels of DSBs. Besides, ATM is not required for meiotic maturation.

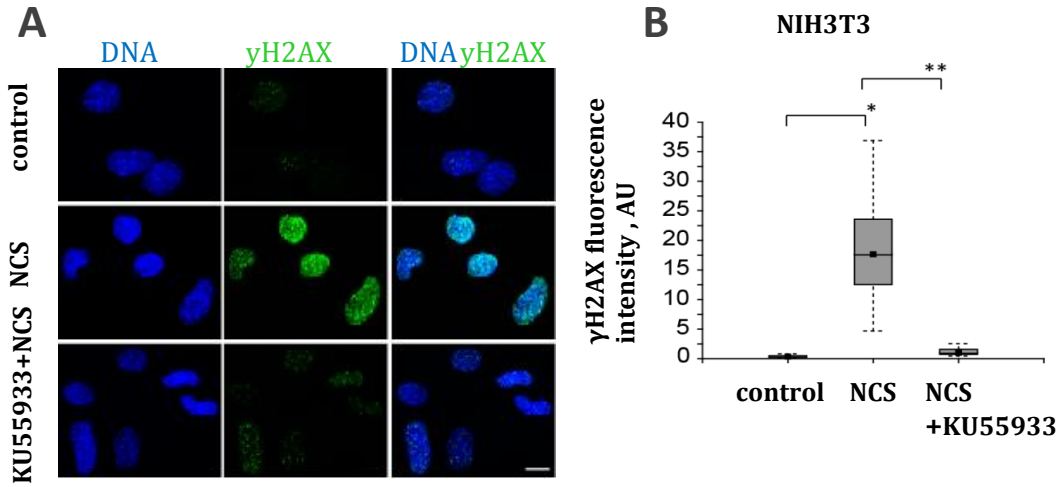

Fig. 38. KU55933 inhibits ATM in somatic cells. A) Immunofluorescence of control, NCS and NCS+KU55933 treated NIH3T3 cells labeled with γH2AX antibody. B) Quantification of γH2AX fluorescence in control, NCS and NCS+KU55933 treated NIH3T3 cells (n= 27, 44, 33).

Further we considered the involvement of MRE11 in regulation of DDR in oocytes. MRE11 is involved in sensing of DSBs and DNA repair (Rass et al., 2009). It is one of the primary sensors of DSBs which is responsible for ATM-mediated signal amplification. We found that in GV stage arrested oocytes MRE11 localizes to the nucleus and is expressed during cell cycle (Fig. 39).

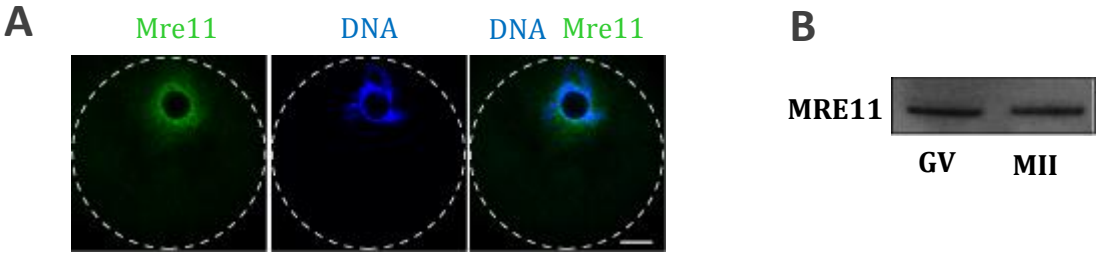

Fig. 39. MRE11 is expressed in oocytes. A) Immunofluorescence of GV-stage oocytes stained with MRE11 antibody and DAPI (DNA). Maximum z-projection is shown. B) Expression of MRE11 in GV-stage and metaphase II detected by Western blot (n=200 oocytes/lane). Scale bar 10um.

To estimate the role of MRE11 in meiotic maturation and H2AX phosphorylation we used a small molecule inhibitor Mirin which inhibits MRE11 nuclease activity and prevents MRN-dependent signal amplification in somatic cells (Dupré et al., 2008; Roques et al., 2009). We found that Mirin did not affect γH2AX/MDC1 foci number at GV-stage arrested oocyte after 1h incubation. However, it reduced the number of γH2AX/MDC1 foci in the oocytes treated simultaneously with NCS for 1h at GV stage (Fig. 39; Fig. 40 A).

Further, inhibition of MRE11 with Mirin during meiotic maturation (MI stage) reduced chromosome associated γH2AX/MDC1 signal compared to control oocytes (Fig. 39; Fig. 40 B). Interestingly, when the oocytes cultured in Mirin reached MII stage we observed both the increase of γH2AX foci and the significant increase of oocytes with at lease 1 γH2AX focus (Fig. 40. C, D).

While Mre11 clearly regulates H2AX phosphorylation during metaphase I, we wondered whether Mre11 is required for this process in MII. We isolated *in vivo* matured metaphase II oocytes and treated them for 1h with Mirin, NCS or Mirin+NCS. Treatment with Mirin alone did not change the number of γH2AX foci, while NCS increased γH2AX foci number as expected (Fig. 41A,B). Concomitant treatment with Mirin and NCS reduced the number of γH2AX foci ($p=0.025$), but this decrease was negligible compared to a dramatic effect of Mirin ($p< 0.0001$) on γH2AX foci number in GV-stage arrested NCS-treated oocytes (Fig. 40A). Moreover, Mirin treatment in MII did not affect the number of metaphase II oocytes with at least 3 γH2AX foci.

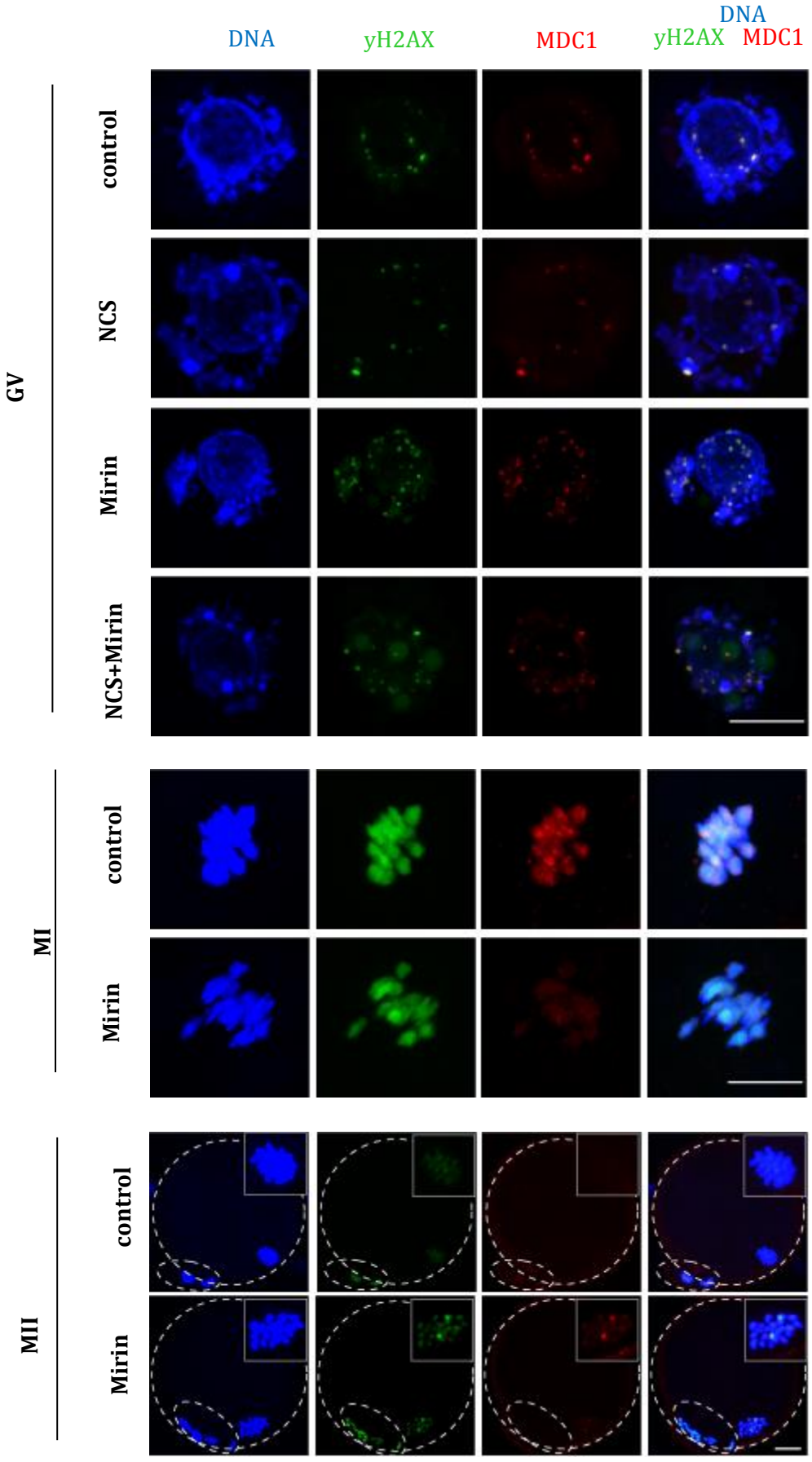

Fig. 39. MRE11 regulates γH2AX phosphorylation during meiotic maturation. Immunofluorescence of GV-stage, MI and MII oocytes labeled with γH2AX and MDC1 antibodies. Maximum z-projection of confocal section across chromatin region is shown. GV-stage oocytes were treated with mirin, NCS or both for 1 h in Milrinone supplemented medium. M I and MII oocytes matured in the presence of Mirin for 7 or 16 h. Insets show magnified images of chromosomes in MII. Scale bar 10µm.

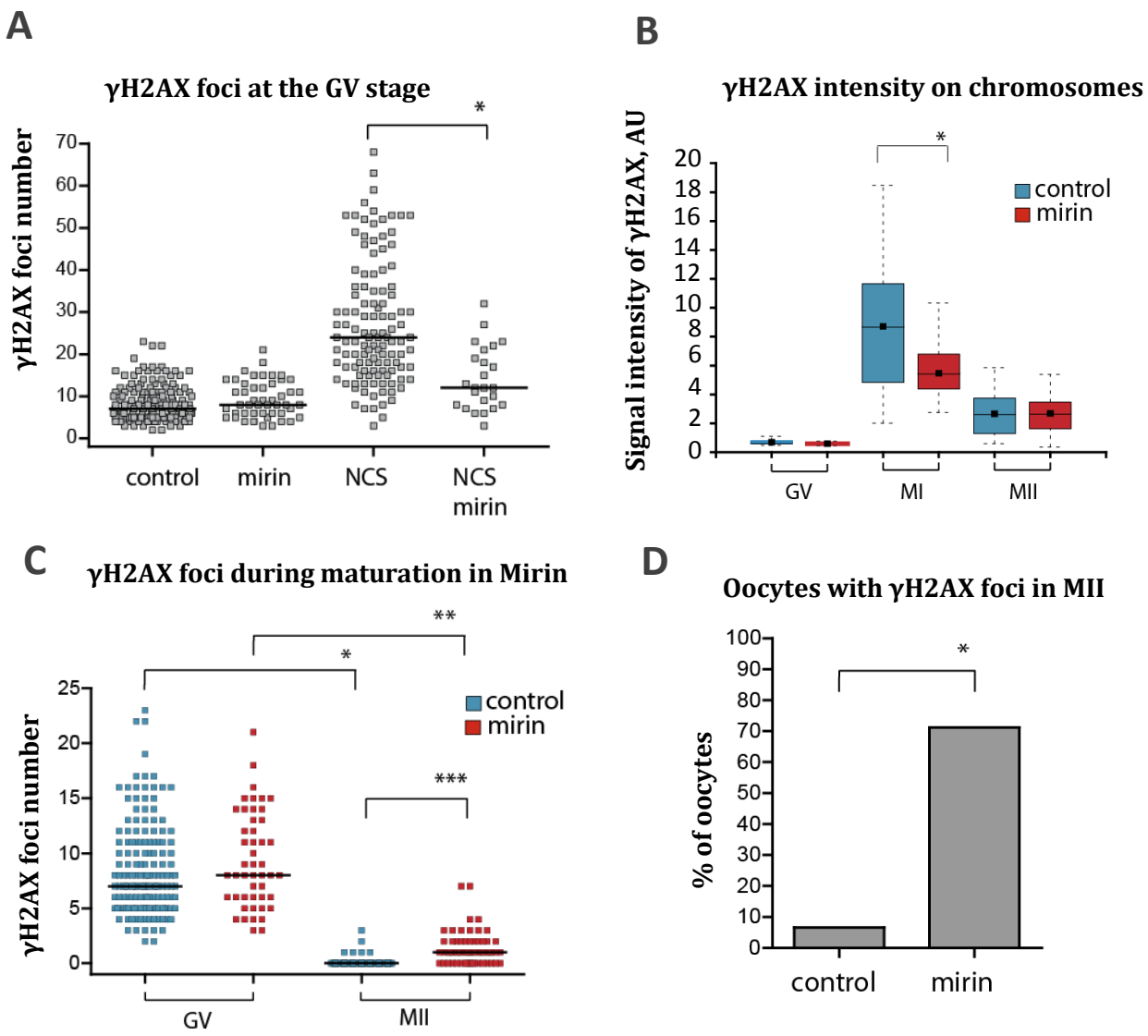

Fig. 40. Quantification of γH2AX phosphorylation in oocytes cultured in mirin. A) Quantification of γH2AX foci number in GV-stage oocytes non-treated (control) or treated with Mirin, NCS or both for 1 h in Milrinone supplemented medium (n=153, 48, 118, 24). B) Quantification of γH2AX during meiotic maturation in control and Mirin treated oocytes (n=26, 8, 15, 21, 14, 32). C) Quantification of γH2AX foci number in GV-stage and MII oocytes treated with mirin in GV stage before meiotic maturation (n=137, 33, 200, 109). D) Percentage of oocytes with at least one γH2AX focus matured into the metaphase II in control or Mirin supplemented medium (n=31, 58).

In summary, our data indicate that ATM is dispensable for meiosis I and H2AX phosphorylation, whereas MRE11 is required both of these processes. Maturation in Mirin leads to increased number of DSBs in MII, but H2AX phosphorylation at MII stage is less dependent on MRE11.

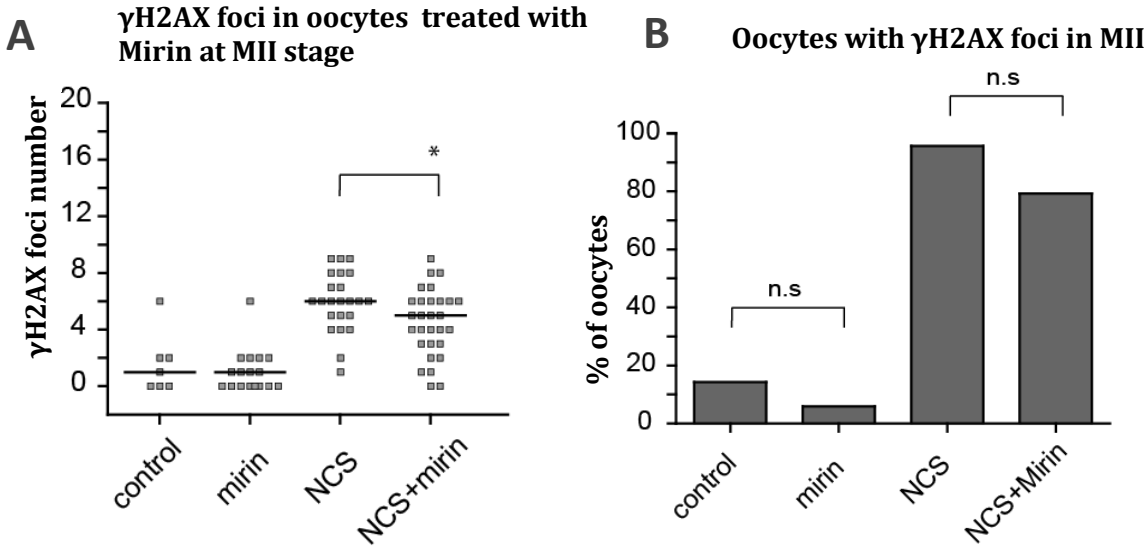

Fig. 41. MRE11 is not required for H2AX phosphorylation in meiosis II. A) Quantification of γH2AX foci number in in vivo matured metaphase II oocytes non-treated (control) or treated with Mirin, NCS or both for 1 h in in metaphase II (n = 7, 17, 23, 29). B) Percentage of oocytes (from A) with at least three γH2AX foci.

4.3.5 MRE11 is required for chromosome segregation and integrity

As described above, maturation in Mirin led to the increase in H2AX foci in MII oocytes. To detect whether these DSBs are generated during MI stage, we monitored by live-cell imaging the maturation and chromosome segregation in oocytes expressing H2B-EGFP and cultured in Mirin. Inhibition of MRE11 induced a significant delay in meiotic resumption and anaphase I onset (Fig.42 A, B). The anaphase I entry in Mirin was marked by significantly increased segregation problems (25%) compared to control oocytes (3%) (Fig. 42 C). Mirin treatment also reduced the rates of NEBD and MII oocytes (Fig. 42 D).

We microinjected the oocytes with MAP4-EGFP and H2B-mCherry to monitor spindle formation and to explore if spindle defects were responsible for missegregation in Mirin. In *Xenopus* mitotic extracts MRE11 is involved in spindle formation and chromosome alignment by regulating RAN-GTP signaling (Rozier et al., 2013). However, Mirin did not affect spindle formation, spindle volume or chromosome alignment in mouse oocytes (Fig. 42 E, F).

Further we aimed to describe the type of segregation problems and therefore monitored by high resolution live-cell imaging the maturation of oocytes expressing H2B-mCherry and a kinetochore marker CENPC- EGFP. In contrast to NCS treatment, chromosome bridges formation was the major phenotype observed in anaphase I (Fig. 43). Chromosome fragments appeared only exceptionally after Mirin treatment.

In conclusion, we demonstrated that MRE11 is required for correct chromosome segregation and maintenance of chromosome integrity and its inhibition leads to increased number of DSBs in Metaphase II and segregation problems in anaphase I.

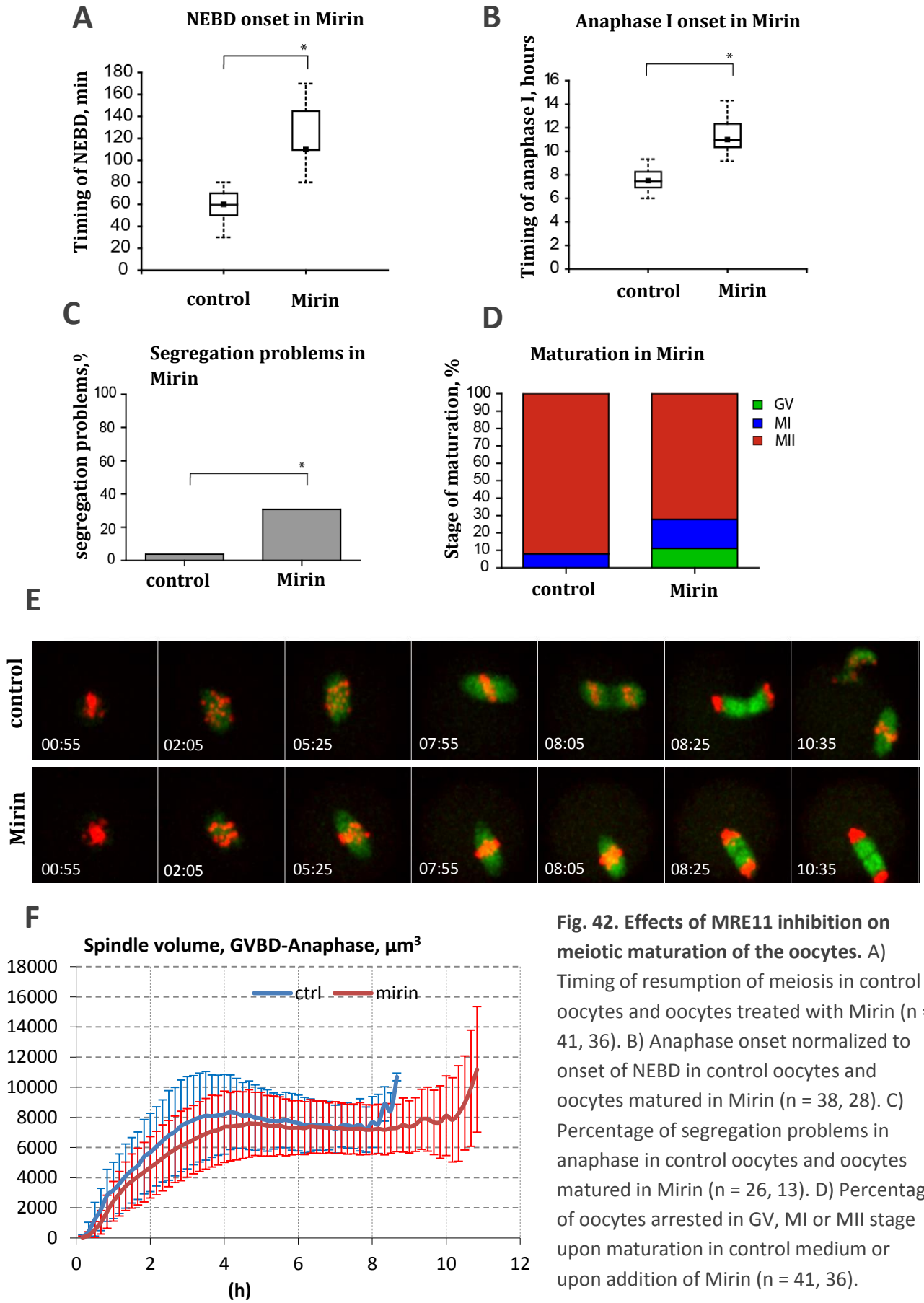

Fig. 42. Effects of MRE11 inhibition on meiotic maturation of the oocytes. A) Timing of resumption of meiosis in control oocytes and oocytes treated with Mirin (n = 41, 36). B) Anaphase onset normalized to onset of NEBD in control oocytes and oocytes matured in Mirin (n = 38, 28). C) Percentage of segregation problems in anaphase in control oocytes and oocytes matured in Mirin (n = 26, 13). D) Percentage of oocytes arrested in GV, MI or MII stage upon maturation in control medium or upon addition of Mirin (n = 41, 36).

E) Time lapse imaging of maturation of oocytes expressing MAP4-EGFP and H2B-mCHERRY in the presence of mirin. Maximum intensity z- projection images are shown. Time is in hh:mm. F) The volume of the spindle (µm3) during oocyte maturation quantified from 3D reconstructed data. Time t=0 corresponds to the time of NEBD. The analyzed timing represents the length of NEBD to anaphase entry period in hours (n=18, 31).

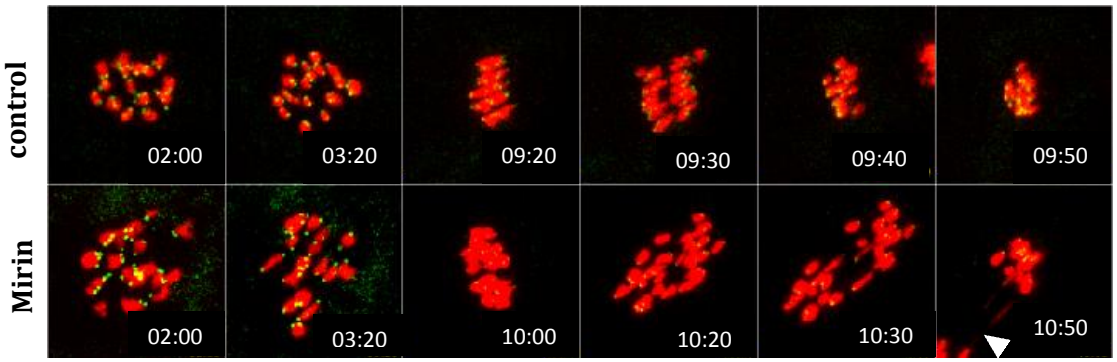

Fig. 43. MRE11 inhibition results in chromosome bridges formation in anaphase I. Imaging of chromosome dynamics and integrity in live oocytes expressing H2B-mCHERRY and EGFP-CENP-C and maturing in control or Mirin supplemented medium. Maximus z-projection of confocal section of selected time intervals is shown. Arrowhead shows anaphase bridges.Time in hh:mm.

5 Discussion

5.1 AURKA and PLK1 role in meiotic resumption and maturation of the oocytes

5.1.1 AURKA in meiotic resumtion in vivo

In our study we triggered meiotic maturation *in vivo* by the surge of luteinizing hormone (LH). LH induces meiotic resumption indirectly, through the expression of EGF-like peptides in mural granulose cells leading to activation of the signaling cascade in cumulus cells which are tightly connected to the oocyte (Panigone et al., 2008; Park et al., 2004). Expression of EGP-like peptides epiregulin and amphiregulin is observed in mural granulose cells within 1h after hCG surge, and we find that AURKA activation corresponds with this timing (Fig. 17, Fig. 18). It is therefore likely that initial AURKA activation is mediated through EGF-like peptides pathway, however we cannot exclude that there is an EGF-like independent signaling mechanism required for AURKA activation.

Although in somatic cells AURKA expression peaks at G2/M transition, it is not essential for normal mitotic entry (Honda et al., 2000; Van Horn et al., 2010; Marumoto et al., 2003). On the other hand, AURKA together with PLK1 and CDC25B is required for G2 checkpoint recovery in somatic cells, which is very similar to physiological meiotic resumption in oocytes (Macůrek et al., 2008; Solc et al., 2010; van Vugt et al., 2004b). Downregulation of AURKA *in vitro* by RNAi or using pharmacological inhibitor in mouse oocytes delays and decreases the rates of meiotic resumption, which implies for an involvement of AURKA in signal amplification leading to meiotic maturation (Saskova et al., 2008; Solc et al., 2010). However we find that overexpression of WT- AURKA in full-grown oocytes does not accelerate meiotic resumption (Fig.22). This finding is consistent with the current view that the main regulation mechanism of prophase I arrest is PKA-mediated inhibition of CDC25B, and the decrease of PKA activity is essential for CDC25B-dependent CDK1 activation (Oh et al., 2010; Pirino et al., 2009; Zhang et al., 2008).

We show that AURKA is involved in MTOC turnover regulation. In contrast to *in vitro* conditions when MTOC multiplication occurs before NEBD, in *in vivo* conditions it takes place shortly after NEBD. However, overexpression of WT-AURKA *in vivo* induces a premature increase in MTOC number already in prophase I arrested oocytes (Fig. 20). Interestingly, we discovered that this increase is transient and the number of MTOC decreases close to normal rates shortly before NEBD. We suggest that prematurely multiplied MTOC are unstable. In somatic cells, AURKA is activated on chromosomes independently of CDK1 activity prior mitotic entry and promotes centrosome separation, whereas later in mitosis AURKA activity is controlled by CDK1(Van Horn et al., 2010). Because CDC25B is essential for full CDK1 activation during resumption of meiosis, we used *Cdc25b-/-* oocytes as a model of low CDK1 activity and found that AURKA is still partially activated (Fig. 21). However multiplication of MTOC requires full AURKA activation mediated by CDK1 because microinjection of a *Gfp-Aurka* cRNA into the *Cdc25b*$^{-/-}$ oocytes restored the increase in MTOC number (Fig.21 D). Our data therefore indicate that first wave of AURKA

activation is independent of CDK1 activity, however full CDK1-mediated activation of AURKA is required for permanent MTOC multiplication.

5.1.2 PLK1 in meiotic resumption

Previous studies discovered that PLK1 activity increases during meiotic resumption and persists throughout meiotic maturation (Pahlavan et al., 2000). We detected that active PLK1 is localized with MTOC marker pericentrin shortly before NEBD (Fig.23) and the maximum activation of PLK1 occurred at the time of NEBD suggesting its involvement in these processes. Besides, in somatic cells chromosome condensation and NEBD are promoted by PLK1. NEBD involves nuclear pore disassembly which is stimulated by phosphorylation of nuclear pore proteins, and mechanical break down of nuclear envelope promoted by microtubule forces followed by depolymerization of nuclear lamina (Beaudouin et al., 2002; Laurell et al., 2011; Lénárt and Ellenberg, 2003). PLK1 is known to phosphorylate many nuclear pore proteins and also to regulate the activity of molecular motor complex dynein-dynactin, which controls microtubule forces (Li et al., 2010; Santamaria et al., 2011). Further, PLK1 phosphorylates cohesin II subunits to facilitate chromosome condensation (Abe et al., 2011).

We confirm that PLK1 plays a role in NEBD and chromosome condensation in oocytes. Unlike in somatic cells PLK1 significantly contributes to nuclear envelope permeabilization and ensures its start before chromosome condensation which seems to be specific for the oocytes (Fig.24). Timely regulation of NEBD and chromosome condensation by PLK1 is independent of CDK1-cyclin B activity as partial inhibition of CDK1 by flavopiridol did not invert the order of NEBD and chromosome condensation (Fig. 24 B). Because lamin disassembly was not affected by PLK1 inhibition it is likely that PLK1 plays a role in phosphorylation of nuclear pore proteins. Altogether, PLK1 contributes to meiotic resumption by ensuring timely NEBD before chromosome condensation.

5.1.3 AURKA in MI phase

While AURKA regulates MTOC multiplication in prophase I oocytes, it does not control MTOC foci number during metaphase I stage, however positively regulates MTOC volume and the amount of γ-tubulin associated with MTOC (Fig. 25). Because MTOC has a crucial role in spindle formation we next focused on analysis of MI spindle formation. In *Xenopus* egg extracts depletion of AURKA leads to formation of shorter spindles and overexpression of AURKA in oocytes *in vitro* leads to formation of multiopolar spindles of increased length accompanied by MI arrest of oocytes(Peset et al., 2005; Saskova et al., 2008). In *in vivo* conditions we found that WT-AURKA, but not KD-AURKA, overexpression leads to formation of longer spindles but does not interfere with chromosome alignment and does not trigger MI arrest (Fig.25 A, B). The explanation why transgenic overexpression of AURKA *in vivo* does not lead to spindle disorganization may be that generating higher amount of AURKA over the long course of oocytes growth elicits a compensatory response resulting in dephosphorylation of AURKA or decrease of AURKA amount. Consistent with this hypothesis is the lower amount of WT-AURKA protein

compared to KD-AURKA (Fig. 19A), although the amount of their transcripts was similar (data not shown). In conclusion, in meiosis I AURKA activity positively regulates spindle length, and in a protein kinase-independent manner AURKA positively regulates the amount of MTOC associated γ-tubulin.

5.1.4 PLK1 in MI phase

Similarly to AURKA, after meiotic resumption PLK1 is concentrated on MTOC, but besides that, we found PLK1 on kinetochores. Like in somatic cell, PLK1 recruits γ-tubulin and pericentrin to acentriolar MTOCs, promoting meiotic spindle formation (Fig. 27). PLK1 inhibition led to a significant delay in spindle elongation timing and also reduced the size of elongated spindles. The localization of PLK1 changed in anaphase I, when it disappeared from spindle poles and kinetochores and relocalized to spindle midzone (Fig. 26). Unlike in somatic cells or *Xenopus* egg extracts, PLK1 is not absolutely required for bipolarization of the spindle (Lane and Nigg, 1996; Liu et al., 2004).

Further our data indicate, that PLK1 regulates APC/C activity in oocytes through multiple pathways. First, PLK1 promotes proper kinetochore-microtubule attachment (Fig. 28 D), which satisfies the SAC and thereby enables APC/C activation. This data is consistent with the data from somatic cells, where PLK1 is required for stabilization of kinetochore-microtuble attachments and its timely removal is nessessary to maintain dynamic microtubules (Liu et al., 2012). Second, PLK1 phosphorylates the APC/C-inhibitor EMI1 promoting its degradation. Interestingly, in somatic cells PLK1 is not required for anaphase entry when SAC is abrogated (Lénárt et al., 2007; Sumara et al., 2004; van Vugt et al., 2004a), whereas oocytes require it (Fig.29). The explanation could be the larger volume of oocytes and larger amounts of EMI1, securin, cyclin B, which need to be degraded by APC/C.

5.1.5 Overlapping functions of AURKA and PLK1

PLK1 and AURKA are distinct kinases, however, their functions are intertwined in many aspects(Macurek et al., 2009). Their localization during somatic cell cycle is quite similar, suggesting that they may regulate the activity of one another. Indeed, AURKA is responsible for initial PLK1 phosphorylation at the G2/M transition (Macůrek et al., 2008; Seki et al., 2008). Inhibition of AURKA interferes with localization of active PLK1 at centosomes in prophase, but also at kinetochores (Macůrek et al., 2008). PLK1and AURKA levels rise in G2, and AURKA cofactor hBora forms a complex with PLK1 in G2 contributing to AURKA-mediated phosphorylation of PLK1 (Chan et al., 2008; Seki et al., 2008). In mitosis, AURKA localizes to centrosomes and spindle poles where it activates PLK1, which in turn regulates the function of AURKA(Chan et al., 2008; Seki et al., 2008). Besides, both kinases regulate KT-MT attachments during mitosis.

In the oocytes we confirm similar functions and localization of AURKA and PLK1 (Fig. 44). Both AURKA and PLK1 are responsible for γ-tubulin and probably pericentrin (no data for AURKA) recruitment to MTOC, they control metaphase I spindle volume and length.

It is therefore possible, that these kinases regulate each other activity also during meiotic maturation, however the evidence still needs to be found.

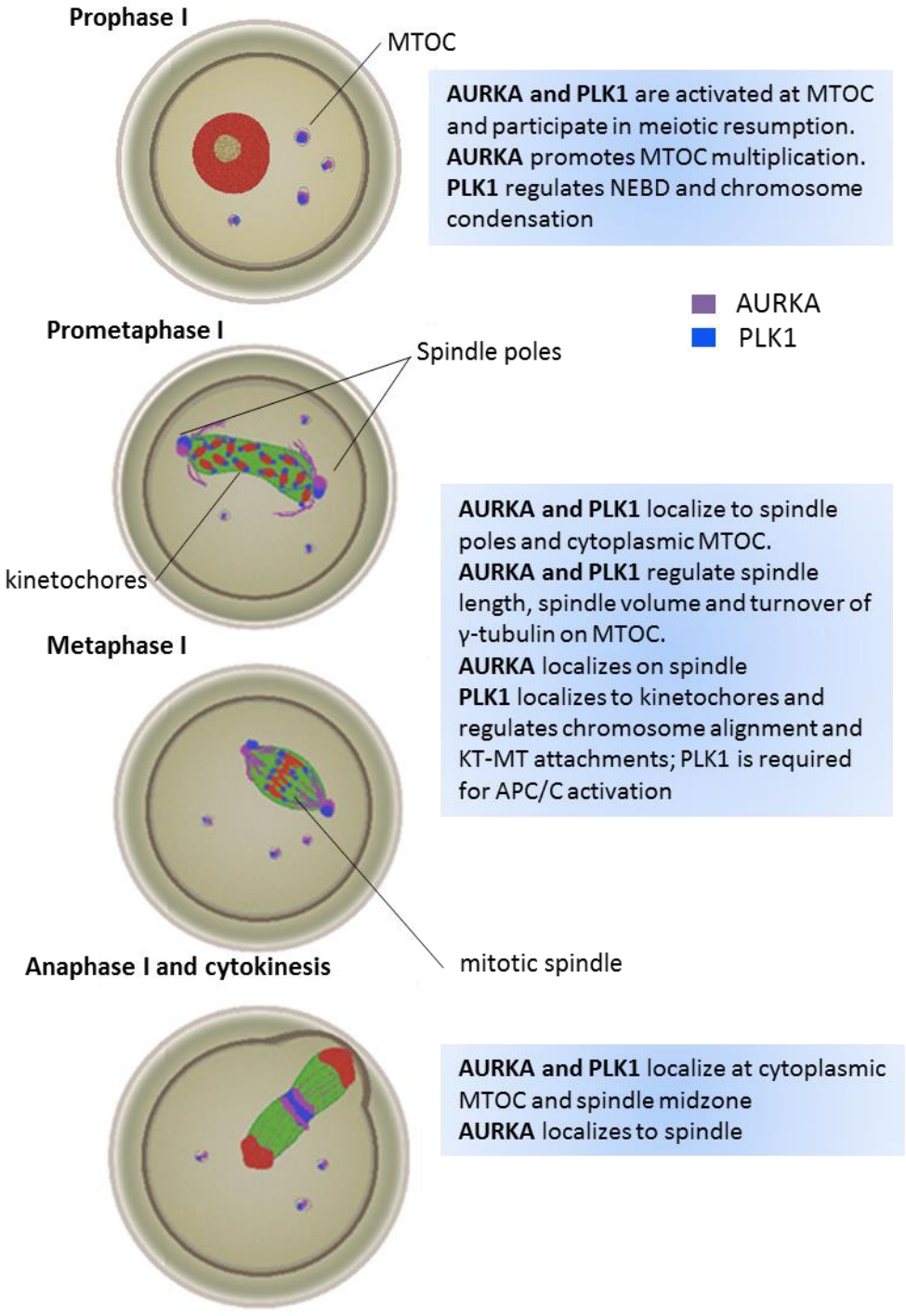

Fig. 44. Localization and function of AURKA and PLK1 in mouse oocytes. AURKA (purple) and PLK1 (violet) localize to MTOC, spindle poles and spindle midzone. Additionally, PLK1 localizes to kinechochores in MI, while AURKA can be found on spindle (green). Chromatin is red.

5.2 DNA damage response in oocytes.

In our experiments we show that phosphorylation of H2AX in mouse prophase I arrested oocytes increases in response to new DSBs induced exogenously by low concentration of NCS which generates a number of DSBs close to physiological (Fig. 31). These results extend the previous findings when DSBs were induced by high concentration of radiomimetic drugs (bleomycin, NCS, zeocin) (Lin et al., 2014; Ma et al., 2013; Yuen et al., 2012). Low levels of NCS lead to an increase of chromosome segregation errors (Fig. 31), however do not activate APC/C and do not induce a delay in the onset of anaphase I (Fig. 34). In contrast, severe levels of DNA damage induce a non-physiological increase in the number of DSBs and result in delayed resumption of meiosis and MI arrest accompanied by fragmented chromosomes (Yuen et al., 2012). Those oocytes which enter anaphase I in the presence of high concentration of radiomimetic drugs exhibit a delay in the time of emission of the first polar body, lower APC/C activation and persistent SAC activity as a consequence of disrupted microtubule-kinetochore attachments (Lin et al., 2014; Ma et al., 2013).

5.2.1 DSBs response in prophase I

Transient induction of DSBs in prophase I arrested oocytes led to a transient increase in DSBs, and the levels of DSBs dropped both in control and NCS treated oocytes after prolonged incubation (Fig.32). This result may indicate the repair processes in GV stage oocytes, supported by the knowledge that some of the repair proteins (BRCA1, BRCA2, RAD51, MRE11 and ATM) were found to be expressed in human oocytes and active repair processes were suggested at this stage (Titus et al., 2013). Further, UV irradiation of GV oocytes induced the highest frequency of ^{3}H-tymidine incorporation compared to MI and MII stages (Masui and Pedersen, 1975).However, we did not observe the decrease in segregation problems corresponding to the decreased amount of DSBs (Fig. 32 D). The explanation may be an incomplete repair process due to short post-NCS incubation of oocytes, while physiologically the oocytes are arrested for a long period.

5.2.2 DSBs lead to fragmentation of chromosomes in anaphase

To understand which type of segregation problems occurs after transient treatment with employed high-resolution imaging of live oocytes treated with NCS (Fig.33). Our findings show that chromosome structure was altered shortly after resumption of meiosis as evidenced by stretched homologues. However, chromosome fragments appeared only after anaphase onset due to mechanical forces during chromosome segregation. It is likely that cohesion loss in anaphase I also contributed to the breakage of those chromosomes that possessed the higher number of DSBs. Before chromosome segregation, DSBs are already present on chromosomes but cohesion between sister chromatids may help to support chromosome structure. Additionally, we observed lagging chromosomes after NCS treatment which may indicate that microtubule-kinetochore attachment was affected by DSBs. It is in agreement with the incidence of lagging chromosomes upon DNA damage induction in mitosis, which appear due to stabilzed microtubule-kinetochore attachments mediated by AURKA and PLK1 kinases (Bakhoum et al., 2014). Because aneuploidy in older females is associated with the loss of cohesion (Chiang et al., 2010), and older oocytes are characterized

by increased level of DSBs (Titus et al., 2013) it rises a question whether DSBs in aged oocytes may be one of the factors leading to aneuploidy.

5.2.3 H2AX phosphorylation is regualted by MRE11, but not ATM in oocytes

While H2AX foci related to DSBs are formed in interphase cells, ATM- mediated H2AX phosphorylation increases during mitosis and spreads over the condensed chromosomes independently of exogenous DNA damage (Burma et al., 2001). However even in the absence of DNA damage ATM and γH2AX may guard genome integrity in mitosis and regulate localization of mitotic checkpoint components (Eliezer et al., 2014; Ichijima et al., 2005; McManus and Hendzel, 2005). Interestingly, in somatic cells γH2AX may appear on intact chromatin throughout the cell cycle and may represent incomplete or halted DDR, whereas the morphology of the foci determines its association with repair proteins (Martín et al., 2014; Soutoglou and Misteli, 2008). Similar to mitosis, we discovered the highest H2AX phosphorylation in MI oocytes and the decrease of signal intensity in MII (Fig. 35 A, C). More importantly, unlike in somatic cells, this pathway is ATM-independent: inhibition of ATM by a specific inhibitor KU55933 did not change γH2AX on MI chromosomes, but also the numer of γH2AX was not altered in prophase I (Fig. 37) (Hickson et al., 2004). Because ATM expression and activation in mouse oocytes is significantly lower compared to somatic cells, other proteins may regulate H2AX phosphorylation in MI (Marangos and Carroll, 2012). We found that H2AX phosphorylation in MI phase is dependent on MRE11 (Fig. 35), suggesting that MRE11 plays a role in chromosome integrity.

Being involved in DSBs signal amplification loop (Stracker et al., 2004), MRE11 appeared to regulate γH2AX phosphorylation also in prophase I: inhibition of MRE11 reduced NCS-mediated increase in γH2AX foci number. However γH2AX signaling in MII was partly independent of MRE11 activity (Fig. 41). Given that DSBs repair in MII eggs is dependent on homologous recombination factor RAD51(Kujjo et al., 2010) and MRE11 is an essential component of homologous recombination it is not clear whether MRE11 is essential for DNA repair at metaphase II.

5.2.4 Regulation of DNA repair during maturation in oocytes

Upon maturation of oocytes in mirin we detected an increase of γH2AX foci in MII, which was likely a consequence of impaired chromosome integrity in metaphase I. Indeed, live imaging of oocytes revealed more stretched homologous chromosomes in prometaphase and MI, which is similar to the effect of NCS treatment. In contrast to mirin effect in *Xenopus* egg extracts (Rozier et al., 2013), we did not observe any abnormality in spindle formation or chromosome alignment in Metaphase I, however anaphase bridges were visible when MRE11 was inhibited during maturation. Anaphase bridges may be associated with incomplete or incorrect DSBs repair (Acilan et al., 2007). Alternatively, anaphase bridges may indicate erroneous „repair“ of deprotected telomeres which are recognized as DSBs in mitosis, given that in primary human telomerase negative G2 cells, MRE11 and NBS1 are recruited to telomeres to ensure their protection (Verdun et al., 2005). Physiologically, DSBs repair is suppressed in mitosis: only early DSBs repair and recognition factors are recruited (γH2AX,

MDC1, MRE11), whereas the recruitment of late repair factors (RNF8/RNF15, 53BP1, BRCA1, DNA ligase XRCC4) is suppressed by CDK1 and PLK1 (Terasawa et al., 2014b). Artificial activation and recruitment of late repair factors to DNA in mitosis results in sister telomere fusion due to NHEJ repair, followed by chromosome segregation errors (Lee et al., 2014; Orthwein et al., 2014). However, down-regulation of MRN binding partner CtIP, which facilitates DSB-end resection and is involved both in NHEJ and HR, significantly increases the incidence of anaphase bridges, suggesting that it is actively involved in the maintenance of genome stability (Montgomery et al., 2003; Terasawa et al., 2014a)

Given that meiotic maturation, which lasts much longer than mitosis in somatic cells, is the last option for the oocytes to precisely repair DNA before fertilization when homologous template is available, we suggest that DNA repair mechanisms should be functional at this stage. Besides, meiotic chromosomes are generally less dense than chromsomes in mitosis, which potentially makes them more accessible for the repair factors (Marko and Siggia, 1997). Our findings support the assumption that the oocytes possess mechanisms protecting their DNA integrity during meiotic maturation. In particular, we observe that the number of γH2AX foci significantly decreases between prophase I and MII during oocyte maturation (Fig. 35 D, Fig. 40 C). Oocytes transiently treated with NCS exhibited a 2.5-fold increase in DSBs number in prophase I, but following maturation, only about 30% of oocytes entered anaphase I with chromosome segregation errors, and also only about 30% of MII eggs had more than 1 detectable DSB. Inhibiting the nuclease activity of MRE11(Dupré et al., 2008), but not DNA tethering function during meiotic maturation resulted in anaphase bridges formation and also increased the number of γH2AX foci in MII eggs.

Collectively, our data suggest that DNA repair occurs after resumption of meiosis during the prolonged MI phase and that MRE11 is critical for such DNA repair. Because MRE11 is involved in all typer of repair (Stracker and Petrini, 2011), further investigations are needed to elucidate the mechanisms of DNA repair operating in oocytes, which seem to differ from somatic cells.

6 Conclusion

In our study we investigated the roles of AURKA and PLK1 during meiotic resumption and maturation. We found that AURKA controls biogenesis of MTOC during meiotic resumption *in vivo* and its inhibition leads to premature and unstable increase of MTOC number, while CDC25B-mediated CDK1 activation is essential for MTOC stabilization. We discovered that PLK1 is involved in the regulation of nuclear envelope break down, which is partly independent of CDK1 activity. Both AURKA and PLK1 localize at MTOC and regulate the amount of centrosomal proteins at MTOC and ensure correct spindle formation. PLK1 regulates kinetochore-microtubule attachments and plays a role in APC/C activation through degradation of EMI1. Therefore, in addition to known function for these two kinases in mitosis, we found their specific involvement in the regulation of meiotic progression.

Further we discovered the response of oocytes to double strand breaks (DSBs). Our data show, that both exogenous DSBs induced by Neocarzionstatin (NCS) and endogenous DSBs which result from cell metabolism, decrease throughout maturation. Prolonged incubation of GV stage arrested oocytes transiently treated with NCS was also characterized by the decrease of DSBs represented by γH2AX foci. We discovered that a component of MRN complex MRE11, but not ATM, regulates the signaling in response to DSBs. Besides, inhibition of MRE11 with mirin results in chromosome instability, marked by the increased incidence of anaphase bridges. Altogether, our data extend previous findings and imply that DNA repair processes operate during oocyte maturation. Given that the oocytes are arrested in prophase I for a long period, the repair of the DNA damage seems to be essential for the maintenance of reproduction capacity. Further experiments are needed to investigate the signaling pathways in oocytes, which are involved in DNA damage detection and repair.

7 Abbreviations

A-NHEJ	alternative NHEJ
ADCY3	adenylate cyclase 3
APC/C	anaphase promoting complex/cyclosome
AREG	amphiregulin
ARP 2/3	actin-related protein 2/3 complex
ATM	Ataxia telangiectasia mutated
ATR	ataxia telangiectasia and Rad3-related
ATP	adenosin triphosphate
AURKA	Aurora kinase A
ATRIP	ATR interacting protein
BRCA1	breast cancer 1, early onset
BTC	betacellulin
BUB1,3	budding uninhibited by benzimidazoles 1,3
C-NHEJ	canonical NHEJ
cAMP	cyclic adenosine monophosphate
CDC	cell division cycle (CDC25 A,B, C, CDC14)
CDH1	cadherin1
CDK1	cycline dependent kinase 1
CENP-E	centromere protein E
cGMP	cyclic guanosine monophosphate
CHK1, 2	checkpoint kinase 1, 2
CPC	chromosomal passenger complex
CtIP	C-terminal binding protein interacting protein
DDR	DNA damage response
DMC1	DNA meiotic recombinase 1
DNA-PK	DNA-dependent protein kinase
DSBs	DNA double strand breaks
EGF	epidermal growth like factors
EGFP	enhanced green fluorescent protein
EGFR	epidermal growth factor receptor
EMI1	early mitotic inhibitor 1
EREG	epiregulin
FANCD2	Fanconi anemia group D2 protein
FSH	follicle stimulating hormone
GTP	guanosine triphosphate
GV	germinal vesicle
GVBD	germinal vesicle breakdown
hCG	human chorionic gonadotropin
HR	homologous recombination
INCENP	inner centromere protein
KT-MT	kinetochore-microtubule
KD	kinase-dead
LH	luteinizing hormone
MI, II	metaphase I
MAD1, 2	mitotic arrest deficient-like 1, 2
MAPK	mitogen activated protein kinase
MCC	mitotic checkpoint complex

MDC1	mediator of DNA damage checkpoint protein 1
MRE11	meiotic recombination 11 homologue
MRN	MRE11, RAD50, NBS1
MTOC	microtubule organizing center
MPF	metaphase promoting factor
Myo II	myosin II
NBS1	Nijmegen breakage syndrome 1
NCS	Neocarzinostatin
NEBD	nuclear envelope break down
NHEJ	non-homologous end joining
PARP-1	poly(ADP-ribose)polymerase 1
PGCs	primordial germ cells
PIKK	phosphatidylinositol 3-kinase-related kinase
PKA, PKB	protein kinase A, protein kinase B
PLK1	polo-like kinase 1
PP2A	protein phosphatase 2A
RAN	Ras-related nuclear protein
RCC1	regulation of chromosome condensation 1
PD3A	phosphodiesterase 3A
PUMAp53	upregulated modulator of apoptosis
Rec8	meiotic recombination protein Rec8
RNF 8, 168	ring finger protein 8, 168
RPA	replication protein A
SA 1, 2	stromal antigen-1, 2
SAC	spindle assembly checkpoint
SCF	Skp, Cullin, F-box containing complex
Sgo1,2	shugosin 1, 2
Smc1β, 1, 3	structural maintenance of chromosome 1β, 1, 3
TOP2	topoisomerase 2
UV	ultraviolet
WT	wild type
XRCC3,4	X-ray repair cross-complementing protein 3,4
ZP1, 2, 3	zona pellucida 1, 2, 3
53BP1	tumor protein p53 binding protein 1

8 References

Abe, S., Nagasaka, K., Hirayama, Y., Kozuka-Hata, H., Oyama, M., Aoyagi, Y., Obuse, C., and Hirota, T. (2011). The initial phase of chromosome condensation requires Cdk1-mediated phosphorylation of the CAP-D3 subunit of condensin II. Genes Dev. *25*, 863–874.

Acilan, C., Potter, D.M., and Saunders, W.S. (2007). DNA repair pathways involved in anaphase bridge formation. Genes. Chromosomes Cancer *46*, 522–531.

Agarwal, S., Tafel, A.A., and Kanaar, R. (2006). DNA double-strand break repair and chromosome translocations. DNA Repair *5*, 1075–1081.

Altmeyer, M., and Lukas, J. (2013). To spread or not to spread--chromatin modifications in response to DNA damage. Curr. Opin. Genet. Dev. *23*, 156–165.

An, J., Huang, Y.-C., Xu, Q.-Z., Zhou, L.-J., Shang, Z.-F., Huang, B., Wang, Y., Liu, X.-D., Wu, D.-C., and Zhou, P.-K. (2010). DNA-PKcs plays a dominant role in the regulation of H2AX phosphorylation in response to DNA damage and cell cycle progression. BMC Mol. Biol. *11*, 18.

Anderson, E., and Albertini, D.F. (1976). Gap junctions between the oocyte and companion follicle cells in the mammalian ovary. J. Cell Biol. *71*, 680–686.

Badie, S., Carlos, A.R., Folio, C., Okamoto, K., Bouwman, P., Jonkers, J., and Tarsounas, M. (2015). BRCA1 and CtIP promote alternative non-homologous end-joining at uncapped telomeres. EMBO J. *34*, 828.

Bakhoum, S.F., Kabeche, L., Murnane, J.P., Zaki, B.I., and Compton, D.A. (2014). DNA-damage response during mitosis induces whole-chromosome missegregation. Cancer Discov. *4*, 1281–1289.

Bannister, L.A., and Schimenti, J.C. (2004). Homologous recombinational repair proteins in mouse meiosis. Cytogenet. Genome Res. *107*, 191–200.

Bartek, J., and Lukas, J. (2007). DNA damage checkpoints: from initiation to recovery or adaptation. Curr. Opin. Cell Biol. *19*, 238–245.

Baudat, F., Manova, K., Yuen, J.P., Jasin, M., and Keeney, S. (2000). Chromosome Synapsis Defects and Sexually Dimorphic Meiotic Progression in Mice Lacking Spo11. Mol. Cell *6*, 989–998.

Beaudouin, J., Gerlich, D., Daigle, N., Eils, R., and Ellenberg, J. (2002). Nuclear envelope breakdown proceeds by microtubule-induced tearing of the lamina. Cell *108*, 83–96.

Bekker-Jensen, S., Lukas, C., Kitagawa, R., Melander, F., Kastan, M.B., Bartek, J., and Lukas, J. (2006). Spatial organization of the mammalian genome surveillance machinery in response to DNA strand breaks. J. Cell Biol. *173*, 195–206.

Belmont, A.S. (2006). Mitotic chromosome structure and condensation. Curr. Opin. Cell Biol. *18*, 632–638.

Boateng, K.A., Bellani, M.A., Gregoretti, I.V., Pratto, F., and Camerini-Otero, R.D. (2013). Homologous pairing preceding SPO11-mediated double-strand breaks in mice. Dev. Cell *24*, 196–205.

Bolte, S., and Cordelières, F.P. (2006). A guided tour into subcellular colocalization analysis in light microscopy. J. Microsc. *224*, 213–232.

Borde, V. (2007). The multiple roles of the Mre11 complex for meiotic recombination. Chromosome Res. Int. J. Mol. Supramol. Evol. Asp. Chromosome Biol. *15*, 551–563.

Bornslaeger, E.A., Mattei, P., and Schultz, R.M. (1986). Involvement of cAMP-dependent protein kinase and protein phosphorylation in regulation of mouse oocyte maturation. Dev. Biol. *114*, 453–462.

Boutros, R., Lobjois, V., and Ducommun, B. (2007). CDC25 phosphatases in cancer cells: key players? Good targets? Nat. Rev. Cancer *7*, 495–507.

Broekmans, F.J., Knauff, E.A.H., Velde, E.R. te, Macklon, N.S., and Fauser, B.C. (2007). Female reproductive ageing: current knowledge and future trends. Trends Endocrinol. Metab. TEM *18*, 58–65.

Brunet, S., Maria, A.S., Guillaud, P., Dujardin, D., Kubiak, J.Z., and Maro, B. (1999). Kinetochore fibers are not involved in the formation of the first meiotic spindle in mouse oocytes, but control the exit from the first meiotic M phase. J. Cell Biol. *146*, 1–12.

Buccione, R., Schroeder, A.C., and Eppig, J.J. (1990). Interactions between somatic cells and germ cells throughout mammalian oogenesis. Biol. Reprod. *43*, 543–547.

Buis, J., Wu, Y., Deng, Y., Leddon, J., Westfield, G., Eckersdorff, M., Sekiguchi, J.M., Chang, S., and Ferguson, D.O. (2008). Mre11 Nuclease Activity has Essential Roles in DNA Repair and Genomic Stability Distinct from ATM Activation. Cell *135*, 85–96.

Burgess, A., Rasouli, M., and Rogers, S. (2014). Stressing mitosis to death. Mol. Cell. Oncol. *4*, 140.

Burma, S., Chen, B.P., Murphy, M., Kurimasa, A., and Chen, D.J. (2001). ATM phosphorylates histone H2AX in response to DNA double-strand breaks. J. Biol. Chem. *276*, 42462–42467.

Busino, L., Donzelli, M., Chiesa, M., Guardavaccaro, D., Ganoth, D., Dorrello, N.V., Hershko, A., Pagano, M., and Draetta, G.F. (2003). Degradation of Cdc25A by beta-TrCP during S phase and in response to DNA damage. Nature *426*, 87–91.

Byskov, A.G., Høyer, P.E., Yding Andersen, C., Kristensen, S.G., Jespersen, A., and Møllgård, K. (2011). No evidence for the presence of oogonia in the human ovary after their final clearance during the first two years of life. Hum. Reprod. Oxf. Engl. *26*, 2129–2139.

Calarco, P.G. (2000). Centrosome precursors in the acentriolar mouse oocyte. Microsc. Res. Tech. *49*, 428–434.

Calarco-Gillam, P.D., Siebert, M.C., Hubble, R., Mitchison, T., and Kirschner, M. (1983). Centrosome development in early mouse embryos as defined by an autoantibody against pericentriolar material. Cell *35*, 621–629.

Can, A., Semiz, O., and Cinar, O. (2003). Centrosome and microtubule dynamics during early stages of meiosis in mouse oocytes. Mol. Hum. Reprod. *9*, 749–756.

Carabatsos, M.J., Combelles, C.M., Messinger, S.M., and Albertini, D.F. (2000). Sorting and reorganization of centrosomes during oocyte maturation in the mouse. Microsc. Res. Tech. *49*, 435–444.

Carson, C.T., Schwartz, R.A., Stracker, T.H., Lilley, C.E., Lee, D.V., and Weitzman, M.D. (2003). The Mre11 complex is required for ATM activation and the G2/M checkpoint. EMBO J. *22*, 6610–6620.

Chan, E.H.Y., Santamaria, A., Silljé, H.H.W., and Nigg, E.A. (2008). Plk1 regulates mitotic Aurora A function through βTrCP-dependent degradation of hBora. Chromosoma *117*, 457–469.

Chen, M.S., Hurov, J., White, L.S., Woodford-Thomas, T., and Piwnica-Worms, H. (2001). Absence of apparent phenotype in mice lacking Cdc25C protein phosphatase. Mol. Cell. Biol. *21*, 3853–3861.

Chiang, T., Duncan, F.E., Schindler, K., Schultz, R.M., and Lampson, M.A. (2010). Evidence that weakened centromere cohesion is a leading cause of age-related aneuploidy in oocytes. Curr. Biol. CB *20*, 1522–1528.

Ciccia, A., and Elledge, S.J. (2010). The DNA damage response: making it safe to play with knives. Mol. Cell *40*, 179–204.

Clarke, P.R., and Zhang, C. (2008). Spatial and temporal coordination of mitosis by Ran GTPase. Nat. Rev. Mol. Cell Biol. *9*, 464–477.

Clift, D., and Schuh, M. (2013). Restarting life: fertilization and the transition from meiosis to mitosis. Nat. Rev. Mol. Cell Biol. *14*, 549–562.

Colledge, W.H., Carlton, M.B., Udy, G.B., and Evans, M.J. (1994). Disruption of c-mos causes parthenogenetic development of unfertilized mouse eggs. Nature *370*, 65–68.

Conti, M., Hsieh, M., Zamah, A.M., and Oh, J.S. (2012). Novel signaling mechanisms in the ovary during oocyte maturation and ovulation. Mol. Cell. Endocrinol. *356*, 65–73.

Coucouvanis, E.C., Sherwood, S.W., Carswell-Crumpton, C., Spack, E.G., and Jones, P.P. (1993). Evidence that the mechanism of prenatal germ cell death in the mouse is apoptosis. Exp. Cell Res. *209*, 238–247.

Darzynkiewicz, Z., Traganos, F., and Wlodkowic, D. (2009). Impaired DNA damage response--an Achilles' heel sensitizing cancer to chemotherapy and radiotherapy. Eur. J. Pharmacol. *625*, 143–150.

Davydenko, O., Schultz, R.M., and Lampson, M.A. (2013). Increased CDK1 activity determines the timing of kinetochore-microtubule attachments in meiosis I. J. Cell Biol. *202*, 221–229.

Debey, P., Szöllösi, M.S., Szöllösi, D., Vautier, D., Girousse, A., and Besombes, D. (1993). Competent mouse oocytes isolated from antral follicles exhibit different chromatin organization and follow different maturation dynamics. Mol. Reprod. Dev. *36*, 59–74.

Denchi, E.L., and Li, J. (2014). Let it go: how to deal with a breakup in mitosis. Nat. Struct. Mol. Biol. *21*, 433–435.

Dimitrova, N., and de Lange, T. (2009). Cell Cycle-Dependent Role of MRN at Dysfunctional Telomeres: ATM Signaling-Dependent Induction of Nonhomologous End Joining (NHEJ) in G1 and Resection-Mediated Inhibition of NHEJ in G2. Mol. Cell. Biol. *29*, 5552–5563.

Ding, J., Swain, J.E., and Smith, G.D. (2011). Aurora kinase-A regulates microtubule organizing center (MTOC) localization, chromosome dynamics, and histone-H3 phosphorylation in mouse oocytes. Mol. Reprod. Dev. *78*, 80–90.

diZerega, G.S., and Hodgen, G.D. (1981). Folliculogenesis in the primate ovarian cycle. Endocr. Rev. *2*, 27–49.

Dumont, J., Petri, S., Pellegrin, F., Terret, M.-E., Bohnsack, M.T., Rassinier, P., Georget, V., Kalab, P., Gruss, O.J., and Verlhac, M.-H. (2007a). A centriole- and RanGTP-independent spindle assembly pathway in meiosis I of vertebrate oocytes. J. Cell Biol. *176*, 295–305.

Dumont, J., Million, K., Sunderland, K., Rassinier, P., Lim, H., Leader, B., and Verlhac, M.-H. (2007b). Formin-2 is required for spindle migration and for the late steps of cytokinesis in mouse oocytes. Dev. Biol. *301*, 254–265.

Duncan, F.E., Moss, S.B., and Williams, C.J. (2006). Knockdown of the cAMP-dependent protein kinase (PKA) Type Ialpha regulatory subunit in mouse oocytes disrupts meiotic arrest and results in meiotic spindle defects. Dev. Dyn. Off. Publ. Am. Assoc. Anat. *235*, 2961–2968.

Dupré, A., Boyer-Chatenet, L., Sattler, R.M., Modi, A.P., Lee, J.-H., Nicolette, M.L., Kopelovich, L., Jasin, M., Baer, R., Paull, T.T., et al. (2008). A forward chemical genetic screen reveals an inhibitor of the Mre11-Rad50-Nbs1 complex. Nat. Chem. Biol. *4*, 119–125.

Durant, S.T., and Nickoloff, J.A. (2005). Good timing in the cell cycle for precise DNA repair by BRCA1. Cell Cycle Georget. Tex *4*, 1216–1222.

Eliezer, Y., Argaman, L., Kornowski, M., Roniger, M., and Goldberg, M. (2014). Interplay between the DNA damage proteins MDC1 and ATM in the regulation of the spindle assembly checkpoint. J. Biol. Chem. *289*, 8182–8193.

Eppig, J.J. (2001). Oocyte control of ovarian follicular development and function in mammals. Reproduction *122*, 829–838.

Faddy, M.J., and Gosden, R.G. (1995). A mathematical model of follicle dynamics in the human ovary. Hum. Reprod. Oxf. Engl. *10*, 770–775.

Falck, J., Coates, J., and Jackson, S.P. (2005). Conserved modes of recruitment of ATM, ATR and DNA-PKcs to sites of DNA damage. Nature *434*, 605–611.

La Fuente, R. De, and Eppig, J.J. (2001). Transcriptional activity of the mouse oocyte genome: companion granulosa cells modulate transcription and chromatin remodeling. Dev. Biol. *229*, 224–236.

Gatti, M., Pinato, S., Maspero, E., Soffientini, P., Polo, S., and Penengo, L. (2012). A novel ubiquitin mark at the N-terminal tail of histone H2As targeted by RNF168 ubiquitin ligase. Cell Cycle Georget. Tex *11*, 2538–2544.

Gaulden, M.E. (1992). Maternal age effect: the enigma of Down syndrome and other trisomic conditions. Mutat. Res. *296*, 69–88.

Di Giacomo, M., Barchi, M., Baudat, F., Edelmann, W., Keeney, S., and Jasin, M. (2005). Distinct DNA-damage-dependent and -independent responses drive the loss of oocytes in recombination-defective mouse mutants. Proc. Natl. Acad. Sci. U. S. A. *102*, 737–742.

Gilbert, S.F. (2000). Developmental Biology 6th ed (Sunderland, Mass: Sinauer Associates Inc.,U.S.).

Giunta, S., and Jackson, S.P. (2011). Give me a break, but not in mitosis: the mitotic DNA damage response marks DNA double-strand breaks with early signaling events. Cell Cycle Georget. Tex *10*, 1215–1221.

Giunta, S., Belotserkovskaya, R., and Jackson, S.P. (2010). DNA damage signaling in response to double-strand breaks during mitosis. J. Cell Biol. *190*, 197–207.

Gorr, I.H., Boos, D., and Stemmann, O. (2005). Mutual inhibition of separase and Cdk1 by two-step complex formation. Mol. Cell *19*, 135–141.

Gueth-Hallonet, C., Antony, C., Aghion, J., Santa-Maria, A., Lajoie-Mazenc, I., Wright, M., and Maro, B. (1993). gamma-Tubulin is present in acentriolar MTOCs during early mouse development. J. Cell Sci. *105 (Pt 1)*, 157–166.

Gui, L., and Homer, H. (2012). Spindle assembly checkpoint signalling is uncoupled from chromosomal position in mouse oocytes. Dev. Camb. Engl. *139*, 1941–1946.

Hadjantonakis, A.-K., and Papaioannou, V.E. (2004). Dynamic in vivo imaging and cell tracking using a histone fluorescent protein fusion in mice. BMC Biotechnol. *4*, 33.

Han, S.J., Chen, R., Paronetto, M.P., and Conti, M. (2005). Wee1B is an oocyte-specific kinase involved in the control of meiotic arrest in the mouse. Curr. Biol. CB *15*, 1670–1676.

Hara, M., Abe, Y., Tanaka, T., Yamamoto, T., Okumura, E., and Kishimoto, T. (2012). Greatwall kinase and cyclin B-Cdk1 are both critical constituents of M-phase-promoting factor. Nat. Commun. *3*, 1059.

Hassold, T., and Hunt, P. (2001). To err (meiotically) is human: the genesis of human aneuploidy. Nat. Rev. Genet. *2*, 280–291.

Herbert, M., Levasseur, M., Homer, H., Yallop, K., Murdoch, A., and McDougall, A. (2003). Homologue disjunction in mouse oocytes requires proteolysis of securin and cyclin B1. Nat. Cell Biol. *5*, 1023–1025.

Hickson, I., Zhao, Y., Richardson, C.J., Green, S.J., Martin, N.M.B., Orr, A.I., Reaper, P.M., Jackson, S.P., Curtin, N.J., and Smith, G.C.M. (2004). Identification and characterization of a novel and specific inhibitor of the ataxia-telangiectasia mutated kinase ATM. Cancer Res. *64*, 9152–9159.

Hirshfield, A.N. (1991). Development of follicles in the mammalian ovary. Int. Rev. Cytol. *124*, 43–101.

Hodges, C.A., Revenkova, E., Jessberger, R., Hassold, T.J., and Hunt, P.A. (2005). SMC1beta-deficient female mice provide evidence that cohesins are a missing link in age-related nondisjunction. Nat. Genet. *37*, 1351–1355.

Holt, J.E., Weaver, J., and Jones, K.T. (2010). Spatial regulation of APCCdh1-induced cyclin B1 degradation maintains G2 arrest in mouse oocytes. Dev. Camb. Engl. *137*, 1297–1304.

Honda, K., Mihara, H., Kato, Y., Yamaguchi, A., Tanaka, H., Yasuda, H., Furukawa, K., and Urano, T. (2000). Degradation of human Aurora2 protein kinase by the anaphase-promoting complex-ubiquitin-proteasome pathway. Oncogene *19*, 2812–2819.

Horner, K., Livera, G., Hinckley, M., Trinh, K., Storm, D., and Conti, M. (2003). Rodent oocytes express an active adenylyl cyclase required for meiotic arrest. Dev. Biol. *258*, 385–396.

Van Horn, R.D., Chu, S., Fan, L., Yin, T., Du, J., Beckmann, R., Mader, M., Zhu, G., Toth, J., Blanchard, K., et al. (2010). Cdk1 activity is required for mitotic activation of aurora A during G2/M transition of human cells. J. Biol. Chem. *285*, 21849–21857.

Hsueh, A.J., Billig, H., and Tsafriri, A. (1994). Ovarian follicle atresia: a hormonally controlled apoptotic process. Endocr. Rev. *15*, 707–724.

Huen, M.S.Y., Sy, S.M.H., and Chen, J. (2010). BRCA1 and its toolbox for the maintenance of genome integrity. Nat. Rev. Mol. Cell Biol. *11*, 138–148.

Hunt, P.A., and Hassold, T.J. (2008). Human female meiosis: what makes a good egg go bad? Trends Genet. TIG *24*, 86–93.

Ichijima, Y., Sakasai, R., Okita, N., Asahina, K., Mizutani, S., and Teraoka, H. (2005). Phosphorylation of histone H2AX at M phase in human cells without DNA damage response. Biochem. Biophys. Res. Commun. *336*, 807–812.

Jackman, M., Lindon, C., Nigg, E.A., and Pines, J. (2003). Active cyclin B1-Cdk1 first appears on centrosomes in prophase. Nat. Cell Biol. *5*, 143–148.

Jazayeri, A., Falck, J., Lukas, C., Bartek, J., Smith, G.C.M., Lukas, J., and Jackson, S.P. (2006). ATM- and cell cycle-dependent regulation of ATR in response to DNA double-strand breaks. Nat. Cell Biol. *8*, 37–45.

Jones, K.T. (2005). Mammalian egg activation: from Ca2+ spiking to cell cycle progression. Reprod. Camb. Engl. *130*, 813–823.

Kalab, P., Pu, R.T., and Dasso, M. (1999). The ran GTPase regulates mitotic spindle assembly. Curr. Biol. CB *9*, 481–484.

Kalous, J., Solc, P., Baran, V., Kubelka, M., Schultz, R.M., and Motlik, J. (2006). PKB/AKT is involved in resumption of meiosis in mouse oocytes. Biol. Cell Auspices Eur. Cell Biol. Organ. *98*, 111–123.

Kang, J., Bronson, R.T., and Xu, Y. (2002). Targeted disruption of NBS1 reveals its roles in mouse development and DNA repair. EMBO J. *21*, 1447–1455.

Katis, V.L., Lipp, J.J., Imre, R., Bogdanova, A., Okaz, E., Habermann, B., Mechtler, K., Nasmyth, K., and Zachariae, W. (2010). Rec8 phosphorylation by casein kinase 1 and Cdc7-Dbf4 kinase regulates cohesin cleavage by separase during meiosis. Dev. Cell *18*, 397–409.

Keeney, S., and Neale, M.J. (2006). Initiation of meiotic recombination by formation of DNA double-strand breaks: mechanism and regulation. Biochem. Soc. Trans. *34*, 523–525.

Kitajima, T.S., Sakuno, T., Ishiguro, K., Iemura, S., Natsume, T., Kawashima, S.A., and Watanabe, Y. (2006). Shugoshin collaborates with protein phosphatase 2A to protect cohesin. Nature *441*, 46–52.

Kitajima, T.S., Ohsugi, M., and Ellenberg, J. (2011). Complete kinetochore tracking reveals error-prone homologous chromosome biorientation in mammalian oocytes. Cell *146*, 568–581.

Kolano, A., Brunet, S., Silk, A.D., Cleveland, D.W., and Verlhac, M.-H. (2012). Error-prone mammalian female meiosis from silencing the spindle assembly checkpoint without normal interkinetochore tension. Proc. Natl. Acad. Sci. U. S. A. *109*, E1858–E1867.

Kudo, N.R., Wassmann, K., Anger, M., Schuh, M., Wirth, K.G., Xu, H., Helmhart, W., Kudo, H., McKay, M., Maro, B., et al. (2006). Resolution of chiasmata in oocytes requires separase-mediated proteolysis. Cell *126*, 135–146.

Kudo, N.R., Anger, M., Peters, A.H.F.M., Stemmann, O., Theussl, H.-C., Helmhart, W., Kudo, H., Heyting, C., and Nasmyth, K. (2009). Role of cleavage by separase of the Rec8 kleisin subunit of cohesin during mammalian meiosis I. J. Cell Sci. *122*, 2686–2698.

Kujjo, L.L., Laine, T., Pereira, R.J.G., Kagawa, W., Kurumizaka, H., Yokoyama, S., and Perez, G.I. (2010). Enhancing survival of mouse oocytes following chemotherapy or aging by targeting Bax and Rad51. PloS One *5*, e9204.

Lamarche, B.J., Orazio, N.I., and Weitzman, M.D. (2010). The MRN complex in Double-Strand Break Repair and Telomere Maintenance. FEBS Lett. *584*, 3682–3695.

Lampson, M.A., and Cheeseman, I.M. (2011). Sensing centromere tension: Aurora B and the regulation of kinetochore function. Trends Cell Biol. *21*, 133–140.

Lane, H.A., and Nigg, E.A. (1996). Antibody microinjection reveals an essential role for human polo-like kinase 1 (Plk1) in the functional maturation of mitotic centrosomes. J. Cell Biol. *135*, 1701–1713.

Lane, S.I.R., and Jones, K.T. (2014). Non-canonical function of spindle assembly checkpoint proteins after APC activation reduces aneuploidy in mouse oocytes. Nat. Commun. *5*.

Lane, S.I.R., Yun, Y., and Jones, K.T. (2012). Timing of anaphase-promoting complex activation in mouse oocytes is predicted by microtubule-kinetochore attachment but not by bivalent alignment or tension. Dev. Camb. Engl. *139*, 1947–1955.

Laurell, E., Beck, K., Krupina, K., Theerthagiri, G., Bodenmiller, B., Horvath, P., Aebersold, R., Antonin, W., and Kutay, U. (2011). Phosphorylation of Nup98 by multiple kinases is crucial for NPC disassembly during mitotic entry. Cell *144*, 539–550.

Leader, B., Lim, H., Carabatsos, M.J., Harrington, A., Ecsedy, J., Pellman, D., Maas, R., and Leder, P. (2002). Formin-2, polyploidy, hypofertility and positioning of the meiotic spindle in mouse oocytes. Nat. Cell Biol. *4*, 921–928.

Lee, J.-H., and Paull, T.T. (2004). Direct activation of the ATM protein kinase by the Mre11/Rad50/Nbs1 complex. Science *304*, 93–96.

Lee, D.-H., Acharya, S.S., Kwon, M., Drane, P., Guan, Y., Adelmant, G., Kalev, P., Shah, J., Pellman, D., Marto, J.A., et al. (2014). Dephosphorylation enables the recruitment of 53BP1 to double-strand DNA breaks. Mol. Cell *54*, 512–525.

Lee, J., Iwai, T., Yokota, T., and Yamashita, M. (2003). Temporally and spatially selective loss of Rec8 protein from meiotic chromosomes during mammalian meiosis. J. Cell Sci. *116*, 2781–2790.

Lénárt, P., and Ellenberg, J. (2003). Nuclear envelope dynamics in oocytes: from germinal vesicle breakdown to mitosis. Curr. Opin. Cell Biol. *15*, 88–95.

Lénárt, P., Petronczki, M., Steegmaier, M., Di Fiore, B., Lipp, J.J., Hoffmann, M., Rettig, W.J., Kraut, N., and Peters, J.-M. (2007). The small-molecule inhibitor BI 2536 reveals novel insights into mitotic roles of polo-like kinase 1. Curr. Biol. CB *17*, 304–315.

Lewandoski, M., Wassarman, K.M., and Martin, G.R. (1997). Zp3-cre, a transgenic mouse line for the activation or inactivation of loxP-flanked target genes specifically in the female germ line. Curr. Biol. CB *7*, 148–151.

Li, H., Liu, X.S., Yang, X., Song, B., Wang, Y., and Liu, X. (2010). Polo-like kinase 1 phosphorylation of p150Glued facilitates nuclear envelope breakdown during prophase. Proc. Natl. Acad. Sci. U. S. A. *107*, 14633–14638.

Li, M., Li, S., Yuan, J., Wang, Z.-B., Sun, S.-C., Schatten, H., and Sun, Q.-Y. (2009). Bub3 is a spindle assembly checkpoint protein regulating chromosome segregation during mouse oocyte meiosis. PloS One *4*, e7701.

Li, X.-M., Yu, C., Wang, Z.-W., Zhang, Y.-L., Liu, X.-M., Zhou, D., Sun, Q.-Y., and Fan, H.-Y. (2013). DNA Topoisomerase II Is Dispensable for Oocyte Meiotic Resumption but Is Essential for Meiotic Chromosome Condensation and Separation in Mice. Biol. Reprod. *89*, 118.

Lin, F., Ma, X.-S., Wang, Z.-B., Wang, Z.-W., Luo, Y.-B., Huang, L., Jiang, Z.-Z., Hu, M.-W., Schatten, H., and Sun, Q.-Y. (2014). Different fates of oocytes with DNA double-strand breaks *in vitro* and *in vivo*. Cell Cycle *13*, 2674–2680.

Lincoln, A.J., Wickramasinghe, D., Stein, P., Schultz, R.M., Palko, M.E., De Miguel, M.P., Tessarollo, L., and Donovan, P.J. (2002). Cdc25b phosphatase is required for resumption of meiosis during oocyte maturation. Nat. Genet. *30*, 446–449.

Lindqvist, A., Rodríguez-Bravo, V., and Medema, R.H. (2009). The decision to enter mitosis: feedback and redundancy in the mitotic entry network. J. Cell Biol. *185*, 193–202.

Littlepage, L.E., Wu, H., Andresson, T., Deanehan, J.K., Amundadottir, L.T., and Ruderman, J.V. (2002). Identification of phosphorylated residues that affect the activity of the mitotic kinase Aurora-A. Proc. Natl. Acad. Sci. U. S. A. *99*, 15440–15445.

Liu, L., and Keefe, D.L. (2008). Defective cohesin is associated with age-dependent misaligned chromosomes in oocytes. Reprod. Biomed. Online *16*, 103–112.

Liu, D., Davydenko, O., and Lampson, M.A. (2012). Polo-like kinase-1 regulates kinetochore–microtubule dynamics and spindle checkpoint silencing. J. Cell Biol. *198*, 491–499.

Liu, J., Lewellyn, A.L., Chen, L.G., and Maller, J.L. (2004). The polo box is required for multiple functions of Plx1 in mitosis. J. Biol. Chem. *279*, 21367–21373.

Llano, E., Gómez, R., Gutiérrez-Caballero, C., Herrán, Y., Sánchez-Martín, M., Vázquez-Quiñones, L., Hernández, T., de Alava, E., Cuadrado, A., Barbero, J.L., et al. (2008). Shugoshin-2 is essential for the completion of meiosis but not for mitotic cell division in mice. Genes Dev. *22*, 2400–2413.

Lobjois, V., Jullien, D., Bouché, J.-P., and Ducommun, B. (2009). The polo-like kinase 1 regulates CDC25B-dependent mitosis entry. Biochim. Biophys. Acta *1793*, 462–468.

Longo, F.J., and Chen, D.Y. (1985). Development of cortical polarity in mouse eggs: involvement of the meiotic apparatus. Dev. Biol. *107*, 382–394.

Luisier, F., Blu, T., and Unser, M. (2011). Image denoising in mixed Poisson-Gaussian noise. IEEE Trans. Image Process. Publ. IEEE Signal Process. Soc. *20*, 696–708.

Lukas, C., Falck, J., Bartkova, J., Bartek, J., and Lukas, J. (2003). Distinct spatiotemporal dynamics of mammalian checkpoint regulators induced by DNA damage. Nat. Cell Biol. *5*, 255–260.

Luo, Y.-B., and Kim, N.-H. (2015). PLK4 is essential for meiotic resumption in mouse oocytes. Biol. Reprod. *92*, 101.

Ma, J.-Y., Ou Yang, Y.-C., Wang, Z.-W., Wang, Z.-B., Jiang, Z.-Z., Luo, S.-M., Hou, Y., Liu, Z.-H., Schatten, H., and Sun, Q.-Y. (2013). The effects of DNA double-strand breaks on mouse oocyte meiotic maturation. Cell Cycle Georget. Tex *12*, 1233–1241.

Ma, Y., Pannicke, U., Schwarz, K., and Lieber, M.R. (2002). Hairpin opening and overhang processing by an Artemis/DNA-dependent protein kinase complex in nonhomologous end joining and V(D)J recombination. Cell *108*, 781–794.

Macůrek, L., Lindqvist, A., Lim, D., Lampson, M.A., Klompmaker, R., Freire, R., Clouin, C., Taylor, S.S., Yaffe, M.B., and Medema, R.H. (2008). Polo-like kinase-1 is activated by aurora A to promote checkpoint recovery. Nature *455*, 119–123.

Macurek, L., Lindqvist, A., and Medema, R.H. (2009). Aurora-A and hBora join the game of Polo. Cancer Res. *69*, 4555–4558.

Madgwick, S., and Jones, K.T. (2007). How eggs arrest at metaphase II: MPF stabilisation plus APC/C inhibition equals Cytostatic Factor. Cell Div. *2*, 4.

Mahaney, B.L., Meek, K., and Lees-Miller, S.P. (2009). Repair of ionizing radiation-induced DNA double-strand breaks by non-homologous end-joining. Biochem. J. *417*, 639–650.

Mailand, N., Falck, J., Lukas, C., Syljuâsen, R.G., Welcker, M., Bartek, J., and Lukas, J. (2000). Rapid destruction of human Cdc25A in response to DNA damage. Science *288*, 1425–1429.

Mailhes, J.B., Marchetti, F., Phillips, G.L., and Barnhill, D.R. (1994). Preferential pericentric lesions and aneuploidy induced in mouse oocytes by the topoisomerase II inhibitor etoposide. Teratog. Carcinog. Mutagen. *14*, 39–51.

Mallette, F.A., Mattiroli, F., Cui, G., Young, L.C., Hendzel, M.J., Mer, G., Sixma, T.K., and Richard, S. (2012). RNF8- and RNF168-dependent degradation of KDM4A/JMJD2A triggers 53BP1 recruitment to DNA damage sites. EMBO J. *31*, 1865–1878.

Mao, Z., Bozzella, M., Seluanov, A., and Gorbunova, V. (2008). Comparison of nonhomologous end joining and homologous recombination in human cells. DNA Repair *7*, 1765–1771.

Marangos, P., and Carroll, J. (2004). The dynamics of cyclin B1 distribution during meiosis I in mouse oocytes. Reprod. Camb. Engl. *128*, 153–162.

Marangos, P., and Carroll, J. (2012). Oocytes progress beyond prophase in the presence of DNA damage. Curr. Biol. CB *22*, 989–994.

Marangos, P., Verschuren, E.W., Chen, R., Jackson, P.K., and Carroll, J. (2007). Prophase I arrest and progression to metaphase I in mouse oocytes are controlled by Emi1-dependent regulation of APC(Cdh1). J. Cell Biol. *176*, 65–75.

Marko, J.F., and Siggia, E.D. (1997). Polymer Models of Meiotic and Mitotic Chromosomes. Mol. Biol. Cell *8*, 2217–2231.

Marston, A.L., and Amon, A. (2004). Meiosis: cell-cycle controls shuffle and deal. Nat. Rev. Mol. Cell Biol. *5*, 983–997.

Martín, M., Terradas, M., Hernández, L., and Genescà, A. (2014). γH2AX foci on apparently intact mitotic chromosomes: not signatures of misrejoining events but signals of unresolved DNA damage. Cell Cycle Georget. Tex *13*, 3026–3036.

Marumoto, T., Honda, S., Hara, T., Nitta, M., Hirota, T., Kohmura, E., and Saya, H. (2003). Aurora-A kinase maintains the fidelity of early and late mitotic events in HeLa cells. J. Biol. Chem. *278*, 51786–51795.

Masciarelli, S., Horner, K., Liu, C., Park, S.H., Hinckley, M., Hockman, S., Nedachi, T., Jin, C., Conti, M., and Manganiello, V. (2004). Cyclic nucleotide phosphodiesterase 3A-deficient mice as a model of female infertility. J. Clin. Invest. *114*, 196–205.

Masui, Y., and Pedersen, R.A. (1975). Ultraviolet light-induced unscheduled DNA synthesis in mouse oocytes during meiotic maturation. Nature *257*, 705–706.

Matson, S., Markoulaki, S., and Ducibella, T. (2006). Antagonists of myosin light chain kinase and of myosin II inhibit specific events of egg activation in fertilized mouse eggs. Biol. Reprod. *74*, 169–176.

McGuinness, B.E., Anger, M., Kouznetsova, A., Gil-Bernabé, A.M., Helmhart, W., Kudo, N.R., Wuensche, A., Taylor, S., Hoog, C., Novak, B., et al. (2009). Regulation of APC/C activity in oocytes by a Bub1-dependent spindle assembly checkpoint. Curr. Biol. CB *19*, 369–380.

McLaren, A., and Southee, D. (1997). Entry of mouse embryonic germ cells into meiosis. Dev. Biol. *187*, 107–113.

McManus, K.J., and Hendzel, M.J. (2005). ATM-dependent DNA damage-independent mitotic phosphorylation of H2AX in normally growing mammalian cells. Mol. Biol. Cell *16*, 5013–5025.

Meek, K., Dang, V., and Lees-Miller, S.P. (2008). DNA-PK: the means to justify the ends? Adv. Immunol. *99*, 33–58.

Mehlmann, L.M., Jones, T.L.Z., and Jaffe, L.A. (2002). Meiotic arrest in the mouse follicle maintained by a Gs protein in the oocyte. Science *297*, 1343–1345.

Mehta, A., and Haber, J.E. (2014). Sources of DNA double-strand breaks and models of recombinational DNA repair. Cold Spring Harb. Perspect. Biol. *6*, a016428.

Miao, Y.-L., Stein, P., Jefferson, W.N., Padilla-Banks, E., and Williams, C.J. (2012). Calcium influx-mediated signaling is required for complete mouse egg activation. Proc. Natl. Acad. Sci. U. S. A. *109*, 4169–4174.

Mimitou, E.P., and Symington, L.S. (2009). DNA end resection: many nucleases make light work. DNA Repair *8*, 983–995.

Mitra, J., and Schultz, R.M. (1996). Regulation of the acquisition of meiotic competence in the mouse: changes in the subcellular localization of cdc2, cyclin B1, cdc25C and wee1, and in the concentration of these proteins and their transcripts. J. Cell Sci. *109 (Pt 9)*, 2407–2415.

Miyara, F., Migne, C., Dumont-Hassan, M., Le Meur, A., Cohen-Bacrie, P., Aubriot, F.-X., Glissant, A., Nathan, C., Douard, S., Stanovici, A., et al. (2003). Chromatin configuration and transcriptional control in human and mouse oocytes. Mol. Reprod. Dev. *64*, 458–470.

Montgomery, E., Wilentz, R.E., Argani, P., Fisher, C., Hruban, R.H., Kern, S.E., and Lengauer, C. (2003). Analysis of anaphase figures in routine histologic sections distinguishes chromosomally unstable from chromosomally stable malignancies. Cancer Biol. Ther. *2*, 248–252.

Moreno-Herrero, F., de Jager, M., Dekker, N.H., Kanaar, R., Wyman, C., and Dekker, C. (2005). Mesoscale conformational changes in the DNA-repair complex Rad50/Mre11/Nbs1 upon binding DNA. Nature *437*, 440–443.

Munné, S., Grifo, J., Cohen, J., and Weier, H.U. (1994). Chromosome abnormalities in human arrested preimplantation embryos: a multiple-probe FISH study. Am. J. Hum. Genet. *55*, 150–159.

Musacchio, A., and Salmon, E.D. (2007). The spindle-assembly checkpoint in space and time. Nat. Rev. Mol. Cell Biol. *8*, 379–393.

Nabti, I., Marangos, P., Bormann, J., Kudo, N.R., and Carroll, J. (2014). Dual-mode regulation of the APC/C by CDK1 and MAPK controls meiosis I progression and fidelity. J. Cell Biol. *204*, 891–900.

Nakajima, H., Toyoshima-Morimoto, F., Taniguchi, E., and Nishida, E. (2003). Identification of a consensus motif for Plk (Polo-like kinase) phosphorylation reveals Myt1 as a Plk1 substrate. J. Biol. Chem. *278*, 25277–25280.

Neale, M.J., Pan, J., and Keeney, S. (2005). Endonucleolytic processing of covalent protein-linked DNA double-strand breaks. Nature *436*, 1053–1057.

Nelson, G., Buhmann, M., and Zglinicki, T. von (2009). DNA damage foci in mitosis are devoid of 53BP1. Cell Cycle Georget. Tex *8*, 3379–3383.

Nixon, V.L., Levasseur, M., McDougall, A., and Jones, K.T. (2002). Ca(2+) oscillations promote APC/C-dependent cyclin B1 degradation during metaphase arrest and completion of meiosis in fertilizing mouse eggs. Curr. Biol. CB *12*, 746–750.

Norris, R.P., Ratzan, W.J., Freudzon, M., Mehlmann, L.M., Krall, J., Movsesian, M.A., Wang, H., Ke, H., Nikolaev, V.O., and Jaffe, L.A. (2009). Cyclic GMP from the surrounding somatic cells regulates cyclic AMP and meiosis in the mouse oocyte. Dev. Camb. Engl. *136*, 1869–1878.

Nurse, P. (1997). Checkpoint pathways come of age. Cell *91*, 865–867.

Oatley, J., and Hunt, P.A. (2012). Of mice and (wo)men: purified oogonial stem cells from mouse and human ovaries. Biol. Reprod. *86*, 196.

Oh, J.S., Han, S.J., and Conti, M. (2010). Wee1B, Myt1, and Cdc25 function in distinct compartments of the mouse oocyte to control meiotic resumption. J. Cell Biol. *188*, 199–207.

Oh, J.S., Susor, A., and Conti, M. (2011). Protein tyrosine kinase Wee1B is essential for metaphase II exit in mouse oocytes. Science *332*, 462–465.

Oh, J.S., Susor, A., Schindler, K., Schultz, R.M., and Conti, M. (2013). Cdc25A activity is required for the metaphase II arrest in mouse oocytes. J. Cell Sci. *126*, 1081–1085.

O'Keefe, S.J., Wolfes, H., Kiessling, A.A., and Cooper, G.M. (1989). Microinjection of antisense c-mos oligonucleotides prevents meiosis II in the maturing mouse egg. Proc. Natl. Acad. Sci. U. S. A. *86*, 7038–7042.

Orthwein, A., Fradet-Turcotte, A., Noordermeer, S.M., Canny, M.D., Brun, C.M., Strecker, J., Escribano-Diaz, C., and Durocher, D. (2014). Mitosis inhibits DNA double-strand break repair to guard against telomere fusions. Science *344*, 189–193.

Otsuki, J., Nagai, Y., and Chiba, K. (2009). Association of spindle midzone particles with polo-like kinase 1 during meiosis in mouse and human oocytes. Reprod. Biomed. Online *18*, 522–528.

Pahlavan, G., Polanski, Z., Kalab, P., Golsteyn, R., Nigg, E.A., and Maro, B. (2000). Characterization of polo-like kinase 1 during meiotic maturation of the mouse oocyte. Dev. Biol. *220*, 392–400.

Panigone, S., Hsieh, M., Fu, M., Persani, L., and Conti, M. (2008). Luteinizing Hormone Signaling in Preovulatory Follicles Involves Early Activation of the Epidermal Growth Factor Receptor Pathway. Mol. Endocrinol. *22*, 924–936.

Park, J.-Y., Su, Y.-Q., Ariga, M., Law, E., Jin, S.-L.C., and Conti, M. (2004). EGF-like growth factors as mediators of LH action in the ovulatory follicle. Science *303*, 682–684.

Peng, X.R., Hsueh, A.J., LaPolt, P.S., Bjersing, L., and Ny, T. (1991). Localization of luteinizing hormone receptor messenger ribonucleic acid expression in ovarian cell types during follicle development and ovulation. Endocrinology *129*, 3200–3207.

Pesce, M., and De Felici, M. (1994). Apoptosis in mouse primordial germ cells: a study by transmission and scanning electron microscope. Anat. Embryol. (Berl.) *189*, 435–440.

Peset, I., Seiler, J., Sardon, T., Bejarano, L.A., Rybina, S., and Vernos, I. (2005). Function and regulation of Maskin, a TACC family protein, in microtubule growth during mitosis. J. Cell Biol. *170*, 1057–1066.

Pines, J. (1999). Four-dimensional control of the cell cycle. Nat. Cell Biol. *1*, E73–E79.

Pirino, G., Wescott, M.P., and Donovan, P.J. (2009). Protein kinase A regulates resumption of meiosis by phosphorylation of Cdc25B in mammalian oocytes. Cell Cycle Georget. Tex *8*, 665–670.

Pittman, D.L., Cobb, J., Schimenti, K.J., Wilson, L.A., Cooper, D.M., Brignull, E., Handel, M.A., and Schimenti, J.C. (1998). Meiotic prophase arrest with failure of chromosome synapsis in mice deficient for Dmc1, a germline-specific RecA homolog. Mol. Cell *1*, 697–705.

Pomerantz, Y., Elbaz, J., Ben-Eliezer, I., Reizel, Y., David, Y., Galiani, D., Nevo, N., Navon, A., and Dekel, N. (2012). From ubiquitin-proteasomal degradation to CDK1 inactivation: requirements for the first polar body extrusion in mouse oocytes. FASEB J. Off. Publ. Fed. Am. Soc. Exp. Biol. *26*, 4495–4505.

Rass, E., Grabarz, A., Plo, I., Gautier, J., Bertrand, P., and Lopez, B.S. (2009). Role of Mre11 in chromosomal nonhomologous end joining in mammalian cells. Nat. Struct. Mol. Biol. *16*, 819–824.

Reimann, J.D.R., and Jackson, P.K. (2002). Emi1 is required for cytostatic factor arrest in vertebrate eggs. Nature *416*, 850–854.

Reimann, J.D., Freed, E., Hsu, J.Y., Kramer, E.R., Peters, J.M., and Jackson, P.K. (2001). Emi1 is a mitotic regulator that interacts with Cdc20 and inhibits the anaphase promoting complex. Cell *105*, 645–655.

Rein, K., and Stracker, T.H. (2014). The MRE11 complex: an important source of stress relief. Exp. Cell Res. *329*, 162–169.

Revenkova, E., Herrmann, K., Adelfalk, C., and Jessberger, R. (2010). Oocyte cohesin expression restricted to predictyate stages provides full fertility and prevents aneuploidy. Curr. Biol. CB *20*, 1529–1533.

Richardson, S.J., Senikas, V., and Nelson, J.F. (1987). Follicular depletion during the menopausal transition: evidence for accelerated loss and ultimate exhaustion. J. Clin. Endocrinol. Metab. *65*, 1231–1237.

Rieder, C.L., and Cole, R.W. (1998). Entry into mitosis in vertebrate somatic cells is guarded by a chromosome damage checkpoint that reverses the cell cycle when triggered during early but not late prophase. J. Cell Biol. *142*, 1013–1022.

Roberts, S.A., Strande, N., Burkhalter, M.D., Strom, C., Havener, J.M., Hasty, P., and Ramsden, D.A. (2010). Ku is a 5'-dRP/AP lyase that excises nucleotide damage near broken ends. Nature *464*, 1214–1217.

Roeder, G.S., and Bailis, J.M. (2000). The pachytene checkpoint. Trends Genet. TIG *16*, 395–403.

Rogakou, E.P., Pilch, D.R., Orr, A.H., Ivanova, V.S., and Bonner, W.M. (1998). DNA Double-stranded Breaks Induce Histone H2AX Phosphorylation on Serine 139. J. Biol. Chem. *273*, 5858–5868.

Rogakou, E.P., Boon, C., Redon, C., and Bonner, W.M. (1999). Megabase Chromatin Domains Involved in DNA Double-Strand Breaks in Vivo. J. Cell Biol. *146*, 905–916.

Roller, R.J., Kinloch, R.A., Hiraoka, B.Y., Li, S.S., and Wassarman, P.M. (1989). Gene expression during mammalian oogenesis and early embryogenesis: quantification of three messenger RNAs abundant in fully grown mouse oocytes. Dev. Camb. Engl. *106*, 251–261.

Roques, C., Coulombe, Y., Delannoy, M., Vignard, J., Grossi, S., Brodeur, I., Rodrigue, A., Gautier, J., Stasiak, A.Z., Stasiak, A., et al. (2009). MRE11-RAD50-NBS1 is a critical regulator of FANCD2 stability and function during DNA double-strand break repair. EMBO J. *28*, 2400–2413.

Rozier, L., Guo, Y., Peterson, S., Sato, M., Baer, R., Gautier, J., and Mao, Y. (2013). The MRN-CtIP pathway is required for metaphase chromosome alignment. Mol. Cell *49*, 1097–1107.

Sakakibara, Y., Hashimoto, S., Nakaoka, Y., Kouznetsova, A., Höög, C., and Kitajima, T.S. (2015). Bivalent separation into univalents precedes age-related meiosis I errors in oocytes. Nat. Commun. *6*, 7550.

Sanfins, A., Lee, G.Y., Plancha, C.E., Overstrom, E.W., and Albertini, D.F. (2003). Distinctions in meiotic spindle structure and assembly during in vitro and in vivo maturation of mouse oocytes. Biol. Reprod. *69*, 2059–2067.

Santamaria, A., Neef, R., Eberspächer, U., Eis, K., Husemann, M., Mumberg, D., Prechtl, S., Schulze, V., Siemeister, G., Wortmann, L., et al. (2007). Use of the novel Plk1 inhibitor ZK-thiazolidinone to elucidate functions of Plk1 in early and late stages of mitosis. Mol. Biol. Cell *18*, 4024–4036.

Santamaria, A., Wang, B., Elowe, S., Malik, R., Zhang, F., Bauer, M., Schmidt, A., Silljé, H.H.W., Körner, R., and Nigg, E.A. (2011). The Plk1-dependent phosphoproteome of the early mitotic spindle. Mol. Cell. Proteomics MCP *10*, M110.004457.

Sartori, A.A., Lukas, C., Coates, J., Mistrik, M., Fu, S., Bartek, J., Baer, R., Lukas, J., and Jackson, S.P. (2007). Human CtIP promotes DNA end resection. Nature *450*, 509–514.

Saskova, A., Solc, P., Baran, V., Kubelka, M., Schultz, R.M., and Motlik, J. (2008). Aurora kinase A controls meiosis I progression in mouse oocytes. Cell Cycle Georget. Tex *7*, 2368–2376.

Sato, E., and Koide, S.S. (1984). Forskolin and mouse oocyte maturation in vitro. J. Exp. Zool. *230*, 125–129.

Schindelin, J., Arganda-Carreras, I., Frise, E., Kaynig, V., Longair, M., Pietzsch, T., Preibisch, S., Rueden, C., Saalfeld, S., Schmid, B., et al. (2012). Fiji: an open-source platform for biological-image analysis. Nat. Methods *9*, 676–682.

Schmitt, A., and Nebreda, A.R. (2002). Inhibition of Xenopus oocyte meiotic maturation by catalytically inactive protein kinase A. Proc. Natl. Acad. Sci. U. S. A. *99*, 4361–4366.

Schneider, M.R., and Wolf, E. (2009). The epidermal growth factor receptor ligands at a glance. J. Cell. Physiol. *218*, 460–466.

Schuh, M., and Ellenberg, J. (2007). Self-organization of MTOCs replaces centrosome function during acentrosomal spindle assembly in live mouse oocytes. Cell *130*, 484–498.

Schuh, M., and Ellenberg, J. (2008). A new model for asymmetric spindle positioning in mouse oocytes. Curr. Biol. CB *18*, 1986–1992.

Schultz, R.M., Montgomery, R.R., and Belanoff, J.R. (1983). Regulation of mouse oocyte meiotic maturation: implication of a decrease in oocyte cAMP and protein dephosphorylation in commitment to resume meiosis. Dev. Biol. *97*, 264–273.

Sebestova, J., Danylevska, A., Novakova, L., Kubelka, M., and Anger, M. (2012). Lack of response to unaligned chromosomes in mammalian female gametes. Cell Cycle *11*, 3011–3018.

Seki, A., Coppinger, J.A., Jang, C.-Y., Yates, J.R., and Fang, G. (2008). Bora and the Kinase Aurora A Cooperatively Activate the Kinase Plk1 and Control Mitotic Entry. Science *320*, 1655–1658.

Sela-Abramovich, S., Edry, I., Galiani, D., Nevo, N., and Dekel, N. (2006). Disruption of gap junctional communication within the ovarian follicle induces oocyte maturation. Endocrinology *147*, 2280–2286.

Sharif, B., Na, J., Lykke-Hartmann, K., McLaughlin, S.H., Laue, E., Glover, D.M., and Zernicka-Goetz, M. (2010). The chromosome passenger complex is required for fidelity of chromosome transmission and cytokinesis in meiosis of mouse oocytes. J. Cell Sci. *123*, 4292–4300.

Sharma, A., Singh, K., and Almasan, A. (2012). Histone H2AX phosphorylation: a marker for DNA damage. Methods Mol. Biol. Clifton NJ *920*, 613–626.

Shen, W., Ahmad, F., Hockman, S., Ma, J., Omi, H., Raghavachari, N., and Manganiello, V. (2010). Female infertility in PDE3A(-/-) mice: polo-like kinase 1 (Plk1) may be a target of protein kinase A (PKA) and involved in meiotic arrest of oocytes from PDE3A(-/-) mice. Cell Cycle Georget. Tex *9*, 4720–4734.

Shibata, A., Moiani, D., Arvai, A.S., Perry, J.J.P., Harding, S.M., Genois, M.-M., Maity, R., van Rossum-Fikkert, S., Kertokalio, A., Romoli, F., et al. (2014). DNA Double Strand Break Repair Pathway Choice Is Directed by Distinct MRE11 Nuclease Activities. Mol. Cell *53*, 7–18.

Shrivastav, M., De Haro, L.P., and Nickoloff, J.A. (2008). Regulation of DNA double-strand break repair pathway choice. Cell Res. *18*, 134–147.

Shuda, K., Schindler, K., Ma, J., Schultz, R.M., and Donovan, P.J. (2009). Aurora kinase B modulates chromosome alignment in mouse oocytes. Mol. Reprod. Dev. *76*, 1094–1105.

Solc, P., Saskova, A., Baran, V., Kubelka, M., Schultz, R.M., and Motlik, J. (2008). CDC25A phosphatase controls meiosis I progression in mouse oocytes. Dev. Biol. *317*, 260–269.

Solc, P., Schultz, R.M., and Motlik, J. (2010). Prophase I arrest and progression to metaphase I in mouse oocytes: comparison of resumption of meiosis and recovery from G2-arrest in somatic cells. Mol. Hum. Reprod. *16*, 654–664.

Soleimani, R., Heytens, E., Darzynkiewicz, Z., and Oktay, K. (2011). Mechanisms of chemotherapy-induced human ovarian aging: double strand DNA breaks and microvascular compromise. Aging *3*, 782–793.

Solomon, M.J., Glotzer, M., Lee, T.H., Philippe, M., and Kirschner, M.W. (1990). Cyclin activation of p34cdc2. Cell *63*, 1013–1024.

Soutoglou, E., and Misteli, T. (2008). Activation of the cellular DNA damage response in the absence of DNA lesions. Science *320*, 1507–1510.

Stewart, G.S., Maser, R.S., Stankovic, T., Bressan, D.A., Kaplan, M.I., Jaspers, N.G., Raams, A., Byrd, P.J., Petrini, J.H., and Taylor, A.M. (1999). The DNA double-strand break repair gene hMRE11 is mutated in individuals with an ataxia-telangiectasia-like disorder. Cell *99*, 577–587.

Stiff, T., O'Driscoll, M., Rief, N., Iwabuchi, K., Löbrich, M., and Jeggo, P.A. (2004). ATM and DNA-PK function redundantly to phosphorylate H2AX after exposure to ionizing radiation. Cancer Res. *64*, 2390–2396.

Stracker, T.H., and Petrini, J.H.J. (2011). The MRE11 complex: starting from the ends. Nat. Rev. Mol. Cell Biol. *12*, 90–103.

Stracker, T.H., Theunissen, J.-W.F., Morales, M., and Petrini, J.H.J. (2004). The Mre11 complex and the metabolism of chromosome breaks: the importance of communicating and holding things together. DNA Repair *3*, 845–854.

Stucki, M., and Jackson, S.P. (2004). MDC1/NFBD1: a key regulator of the DNA damage response in higher eukaryotes. DNA Repair *3*, 953–957.

Stucki, M., and Jackson, S.P. (2006). gammaH2AX and MDC1: anchoring the DNA-damage-response machinery to broken chromosomes. DNA Repair *5*, 534–543.

Stucki, M., Clapperton, J.A., Mohammad, D., Yaffe, M.B., Smerdon, S.J., and Jackson, S.P. (2005). MDC1 directly binds phosphorylated histone H2AX to regulate cellular responses to DNA double-strand breaks. Cell *123*, 1213–1226.

Suh, E.-K., Yang, A., Kettenbach, A., Bamberger, C., Michaelis, A.H., Zhu, Z., Elvin, J.A., Bronson, R.T., Crum, C.P., and McKeon, F. (2006). p63 protects the female germ line during meiotic arrest. Nature *444*, 624–628.

Sulli, G., Di Micco, R., and di Fagagna, F. d'Adda (2012). Crosstalk between chromatin state and DNA damage response in cellular senescence and cancer. Nat. Rev. Cancer *12*, 709–720.

Sumara, I., Giménez-Abián, J.F., Gerlich, D., Hirota, T., Kraft, C., la Torre, C. de, Ellenberg, J., and Peters, J.-M. (2004). Roles of polo-like kinase 1 in the assembly of functional mitotic spindles. Curr. Biol. CB *14*, 1712–1722.

Sun, S.-C., Wang, Z.-B., Xu, Y.-N., Lee, S.-E., Cui, X.-S., and Kim, N.-H. (2011). Arp2/3 complex regulates asymmetric division and cytokinesis in mouse oocytes. PloS One *6*, e18392.

Sun, S.-C., Liu, H.-L., and Sun, Q.-Y. (2012). Survivin regulates Plk1 localization to kinetochore in mouse oocyte meiosis. Biochem. Biophys. Res. Commun. *421*, 797–800.

Szollosi, D., Calarco, P., and Donahue, R.P. (1972). Absence of centrioles in the first and second meiotic spindles of mouse oocytes. J. Cell Sci. *11*, 521–541.

Tachibana-Konwalski, K., Godwin, J., van der Weyden, L., Champion, L., Kudo, N.R., Adams, D.J., and Nasmyth, K. (2010). Rec8-containing cohesin maintains bivalents without turnover during the growing phase of mouse oocytes. Genes Dev. *24*, 2505–2516.

Tachibana-Konwalski, K., Godwin, J., Borsos, M., Rattani, A., Adams, D.J., and Nasmyth, K. (2013). Spindle Assembly Checkpoint of Oocytes Depends on a Kinetochore Structure Determined by Cohesin in Meiosis I. Curr. Biol. *23*, 2534–2539.

Takata, M., Sasaki, M.S., Sonoda, E., Morrison, C., Hashimoto, M., Utsumi, H., Yamaguchi-Iwai, Y., Shinohara, A., and Takeda, S. (1998). Homologous recombination and non-homologous end-joining pathways of DNA double-strand break repair have overlapping roles in the maintenance of chromosomal integrity in vertebrate cells. EMBO J. *17*, 5497–5508.

Tan, J.-H., Wang, H.-L., Sun, X.-S., Liu, Y., Sui, H.-S., and Zhang, J. (2009). Chromatin configurations in the germinal vesicle of mammalian oocytes. Mol. Hum. Reprod. *15*, 1–9.

Tanno, Y., Kitajima, T.S., Honda, T., Ando, Y., Ishiguro, K.-I., and Watanabe, Y. (2010). Phosphorylation of mammalian Sgo2 by Aurora B recruits PP2A and MCAK to centromeres. Genes Dev. *24*, 2169–2179.

Terasawa, M., Shinohara, A., and Shinohara, M. (2014a). Canonical Non-Homologous End Joining in Mitosis Induces Genome Instability and Is Suppressed by M-phase-Specific Phosphorylation of XRCC4. PLoS Genet. *10*.

Terasawa, M., Shinohara, A., and Shinohara, M. (2014b). Double-strand break repair-adox: Restoration of suppressed double-strand break repair during mitosis induces genomic instability. Cancer Sci. *105*, 1519–1525.

Titus, S., Li, F., Stobezki, R., Akula, K., Unsal, E., Jeong, K., Dickler, M., Robson, M., Moy, F., Goswami, S., et al. (2013). Impairment of BRCA1-related DNA double-strand break repair leads to ovarian aging in mice and humans. Sci. Transl. Med. *5*, 172ra21.

Tong, C., Fan, H.-Y., Lian, L., Li, S.-W., Chen, D.-Y., Schatten, H., and Sun, Q.-Y. (2002). Polo-like kinase-1 is a pivotal regulator of microtubule assembly during mouse oocyte meiotic maturation, fertilization, and early embryonic mitosis. Biol. Reprod. *67*, 546–554.

Toyoshima-Morimoto, F., Taniguchi, E., and Nishida, E. (2002). Plk1 promotes nuclear translocation of human Cdc25C during prophase. EMBO Rep. *3*, 341–348.

Tsafriri, A., Chun, S.Y., Zhang, R., Hsueh, A.J., and Conti, M. (1996). Oocyte maturation involves compartmentalization and opposing changes of cAMP levels in follicular somatic and germ cells: studies using selective phosphodiesterase inhibitors. Dev. Biol. *178*, 393–402.

Tsutsumi, M., Fujiwara, R., Nishizawa, H., Ito, M., Kogo, H., Inagaki, H., Ohye, T., Kato, T., Fujii, T., and Kurahashi, H. (2014). Age-related decrease of meiotic cohesins in human oocytes. PloS One *9*, e96710.

Uppangala, S., Dhiman, S., Salian, S.R., Singh, V.J., Kalthur, G., and Adiga, S.K. (2015). In vitro matured oocytes are more susceptible than in vivo matured oocytes to mock ICSI induced functional and genetic changes. PloS One *10*, e0119735.

Uziel, T., Lerenthal, Y., Moyal, L., Andegeko, Y., Mittelman, L., and Shiloh, Y. (2003). Requirement of the MRN complex for ATM activation by DNA damage. EMBO J. *22*, 5612–5621.

Vaccari, S., Horner, K., Mehlmann, L.M., and Conti, M. (2008). Generation of mouse oocytes defective in cAMP synthesis and degradation: endogenous cyclic AMP is essential for meiotic arrest. Dev. Biol. *316*, 124–134.

Vagnarelli, P. (2012). Mitotic chromosome condensation in vertebrates. Exp. Cell Res. *318*, 1435–1441.

Valdiglesias, V., Giunta, S., Fenech, M., Neri, M., and Bonassi, S. (2013). γH2AX as a marker of DNA double strand breaks and genomic instability in human population studies. Mutat. Res. *753*, 24–40.

Velde, E.R. te, Dorland, M., and Broekmans, F.J. (1998). Age at menopause as a marker of reproductive ageing. Maturitas *30*, 119–125.

Verdun, R.E., Crabbe, L., Haggblom, C., and Karlseder, J. (2005). Functional Human Telomeres Are Recognized as DNA Damage in G2 of the Cell Cycle. Mol. Cell *20*, 551–561.

Virant-Klun, I., Stimpfel, M., and Skutella, T. (2012). Stem cells in adult human ovaries: from female fertility to ovarian cancer. Curr. Pharm. Des. *18*, 283–292.

Vogel, G. (2012). Reproductive biology. Potential egg stem cells reignite debate. Science *335*, 1029–1030.

Vogt, E., Kirsch-Volders, M., Parry, J., and Eichenlaub-Ritter, U. (2008). Spindle formation, chromosome segregation and the spindle checkpoint in mammalian oocytes and susceptibility to meiotic error. Mutat. Res. *651*, 14–29.

van Vugt, M.A.T.M., van de Weerdt, B.C.M., Vader, G., Janssen, H., Calafat, J., Klompmaker, R., Wolthuis, R.M.F., and Medema, R.H. (2004a). Polo-like Kinase-1 Is Required for Bipolar Spindle Formation but Is Dispensable for Anaphase Promoting Complex/Cdc20 Activation and Initiation of Cytokinesis. J. Biol. Chem. *279*, 36841–36854.

van Vugt, M.A.T.M., Brás, A., and Medema, R.H. (2004b). Polo-like kinase-1 controls recovery from a G2 DNA damage-induced arrest in mammalian cells. Mol. Cell *15*, 799–811.

van Vugt, M.A.T.M., Gardino, A.K., Linding, R., Ostheimer, G.J., Reinhardt, H.C., Ong, S.-E., Tan, C.S., Miao, H., Keezer, S.M., Li, J., et al. (2010). A mitotic phosphorylation feedback network connects Cdk1, Plk1, 53BP1, and Chk2 to inactivate the G(2)/M DNA damage checkpoint. PLoS Biol. *8*, e1000287.

Wallace, W.H.B., and Kelsey, T.W. (2010). Human Ovarian Reserve from Conception to the Menopause. PLoS ONE *5*, e8772.

Wang, M., Wu, W., Wu, W., Rosidi, B., Zhang, L., Wang, H., and Iliakis, G. (2006). PARP-1 and Ku compete for repair of DNA double strand breaks by distinct NHEJ pathways. Nucleic Acids Res. *34*, 6170–6182.

Ward, I.M., and Chen, J. (2001). Histone H2AX is phosphorylated in an ATR-dependent manner in response to replicational stress. J. Biol. Chem. *276*, 47759–47762.

Wassmann, K. (2013). Sister chromatid segregation in meiosis II. Cell Cycle *12*, 1352–1359.

Wassmann, K., Niault, T., and Maro, B. (2003). Metaphase I arrest upon activation of the Mad2-dependent spindle checkpoint in mouse oocytes. Curr. Biol. CB *13*, 1596–1608.

Watanabe, Y., and Nurse, P. (1999). Cohesin Rec8 is required for reductional chromosome segregation at meiosis. Nature *400*, 461–464.

Watanabe, N., Arai, H., Iwasaki, J.-I., Shiina, M., Ogata, K., Hunter, T., and Osada, H. (2005). Cyclin-dependent kinase (CDK) phosphorylation destabilizes somatic Wee1 via multiple pathways. Proc. Natl. Acad. Sci. U. S. A. *102*, 11663–11668.

Wei, L., Liang, X.-W., Zhang, Q.-H., Li, M., Yuan, J., Li, S., Sun, S.-C., Ouyang, Y.-C., Schatten, H., and Sun, Q.-Y. (2010). BubR1 is a spindle assembly checkpoint protein regulating meiotic cell cycle progression of mouse oocyte. Cell Cycle Georget. Tex *9*, 1112–1121.

White, Y.A.R., Woods, D.C., Takai, Y., Ishihara, O., Seki, H., and Tilly, J.L. (2012). Oocyte formation by mitotically active germ cells purified from ovaries of reproductive-age women. Nat. Med. *18*, 413–421.

Williams, R.S., and Tainer, J.A. (2005). A nanomachine for making ends meet: MRN is a flexing scaffold for the repair of DNA double-strand breaks. Mol. Cell *19*, 724–726.

Williams, R.S., Moncalian, G., Williams, J.S., Yamada, Y., Limbo, O., Shin, D.S., Groocock, L.M., Cahill, D., Hitomi, C., Guenther, G., et al. (2008). Mre11 dimers coordinate DNA end bridging and nuclease processing in double-strand-break repair. Cell *135*, 97–109.

Woodcock, C.L., and Ghosh, R.P. (2010). Chromatin Higher-order Structure and Dynamics. Cold Spring Harb. Perspect. Biol. *2*.

Xiao, Y., and Weaver, D.T. (1997). Conditional gene targeted deletion by Cre recombinase demonstrates the requirement for the double-strand break repair Mre11 protein in murine embryonic stem cells. Nucleic Acids Res. *25*, 2985–2991.

Xie, A., Kwok, A., and Scully, R. (2009). Role of mammalian Mre11 in classical and alternative non-homologous end joining. Nat. Struct. Mol. Biol. *16*, 814–818.

Xiong, B., Sun, S.-C., Lin, S.-L., Li, M., Xu, B.-Z., OuYang, Y.-C., Hou, Y., Chen, D.-Y., and Sun, Q.-Y. (2008). Involvement of Polo-like kinase 1 in MEK1/2-regulated spindle formation during mouse oocyte meiosis. Cell Cycle Georget. Tex *7*, 1804–1809.

Yang, K.-T., Li, S.-K., Chang, C.-C., Tang, C.-J.C., Lin, Y.-N., Lee, S.-C., and Tang, T.K. (2010). Aurora-C Kinase Deficiency Causes Cytokinesis Failure in Meiosis I and Production of Large Polyploid Oocytes in Mice. Mol. Biol. Cell *21*, 2371–2383.

Yao, L.-J., Zhong, Z.-S., Zhang, L.-S., Chen, D.-Y., Schatten, H., and Sun, Q.-Y. (2004). Aurora-A is a critical regulator of microtubule assembly and nuclear activity in mouse oocytes, fertilized eggs, and early embryos. Biol. Reprod. *70*, 1392–1399.

Ye, Q., Chen, L., Yin, X., Liu, Y.J.C., Ji, Q., and Zhao, E. (2014). Development of serous ovarian cancer is associated with the expression of homologous recombination pathway proteins. Pathol. Oncol. Res. POR *20*, 931–938.

Yi, K., Unruh, J.R., Deng, M., Slaughter, B.D., Rubinstein, B., and Li, R. (2011). Dynamic maintenance of asymmetric meiotic spindle position through Arp2/3-complex-driven cytoplasmic streaming in mouse oocytes. Nat. Cell Biol. *13*, 1252–1258.

You, Z., and Bailis, J.M. (2010). DNA damage and decisions: CtIP coordinates DNA repair and cell cycle checkpoints. Trends Cell Biol. *20*, 402–409.

You, Z., Chahwan, C., Bailis, J., Hunter, T., and Russell, P. (2005). ATM activation and its recruitment to damaged DNA require binding to the C terminus of Nbs1. Mol. Cell. Biol. *25*, 5363–5379.

You, Z., Shi, L.Z., Zhu, Q., Wu, P., Zhang, Y.-W., Basilio, A., Tonnu, N., Verma, I.M., Berns, M.W., and Hunter, T. (2009). CtIP links DNA double-strand break sensing to resection. Mol. Cell *36*, 954–969.

Yuen, W.S., Merriman, J.A., O'Bryan, M.K., and Jones, K.T. (2012). DNA double strand breaks but not interstrand crosslinks prevent progress through meiosis in fully grown mouse oocytes. PloS One *7*, e43875.

Zhai, R., Yuan, Y.-F., Zhao, Y., Liu, X.-M., Zhen, Y.-H., Yang, F.-F., Wang, L., Huang, C.-Z., Cao, J., and Huo, L.-J. (2013). Bora regulates meiotic spindle assembly and cell cycle during mouse oocyte meiosis. Mol. Reprod. Dev. *80*, 474–487.

Zhang, D., Hirota, T., Marumoto, T., Shimizu, M., Kunitoku, N., Sasayama, T., Arima, Y., Feng, L., Suzuki, M., Takeya, M., et al. (2004). Cre-loxP-controlled periodic Aurora-A overexpression induces mitotic abnormalities and hyperplasia in mammary glands of mouse models. Oncogene *23*, 8720–8730.

Zhang, D., Zhang, X., Zeng, M., Yuan, J., Liu, M., Yin, Y., Wu, X., Keefe, D.L., and Liu, L. (2015). Increased DNA damage and repair deficiency in granulosa cells are associated with ovarian aging in rhesus monkey. J. Assist. Reprod. Genet.

Zhang, W., Peng, G., Lin, S.-Y., and Zhang, P. (2011). DNA damage response is suppressed by the high cyclin-dependent kinase 1 activity in mitotic mammalian cells. J. Biol. Chem. *286*, 35899–35905.

Zhang, Y., Zhang, Z., Xu, X.-Y., Li, X.-S., Yu, M., Yu, A.-M., Zong, Z.-H., and Yu, B.-Z. (2008). Protein kinase A modulates Cdc25B activity during meiotic resumption of mouse oocytes. Dev. Dyn. Off. Publ. Am. Assoc. Anat. *237*, 3777–3786.

Zhao, X., Feng, C., Yu, D., Deng, X., Wu, D., Jin, M., Wang, E., Wang, X., and Yu, B. (2015). Successive recruitment of p-CDC25B-Ser351 and p-cyclin B1-Ser123 to centrosomes contributes to the release of mouse oocytes from prophase I arrest. Dev. Dyn. Off. Publ. Am. Assoc. Anat. *244*, 110–121.

Zou, L., and Elledge, S.J. (2003). Sensing DNA damage through ATRIP recognition of RPA-ssDNA complexes. Science *300*, 1542–1548.

9 Supplementary material

9.1 List of publications

Aurora kinase A drives MTOC biogenesis but does not trigger resumption of meiosis in mouse oocytes matured in vivo.

Solc P, Baran V, Mayer A, Bohmova T, Panenkova-Havlova G, Saskova A, Schultz RM, Motlik J.

Biol.Reprod. 2012 Oct 11;87(4):85. doi: 10.1095/biolreprod.112.101014 IF: 4.027 (2012)

A.M. performed experiments (immunostaining, confocal microscopy) and analysed the data.

Multiple requirements of PLK1 during mouse oocyte maturation.

Solc P, Kitajima TS, Yoshida S, Brzakova A, Kaido M, Baran V, Mayer A, Samalova P, Motlik J, Ellenberg J.

PLoS One. 2015 Feb 6;10(2):e0116783. doi: 10.1371/journal.pone.0116783. IF: 3.234 (2014).

A.M. performed experiments (immunostaining, confocal microscopy) and analysed the data.

MRE11 is involved in H2AX phosphorylation and protects chromosome integrity during mouse oocyte maturation.

Mayer A, Baran V, Sakakibara Y, Adela Brzakova, Ferencova I, Motlik J, Kitajima TS, Schultz RM, Solc P.

Journal of Cell Science, submitted, under revision. IF: 5.4 (2014).

A.M designed and performed experiments (immunostaining and confocal microscopy, live-cell imaging, Western blot, kinetochore tracking in mirin), analysed the data, wrote the manuscript.

Odpověď na poškození DNA v oocytech.

Mayer A, Šolc P.

Bioprospect 25, 2/2015, p.41-43.

A.M. wrote the manuscript.

BIOLOGY OF REPRODUCTION (2012) **87**(4):85, 1–12
Published online before print 25 July 2012.
DOI 10.1095/biolreprod.112.101014

Aurora Kinase A Drives MTOC Biogenesis but Does Not Trigger Resumption of Meiosis in Mouse Oocytes Matured In Vivo[1]

Petr Solc,[2,3,5] Vladimir Baran,[3,6] Alexandra Mayer,[5] Tereza Bohmova,[5] Gabriela Panenkova-Havlova,[4,5] Adela Saskova,[5] Richard M. Schultz,[7] and Jan Motlik[5]

[5]*Institute of Animal Physiology and Genetics, Academy of Sciences of the Czech Republic, Libechov, Czech Republic*
[6]*Institute of Animal Physiology, Slovak Academy of Sciences, Kosice, Slovakia*
[7]*Department of Biology, University of Pennsylvania, Philadelphia, Pennsylvania*

ABSTRACT

Aurora kinase A (AURKA) is an important mitotic kinase involved in the G2/M transition, centrosome maturation and separation, and spindle formation in somatic cells. We used transgenic models that specifically overexpress in mouse oocytes either wild-type (WT-AURKA) or a catalytically inactive (kinase-dead) (KD-AURKA) AURKA to gain new insights regarding the role of AURKA during oocyte maturation. AURKA activation occurs shortly after hCG administration that initiates maturation in vivo. Although AURKA activity is increased in WT-AURKA oocytes, resumption of meiosis is not observed in the absence of hCG administration. Control oocytes contain one to three microtubule organizing centers (MTOCs; centrosome equivalent) at prophase I. At the time of germinal vesicle breakdown (GVBD), the first visible marker of resumption of meiosis, the MTOC number increases. In WT-AURKA oocytes, the increase in MTOC number occurs prematurely but transiently without GVBD, whereas the increase in MTOC number does not occur in control and KD-AURKA oocytes. AURKA activation is biphasic with the initial activation not requiring CDC25B-CDK1 activity, whereas full activation, which is essential for the increase in MTOCs number, depends on CDK1 activity. AURKA activity also influences spindle length and regulates, independent of its protein kinase activity, the amount of MTOC associated with gamma-tubulin. Both WT-AURKA and KD-AURKA transgenic mice have normal fertility during first 6 mo of life. These results suggest that although AURKA is not a trigger kinase for G2/M transition in mouse oocytes, it regulates MTOC number and spindle length, and, independent of its protein kinase activity, gamma-tubulin recruitment to MTOCs.

AURKA, CDC25B, centrosome, γ-tubulin, mouse oocytes, MTOC, resumption of meiosis, spindle formation

INTRODUCTION

The members of the Aurora family of serine/threonine kinase (Aurora kinase A, B, and C) have emerged as crucial regulators of mitosis and meiosis. Although these kinases share sequence homology in their central catalytic domains, they have distinct localizations and functions. Aurora kinase A (AURKA) is a key mitotic protein kinase that associates with centrosomes [1] and the spindle [2], and drives centrosome maturation, separation, and spindle formation [1, 3–7]. AURKA facilitates mitotic entry by recruiting cyclin B (CCNB) to the centrosome [4] and by phosphorylating CDC25B [8, 9]. AURKA is also responsible for the initial activation of Polo-like kinase (PLK1) before mitotic entry by phosphorylating T210 [10, 11]. AURKA was initially proposed to be upstream of CDK1 activation during mitotic entry because RNA interference (RNAi)-mediated AURKA knockdown in synchronized HeLa cells prevents CDK1 activation and mitotic entry [4]. Other works demonstrated, however, that inhibition of AURKA causes only a delay in mitotic entry during a normal cell cycle for both cancerous and non-transformed mammalian cells [6, 12, 13]. AURKA activity is essential for G2 checkpoint recovery following DNA-damage induced G2 arrest [10, 14, 15].

In mouse oocytes, AURKA localizes to microtubule organizing centers (MTOCs) at the germinal vesicle (GV) stage, to proximal microtubules (MTs) in metaphase I, and to the midbody during telophase I [16, 17]. We previously demonstrated that RNAi-mediated reduction of AURKA during in vitro meiotic maturation results in a small but significant delay in resumption of meiosis [16], a finding consistent with the AURKA inhibitor MLN8054 eliciting a delay in resumption of meiosis [18]. Moreover, RNAi-mediated knockdown of AURKA results in mouse oocytes arrested in metaphase I with disorganized spindles [16]. These findings are consistent with TPX2, a known activator of AURKA [19, 20], control of meiotic spindle formation by regulating TACC3 phosphorylation on MTOCs [21]. In addition, microinjection of a constitutively active AURKA into *Xenopus* oocytes induces hormone-independent resumption of meiosis [22] and overexpression of a mutant form of AURKA, in which inhibitory phosphorylation sites Ser-283 and Ser-284 are replaced by Ala residues, accelerates resumption of meiosis in porcine oocytes cultured in vitro by increasing CCNB accumulation [23].

AURKB is a critical component of the chromosome passenger complex, which also contains INCENP, Survivin, and Borealin, and is required for correct MT attachment to kinetochores, a robust spindle assembly checkpoint (SAC), and for cytokinesis [15]. Moreover, vertebrates also have AURKC,

[1]This research was performed in the frame of IRP IAPG No. AV0Z50450515. This study was supported mainly by grant ME08030 (Czech-US scientific program) to J.M. The finalization of this study was supported by grant LH12057 (Czech-US scientific program) to P.S. V.B. was supported by grant APVV-0237-10 of the Slovak Grant Agency. P.S was also supported by P301/11/P081 and R.M.S. by a grant from NIH (HD022681).
[2]Correspondence: E-mail: solc@iapg.cas.cz
[3]These authors contributed equally to this work.
[4]Current address: Biology and Medical Genetics, Motol University Hospital, V Uvalu 84, Praha 5, 150 00, Czech Republic.

Received: 30 March 2012.
First decision: 19 April 2012.
Accepted: 17 July 2012.
© 2012 by the Society for the Study of Reproduction, Inc.
eISSN: 1529-7268 http://www.biolreprod.org
ISSN: 0006-3363

Downloaded from www.biolreprod.org.

which is highly similar to AURKB and whose expression is restricted to the germ line and some types of cancerous cells [24–26], where it competes with AURKB for binding to INCENP [27]. In mouse oocytes meiosis I, both AURKB and AURKC localize to the centromeric region, but AURKC also is found along the chromosome arms [28]. In metaphase II, only AURKC localizes to the centromere, and AURKB expression is very low without a clear localized signal [28]. Pharmacological inhibition of AURKB and AURKC results in abnormal chromosome congression, attenuation of the SAC activity, and cytokinesis defects. Although securin is destroyed in anaphase and homologous chromosomes separate in meiosis I following overexpression of AURKC, overexpression of AURKB blocks proper anaphase-promoting complex/cyclosome activation and securin destruction [28]. The results of recent experiments find that female mice lacking AURKC are subfertile partly as a result of chromosome misalignment that leads to MI arrest and that AURKB protein is less stable than AURKC during meiotic maturation [29].

Mammalian oocytes removed from their follicle spontaneously resume meiosis when placed in a suitable culture medium, and maturation is inhibited by maintaining elevated concentrations of cAMP using PDE inhibitors [30–32]. Resumption of meiosis in vivo, however, is induced by luteinizing hormone (LH) binding to LH receptors located mainly on mural granulosa cells. Activation of the LH receptor, via an EGF-like signaling pathway, ultimately results in a decreased flow of cGMP from cumulus cells to the oocyte, thereby relieving cGMP-mediated inhibition of oocyte PDE3A [33]. Thus, mechanisms that promote the maturation-associated decrease in oocyte cAMP could, in principle, differ in vitro and in vivo, and in particular with respect to upstream regulators of CDK1 such as CDC25B and WEE1B [34–36]. For example, WEE1B activity, which inhibits CDK1 activity, is inhibited following AURKA-PLK1-mediated phosphorylation [37, 38] whereas CDC25B, which activates CDK1 activity, is activated by AURKA-mediated phosphorylation [8, 9]; AURKA is activated prior to germinal vesicle breakdown (GVBD) [16].

We previously examined the effect of overexpressing AURKA on mouse oocyte maturation in vitro with particular attention focused on its ability to activate CDK1 and MTOCs [16]. Because of potential differences between in vitro and in vivo regulation of oocyte maturation, we employed two in vivo models: the first expresses wild-type AURKA (WT-AURKA) and a second expresses a catalytically inactive, that is, kinase dead, AURKA (KD-AURKA) to establish kinase-dependent and -independent functions during meiotic maturation. In addition, we investigated the relationship between AURKA and CDC25B-CDK1 activity in vivo using *Cdc25b*$^{-/-}$ oocytes. Consistent with our previous findings [16], we find that AURKA in vivo is essential for proper spindle formation during meiosis I and regulates MTOC number. We extend these findings using our in vivo model by demonstrating that (1) AURKA is not a trigger kinase for resumption of meiosis in vivo; (2) although AURKA activation occurs very early during resumption of meiosis, full activation of AURKA depends on CDC25B-CDK1; (3) an increase in MTOC number occurs in vivo after GVBD and can be uncoupled from GVBD by premature AURKA activation; (4) the increase in MTOC number (parallel to centrosome separation) depends on CDC25B-CDK1 signaling, which differs from what occurs during mitosis and centrosome separation; and (5) AURKA influences MTOC associated γ-tubulin independent of its kinase activity.

MATERIALS AND METHODS

Generation of Aurka *Transgenic and* Cdc25b$^{-/-}$ *Mice and Their Genotyping*

To generate mice overexpressing human WT-AURKA or catalytically inactive KD-AURKA, we employed a Cre-lox system. We bred previously described CAG-CAT-*Aurka* [39] female mice to *Zp3-Cre* males [40]. These CAG-CAT-*Aurka*; *Zp3-Cre* mice are called hereafter WT-*Aurka* or KD-*Aurka*, respectively. The CAT sequence contains a polyA signal that terminates transcription. Because the CAT sequence is flanked by two loxP sites, it can be removed by Cre-mediated recombination, and because *Cre* expression is restricted only to oocytes by *Zp3* promotor, WT- or KD-*Aurka* mice express AURKA only in oocytes. *Cdc25b*-deficient oocytes were obtained from *Cdc25b* germ line knockout mice [35].

Mice were genotyped using tail DNA by PCR as previously described [35, 39]. In experiments using WT- and KD-A*urka* mice, we used CAG-CAT-*Aurka* and/or *Zp3-Cre* mice as controls; these mice have normal WT phenotypes. For experiments with *Cdc25b*$^{-/-}$ mice, we used as controls WT C57BL/6NCrl because *Cdc25b*$^{-/-}$ mice are in a C57BL genetic background.

In Vivo Oocyte Maturation

Oocytes were matured in vivo by administering 5 international units (I.U.) of equine chorionic gonadotropin (eCG) intraperitoneally (i.p.) (Intervet) and 44 h later by 5.I.U. human chorionic gonadotropin (hCG) i.p. (Intervet) to initiate resumption of meiosis. Cumulus cell-enclosed oocytes were isolated in M2 medium (M7167; Sigma Aldrich) at different times after hCG administration; GVBD occurs 3–4 h, MI 7 h, and MII 12 h post-hCG administration. GV-stage oocytes (t = 0) were isolated from eCG-primed mice. GV-intact oocytes, and oocytes that had undergone GVBD or reached MI were isolated from ovaries, whereas MII-ovulated eggs were recovered from the ampullae of the oviduct. Cumulus cells of oocytes recovered from ovaries were removed mechanically, and expanded cumulus cells surrounding MII eggs were removed by hyaluronidase (H4272; Sigma Aldrich) treatment. The use of animals for these experiments was approved by the Animal Care and Use Committee of the Institute of Animal Physiology and Genetics, Academy of Sciences of the Czech Republic.

Oocytes Microinjection and In Vitro Culture

Oocytes were isolated from eCG-primed mice into M2 medium supplemented with 0.1 mM IBMX (I5879; Sigma Aldrich). *Cdc25b*$^{-/-}$ oocytes were microinjected with *Gfp-Aurka* cRNA in IBMX-supplemented medium. Two hours later IBMX was washed-out, and the oocytes were cultured in control M16 medium (M7292; Sigma Aldrich) for 4 or 7 h. Production and microinjection of cRNA was performed as described previously [16].

Quantitative Immunofluorescence Confocal Microscopy

After briefly washing oocytes in PBS, the cells were fixed in 3.7% paraformaldehyde diluted in PBS for 60 min at room temperature; the zona pellucida was not removed. We decided not to remove the zona pellucida for technical reasons: removing the zona pellucida either enzymatically (pronase) or chemically (Tyrode acidic solution) shortly after oocyte isolation and cumulus cells removal produced a strong immunostaining artifact on the oocyte's surface, and such was not case when oocytes were cultured in vitro after isolation. After washing in PBS (3 × 20 min), oocytes were permeabilized with 0.5% Triton X-100 in PBS for 30 min at room temperature and incubated with heat-inactivated 2% normal goat serum in PBS containing 0.2% bovine serum albumin (BSA) for 2 h at room temperature. The oocytes were then incubated overnight at 4°C with primary antibodies diluted in PBS/0.2% BSA. After washing the oocytes in PBS (3 × 20 min), the cells were incubated for 60 min at room temperature with the secondary antibodies conjugated with fluorescein isothiocyanate or Texas Red (15 ng/ml). The specificity of the immunostaining was established by omitting the primary antibodies or using another species-specific secondary antibody conjugated to fluorescein. DNA staining was done with 4′6-diamidino-2-phenylindole. AURKA phosphorylated on T288 was detected with a rabbit polyclonal antibody (NB100-2371; Novus Biological) at a 1:200 dilution, acetylated αtubulin with a mouse monoclonal antibody (T7451; Sigma) at a 1:1000 dilution; γ-tubulin with a rabbit polyclonal antibody (620901; Biolegend) at a 1:200 dilution, and pericentrin with a mouse monoclonal antibody (611815; BD Biosciences) at a 1:50 dilution. After a final wash in PBS/BSA, the oocytes were mounted in

Downloaded from www.biolreprod.org.

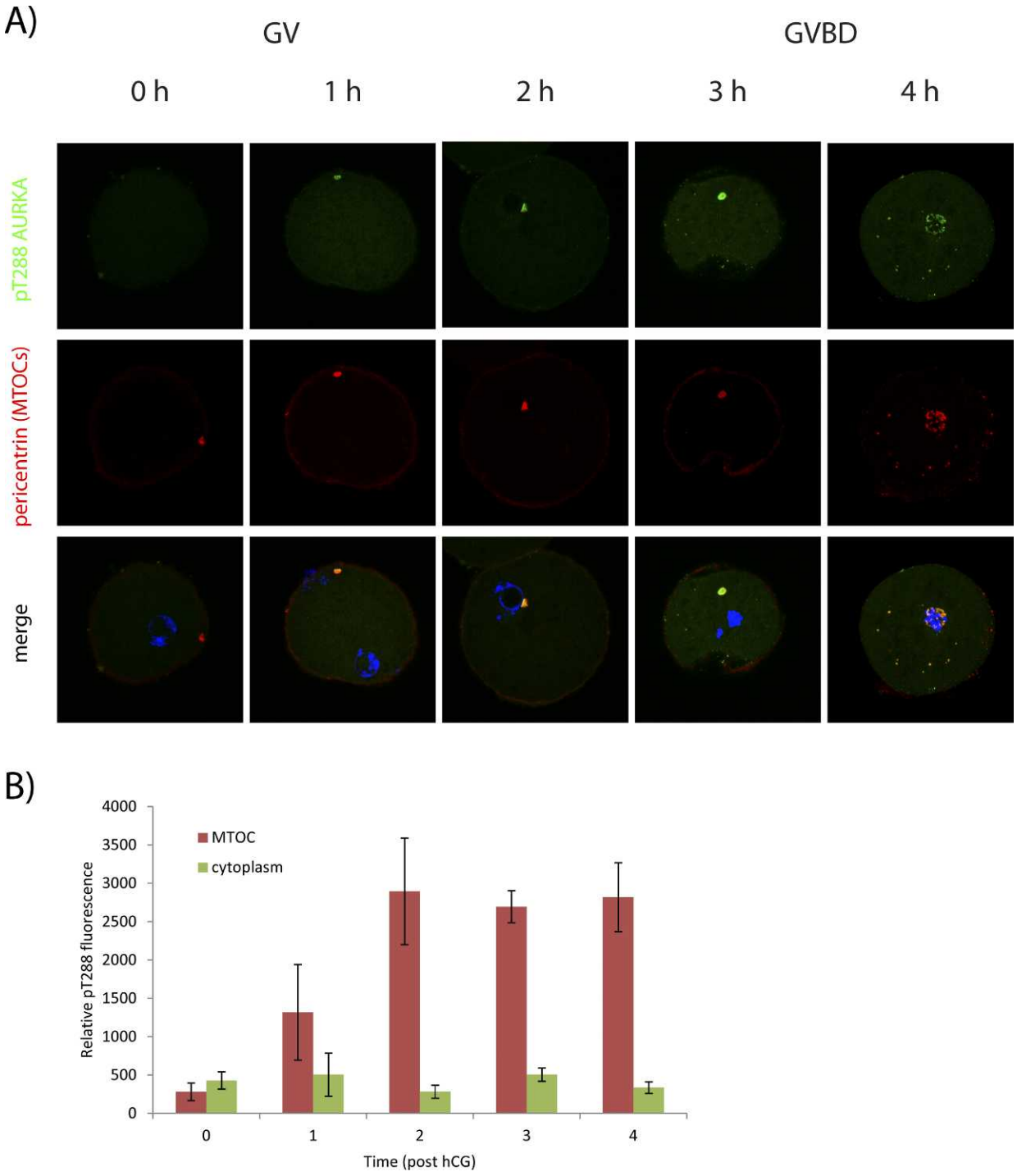

FIG. 1. Activation of AURKA during resumption of meiosis induced by hCG in 0–4 h intervals. **A**) The time course of the AURKA activating T288 phosphorylation on MTOC and in the cytoplasm. At 0-, 1-, and 2-h intervals, pericentrin (MTOC marker) and pT288 AURKA are shown in a single confocal section through the MTOC whereas at the 3- and 4-h intervals. the pictures represent maximum projections of 9–11 and 12–19 sections, respectively, to cover MTOC multiplication. DNA is always presented as a maximum projection. Note that pericentrin staining also nonspecifically detected the zona pellucida and precluded using a maximum projection of the entire stack. Entire stacks are available in Supplemental Movie S1. Original magnification ×63, zoom ×3. **B**) Quantification of AURKA phosphorylation. Data are means with 95% confidence intervals in arbitrary units.

Mowiol (Merck, 475904) between a slide and cover glass using a spacer to preserve the three-dimensional (3D) structure of the oocytes.

Oocytes were scanned using either a Leica TCS SP2 or Leica TCS SP5 laser scanning confocal microscope. The same power setting was used, and the signal was not saturated. To avoid spectral overlap, a sequential scan was applied in the 12-bit image depth with a 1024 × 1024 or 512 × 512 pixel image resolution. Three-dimensional scanning was performed using 1-μm optical sections through the oocyte volume.

Image Analysis

For pT288 AURKA MTOC-associated signal quantification (see Fig. 1), MTOC(s) mask (selection) was created by intensity thresholding of the pericentrin channel and the immunofluorescent intensity measurement was redirected to the pT288 AURKA channel. The same approach was used for quantifying MTOC-associated γ-tubulin. Image analysis was done using FiJi, an ImageJ distribution (http://fiji.sc).

Downloaded from www.biolreprod.org.

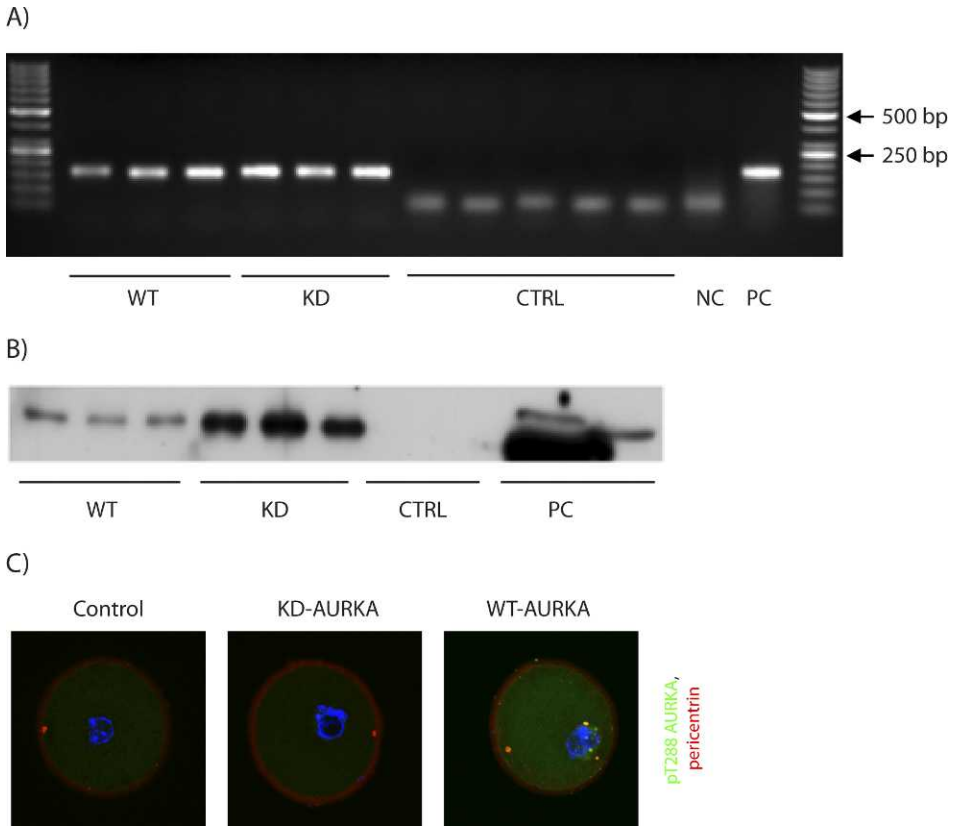

FIG. 2. Conditional expression of human wild-type (WT) and kinase-dead (KD) AURKA transgenes in mouse oocytes. **A**) RT-PCR analysis of single oocytes using primers detecting human *AURKA* mRNA but not the endogenous mouse mRNA. Mouse NIH3T cells were used as negative (NC) and human HeLa cells as positive (PC) controls. **B**) Immunoblot of samples with 20 oocytes. Note that to detect endogenous mouse AURKA, about 200 oocytes were required. PC, HeLa cells. **C**) Premature T288 AURKA activating phosphorylation in GV-stage oocytes (time = 0 h) from WT-AURKA but not KD-AURKA and control mice. Note MTOC multiplication in WT-AURKA oocyte. Pericentrin (red) was used as MTOC marker. Both pT288 and pericentrin are shown in a single confocal section for control and KD-AURKA, and as maximum projection of 8-22 sections for WT-AURKA, to cover MTOC multiplication. DNA is always presented as a maximum projection. Entire stacks are available in Supplemental Movie S2. Original magnification ×63, zoom ×3.

To measure the total MTOC volume (see Figs. 4B and 6C), the γ-tubulin 12-bit channel was converted by intensity thresholding into the binary channel, individual MTOCs were identified with a 3D object counter, and the MTOC volume was measured. For spindle length measurement (see Fig. 6B), x, y, z coordinates of spindle poles stained by γ-tubulin were stored and the spindle length was calculated as the distance between spindle poles using the Pythagorean theorem. The spindle volume (see Fig. 6B) was measured from the intensity threshold binary channel of α-tubulin, where spindles were again detected by 3D object counter and where spindle volume was measured using a 3D ROI manager plug-in [41].

RT-PCR and Western Blot

RT-PCR was done using FastLane Cell SYBR Green Kit (216213; Qiagen) when single oocytes were used directly as substrate for single-step RT-PCR without mRNA purification. To detect human WT or KD-*Aurka* mRNAs as a product of *Aurka* transgenes, we designed primers that specifically detected human but not mouse *Aurka* mRNA. These primers do not discriminate between WT- and KD-*Aurka* mRNAs. The primers sequences are: TTC CTT GTC AGA ATC CAT TAC and ATG AGG TAC ACT GGT TGC.

For immunoblot detection of overexpressed WT or KD-AURKA, 20 oocytes per sample were used. The antibody was a rabbit polyclonal antibody (3092; Cell Signaling) diluted 1:500 in 5% milk.

Statistics

NCSS2007 software was used (NCSS). Differences in imunofluorescence intensities were evaluated using the Student *t*-test or its variant Aspin-Welch in the case of unequal variance. When a nonnormal distribution was observed, we used the Mann-Whitney test for differences in the medians. Differences in meiotic maturation progression (GV, GVBD, MII) and differences in the amount of MTOCs between groups were tested by chi-square.

RESULTS

Activation of AURKA in Oocytes Occurs Shortly after hCG Administration and Precedes Resumption of Meiosis

We have shown previously that AURKA activation occurs within 20 min after initiation of maturation in vitro [16]. Because of the differences in spindle morphology when oocytes are matured either in vitro or in vivo [42], coupled with the role of AURKA in increase in MTOC number, we closely monitored the temporal-spatial time course of AURKA activation during maturation in vivo using quantitative confocal microscopy to detect pT288 AURKA, which serves as a proxy for AURKA activation; the functional relationship between T288 autophosphorylation in the activation loop and kinase activity is well established [43, 44].

The results of these experiments demonstrated that significant activation of AURKA on MTOCs occurred within 1 h of initiation of maturation and full activation was achieved by 2 h, after which it remained essentially constant (Fig. 1; see also Supplemental Movie S1) [all the Supplemental Data are available online at www.biolreprod.org]. After GVBD, when MTOC multiplication occurred, active AURKA was localized on all the MTOCs. The increase in AURKA activation was apparently restricted to MTOCs because no significant changes in the amount of phosphorylated AURKA were detected in the cytoplasm (Fig. 1B).

Downloaded from www.biolreprod.org.

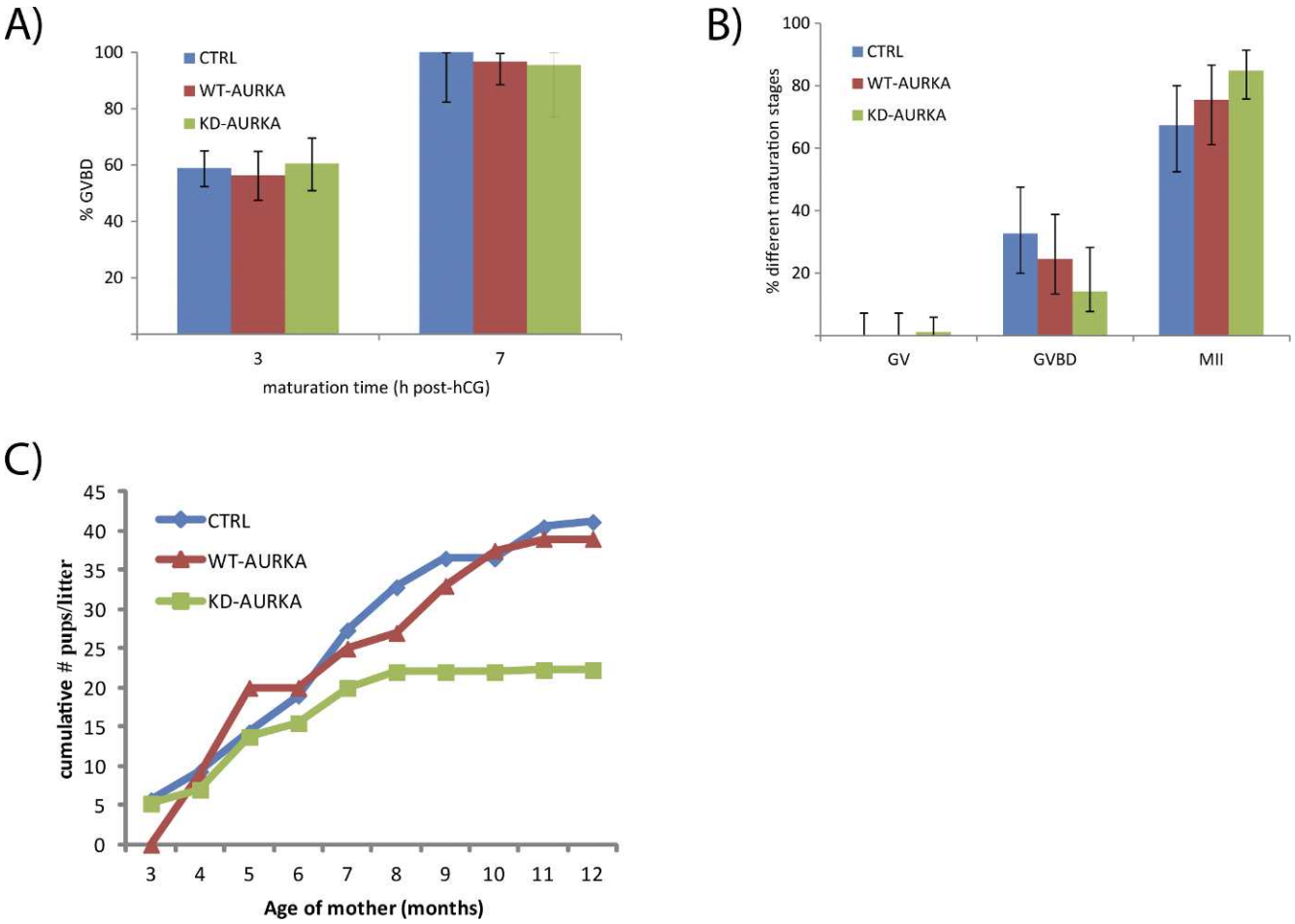

FIG. 3. Meiotic maturation and fertility of AURKA transgenic mice. **A**) Resumption of meiosis (GVBD) at 3 and 7 h after hCG administration. The number of oocytes examined was 262 for controls (CTRL), 195 for WT-AURKA, and 136 for KD-AURKA. **B**) Incidence of maturation 12 h after hCG administration. The number of oocytes examined was 49 for controls, 49 for WT-AURKA, and 92 for KD-AURKA. Error bars in both graphs represent 95% confidence intervals. Differences between groups are statistically significant at $P < 0.05$. **C**) Fertility expressed as cumulative numbers of pups per litter during a 3–12 mo breeding trial. Data are expressed as mean from four mice per each group.

Conditional Overexpression of AURKA in Oocytes Does Not Influence Resumption of Meiosis, Meiotic Maturation, and Developmental Competence

In somatic cells, AURKA is implicated as a positive regulator of CDC25B during normal mitotic entry [9] and is essential for G2 checkpoint recovery [10]. The latter situation is very similar in many aspects to resumption of meiosis in oocytes [18]. Because CDC25B is essential for resumption of meiosis [35], and given the very early activation of AURKA at the onset of initiating maturation and the aforementioned similarity, we tested whether AURKA regulates CDC25B. We found that overexpressing AURKA by microinjecting a cRNA encoding AURKA did not induce resumption of meiosis when maturation was inhibited by including the PDE3A inhibitor, milrinone, in the medium for 18 h [16]. Because meiotic arrest is the result of a highly complex pathway that involves not only cAMP but cGMP as well [45, 46], this failure may not reflect the role of AURKA in a more physiological context. We, therefore, took an approach that examined the effect of overexpressing AURKA in oocytes within follicles.

We employed a previously published transgenic mouse that carries human WT- or KD-*Aurka* transgenes under the control of a constitutive CAG promoter [39]. The transgenes are only transcribed after *Cre*-mediated excision of the floxed CAT inhibitory sequence. Breeding these mice with *Zp3-Cre* mice allowed us to overexpress WT- or KD-AURKA only in oocytes. Both transgenes were expressed, with higher amounts of KD-AURKA accumulating when compared to WT-AURKA (Fig. 2, see also Supplemental Movie S2). The amount of WT-AURKA was ~10 times greater than endogenous AURKA because only 20 WT-AURKA oocytes were required to detect a signal following immunoblotting, whereas 200 oocytes were required to detect endogenous AURKRA (data not shown and [16]). In addition, MTOCs in WT-AURKA oocytes were already associated with activated AURKA (Fig. 2C), demonstrating that WT-AURKA overexpression lead to the premature AURKA activation.

We next analyzed whether WT-AURKA overexpression induces resumption of meiosis of oocytes enclosed in preovulatory antral follicles. We isolated oocytes from eCG-stimulated and -unstimulated mice and found that all the oocytes from the control and WT- and KD-AURKA groups had an intact nucleus, suggesting maintenance of prophase I arrest despite increased AURKA activity in WT-AURKA oocytes. In addition, the kinetics of meiotic resumption (Fig. 3A) and meiotic maturation to metaphase II (Fig. 3B) after hCG administration were unaffected by either WT- or KD-AURKA overexpression. Metaphase II eggs were also able to support normal embryonic development as evidenced by

Downloaded from www.biolreprod.org.

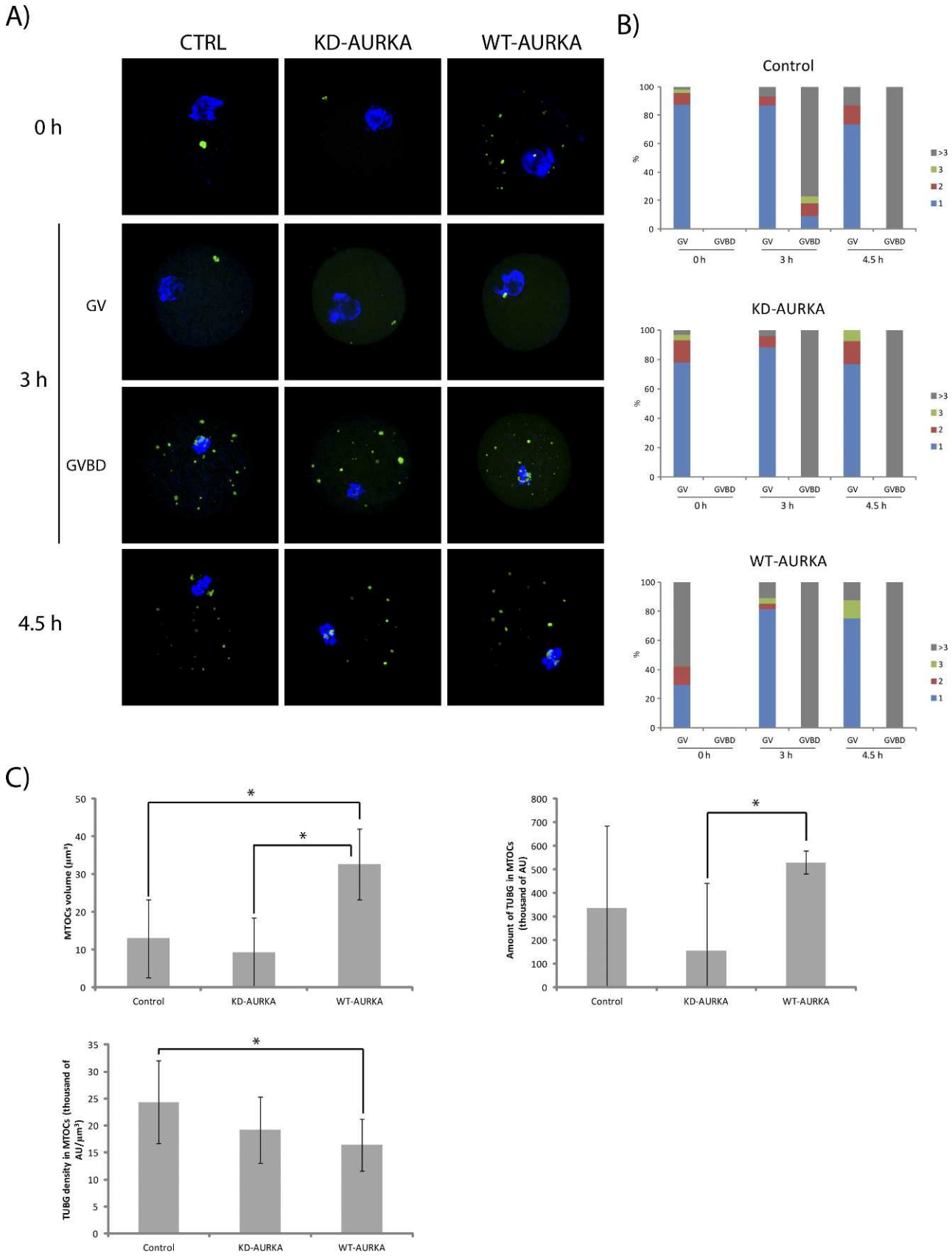

FIG. 4. WT-AURKA overexpression induces a transient and premature increase in MTOC number in prophase I arrested oocytes. **A**) MTOC biogenesis of control and KD- and WT-AURKA oocytes. Images are presented as maximum projections for γ-tubulin and DNA staining. All the MTOCs are also positive for pericentrin that is clearly visible; see Supplemental Movies S3–S5 showing entire stacks. The zona pellucida is nonspecifically stained, which precludes using a maximum projection of the entire stack of the pericentrin channel. Original magnification ×63, zoom ×3. **B**) Quantitative data regarding MTOC(s) number at 0, 3, and 4.5 h after hCG administration and sorted according to GV and GVBD stages. The number of oocytes examined was 146 for

Downloaded from www.biolreprod.org.

breeding trials conducted over a period of 3–6 mo (Fig. 3C). We did find, however, that in older mice (7–12 mo), KD-AURKA overexpression led to infertility for unknown reasons. Taken together, these data strongly suggest that activation of AURKA in prophase I arrested oocytes does not trigger resumption of meiosis.

Premature AURKA Activation Leads to the Premature Increase in MTOCs Number

Mouse oocytes, which lack centrosome-containing centrioles [47, 48], have one to three MTOCs that contain both pericentrin [49] and γ-tubulin [50]; although some authors term MTOCs in oocytes as centrosomes [51], we use in this report only the term MTOC because a typical centrosome contains centrioles [52]. In addition, MTs form an interphaselike dense network in germinal vesicle (GV)-intact oocytes that are arrested in prophase I, but following initiation of meiotic maturation and prior to GVBD, the number of MTOCs increases and the MT dense network diminishes [53, 54]. Following GVBD, MTOCs congress in the vicinity of the condensed chromosomes and nucleate MTs to form a ball-like structure with MTOCs decorating the surface [54]. The increase in MTOC number and total MTOC volume during resumption of meiosis [53, 54] can be viewed as analogous to centrosome maturation and separation in somatic cells, with both process requiring AURKA activity [14, 52, 55]. A bipolar meiotic spindle forms by the progressive clustering of multiple MTOCs ejected from the MT balls. MTOC clustering, also termed sorting, is governed by hepatoma up-regulated protein (HURP) that is loaded on interpolar MTs in the vicinity of chromosomes via kinesin-5 activity. By promoting MT stability in the spindle's central domain, HURP allows efficient MTOC sorting into distinct poles [56].

A previous study reported increase in MTOC number, probably due to de novo formation, occurs prior to GVBD when oocytes are matured in vitro [54]. We have shown that overexpression of AURKA induces an increase in MTOC number in prophase I-arrested oocytes as well as later during in vitro meiotic maturation, resulting in formation of defective multipolar spindles and arrest in meiosis I [16]. The observed normal meiotic progression to and arrest at metaphase II in WT-AURKA oocytes matured in vivo, coupled with the normal fertility of the female mice, appears not consistent with the aforementioned in vitro observations.

To gain better insight into the source of these differences we quantified the number of MTOCs during the course of maturation in vivo; we define an increase in MTOC number to have occur when >3 MTOCs are detected. Oocytes arrested within follicles have one to three cytoplasmic MTOC(s). Three to four hours after hCG stimulation to induce maturation, oocytes with a GV still contained one to three MTOC(s) whereas an increase in MTOC number occurred in those that underwent GVBD (Fig. 4, A and B; see also Supplemental Movies S3–S5). When AURKA activation was accelerated using WT-AURKA oocytes, an increase in MTOC number was already observed in GV-intact oocytes at $t = 0$ (Fig. 4, A and B). This increase, however, was transient because oocytes that were still at the GV-stage 3 h post-hCG only had one to three MTOCs, whereas an increase in MTOC number had occurred in both control and WT-AURKA oocytes during the same time interval in oocytes after GVBD. The transient and premature increase in MTOC number required AURKA kinase activity because KD-AURKA oocytes have the same kinetics of increase in the number of MTOCs as controls. The increase in MTOC number in WT-AURKA GV-intact oocytes at $t = 0$ was associated with an increase of total MTOC volume (Fig. 4C), suggesting that this increase was not due to fragmentation of preexisting MTOC(s). The small increase in the total MTOC-associated γ-tubulin in WT-AURKA oocytes and decrease in KD-AURKA oocytes were not significant. The significant differences in the amount of γ-tubulin between WT- and KD-AURKA oocytes (Fig. 4C), however, implied that AURKA activity positively regulates the amount of γ-tubulin in MTOCs and that KD-AURKA exhibits in oocytes a dominant negative effect. Although γ-tubulin slightly increased in WT-AURKA oocytes, this increase did not fully compensate for the increase in MTOC number and total volume leading to a decline in γ-tubulin intensity on MTOC in WT-AURKA oocytes.

Full Activation of AURKA Essential for Increase in MTOCs Number Depends on CDC25B-CDK1 Activity

The results described above strongly implicate AURKA in an increase in MTOC number and raise the question of the role of CDK1 in this process, that is, whether it is CDK1 dependent or independent. Interestingly, in somatic cells, CDK1-independent activation of AURKA on centrosomes drives centrosome separation [13]. Accordingly, we measured T288 AURKA phosphorylation after hCG administration in oocytes derived from *Cdc25b*$^{-/-}$ mice; CDC25B is essential for CDK1 activation and resumption of meiosis [35]. At 4 and 7 h post-hCG administration, AURKA was activated on MTOCs and MTOC multiplication had occurred in WT oocytes. In contrast, AURKA was only partially activated, and an increase in MTOC number did not occur in *Cdc25b*$^{-/-}$ oocytes (Fig. 5, A and B; see also Supplemental Movies S6 and S7), that is, CDC25B-dependent CDK1 activation was essential for complete AURKA activation.

The remaining question was whether the increase in MTOC number deficiency was due to partial AURKA activation in *Cdc25b*$^{-/-}$ oocytes. Because AURKA overexpression induced MTOC multiplication in WT oocytes in vitro [16], we microinjected a *Gfp-Aurka* cRNA into the *Cdc25b*$^{-/-}$ oocytes matured in vitro. We found that GFP-AURKA restored the increase in MTOC number in these oocytes, although they remained arrested in prophase I because of the absence of CDC25B (Fig. 5C).

AURKA Influences Spindle Length and Regulates, Independent of Its Kinase Activity, MTOC-Associated γ-Tubulin

We previously demonstrated that overexpressing AURKA during in vitro maturation leads to an elongated metaphase I spindle or multipolar spindle formation that in each case is accompanied by metaphase I arrest [16]. In contrast, results from the in vivo maturation studies of WT-AURKA oocytes show normal maturation with arrest at metaphase II and normal embryonic development after fertilization. Therefore, we

controls, 119 for WT-AURKA, and 110 for KD-AURKA. **C**) Quantification of total MTOCs volume per oocytes, the total of γ-tubulin associated with MTOCs and γ-tubulin density in MTOCs in control and KD- and WT-oocytes at 0 h.

Downloaded from www.biolreprod.org.

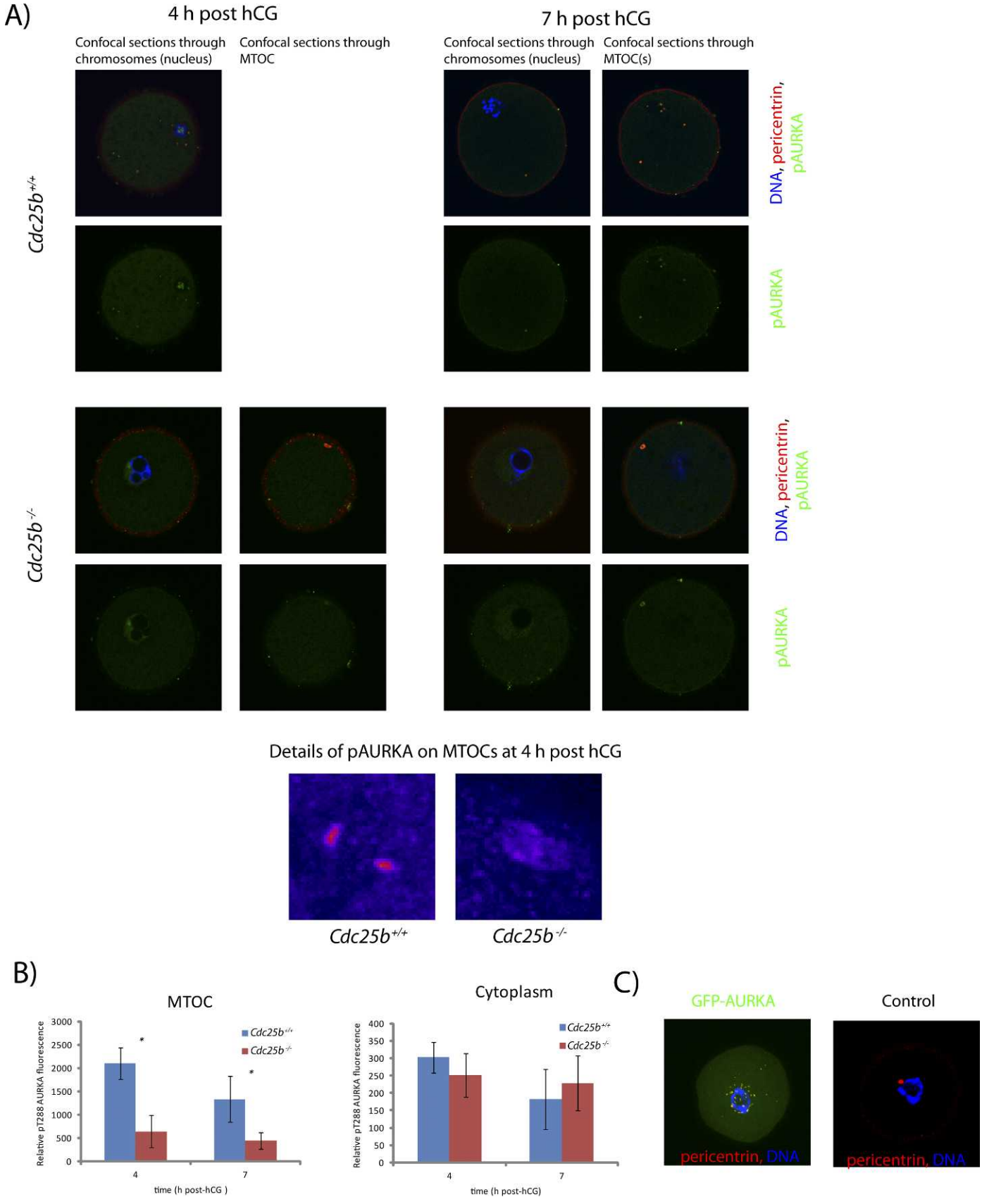

FIG. 5. Full activation of AURKA is essential for the increase in MTOCs number and depends on CDC25B-CDK1 activity. **A**) Partial activation of AURKA in *Cdc25b*$^{-/-}$ oocytes at 4 and 7 h after hCG administration is not sufficient to induce the increase in MTOC number. Images show confocal sections through chromosomes and MTOCs. For 4-h interval, detailed pseudocolored (fire) images of pAURKA MTOC-associated signal are provided. All the MTOCs are clearly visible on complete stacks in Supplemental Movie S6. Original magnification ×63, zoom ×3. **B**) Quantification of partial activation of AURKA on MTOCs in *Cdc25b*$^{+/+}$ and *Cdc25b*$^{-/-}$ oocytes. There are not significant changes in pT288 AURKA in the cytoplasm. The number of oocytes

Downloaded from www.biolreprod.org.

ascertained the effect of WT- and KD-AURKA on spindle morphology of metaphase I oocytes.

WT-AURKA oocytes exhibited a normal bipolar spindle that was elongated (Fig. 6, A and B). This elongation depended on protein kinase activity because spindle length was unaffected in KD-AURKA oocytes (Fig. 6, A and B). The elongated WT-AURKA spindles had the same volume as control (Fig. 6B), documenting that elongation was not a result of increased spindle volume. Surprisingly, KD-AURKA spindles were slightly but significantly smaller in volume than controls, suggesting that KD-AURKA exhibited a dominant negative effect similar to that observed for the amount of MTOC-associated γ-tubulin in prophase I arrested oocytes (Fig. 4C). γ-Tubulin staining revealed that metaphase I oocytes had a normal number of MTOCs focused on spindle poles as well as in the cytoplasm regardless of AURKA status (Fig. 6, A and C). However, total MTOC volume (Fig. 6C), total amount of MTOC associated γ-tubulin, and γ-tubulin density on MTOCs were higher both in WT-AURKA and KD-AURKA oocytes (Fig. 6, A and C). This finding suggests that AURKA regulates γ-tubulin turnover independent of its protein kinase activity.

DISCUSSION

The LH surge is the primary trigger that initiates ovulation, cumulus cell expansion, and meiotic maturation by its binding to LH receptors located on follicle cells. Luteinizing hormone's ability to initiate oocyte maturation is indirect and occurs by driving expression of EGF-like peptides in mural granulosa cells that in turn leads to signaling events in cumulus cells that result not only in cumulus cell expansion but also meiosis resumption in the oocyte [57, 58]. Our finding that AURKA activation occurs as early as 1 h after hCG stimulation (Fig. 1) is interesting given that increased mRNA expression of the EGF-like peptides amphiregulin and epiregulin is also observed in mural granulosa cells within an hour [58]. The timing of these events suggests that the initial activation of AURKA is mediated by shedding of a preexisting pool of EGF-like ligands [57]. Alternatively, there may exist an EGF-like independent signaling mechanism that triggers AURKA activation in oocytes.

AURKA-dependent CDC25B phosphorylation facilitates mitotic entry in cancerous somatic cells [9], although AURKA is not absolutely essential for normal mitotic entry [6, 12, 13]. On the other hand both AURKA [10, 15] and CDC25B [59, 60] are crucial for G2 checkpoint recovery following prolonged DNA-damage induced G2-arrest that is very similar in many aspects to resumption of meiosis in oocytes after long prophase I arrest [18]. CDC25B is essential for resumption of meiosis in mouse oocytes [35]. Microinjection of a constitutively active AURKA into *Xenopus* oocytes induces hormone-independent resumption of meiosis [22] and forces activation of AURKA in porcine oocytes that facilitates resumption of meiosis by increasing CCNB synthesis [23]. Although these results implicate AURKA as a triggering protein kinase for resumption of meiosis, we find that overexpressing WT-AURKA in oocytes neither triggers meiosis resumption nor accelerates the time to GVBD (Fig. 3A) in oocytes present in preovulatory antral follicles. This finding is consistent with the current view that prophase I arrest depends mainly on PKA-mediated CDC25B inhibition in which resumption of meiosis is linked to increased CDC25B activity as a consequence of decreased PKA activity; PKA catalyzes an inhibitory phosphorylation of CDC25B [36, 61, 62]. On the other hand, both RNAi-mediated [16] or pharmacological AURKA [18] inhibition delay resumption of meiosis, suggesting that although AURKA is involved in amplification of signaling leading to meiosis resumption, other molecules are rate-limiting because AURKA overexpression does not accelerate GVBD.

During hCG-induced resumption of meiosis, the increase in MTOC number occurs shortly after GVBD (Fig. 4), which differs from in vitro maturation in which an increase in MTOC number occurs before GVBD [53]; overexpression of WT-AURKA induces premature increase in MTOC number in prophase I-arrested oocytes. Surprisingly, this induced increase that occurs during maturation in vivo is transient and is not observed ~3 h after hCG administration, that is, very shortly before GVBD. Thus, oocytes may have a mechanism that tightly controls the number of MTOCs before GVBD. This mechanism may be similar to centrosome clustering that occurs in many cancer cells but also during physiological hepatocyte polyploidization [63]. Alternatively, prematurely formed new MTOCs may not be fully mature and therefore unstable. If the second possibility is true, it raises the question why prematurely multiplied MTOCs are unstable in oocytes shortly before GVBD but not in oocytes arrested in prophase I? One explanation is that MTOC instability is a consequence of a decline in γ-tubulin density in WT-AURKA prophase I-arrested oocytes (Fig. 4C). Alternatively, the concentration of an AURKA activator such as TPX2, may be limiting, because TPX2 increases progressively during meiotic maturation, reaching its highest levels only at metaphase I and II [21].

Another contributing factor to MTOC instability could be dephosphorylation of AURKA substrates important for MTOC development following hCG administration and prior to GVBD. One possible candidate is TACC3, which is phosphorylated during meiotic maturation [21]. We observed in preliminary studies, however, that the p-TACC3 signal is already associated with MOTCs in prophase I-arrested oocytes and transiently decreases between 1 and 2 h post-hCG administration and then increased from 3–4 h (data not shown). Thus, phosphorylation of TACC3 does not correlate with AURKA phosphorylation, that is, it is likely that other protein kinases (and phosphatases) are involved. Moreover, in prophase I-arrested oocytes, the amount of p-TACC3 associated with MTOC is very high in WT-AURKA oocytes when compared to control oocytes (data not shown).

In metaphase I oocytes AURKA overexpression induces increase both in total MTOC volume and the total amount of MTOC associated γ-tubulin independent of its activity although the number of MTOC is the same in control WT- and KD-AURKA oocytes (Fig. 6). These data document a cell cycle stage different role for AURKA in MTOC metabolism. In prophase I, AURKA activity increases MTOC number, total MTOC volume, and amount of γ-tubulin in MTOCs—a process that can be viewed as analogous to centrosome maturation and separation in somatic cells [14, 52, 55]. However, later in meiosis in metaphase I, AURKA, independent of its protein kinase activity, positively regulates MTOC

examined was 14 for $Cdc25b^{+/+}$ and 19 for $Cdc25b^{-/-}$ oocytes. The asterisk indicates $P < 0.001$. **C**) Overexpression of GFP-AURKA in $Cdc25b^{-/-}$ oocytes restores MTOCs multiplication in the absence of CDK1 activity. Control oocytes were microinjected with water. Maximum projections are shown. The entire Z-stacks are available as Supplemental Movie S7. Original magnification ×63, zoom ×3.

Downloaded from www.biolreprod.org.

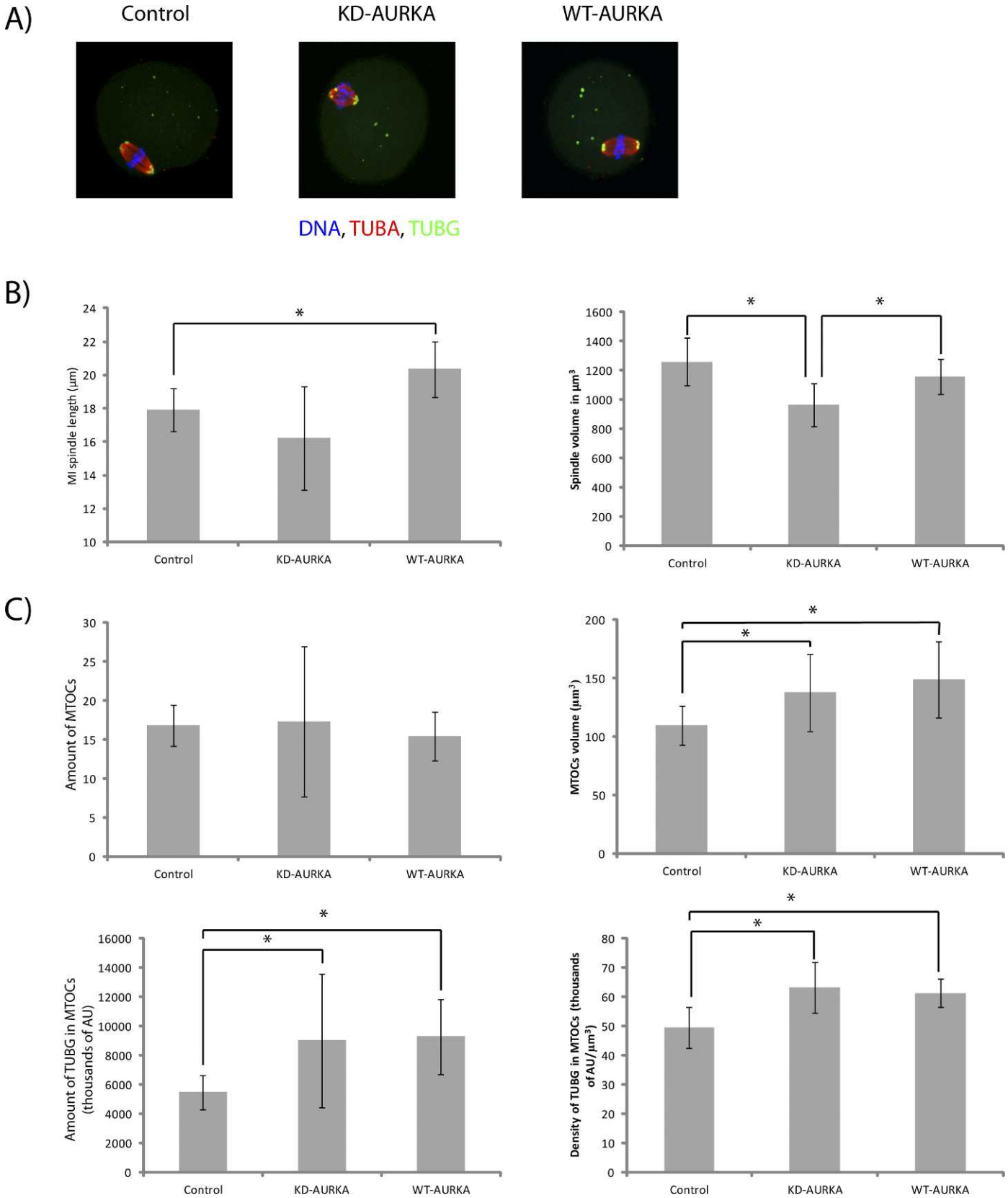

FIG. 6. Spindle length, volume, and γ-tubulin expression in metaphase I oocytes. **A**) Images of control, KD-AURKA, and WT-AURKA oocytes stained for tubulin and DNA. Original magnification ×63, zoom ×2.6. **B**) Quantification of the effect of AURKA on spindle length and volume. The number of oocytes examined was 19 for controls, 13 for WT-AURKA, and 11 for KD-AURKA. DNA staining (blue) and γ-tubulin staining (green) are shown as maximum projections of the entire stacks, but γ-tubulin staining are shown as a maximum projection of confocal sections that contain the spindle. The entire stacks are available as Supplemental Movie S8. The asterisk indicates $P = 0.017$. **C**) Quantification of the total number of MTOCs per oocytes, total MTOCs volume, the total of γ-tubulin associated with MTOCs, and γ-tubulin density in MTOCs in control and KD- and WT-oocytes in KD- and WT-AURKA oocytes. The number of oocytes examined was 10 for controls, 10 for WT-AURKA, and 7 for KD-AURKA. All the data are expressed with 95% confidence intervals. The asterisk indicates $P < 0.05$.

Downloaded from www.biolreprod.org.

volume and the amount of MTOC-associated γ-tubulin, but has little effect on total MTOC number. In somatic cells, AURKA associates with centrosomin and localizes to spindle poles that target γ-tubulin to centrosomes [1]. In *Caenorhabditis elegans* early embryos, AURKA independent of its protein-kinase activity regulates assembly of γ-tubulin-independent microtubules [64].

Our data showing that WT-AURKA overexpression triggers a premature increase in MTOC number without triggering resumption of meiosis is consistent with an uncoupling of the resumption of meiosis (in term of GVBD and chromosome condensation) from the increase in MTOC number. For oocytes present in follicles, the two are coupled during in vivo maturation, possibly by CDK1 activating AURKA (see below). In mammalian somatic cells, AURKA is activated on centrosomes in G2 independent of CDK1 activity and promotes centrosome separation. Later in mitosis, AURKA activity depends on CDK1 [13], whose activation during resumption of meiosis in mouse oocytes requires CDC25B [35]. We find that AURKA is partially activated on MTOCs in *Cdc25b*$^{-/-}$ oocytes. MTOC multiplication, however, is a CDK1-dependent process and requires full AURKA activation (Fig. 5, A and B). CDK1 activity is involved in increase in MTOC number indirectly through full AURKA activation because microinjection of a *Gfp-Aurka* cRNA into the *Cdc25b*$^{-/-}$ oocytes restores increase in MTOC number (Fig. 5C). These data suggest that the first wave of AURKA activation is CDK1 independent, but full AURKA activation, essential for increase in MTOCs number, is CDK1 dependent. In contrast, in somatic cells, the initial G2-associated CDK1-independent AURKA activation drives centrosome separation [13].

WT-AURKA, but not KD-AURKA, oocytes exhibit longer spindle than controls (Fig. 6, A and B; see also Supplemental Movie S8); chromosome alignment is not affected. Of note is that in *Xenopus* egg extracts, depletion of either AURKA (Eg2) or its substrate TACC3 (Maskin) leads to formation of shorter spindles [65]. We previously observed spindle elongation or spindle disorganization [16] following GFP-AURKA overexpression and maturation in vitro. There are several explanations why in vivo WT-AURKA overexpression does not disorganize spindles. For example, the extent of overexpression in the two models may differ; in the in vitro model, low levels of AURKA expression permitted normal spindle formation, whereas high levels resulted in disorganized spindles. Alternatively, as described above, the concentration of AURKA activator such TPX2 may be rate limiting. Last, because transgenic overexpression occurs over the course of oocyte growth, that is, weeks (and is not short-term as it is in the in vitro model, i.e., hours), the higher amount of AURKA activity may elicit a compensatory response, for example, increasing phosphatase activity or decreasing the amount of AURKA protein. Consistent with the latter proposal is the lower amount of WT-AURKA than KD-AURKA, although their transcript abundance is quite similar (Fig. 2). Note that different spindle lengths are observed in oocytes from different strains [66], and therefore AURKA could contribute to these differences.

In conclusion, we show that during in vivo meiotic maturation AURKA is activated as early as 1 h post-hCG administration and the initial AURKA activation does not require CDK1 activity. A physiological increase in MTOC number occurs in vivo shortly after GVBD, and CDC25B-CDK1 is required for full AURKA activation that drives MTOC increase. Later in meiosis I, AURKA activity positively regulates spindle length, and in a protein kinase-independent manner, AURKA positively regulates the amount of MTOC associated γ-tubulin. Although AURKA was proposed in *Xenopus* oocytes as a trigger protein kinase for resumption of meiosis, our finding suggest such is not the case, at least in mouse, because AURKA overexpression using a transgenic model does not induce resumption of meiosis of oocytes within preovulatory antral follicles in the absence of an hCG stimulus.

ACKNOWLEDGMENT

We greatly thank to Dongwei Zhang and Hideyuki Saya (Institute for Advanced Medical Research, Keio University School of Medicine, Japan) for providing *Aurka* transgenic mice.

REFERENCES

1. Terada Y, Uetake Y, Kuriyama R. Interaction of Aurora-A and centrosomin at the microtubule-nucleating site in *Drosophila* and mammalian cells. J Cell Biol 2003; 162:757–763.
2. Kufer TA, Sillje HH, Korner R, Gruss OJ, Meraldi P, Nigg EA. Human TPX2 is required for targeting Aurora-A kinase to the spindle. J Cell Biol 2002; 158:617–623.
3. De Luca M, Lavia P, Guarguaglini G. A functional interplay between Aurora-A, Plk1 and TPX2 at spindle poles: Plk1 controls centrosomal localization of Aurora-A and TPX2 spindle association. Cell Cycle 2006; 5:296–303.
4. Hirota T, Kunitoku N, Sasayama T, Marumoto T, Zhang D, Nitta M, Hatakeyama K, Saya H. Aurora-A and an interacting activator, the LIM protein Ajuba, are required for mitotic commitment in human cells. Cell 2003; 114:585–598.
5. Hoar K, Chakravarty A, Rabino C, Wysong D, Bowman D, Roy N, Ecsedy JA. MLN8054, a small-molecule inhibitor of Aurora A, causes spindle pole and chromosome congression defects leading to aneuploidy. Mol Cell Biol 2007; 27:4513–4525.
6. Marumoto T, Honda S, Hara T, Nitta M, Hirota T, Kohmura E, Saya H. Aurora-A kinase maintains the fidelity of early and late mitotic events in HeLa cells. J Biol Chem 2003; 278:51786–51795.
7. Mori D, Yano Y, Toyo-oka K, Yoshida N, Yamada M, Muramatsu M, Zhang D, Saya H, Toyoshima YY, Kinoshita K, Wynshaw-Boris A, Hirotsune S. NDEL1 phosphorylation by Aurora-A kinase is essential for centrosomal maturation, separation, and TACC3 recruitment. Mol Cell Biol 2007; 27:352–367.
8. Cazales M, Schmitt E, Montembault E, Dozier C, Prigent C, Ducommun B. CDC25B phosphorylation by Aurora-A occurs at the G2/M transition and is inhibited by DNA damage. Cell Cycle 2005; 4:1233–1238.
9. Dutertre S, Cazales M, Quaranta M, Froment C, Trabut V, Dozier C, Mirey G, Bouche JP, Theis-Febvre N, Schmitt E, Monsarrat B, Prigent C, et al. Phosphorylation of CDC25B by Aurora-A at the centrosome contributes to the G2-M transition. J Cell Sci 2004; 117:2523–2531.
10. Macurek L, Lindqvist A, Lim D, Lampson MA, Klompmaker R, Freire R, Clouin C, Taylor SS, Yaffe MB, Medema RH. Polo-like kinase-1 is activated by aurora A to promote checkpoint recovery. Nature 2008; 455: 119–123.
11. Seki A, Coppinger JA, Jang CY, Yates JR, Fang G. Bora and the kinase Aurora a cooperatively activate the kinase Plk1 and control mitotic entry. Science 2008; 320:1655–1658.
12. Manfredi MG, Ecsedy JA, Meetze KA, Balani SK, Burenkova O, Chen W, Galvin KM, Hoar KM, Huck JJ, LeRoy PJ, Ray ET, Sells TB, et al. Antitumor activity of MLN8054, an orally active small-molecule inhibitor of Aurora A kinase. Proc Natl Acad Sci U S A 2007; 104:4106–4111.
13. Van Horn RD, Chu S, Fan L, Yin T, Du J, Beckmann R, Mader M, Zhu G, Toth J, Blanchard K, Ye XS. Cdk1 activity is required for mitotic activation of aurora A during G2/M transition of human cells. J Biol Chem 2010; 285:21849–21857.
14. Barr AR, Gergely F. Aurora-A: the maker and breaker of spindle poles. J Cell Sci 2007; 120:2987–2996.
15. Lens SM, Voest EE, Medema RH. Shared and separate functions of polo-like kinases and aurora kinases in cancer. Nat Rev Cancer 2010; 10: 825–841.
16. Saskova A, Solc P, Baran V, Kubelka M, Schultz RM, Motlik J. Aurora kinase A controls meiosis I progression in mouse oocytes. Cell Cycle 2008; 7:2368–2376.
17. Shuda K, Schindler K, Ma J, Schultz RM, Donovan PJ. Aurora kinase B modulates chromosome alignment in mouse oocytes. Mol Reprod Dev 2009; 76:1094–1105.
18. Solc P, Schultz RM, Motlik J. Prophase I arrest and progression to metaphase I in mouse oocytes: comparison of resumption of meiosis and recovery from G2-arrest in somatic cells. Mol Hum Reprod 2010; 16: 654–664.

Downloaded from www.biolreprod.org.

19. Bayliss R, Sardon T, Vernos I, Conti E. Structural basis of Aurora-A activation by TPX2 at the mitotic spindle. Mol Cell 2003; 12:851–862.
20. Tsai MY, Wiese C, Cao K, Martin O, Donovan P, Ruderman J, Prigent C, Zheng YA. Ran signalling pathway mediated by the mitotic kinase Aurora A in spindle assembly. Nat Cell Biol 2003; 5:242–248.
21. Brunet S, Dumont J, Lee KW, Kinoshita K, Hikal P, Gruss OJ, Maro B, Verlhac MH. Meiotic regulation of TPX2 protein levels governs cell cycle progression in mouse oocytes. PLoS ONE 2008; 3:e3338.
22. Ma C, Cummings C, Liu XJ. Biphasic activation of Aurora-A kinase during the meiosis I- meiosis II transition in Xenopus oocytes. Mol Cell Biol 2003; 23:1703–1716.
23. Nishimura Y, Endo T, Kano K, Naito K. Porcine Aurora A accelerates Cyclin B and Mos synthesis and promotes meiotic resumption of porcine oocytes. Anim Reprod Sci 2009; 113:114–124.
24. Hu HM, Chuang CK, Lee MJ, Tseng TC, Tang TK. Genomic organization, expression, and chromosome localization of a third aurora-related kinase gene, Aie1. DNA Cell Biol 2000; 19:679–688.
25. Kimmins S, Crosio C, Kotaja N, Hirayama J, Monaco L, Hoog C, van Duin M, Gossen JA, Sassone-Corsi P. Differential functions of the Aurora-B and Aurora-C kinases in mammalian spermatogenesis. Mol Endocrinol 2007; 21:726–739.
26. Kimura M, Matsuda Y, Yoshioka T, Okano Y. Cell cycle-dependent expression and centrosome localization of a third human aurora/Ipl1-related protein kinase, AIK3. J Biol Chem 1999; 274:7334–7340.
27. Chen HL, Tang CJ, Chen CY, Tang TK. Overexpression of an Aurora-C kinase-deficient mutant disrupts the Aurora-B/INCENP complex and induces polyploidy. J Biomed Sci 2005; 12:297–310.
28. Sharif B, Na J, Lykke-Hartmann K, McLaughlin SH, Laue E, Glover DM, Zernicka-Goetz M. The chromosome passenger complex is required for fidelity of chromosome transmission and cytokinesis in meiosis of mouse oocytes. J Cell Sci 2010; 123:4292–4300.
29. Schindler K, Davydenko O, Fram G, Lampson MA, Schultz RM. Maternally recruited Aurora C kinase is more stable than Aurora B to support mouse oocyte maturation and early development. Proc Natl Acad Sci U S A 2012; 109:E2215–E2222.
30. Bornslaeger EA, Mattei P, Schultz RM. Involvement of cAMP-dependent protein kinase and protein phosphorylation in regulation of mouse oocyte maturation. Dev Biol 1986; 114:453–462.
31. Downs SM, Daniel SA, Bornslaeger EA, Hoppe PC, Eppig JJ. Maintenance of meiotic arrest in mouse oocytes by purines: modulation of cAMP levels and cAMP phosphodiesterase activity. Gamete Res 1989; 23:323–334.
32. Masciarelli S, Horner K, Liu C, Park SH, Hinckley M, Hockman S, Nedachi T, Jin C, Conti M, Manganiello V. Cyclic nucleotide phosphodiesterase 3A-deficient mice as a model of female infertility. J Clin Invest 2004; 114:196–205.
33. Conti M, Hsieh M, Zamah AM, Oh JS. Novel signaling mechanisms in the ovary during oocyte maturation and ovulation. Mol Cell Endocrinol 2012; 356:65–73.
34. Han SJ, Chen R, Paronetto MP, Conti M. Wee1B is an oocyte-specific kinase involved in the control of meiotic arrest in the mouse. Curr Biol 2005; 15:1670–1676.
35. Lincoln AJ, Wickramasinghe D, Stein P, Schultz RM, Palko ME, De Miguel MP, Tessarollo L, Donovan PJ. Cdc25b phosphatase is required for resumption of meiosis during oocyte maturation. Nat Genet 2002; 30: 446–449.
36. Oh JS, Han SJ, Conti M. Wee1B, Myt1, and Cdc25 function in distinct compartments of the mouse oocyte to control meiotic resumption. J Cell Biol 2010; 188:199–207.
37. Nakajima H, Toyoshima-Morimoto F, Taniguchi E, Nishida E. Identification of a consensus motif for Plk (Polo-like kinase) phosphorylation reveals Myt1 as a Plk1 substrate. J Biol Chem 2003; 278:25277–25280.
38. Watanabe N, Arai H, Iwasaki J, Shiina M, Ogata K, Hunter T, Osada H. Cyclin-dependent kinase (CDK) phosphorylation destabilizes somatic Wee1 via multiple pathways. Proc Natl Acad Sci U S A 2005; 102: 11663–11668.
39. Zhang D, Hirota T, Marumoto T, Shimizu M, Kunitoku N, Sasayama T, Arima Y, Feng L, Suzuki M, Takeya M, Saya H. Cre-loxP-controlled periodic Aurora-A overexpression induces mitotic abnormalities and hyperplasia in mammary glands of mouse models. Oncogene 2004; 23: 8720–8730.
40. Lewandoski M, Wassarman KM, Martin GR. Zp3-cre, a transgenic mouse line for the activation or inactivation of loxP-flanked target genes specifically in the female germ line. Curr Biol 1997; 7:148–151.
41. Iannuccelli E, Mompart F, Gellin J, Lahbib-Mansais Y, Yerle M, Boudier T. NEMO: a tool for analyzing gene and chromosome territory distributions from 3D-FISH experiments. Bioinformatics 2010; 26: 696–697.
42. Sanfins A, Lee GY, Plancha CE, Overstrom EW, Albertini DF. Distinctions in meiotic spindle structure and assembly during in vitro and in vivo maturation of mouse oocytes. Biol Reprod 2003; 69: 2059–2067.
43. Littlepage LE, Wu H, Andresson T, Deanehan JK, Amundadottir LT, Ruderman JV. Identification of phosphorylated residues that affect the activity of the mitotic kinase Aurora-A. Proc Natl Acad Sci U S A 2002; 99:15440–15445.
44. Satinover DL, Leach CA, Stukenberg PT, Brautigan DL. Activation of Aurora-A kinase by protein phosphatase inhibitor-2, a bifunctional signaling protein. Proc Natl Acad Sci U S A 2004; 101:8625–8630.
45. Norris RP, Freudzon M, Nikolaev VO, Jaffe LA. Epidermal growth factor receptor kinase activity is required for gap junction closure and for part of the decrease in ovarian follicle cGMP in response to LH. Reproduction 2010; 140:655–662.
46. Norris RP, Ratzan WJ, Freudzon M, Mehlmann LM, Krall J, Movsesian MA, Wang H, Ke H, Nikolaev VO, Jaffe LA. Cyclic GMP from the surrounding somatic cells regulates cyclic AMP and meiosis in the mouse oocyte. Development 2009; 136:1869–1878.
47. Calarco-Gillam PD, Siebert MC, Hubble R, Mitchison T, Kirschner M. Centrosome development in early mouse embryos as defined by an autoantibody against pericentriolar material. Cell 1983; 35:621–629.
48. Szollosi D, Calarco P, Donahue RP. Absence of centrioles in the first and second meiotic spindles of mouse oocytes. J Cell Sci 1972; 11:521–541.
49. Carabatsos MJ, Combelles CM, Messinger SM, Albertini DF. Sorting and reorganization of centrosomes during oocyte maturation in the mouse. Microsc Res Tech 2000; 49:435–444.
50. Gueth-Hallonet C, Antony C, Aghion J, Santa-Maria A, Lajoie-Mazenc I, Wright M, Maro B. gamma-Tubulin is present in acentriolar MTOCs during early mouse development. J Cell Sci 1993; 105(Pt 1):157–166.
51. Schatten H, Sun QY. Centrosome dynamics during mammalian oocyte maturation with a focus on meiotic spindle formation. Mol Reprod Dev 2011; 78:757–768.
52. Nigg EA, Stearns T. The centrosome cycle: centriole biogenesis, duplication and inherent asymmetries. Nat Cell Biol 2011; 13:1154–1160.
53. Can A, Semiz O, Cinar O. Centrosome and microtubule dynamics during early stages of meiosis in mouse oocytes. Mol Hum Reprod 2003; 9: 749–756.
54. Schuh M, Ellenberg J. Self-organization of MTOCs replaces centrosome function during acentrosomal spindle assembly in live mouse oocytes. Cell 2007; 130:484–498.
55. Mahen R, Venkitaraman AR. Pattern formation in centrosome assembly. Curr Opin Cell Biol 2012; 24:14–23.
56. Breuer M, Kolano A, Kwon M, Li CC, Tsai TF, Pellman D, Brunet S, Verlhac MH. HURP permits MTOC sorting for robust meiotic spindle bipolarity, similar to extra centrosome clustering in cancer cells. J Cell Biol 2010; 191:1251–1260.
57. Panigone S, Hsieh M, Fu M, Persani L, Conti M. Luteinizing hormone signaling in preovulatory follicles involves early activation of the epidermal growth factor receptor pathway. Mol Endocrinol 2008; 22: 924–936.
58. Park JY, Su YQ, Ariga M, Law E, Jin SL, Conti M. EGF-like growth factors as mediators of LH action in the ovulatory follicle. Science 2004; 303:682–684.
59. Jullien D, Bugler B, Dozier C, Cazales M, Ducommun B. Identification of N-terminally truncated stable nuclear isoforms of CDC25B that are specifically involved in G2/M checkpoint recovery. Cancer Res 2011; 71: 1968–1977.
60. van Vugt MA, Bras A, Medema RH. Polo-like kinase-1 controls recovery from a G2 DNA damage-induced arrest in mammalian cells. Mol Cell 2004; 15:799–811.
61. Pirino G, Wescott MP, Donovan PJ. Protein kinase A regulates resumption of meiosis by phosphorylation of Cdc25B in mammalian oocytes. Cell Cycle 2009; 8:665–670.
62. Zhang Y, Zhang Z, Xu XY, Li XS, Yu M, Yu AM, Zong ZH, Yu BZ. Protein kinase A modulates Cdc25B activity during meiotic resumption of mouse oocytes. Dev Dyn 2008; 237:3777–3786.
63. Kramer A, Maier B, Bartek J. Centrosome clustering and chromosomal (in)stability: a matter of life and death. Mol Oncol 2011; 5:324–335.
64. Toya M, Terasawa M, Nagata K, Iida Y, Sugimoto A. A kinase-independent role for Aurora A in the assembly of mitotic spindle microtubules in *Caenorhabditis elegans* embryos. Nat Cell Biol 2011; 13: 708–714.
65. Peset I, Seiler J, Sardon T, Bejarano LA, Rybina S, Vernos I. Function and regulation of Maskin, a TACC family protein, in microtubule growth during mitosis. J Cell Biol 2005; 170:1057–1066.
66. Ibanez E, Sanfins A, Combelles CM, Overstrom EW, Albertini DF. Genetic strain variations in the metaphase-II phenotype of mouse oocytes matured in vivo or in vitro. Reproduction 2005; 130:845–855.

Downloaded from www.biolreprod.org.

PLOS ONE

RESEARCH ARTICLE

Multiple Requirements of PLK1 during Mouse Oocyte Maturation

Petr Solc[1]*‡, Tomoya S. Kitajima[2,4]*‡, Shuhei Yoshida[4], Adela Brzakova[1], Masako Kaido[4], Vladimir Baran[3], Alexandra Mayer[1], Pavlina Samalova[1], Jan Motlik[1], Jan Ellenberg[2]

1 Institute of Animal Physiology and Genetics, Libechov, Czech Republic, **2** Cell Biology and Biophysics Unit, European Molecular Biology Laboratory, Heidelberg, Germany, **3** Institute of Animal Physiology, Kosice, Slovakia, **4** Laboratory for Chromosome Segregation, RIKEN Center for Developmental Biology, Kobe, Japan

‡ These authors contributed equally to this work.
* solc@iapg.cas.cz (PS); tkitajima@cdb.riken.jp (TSK)

CrossMark
click for updates

OPEN ACCESS

Citation: Solc P, Kitajima TS, Yoshida S, Brzakova A, Kaido M, Baran V, et al. (2015) Multiple Requirements of PLK1 during Mouse Oocyte Maturation. PLoS ONE 10(2): e0116783. doi:10.1371/journal.pone.0116783

Academic Editor: Kyung S. Lee, National Cancer Institute, NIH, UNITED STATES

Received: September 29, 2014

Accepted: December 12, 2014

Published: February 6, 2015

Copyright: © 2015 Solc et al. This is an open access article distributed under the terms of the Creative Commons Attribution License, which permits unrestricted use, distribution, and reproduction in any medium, provided the original author and source are credited.

Data Availability Statement: All relevant data are within the paper and its Supporting Information files.

Funding: This work was supported by the research grants from Ministry of Education, Youth and Sports of the Czech Republic (http://www.msmt.cz, LH12057) and from Grant Agency of the Czech Republic (http://www.gacr.cz, P301-11-P081) to P. S.; Japan Society for the Promotion of Science KAKENHI (https://www.jsps.go.jp, 00376641), Nakajima Foundation (http://www.nakajimafound.or.jp), Uehara Memorial Foundation (http://www.ueharazaidan.or.jp) to T. S. K.; Grant Agency of the Czech Republic (http://www.gacr.cz, 301-09-J036) to

Abstract

Polo-like kinase 1 (PLK1) orchestrates multiple events of cell division. Although PLK1 function has been intensively studied in centriole-containing and rapidly cycling somatic cells, much less is known about its function in the meiotic divisions of mammalian oocytes, which arrest for a long period of time in prophase before meiotic resumption and lack centrioles for spindle assembly. Here, using specific small molecule inhibition combined with live mouse oocyte imaging, we comprehensively characterize meiotic PLK1's functions. We show that PLK1 becomes activated at meiotic resumption on microtubule organizing centers (MTOCs) and later at kinetochores. PLK1 is required for efficient meiotic resumption by promoting nuclear envelope breakdown. PLK1 is also needed to recruit centrosomal proteins to acentriolar MTOCs to promote normal spindle formation, as well as for stable kinetochore-microtubule attachment. Consequently, PLK1 inhibition leads to metaphase I arrest with misaligned chromosomes activating the spindle assembly checkpoint (SAC). Unlike in mitosis, the metaphase I arrest is not bypassed by the inactivation of the SAC. We show that PLK1 is required for the full activation of the anaphase promoting complex/cyclosome (APC/C) by promoting the degradation of the APC/C inhibitor EMI1 and is therefore essential for entry into anaphase I. Moreover, our data suggest that PLK1 is required for proper chromosome segregation and the maintenance of chromosome condensation during the meiosis I-II transition, independently of the APC/C. Thus, our results define the meiotic roles of PLK1 in oocytes and reveal interesting differential requirements of PLK1 between mitosis and oocyte meiosis in mammals.

Introduction

Polo-like kinase 1 (PLK1) plays a variety of roles in mitotic cell division[1–3]. PLK1 controls the timing of mitotic entry[4], centrosome maturation[5], chromosome cohesion[6], kinetochore-microtubule attachment[4,7], and cytokinesis[8–12]. Although much information about

J. M.; European Community's Seventh Framework Programme [FP7/2007-2013] (http://cordis.europa.eu/fp7/home_en.html) under grant agreement n° [241548] "Mitosys" and the German Research Foundation DFG (http://www.dfg.de/en/, EL246/4-1,2) within the SPP 1384 "Mechanisms of Genome Haploidization" to J. E. T. S. K. was partly supported by the long-term fellowship from Human Frontier Science Program (http://www.hfsp.org/). A. B. and A. M. were partly supported by Grant Agency of the Czech Republic (http://www.gacr.cz, P502/11/0593). V. B. was supported by Slovak Research and Development Agency (http://www.apvv.sk, APVV-0237-10). Work at IAPG was supported by Institutional Research Concept 67985904 (IAPG AS CR, v.v.i., http://www.iapg.cas.cz/). This work significantly benefited from European Regional Development Fund (http://ec.europa.eu/regional_policy/thefunds/regional/index_en.cfm, ExAM CZ.1.05/2.1.00/03.0124) to J. M. The funders had no role in study design, data collection and analysis, decision to publish, or preparation of the manuscript.

Competing Interests: The authors have declared that no competing interests exist.

the mitotic roles of PLK1 has been accumulated, our understanding of PLK1 function during meiosis in mammalian oocytes remains relatively poor. It has been reported that in mammalian oocytes, PLK1 is involved in resumption of meiosis[13–15], spindle formation[15,16], and RhoA-mediated cytokinesis[17]. However, how PLK1 controls resumption of meiosis and spindle formation, as well as in other meiotic processes such as kinetochore-microtubule attachment, APC/C activation, and meiosis I—meiosis II transition, are largely unknown in oocytes.

One unique feature of the oocyte is that it undergoes a long prophase arrest before entering M-phase of meiosis I. Resumption of meiosis is characterized by two visible, tightly coupled events: nuclear envelope breakdown (NEBD) and chromosome condensation. The resumption depends on the activity of CDK1, which is positively regulated by the phosphatases CDC25A/B [18,19]. PLK1 controls meiotic resumption in oocytes by participation in CDK1 autoamplification loop[14]. In somatic cells, PLK1 controls the activity of CDK1 by phosphorylating cyclin B[20] and multiple regulators, such as CDC25B[21], CDC25C[22,23] and WEE1[24], although it is not absolutely essential for mitotic entry[4,25]. Moreover, after DNA damage and subsequent arrest at the G2 phase in somatic cells, PLK1 promotes G2-checkpoint recovery[26,27], which is very similar in many aspects to the resumption of meiosis I[28]. However, a direct requirement of PLK1 independent of CDK1 activity for the resumption of meiosis I in oocytes has not been experimentally demonstrated.

Another unique feature of the oocyte is that it lacks centriole-containing centrosomes. In oocytes, instead of centrosomes, there are many acentriolar MTOCs throughout the cytoplasm, which self-assemble into an acentriolar bipolar spindle[29]. It is known that in somatic cells, PLK1 localizes to centrosomes[30] and promotes microtubule nucleation by recruiting the γ-tubulin complex. In mouse oocytes, PLK1 localizes to MTOCs[15,16] and microinjection of PLK1 antibody disturbs normal bipolar spindle formation[15]. However, it is unknown whether PLK1 regulates the maturation of acentriolar MTOCs and how PLK1 impacts the kinetics of spindle formation and bipolarization.

As the spindle forms, condensed chromosomes gradually congress towards the equatorial plane of the forming spindle, resulting in a belt-like spatial arrangement of chromosomes, the prometaphase belt[31]. After the prometaphase belt is formed, microtubules begin the process of chromosome biorientation by attaching to kinetochores. In contrast to somatic cells, the most prominent kinetochore fibers that can be detected in oocytes with electron microscopy form at the very late stage of metaphase I[32], suggesting an oocyte-specific regulation of kinetochore-microtubule attachments. Although it is known that in somatic cells, PLK1 stabilizes kinetochore-microtubule attachments during prometaphase and maintains correct attachment during metaphase[4,7,25,33,34], it remains unclear whether PLK1 plays a similar role in kinetochore-microtubule attachment during oocyte meiosis.

Kinetochore-microtubule attachment silences the SAC, a surveillance mechanism that inhibits anaphase onset[35]. Once the SAC is silenced, the APC/C becomes activated. The APC/C mediates the degradation of securin and cyclin B to trigger anaphase. In mitosis, PLK1 inhibition leads to a failure in APC/C activation because a defect in kinetochore-microtubule attachment activates the SAC[4,7,25]. In addition, PLK1 has been speculated to regulate APC/C activity. PLK1 phosphorylates the APC/C inhibitor EMI1, mediating its degradation during prometaphase[36,37]. PLK1 also directly phosphorylates the APC/C, which is implicated in regulating APC/C activity[38–40]. However, neither the EMI1 degradation nor APC/C phosphorylation is essential for anaphase entry in mammalian somatic cells because the mitotic arrest caused by PLK1 perturbation can be released by the inactivation of the SAC alone [4,7,25,40]. It is unknown whether PLK1 is involved in these pathways that activate the APC/C during oocyte meiosis I, and if so, whether they are essential for anaphase I onset.

In this study, we comprehensively investigate the multiple functions of PLK1 in mouse oocyte meiosis by using specific and acute temporal pharmacological inhibition, combined with live imaging and quantitative immunostaining. We demonstrate that PLK1 promotes nuclear envelope permeabilization during NEBD independently of CDK1 activity. Similarly as in mitosis, PLK1 recruits centrosomal proteins to acentriolar MTOCs, promotes efficient spindle formation and kinetochore-microtubule attachment, and thus is required for satisfying the SAC. In contrast to mitosis, SAC silencing is not sufficient for anaphase I entry in PLK1-inhibited oocytes because PLK1 is essential for APC/C activation through at least two pathways independently of the SAC satisfaction. In addition, our data suggest meiotic-specific requirements of PLK1 for chromosome segregation and the maintenance of the condensed state of chromosomes during the meiosis I—meiosis II transition.

Results

PLK1 dynamically changes its localization during meiotic maturation

It has been reported that PLK1 localizes uniformly in the cytoplasm at the germinal vesicle (GV) stage, at MTOCs and kinetochores from NEBD to metaphase I, and at the spindle midzone at anaphase I in mouse oocytes [14,15,41]. However, the changes in PLK1 localization in live oocytes have not been quantitatively analyzed. To address this question, we recorded 4D datasets of EGFP-PLK1 localization in live oocytes. EGFP-PLK1 exhibited punctate signals throughout the cytoplasm at the GV stage (S1A Fig.), and localized to the spindle poles from prometaphase to metaphase I (Fig. 1A, S1 Movie). The EGFP-PLK1 also co-localized with the kinetochore marker 3mCherry-CENP-C (Fig. 1A, S1 Movie). The localizations at MTOCs and kinetochores were further confirmed by immunostaining of endogenous PLK1 (Fig. 1B, C). At anaphase I, EGFP-PLK1 disappeared from the spindle poles and kinetochores and relocated to the spindle midzone (Fig. 1A, S1A Fig., S1 Movie) with approximately 12-fold enrichment above the levels on the earlier kinetochores (S1B Fig.). Thus, these results confirm that PLK1 dynamically changes its localization between three key cell division structures during meiosis I in mouse oocytes.

PLK1 becomes activated during the resumption of meiosis

Previous biochemical analysis has indicated that PLK1 activity increases before resumption of meiosis and persists during meiotic maturation[14]. To examine the local PLK1 activity in individual oocytes in a time course, we used quantitative immunofluorescence staining for the phosphorylation of T210 (pPLK1), which specifically labels the activated form of PLK1[26]. The pPLK1 signals began to be detected 20 minutes before NEBD (40 minutes after the induction of meiotic resumption) colocalizing with the MTOC marker pericentrin, and reached its maximum level at the time of NEBD (Fig. 1B). From prometaphase to metaphase I, pPLK1 was highly concentrated on MTOCs and kinetochores (Fig. 1B,C), which is consistent with the results of EGFP-PLK1. These data demonstrate that PLK1 becomes activated around NEBD at MTOCs during the resumption of meiosis and, later, also at kinetochores.

PLK1 localizations on MTOCs and kinetochores are differentially regulated by its own activity

The temporal difference in PLK1 localizations between MTOCs and kinetochores prompted us to ask whether these localizations are differentially controlled by PLK1's own activity. To this end, we treated oocytes with BI2536, a small molecule inhibitor known to specifically inhibit PLK1 in somatic cells [25] and in oocytes [42] as well as in chemical genetics studies [43,44].

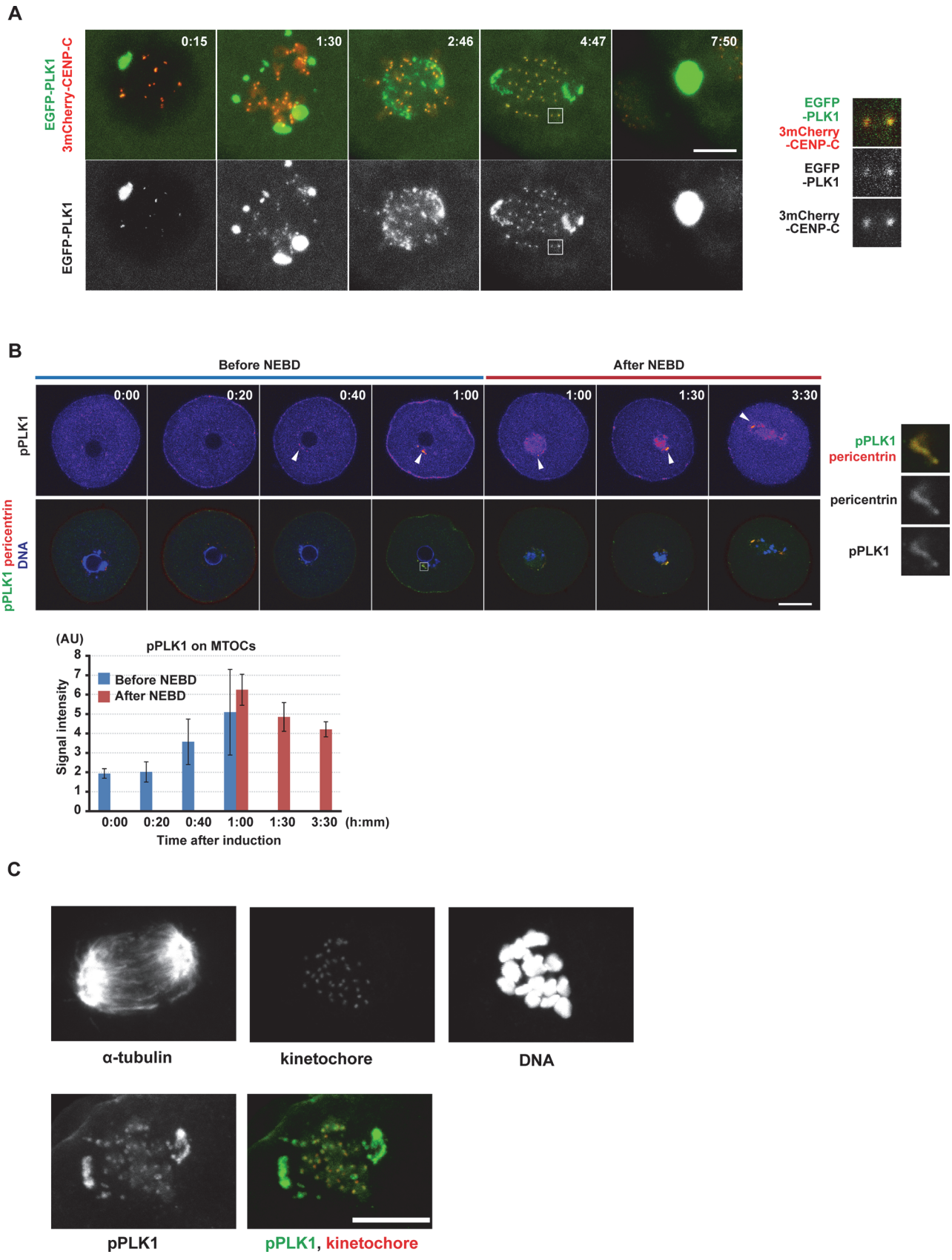
A
EGFP-PLK1
3mCherry-CENP-C
0:15
1:30
2:46
4:47
7:50
EGFP-PLK1
EGFP -PLK1 3mCherry -CENP-C
EGFP -PLK1
3mCherry -CENP-C
B
Before NEBD
After NEBD
pPLK1
pPLK1 pericentrin DNA
0:00
0:20
0:40
1:00
1:00
1:30
3:30
pPLK1 pericentrin
pericentrin
pPLK1
(AU)
pPLK1 on MTOCs
Before NEBD
After NEBD
Signal intensity
0 1 2 3 4 5 6 7 8
0:00 0:20 0:40 1:00 1:30 3:30 (h:mm)
Time after induction
C
α-tubulin
kinetochore
DNA
pPLK1
pPLK1, kinetochore

Fig 1. PLK1 localizes to MTOCs and kinetochores and becomes activated around NEBD. (A) Imaging of meiosis I in oocytes expressing EGFP-PLK1 (green) and 3mCherry-CENP-C (kinetochores, red). Maximum intensity z-projection images are shown. At 7:50, the saturated signal locates at the spindle midzone, as shown in S1A Fig. Time after induction of meiotic resumption (h:mm). Scale bar = 10 μm. Insets show magnified images on kinetochores. Also see S1 Movie. (B) Immunostaining of active PLK1 phosphorylated on T210 (pPLK1) during meiosis I. Pictures represent single selected confocal sections through MTOCs for pPLK1 (fire-pseudocolored or green) and pericentrin (MTOCs, red) and maximum intensity z-projection for DAPI (DNA, blue). Arrowheads indicate pPLK1 signals on MTOCs. Time after induction of meiotic resumption (h:mm). Quantification of MTOC-associated pPLK1 signals (n = 11, 5, 7, 5, 5, 9, 17 oocytes). Averages with the 95% confidence intervals are shown. Scale bar = 20 μm. Insets show magnified images on MTOCs. (C) Localization of pPLK1 on kinetochores in metaphase I oocytes. Oocytes stained for pPLK1 (green), kinetochores (CREST, red), acetylated α-tubulin, and DAPI (DNA). Scale bar = 10 μm.

doi:10.1371/journal.pone.0116783.g001

We tested the concentrations of 20–200 nM BI2536, and found that the 100 nM concentration maximally reduced the phosphorylation of BUBR1 at T669 (S1C Fig.), the residue that corresponds to the known PLK1 target T680 of human BUBR1 on mitotic kinetochores [45]. Because this concentration had no detectable effect on the histone H3 S28 phosphorylation (S1D Fig.), which depends on Aurora kinases in oocytes [46], and is shown to specifically inhibit PLK1 in somatic cells[25], we used the 100 nM concentration in all experiments to inhibit PLK1 in this study. In BI2536-treated oocytes, the EGFP-PLK1 localization on MTOCs dramatically decreased (S1E Fig.), whereas the level on kinetochores significantly increased (S1E Fig.). Thus, these results suggest that in oocytes, the PLK1 localizations at MTOCs and kinetochores are differentially regulated by its own activity.

PLK1 is required for the timing of nuclear envelope permeabilization

The activation of PLK1 before NEBD (Fig. 1 B,C) is consistent with its known role in CDK1 autoamplification during resumption of meiosis[14,47]. The resumption of meiosis is associated with two clearly visible changes in the oocytes: NEBD and chromosome condensation. To explore the possibility that PLK1 plays a role in these processes, we microinjected fluorescent 70 kDa-dextran into the cytoplasm of H2B-EGFP-expressing oocytes and treated them with BI2536 immediately after the induction of meiotic resumption. To analyze the progression of chromosome condensation, we reconstructed the H2B-EGFP chromosome signals in 3D and measured its volume. To analyze the permeabilization of nuclear membranes as the first step of NEBD, we measured the entry of 70 kDa-dextran into the nucleus (Fig. 2A-C, S2 Fig. and S2 Movie). In BI2536-treated oocytes, both NEBD and chromosome condensation were significantly delayed (Fig. 2B), indicating that PLK1 is required for promoting these processes. Moreover, we noticed that the onset of NEBD was more affected than that of chromosome condensation by the BI2536 treatment (Fig. 2B), which was manifested by the presence of condensed chromosomes inside of the intact nucleus (Fig. 2A, BI2536 arrowheads). Chromosome condensation was triggered prematurely 8.0 ± 5.5 minutes before the onset of dextran entry when PLK1 was inhibited, while chromosome condensation normally started 3.8 ± 1.7 minutes after the onset of dextran entry in control oocytes (Fig. 2B-D). Thus, these results suggest that PLK1 is required for timely initiation of NEBD followed by the onset of chromosome condensation.

Because PLK1 is involved in an autoamplification loop activating CDK1[20,21], it was possible that the effects on the timing of NEBD and chromosome condensation by PLK1 inhibition are solely consequences of impaired CDK1 activity. To address this possibility, we used partial pharmacological CDK1 inhibition by 1 μM flavopiridol [48]. As anticipated, flavopiridol-treated oocytes were overall delayed in chromosome condensation and NEBD onsets oocytes (Fig. 2A, B). However, in contrast to PLK1 inhibition, CDK1 inhibition delayed the onset of chromosome condensation much more than that of NEBD (Fig. 2B-D). Live imaging of lamin B1-EGFP further demonstrated distinct effects of CDK1 versus PLK1 inhibition. While lamin disassembly was delayed by flavopirodol, it was not affected by BI2536 (S3A–B Fig.).

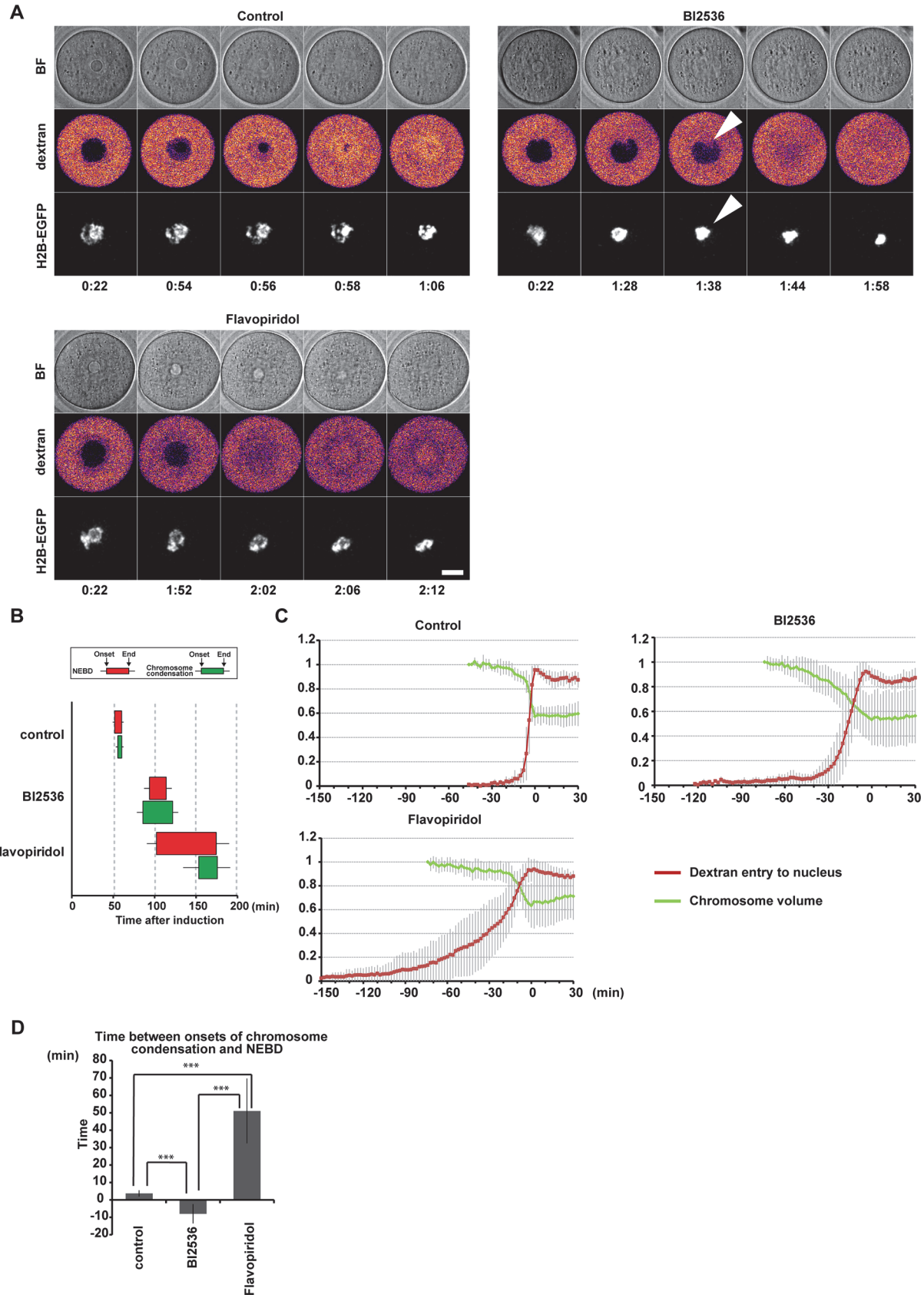
A
Control
BI2536
BF
dextran
H2B-EGFP
0:22
0:54
0:56
0:58
1:06
0:22
1:28
1:38
1:44
1:58
Flavopiridol
0:22
1:52
2:02
2:06
2:12
B
Onset
End
NEBD
Chromosome condensation
control
BI2536
Flavopiridol
0
50
100
150
200 (min)
Time after induction
C
Control
BI2536
Flavopiridol
Dextran entry to nucleus
Chromosome volume
-150
-120
-90
-60
-30
0
30
(min)
D
Time between onsets of chromosome condensation and NEBD
(min)
Time
***
control
BI2536
Flavopiridol

Fig 2. PLK1 promotes NEBD during meiotic resumption. (A) Imaging of H2B-EGFP-expressing oocytes microinjected with 70kDa-dextran-TAMRA in control, 100 nM BI2536 and 1 μM flavopiridol medium. Pictures represent single section from bright field (BF), single confocal section of 70kDa-dextran-TAMRA signals (fire-pseudocolored) and maximum intensity z-projection for H2B-EGFP (gray). Arrowheads indicate condensed chromosomes in the intact nucleus, specifically observed in BI2536-treated oocytes. Time after induction of meiotic resumption (h:mm). Scale bar = 20 μm. Also see S2 Movie. (B) Onsets and ends of chromosome condensation (green) and NEBD (red) in control, BI2536, and flavopiridol oocytes were defined according to S2 Fig. by measuring chromosome volume and the nuclear entry of 70 kDa dextran-TAMRA. The left and right sides of the box indicates the mean timings of the onset and end of the process, respectively, with the 95% confidence intervals (n = 16, 17, 15). (C) Kinetics of chromosome condensation (green) and 70 kDa-dextran-TAMRA nuclear entry (red) in control, BI2536 and flavopiridol oocytes. Curves represents mean values with s.d. (n = 16, 17, 15). Time at the point when chromosomes reached minimum volume was defined as t = 0. Chromosome volumes were normalized to 1 at -46 minutes in control and at -74 minutes in BI2536 and flavoporidol groups. Nuclear dextran signals were scaled between 0 and 1, according to the global minimum and maximum. (D) Time delay between onsets of chromosome condensation and dextran nuclear entry (delay = t2 - t1, according to S2 Fig.). Averages with the 95% confidence intervals are shown (n = 16, 17, 15; ***$p<0.001$).

doi:10.1371/journal.pone.0116783.g002

These results suggest that effect of PLK1 on NEBD and chromosome condensation cannot be explained only by the known role of PLK1 in CDK1 activation but PLK1 has probably additional functions in regulatiing these processes. Collectively, our results suggest that PLK1 promotes timely initiation of NEBD.

PLK1 promotes the formation of acentriolar bipolar spindles

In mitosis, PLK1 activity is required for centrosomal microtubule nucleation and the establishment of spindle bipolarity[4,5,7,25]. To explore the role of PLK1 in acentriolar spindle formation in oocytes, we imaged the microtubule marker EGFP-MAP4[29] in live oocytes treated with BI2536 (Fig. 3A, S3 Movie). In control oocytes, after NEBD, microtubules formed an apolar ball-like spindle, the microtubule ball, which elongated into a bipolar spindle 2.4 ± 0.4 hours after NEBD (Fig. 3A,B). In the BI2536-treated oocytes, however, the time of spindle elongation was significantly delayed to 3.7 ± 0.8 hours after NEBD. Furthermore, the sizes of the formed microtubule ball and elongated bipolar spindle were significantly smaller in the BI2536-treated oocytes (Fig. 3C, S4A–B Fig.). Thus, PLK1 is required for efficient bipolarization and establishment of the proper size of the acentriolar spindle.

PLK1 promotes the recruitment of γ-tubulin and pericentrin to MTOCs

In somatic cells, PLK1 facilitates the recruitment of centrosomal material including γ-tubulin and pericentrin[5,49–52]. We found that in BI2536-treated oocytes, the poles of the metaphase I spindle contained a markedly lower amount of γ-tubulin and considerably reduced pericentrin (Fig. 3D,E). Moreover, whereas control oocytes contained several cytoplasmic MTOCs that were not associated with the spindle poles, such MTOCs were never observed in the BI2536-treated oocytes (Fig. 3D,E). Collectively, these data indicate that the defects in spindle assembly kinetics in PLK1-inhibited oocytes are at least partly a consequence of strongly compromised MTOCs.

Prometaphase belt formation in PLK1-inhibited oocytes

Although the MTOC function is impaired in BI2536-treated oocytes, a bipolar spindle is still formed. Nevertheless, the BI2536-treated oocytes showed chromosome misalignment at metaphase I (Fig. 3A,D). To address how chromosomes fail to align in these oocytes, we analyzed chromosome dynamics in detail by high resolution live imaging and the complete tracking of kinetochores[31] (Fig. 4A, S4 Movie). We observed a slight but not significant delay in the prometaphase belt formation (S5A–B Fig.) (2.5 ± 0.2 hours after NEBD in control v.s. 2.8 ± 0.5 hours in BI2536-treated oocytes, p = 0.81), although the arrangement was somewhat distorted (S5A Fig.). In this arrangement, most of the chromosomes were nevertheless located around the spindle equator (Fig. 4B, 0:00), exhibiting a mean chromosome-equator distance that was

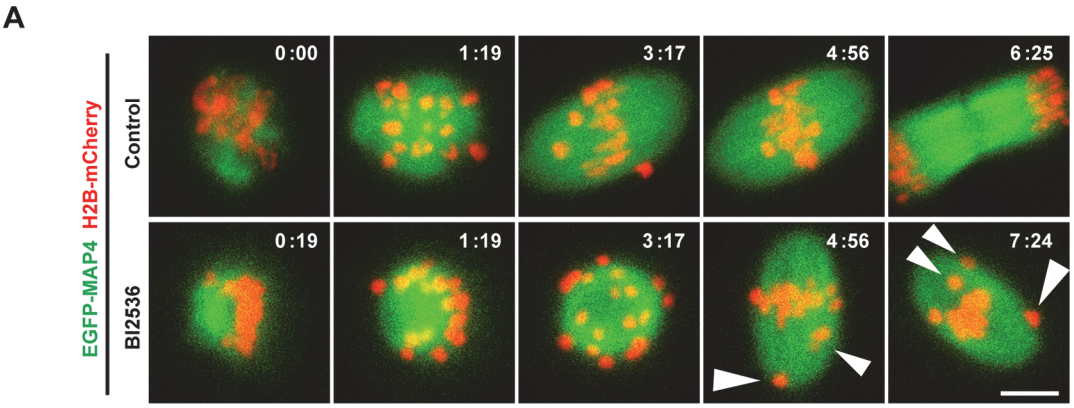
A
EGFP-MAP4 H2B-mCherry
Control
BI2536
0:00
1:19
3:17
4:56
6:25
0:19
1:19
3:17
4:56
7:24

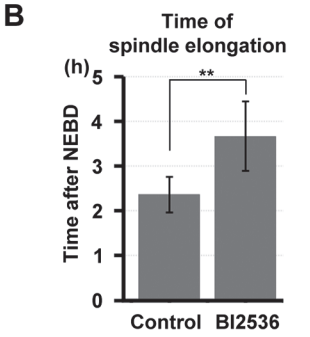
B
Time of spindle elongation
(h)
Time after NEBD
**
Control
BI2536

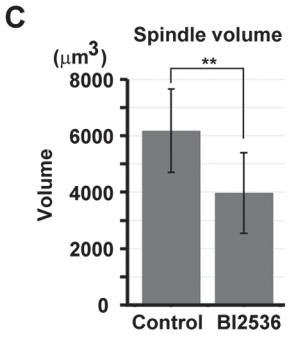
C
Spindle volume
(μm3)
Volume
**
Control
BI2536

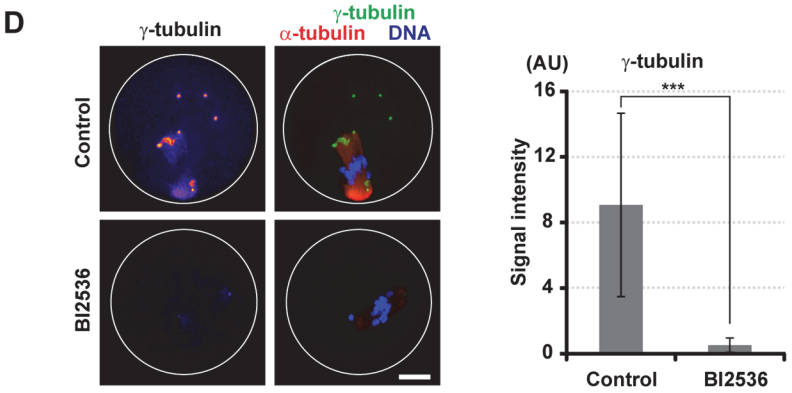
D
γ-tubulin
γ-tubulin
α-tubulin DNA
Control
BI2536
(AU)
γ-tubulin
Signal intensity
***
Control
BI2536

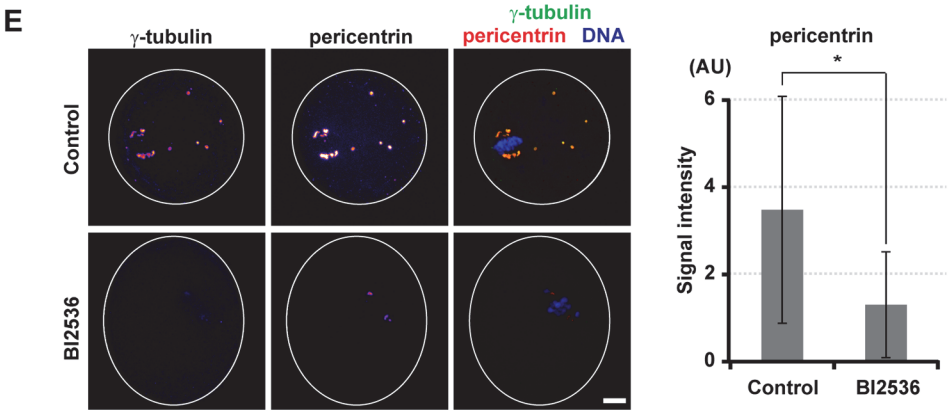
E
γ-tubulin
pericentrin
γ-tubulin
pericentrin DNA
Control
BI2536
pericentrin
(AU)
Signal intensity
*
Control
BI2536

Fig 3. PLK1 is required for spindle formation with acentriolar MTOCs. (A) Imaging of meiosis I in oocytes expressing EGFP-MAP4 (microtubules, green) and H2B-mCherry (chromosomes, red) in the presence of DMSO (control) or 100 nM BI2536. Maximum intensity z-projection images are shown. Arrowheads indicate misaligned chromosomes. Time after NEBD (h:mm). Scale bar = 10 μm. Also see S3 Movie. (B) The EGFP-MAP4 signals were reconstructed in 3D (see S4A Fig.) and the time of spindle elongation was determined. Averages and s.d. are shown (n = 8, 17. $^{**}p < 0.01$). (C) The volume of the spindle at 6 hours after NEBD was measured after 3D reconstruction of EGFP-MAP4 signals. Average and s.d (n = 8, 17. $^{**}p < 0.01$). (D) Control and BI2536-treated oocytes at metaphase I were stained either for γ-tubulin (green) and acetylated α-tubulin (red) or (E) for γ-tubulin (green) and pericentrin (red). DNA was stained with DAPI (blue). Maximum z-projections of entire confocal stacks are shown. Scale bar = 10 μm. Quantifications of the spindle pole-associated integrated signals of γ-tubulin and pericentrin. Averages with the 95% confidence intervals are shown (n = 6, 7, 4, 4. $^{***}p < 0.002$, $^{*}p < 0.05$).

doi:10.1371/journal.pone.0116783.g003

comparable to that in the control oocytes (2.4 ± 1.8 μm in the control vs. 3.1 ± 2.1 μm in the BI2536-treated, p = 0.053) (Fig. 4D, 0 hour). Thus, the defect in prometaphase belt formation could contribute to, but does not fully account for, the chromosome misalignment that was observed at metaphase I in the PLK1-inhibited oocytes.

PLK1 is required for proper kinetochore-microtubule attachment

In oocytes, kinetochore-microtubule attachment begins to be detected after the establishment of the prometaphase belt[31,32]. In mitosis, PLK1 is required for stable kinetochore-microtubule attachment[4,7,25,34]. To assess whether PLK1 plays a similar role in oocytes, we analyzed chromosome movements after prometaphase belt formation. In control oocytes, the majority of the chromosomes began biorientation 20 minutes after the establishment of the prometaphase belt, oscillating within 8 μm around the spindle equator, and the chromosome alignment was maintained until the onset of anaphase I (Fig. 4B,C). However, in BI2536-treated oocytes, the chromosomes moved towards the spindle poles during biorientation attempts, and their positions reached a maximum of 16 μm away from the spindle equator (Fig. 4B,C). The mean chromosome-equator distance became markedly different between the control and BI2536-treated oocytes 2 hours after establishment of the prometaphase belt (1.8 ± 1.6 μm in the control vs. 5.2 ± 4.4 μm in the BI2536-treated oocytes, $p < 0.0001$) (Fig. 4D). These misaligned chromosomes frequently remained at the polar region of the spindle until late metaphase I (Fig. 4C). These data indicate that the majority of misaligned chromosomes observed in the BI2536-treated metaphase I oocytes were generated after the completion of prometaphase belt formation.

To examine whether this defect is related to kinetochore-microtubule attachments, we immunostained stable microtubules after cold treatment. In BI2536-treated oocytes, the population of unattached kinetochores was significantly increased (Fig. 4E), indicating that PLK1 activity is required for stable kinetochore-microtubule attachment. Consistently, we found that the distance between homologous kinetochores at metaphase I was significantly shorter in BI2536-treated oocytes (S5C Fig.). In human somatic cells, one of the PLK1 targets critical for kinetochore function is the residue T680 of BUBR1[45], which corresponds to T669 of mouse BUBR1. We found that the BUBR1 phosphorylation level at T669 was significantly decreased in BI2536-treated oocytes (S1C Fig.). Collectively, our data suggest that PLK1 phosphorylates BUBR1 and promotes stable kinetochore-microtubule attachment.

The APC/C is not activated in PLK1-inhibited oocytes

In somatic cells, PLK1-inhibited cells arrest at mitosis with misaligned chromosomes because the APC/C is not activated due to the prolonged activity of the SAC[4,7,25]. Consistent with this, we found that BI2536-treated oocytes failed to enter anaphase I with misaligned chromosomes (Figs. 3 and 4). To confirm that this arrest is due to the absence of APC/C activation, we monitored the change in APC/C activity using the established marker securin-EGFP[53]. In control oocytes, the securin-EGFP level began to decline at approximately 6 hours after NEBD,

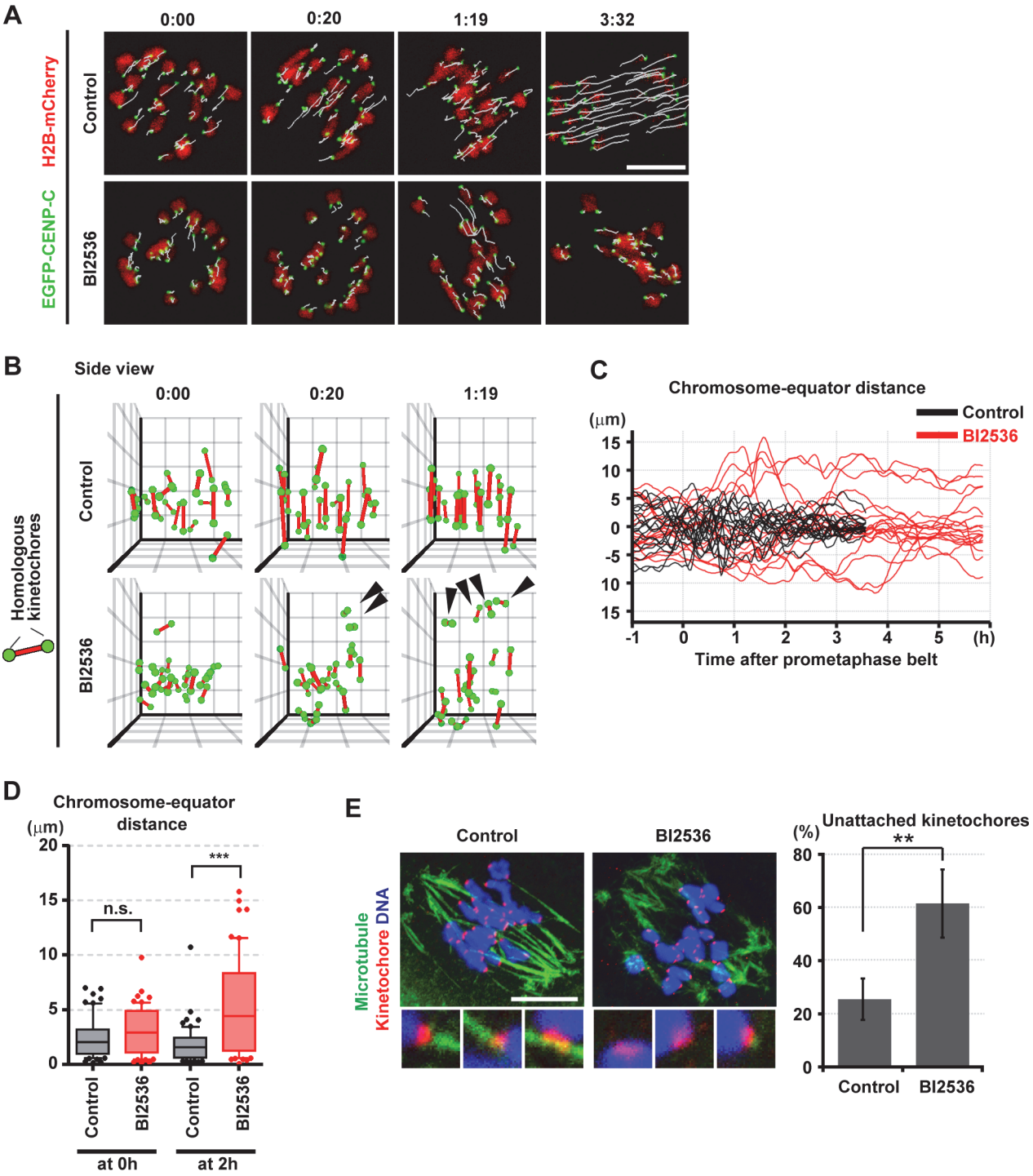

Fig 4. PLK1 is required for chromosome alignment. (A) Imaging of meiosis I in oocytes expressing EGFP-CENP-C (kinetochores, green) and H2B-mCherry (chromosomes, red) in the presence of DMSO (control) or 100 nM BI2536. Maximum intensity z-projection images are shown. White lines indicate kinetochore tracks over 5 timepoints. Time after NEBD (h:mm). Scale bar = 10 μm. Also see S4 Movie. (B) Kinetochore positions were determined from (A) and shown in the 3D plot as green spheres. Red bars connect homologous kinetochores. The view along the chromosome distribution equator (side view) is shown. Black arrowheads indicate misaligned chromosomes. Time after prometaphase belt formation (h:mm). The unit of the grid is 5 μm. (C) Chromosome positions along the estimated spindle axis were plotted for all twenty chromosomes of a single oocyte cultured in the presence of DMSO (control, black) or 100 nM BI2536 (red). (D) Distances between chromosomes and the equator at 0 and 2 hours after the prometaphase belt formation were potted. The box indicates 10–90 percentile (n = 60, 60, 60, 60 from three oocytes for each condition). ***$p < 0.0001$. (E) Oocytes 4 hours after NEBD were briefly treated with a cold buffer and fixed for immunostaining of microtubules (blue) and kinetochores (red). 100 nM BI2536 was added at 2 hours after NEBD. DNA was

stained with Hoechst33342 (blue). Insets show magnified images of kinetochore-microtubule attachments. Scale bar = 10 μm. Average and s.d. of the population of unattached kinetochores are shown (n = 5, 5. **p < 0.01).

doi:10.1371/journal.pone.0116783.g004

indicating that the APC/C became activated, and the securin-EGFP level reached the minimum of approximately 20% at 9 hour, which coincided with the onset of anaphase I (Fig. 5A,B, S5 Movie). However, in BI2536-treated oocytes, the securin-EGFP level was virtually constant for 12 hours after NEBD, indicating that the APC/C is not activated in the absence of PLK1 activity.

PLK1 is required for full APC/C activation, independently of satisfying the SAC

To test whether the block of APC/C activation in PLK1-inhibited oocytes is SAC-dependent, we inhibited MPS1, an essential kinase for the SAC function, using the specific inhibitor reversine[54]. As anticipated, the oocytes that were treated with reversine alone prematurely triggered securin-EGFP destruction and entered anaphase I with defective chromosome segregation (Fig. 5A-D, S5 Movie), consistent with the known function of MPS1 in mouse oocytes[55]. In the oocytes that were treated with reversine in addition to BI2536, a decrease in the securin-EGFP level was observed (Fig. 5A,B), indicating that the activation of the APC/C occurred. Thus, the block of APC/C activation in BI2536-treated oocytes depends, at least partly, on the SAC activity. Importantly, BI2536 did not delay the initiation of APC/C activation in the presence of reversine (Fig. 5B,D), confirming that our condition of reversine treatment largely, if not completely, abolished the SAC function. Nevertheless, BI2536 treatment significantly slowed the kinetics of the securin degradation in the presence of reversine (Fig. 5B,E). In these double-treated oocytes, approximately 50% of the securin-EGFP remained after the degradation, and none of the oocytes entered anaphase I (n = 15). Taken together, our results strongly suggest that PLK1 is required for the APC/C to be fully activated, independently of its primary function in satisfying the SAC. This PLK1 function is essential for entry into anaphase I in oocytes, unlike in somatic cells[4,7,25,40].

PLK1 is required for degradation of the APC/C inhibitor EMI1

Next, we sought to identify PLK1-dependent pathways that activate the APC/C independently of satisfying the SAC. To address whether PLK1 is required for degradation of the APC/C inhibitor EMI1, we monitored EGFP-EMI1 degradation in oocytes[56]. In the BI2536-treated oocytes, EGFP-EMI1 degradation was severely compromised (Fig. 6A,B), indicating that PLK1 is also required for EMI1 degradation in meiosis. EMI1-2A, which harbors mutations that substitute 124S and 128S—the residues corresponding to the PLK1-dependent phosphorylation sites 145S and 149S of human EMI1—with alanines, was less efficiently phosphorylated by PLK1 than wild-type EMI1 *in vitro* (S6 Fig.). In oocytes, EGFP-EMI1-2A failed to be degraded after NEBD (Fig. 6A,B). Thus, these data suggest that PLK1 promotes EMI1 degradation by phosphorylating EMI1 to activate the APC/C.

PLK1 likely activates the APC/C through a third pathway

We further explored the possibility that PLK1 has more pathways that activate the APC/C. To address this, we added BI2536 to the oocytes at late metaphase I, during which all chromosomes had been established stable alignment. We reasoned that the oocytes at this stage should already have degraded EMI1 and satisfied the SAC, thus allowing us to target a pathway independent of EMI1 degradation and SAC satisfaction. In this condition, we found that the

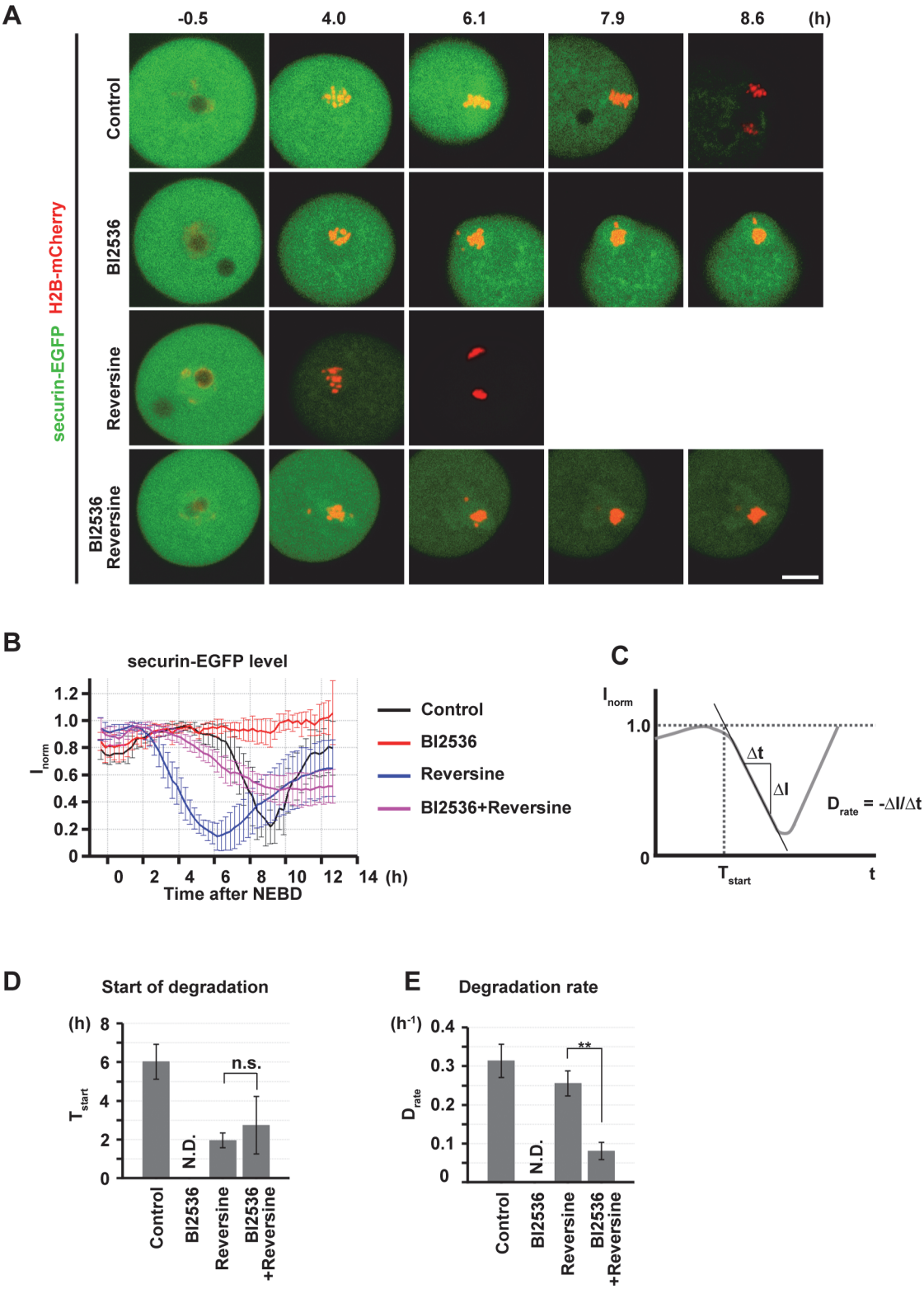

Fig 5. PLK1 activates the APC/C through multiple pathways. (A) Imaging of oocytes expressing securin-EGFP (green) and H2B-mCherry (chromosomes, red) in the presence of DMSO (control), 100 nM BI2536 and/or 1 μM reversine. Maximum intensity z-projection images are shown. Time after NEBD (h). Scale bar = 10 μm. Also see S5 Movie. (B) Normalized intensities of cytoplasmic securin-EGFP signals (I_{norm}) were plotted. Average and s.d. are shown (n = 6, 4, 12, 15). (C-E) A line was fitted to the decrease of I_{norm} (C). Time for the start of securin-EGFP degradation (T_{start}) was defined as the time

when the fitted line reaches the I_{norm} value 1.0. The degradation rate (D_{rate}) was defined as the negative value of the slope of the fitted line. Averages with s.d. of T_{start} and D_{rate} are shown in (D) and (E), respectively (n = 6, 12, 15. **$p < 0.01$).

doi:10.1371/journal.pone.0116783.g005

degradation of securin-EGFP was significantly slower than that in the control oocytes (Fig. 6C, D,E, S6 Movie). It is unlikely that this is due to reactivation of the SAC because chromosome alignment was stably maintained (Fig. 6C, S6 Movie). The BI2536-treated oocytes were unable to reach the same minimal securin-EGFP level as controls until 8 hours after the addition of BI2536 (Fig. 6D), and they remained arrested at metaphase I without any signs of chromosome segregation (Fig. 6C). Thus, these data suggest the presence of a third pathway through which PLK1 activates the APC/C.

PLK1 is required for chromosome segregation and maintenance of the condensed state of chromosomes as well as for cytokinesis

Although our data revealed that PLK1 is required for APC/C activation through multiple pathways, there can be additional PLK1 functions that occur later than APC/C activation that have not been uncovered by the above-mentioned approaches due to the strong metaphase I arrest of the BI2536-treated oocytes. To solve this problem, we arrested oocytes at the metaphase/anaphase I transition by adding of the proteasome inhibitor MG132 after 6 hours of meiotic maturation when EMI1 is already depleted[56,57]. Thereafter, we released them into anaphase I by washout (Fig. 7A). We reasoned that if APC/C substrates are largely ubiquitinated during the MG132 arrest, the oocytes after MG132 washout could have a reduced requirement of PLK1 for APC/C activation to enter anaphase I. Indeed, when we added BI2536 immediately after washing out MG132, 37% of the oocytes exhibited a comparable kinetics of securin degradation to control oocytes and entered anaphase I at a normal timing (Fig. 7B,C,D,E, S7 Movie). The intact degradation of APC/C substrates was further supported by the observation of the normal kinetics of cyclin B degradation in the same experimental condition (S7B–D Fig.). In these oocytes, however, we detected strong chromosome segregation problems, such as many lagging chromosomes and chromosome bridges, whereas only 4% of the controls exhibited segregation problems with only one lagging chromosome (Fig. 7B,C). None of these BI2536-treated oocytes extruded the first polar body (Fig. 7B), which is in good agreement with the known role of PLK1 in cytokinesis in mitosis and meiosis[8–12,17]. Moreover, in 13% of the BI2536-treated oocytes, chromosomes that had failed segregation partially decondensed at metaphase II (Fig. 7B), forming two pronucleus-like structures (Fig. 7C). Collectively, our data suggest that PLK1 is required for chromosome segregation independently of APC/C activation and maintenance of the condensed state of chromosomes during the meiosis I-meiosis II transition.

Discussion

PLK1 localizations on MTOCs and kinetochores are differentially regulated by its own activity

The polo-box domain (PBD) of PLK1 is required for the localization of PLK1 to centrosomes and unattached kinetochores in mitotic cells [58]. PLK1 phosphorylates kinetochore protein PBIP1 (also known as CENP-U) at T78, creating a binding site for the PBD and thus targeting PLK1 to kinetochores [59]. Inhibition of PLK1 by BI2536 in mitotic cells prevents PLK1 recruitment to centrosomes and kinetochores [25]. As expected, BI2536 treatment decreased the EGFP-PLK1 level on MTOCs in oocytes. However, inhibition of PLK1 activity increased the level of EGFP-PLK1 at kinetochores (S1E Fig.). Thus, it is possible that PLK1 is recruited to

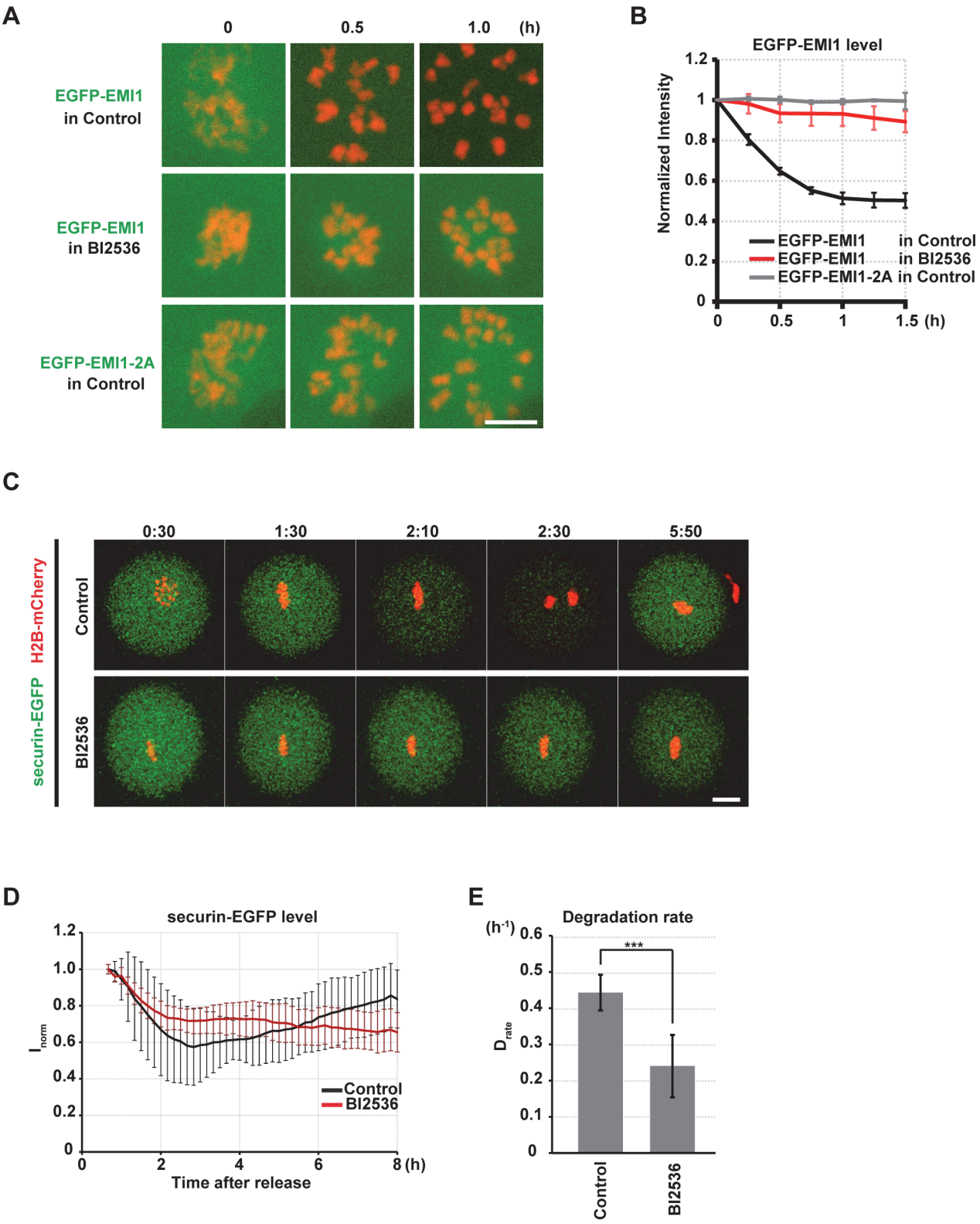

Fig 6. PLK1 is required for EMI1 destruction and full APC/C activation. (A) Imaging of oocytes expressing EGFP-EMI1 or EGFP-EMI1–2A (green) and H2B-mCherry (red) in the presence of DMSO (control) or 100 nM BI2536. Scale bar = 10 μm. Time after NEBD (h). (B) Cytoplasmic EGFP-EMI1 signals were measured and normalized. Average and s.d. are shown (n = 7, 5, 3). Time after NEBD (h). (C) Imaging of securin-EGFP (green) and H2B-mCherry (red) after DMSO (control, top) or 100 nM BI2536 (bottom) was added at the time of metaphase I (6.5 hours after the induction of meiotic resumption). Note that in the

control oocyte at 0:30, the metaphase plate is viewed from the top of the spindle. Time after BI2536 addition (h:mm). Scale bar = 20 μm. Also see S6 Movie. (D) Quantification of securin-EGFP destruction. Values were normalized to 1 at the time when imaging was started (n = 11, 18). Time is relative to BI2536 addition (h). (E) Degradation rate of securin-EGFP in oocytes with BI2536 addition during metaphase I. Average and s.d. are shown.***$p < 0.001$.

doi:10.1371/journal.pone.0116783.g006

kinetochores through unknown pathways in oocytes, in addition to the PLK1 activity-dependent pathways used in mitotic cells.

PLK1 ensures the correct timing of NEBD and chromosome condensation

Chromosome condensation and NEBD are clearly visible hallmarks of the mitotic entry of somatic cells and the meiotic resumption of oocytes. In somatic cells, chromosome condensation and NEBD are promoted by PLK1. NEBD is a step-wise process that involves nuclear pore disassembly and microtubule-dependent mechanical tearing of the nuclear envelope, followed by depolymerization of the nuclear lamina[60,61]. Nuclear pore disassembly is dependent on the phosphorylation of nuclear pore proteins[62]. Recently, many nuclear pore proteins were determined to be phosphorylated by PLK1[63]. Microtubule-dependent forces on the nuclear envelope are mainly generated by the dynein-dynactin complex[64], whose activity at NEBD depends on PLK1-mediated phosphorylation of the p150Glued subunit[65]. To facilitate chromosome condensation, PLK1 is recruited to chromosome axes through binding to the CAP-D3 condensin II subunit that is phosphorylated by CDK1 and phosphorylates many other subunits of the condensin II complex[66].

In oocytes, we confirmed that PLK1 promotes both chromosome condensation and NEBD. Unlike in somatic cells, PLK1 significantly contributes to nuclear envelope permeabilization as a first step of NEBD and ensures that it starts before chromosome condensation (Fig. 2), suggesting an oocyte-specific function of PLK1. This timing function of PLK1 is not solely a consequence of impaired CDK1-cyclin B activation because PLK1 inhibition but not partial CDK1 inhibition inverted the order of NEBD and chromosome condensation (Fig. 2). Unlike in somatic cells, microtubules are not involved in NEBD in starfish [60] and mouse oocytes (data not shown). Because lamin disassembly was not affected by PLK1 inhibition (S3 Fig.), it is likely that PLK1 plays a major role in promoting NEBD by phosphorylation of nuclear pore proteins. In contrast, PLK1 likely plays a relatively minor role in chromosome condensation, as PLK1 is not absolutely essential for chromosome condensation in mitosis [4,7]. Thus, PLK1 could support the timely onset of NEBD just before chromosome condensation by contributing to each process at different levels, in coordination with PLK1-independent pathways.

PLK1 promotes the meiotic spindle assembly

Our data revealed that PLK1 plays a crucial role in acentriolar spindle formation in oocytes (Fig. 3, S4 Fig.). Similar to what occurs in centriolar somatic cells, PLK1 recruits centrosomal materials such as γ-tubulin and pericentrin to acentriolar MTOCs, promoting meiotic spindle formation. It is worth noting that, unlike in somatic cells[5] and acentriolar Xenopus egg extracts[67], PLK1 function was not absolutely required for spindle bipolarization in mouse oocytes (Fig. 3A). It is unlikely that this was due to the partial inhibition of PLK1 activity because bipolar spindle formation was observed at even higher BI2536 concentrations such as 1–2 μM (data not shown).

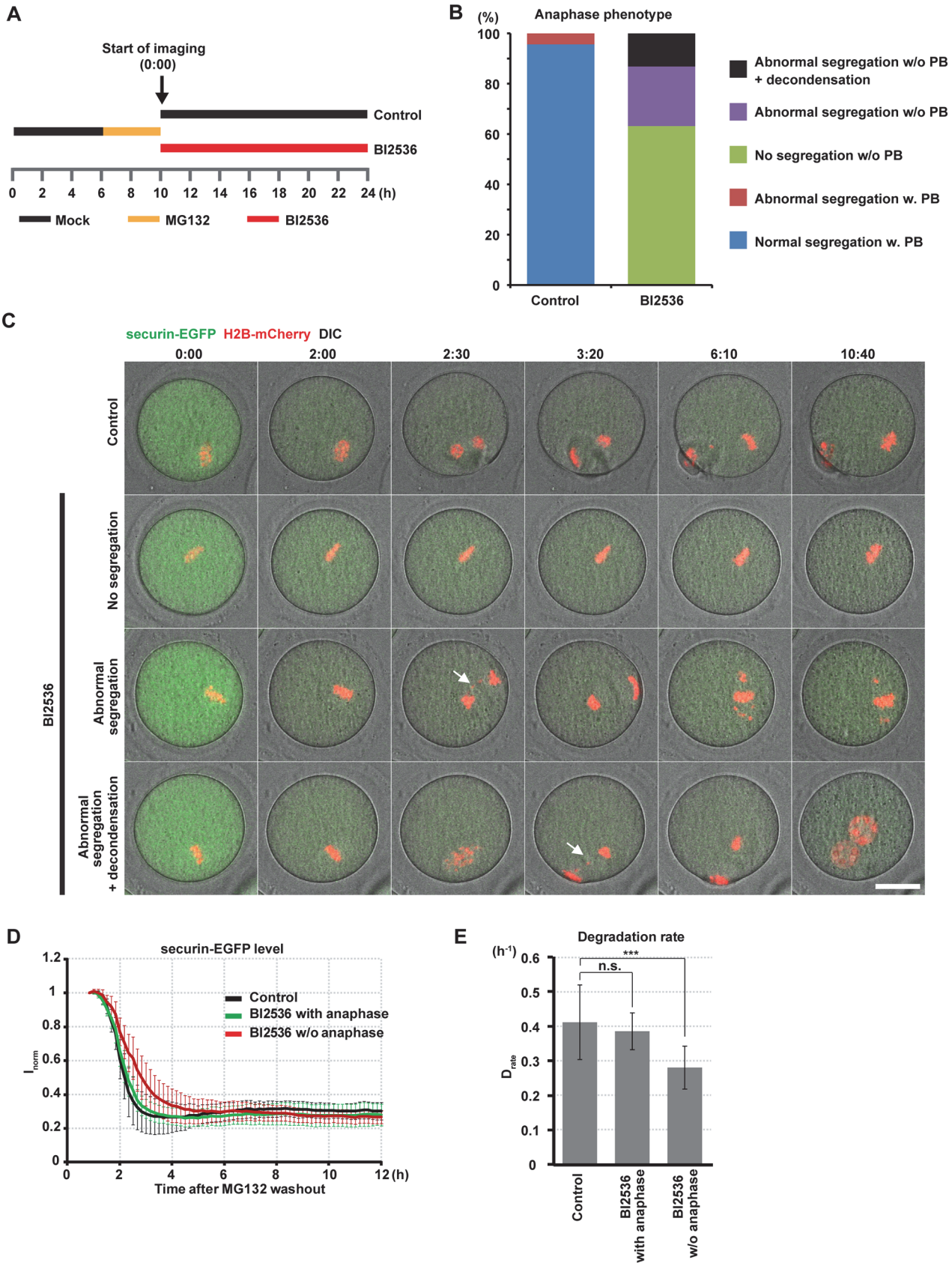
A
Start of imaging
(0:00)
Control
BI2536
0 2 4 6 8 10 12 14 16 18 20 22 24 (h)
Mock
MG132
BI2536
B
Anaphase phenotype
(%)
100
80
60
40
20
0
Control
BI2536
Abnormal segregation w/o PB + decondensation
Abnormal segregation w/o PB
No segregation w/o PB
Abnormal segregation w. PB
Normal segregation w. PB
C
securin-EGFP H2B-mCherry DIC
0:00
2:00
2:30
3:20
6:10
10:40
Control
No segregation
Abnormal segregation
Abnormal segregation + decondensation
BI2536
D
securin-EGFP level
Control
BI2536 with anaphase
BI2536 w/o anaphase
I norm
Time after MG132 washout
E
Degradation rate
(h-1)
***
n.s.
D rate
Control
BI2536 with anaphase
BI2536 w/o anaphase

Fig 7. PLK1 is required for chromosome segregation, first polar body extrusion, and maintenance of the condensed state of chromosomes. (A) Experimental scheme. Oocytes were cultured for 6 hours incontrol medium, and then MG132 was added. The oocytes were incubated for 4 hours to arrest oocytes at the late metaphase I. After release from MG132, 100 nM BI2536 was added and oocytes were imaged. (B) Anaphase phenotypes after MG132 release in control and BI2536-treated oocytes. PB = the first polar body. (C) Imaging of securin-EGFP (green) and H2B-mCherry (red) after DMSO (control, top) or 100 nM BI2536 (lower panels) was added at the time of the MG132 washout. Each phenotype from Fig. 6B is shown on a representative image sequence. Arrows indicate lagging chromosomes. Note that none of the BI2536-treated oocytes undergoing abnormal chromosome segregation extruded the first polar body. Time after MG132 washout (h:mm). Scale bar = 30 μm. Also see S7 Movie. (D) Quantification of securin-EGFP destruction. Values were normalized to 1 when the imaging was started. Time relative to MG132 washout (h). The 'BI2536 with anaphase' curve represents BI2536-treated oocytes that underwent abnormal chromosome segregation either with or without DNA decondensation (3rd and 4th rows in Fig. 7C). The 'BI2536 w/o anaphase' curve represents BI2536-treated oocytes that did not undergo chromosome segregation (2nd row in Fig. 7C). Average and s.d. are shown (n = 23, 40). (E) Degradation rate of securin-EGFP calculated from (D). Average and s.d. are shown. ***$p < 0.001$.

doi:10.1371/journal.pone.0116783.g007

PLK1 activates the APC/C through multiple pathways

Our data strongly suggest that PLK1 regulates APC/C activity through multiple pathways in oocytes. First, PLK1 promotes proper kinetochore-microtubule attachment (Fig. 4, S5 Fig.), which satisfies the SAC and thereby enables APC/C activation (Fig. 5). Second, PLK1 phosphorylates the APC/C-inhibitor EMI1 promoting its degradation (Fig. 6A,B, S6 Fig.). Future studies are needed to confirm the existence of the third pathway (Fig. 6C,D), which could involve APC/C phosphorylation by PLK1[38–40]. Importantly, our data highlighted a clear difference between somatic cells and oocytes in the requirement of the PLK1-dependent APC/C activation. Somatic cells do not require PLK1 to enter anaphase if the SAC is abrogated[4,7,25], whereas oocytes require it (Figs. 5 and 6C,D). This difference could stem from the large volume of oocytes. Oocytes could have larger amounts of EMI1, securin, and cyclin B than somatic cells, and thus more APC/C activity would be needed to degrade them.

PLK1 functions in the meiosis I—II transition

Our results suggested that PLK1 promotes chromosome segregation at anaphase I independently of APC/C activation (Fig. 7). This could involve the PLK1-dependent phosphorylation of cohesin REC8, which allows REC8 to be cleaved by separase *in vitro*[68]. Consistent with this concept, a significant fraction (approximately 60%) of BI2536-treated oocytes after MG132 washout remained arrested at metaphase I, despite the observation that they degraded securin (Fig. 7D) and cyclin B (S7C Fig.) to the same minimal level as control oocytes. Our results also suggested that PLK1 maintains the condensed state of chromosomes at metaphase II (Fig. 7C). Because chromosome decondensation at metaphase II in BI2536-treated oocytes was rescued by introducing exogenous cyclin B-EGFP (S7A,B Fig.), PLK1 could prevent chromosome decondensation by ensuring a minimal essential CDK1-cyclin B activity at metaphase II.

Conclusions

Taken together, our results define the meiotic roles of PLK1 in mammalian oocytes and reveal different requirements between mitosis and oocyte meiosis. PLK1 in oocytes not only promotes resumption of meiosis similar to what occurs in mitotic entry but also controls the onset of nuclear envelope permeabilization. Similar to what occurs in centriolar mitosis, PLK1 in oocytes facilitates meiotic spindle formation by recruiting centrosomal proteins to acentriolar MTOCs, and it promotes stable kinetochore-microtubule attachment, leading to the SAC satisfaction. In addition, in contrast to mitosis, it is essential in oocytes that PLK1 fully activates the APC/C through multiple pathways, one of which is EMI1 degradation, for anaphase I entry. Lastly, PLK1 ensures correct chromosome segregation, mediates first polar body extrusion, and prevents chromosome decondensation during the meiosis I—meiosis II transition in oocytes.

Materials and Methods

Animal use ethical statement

Using mice in this study was approved by the Departmental Expert Committee for the Approval of Projects of Experiments on Animals of the Academy of Sciences of the Czech Republic (for IAPG CAS), by The Animal Care and Use Committee of RIKEN CDB and by EMBL Institutional Animal Care and Use Committee. Animal welfare was under control of local committees. Mice were housed in a temperature-controlled room with proper 12/12 darkness-light cycles, fed with a regular ad libitum diet.

Culture of oocytes and microinjection

For oocyte isolation 8–12-week-old CD1, BDF1, FVB or H2B-EGFP [69] mice were stimulated by 5 IU of pregnant mare's serum gonadotropin (PMSG) 46 hours before experiment and killed by cervical dislocation. Oocytes were collected into the M2 medium and cultured either in Opti-MEM medium (Life Technologies) supplemented with 10% FCS in 5% CO_2 atmosphere or in M2 at 37°C. Meiotic maturation was prevented by 2.5 μM milrinone (Sigma-Aldrich). BI2536 (ChemieTek or Axon Medchem BV), reversine (Cayman Chemical or Merck Millipore), MG132 (Calbiochem or Sigma-Aldrich) and flavopiridol (Sigma Aldrich) were used at 100 nM, 1 μM, 1 μM, and 1 μM respectively.

We microinjected oocytes[70] with 2 pl mEGFP-PLK1, 1 pl EGFP-CENP-C[31], 4pl 3mCherry-CENP-C[31], 0.2 pl H2B-mCherry[31], 1.5 pl EGFP-MAP4[29], 1 pl securin-EGFP [71], 0.5 pl cyclin B1-EGFP[72], and 1 pl mEGFP-EMI1, from 1 μg/μl mRNA stocks. For nuclear envelope permeability measurement, H2B-EGFP oocytes were microinjected with 5 pl of 2 mg/ml 70-kDa dextran conjugated with tetramethylrhodamine (TAMRA) (Sigma Aldrich, D-1819).

Live confocal microscopy and image analysis

Time-lapse image acquisitions in Figs. 1, 3, 4, 5, 6A, and S1 Fig. were performed using a Zeiss LSM710 equipped with a 40x C-Apochromat 1.2 W Corr M27 objective lens (Carl Zeiss). Using a 3D multi-location tracking macro[73], we recorded the subvolume centered around chromosomes at every time point. Kinetochore tracking, determination of the chromosome distribution equator, and estimation of the spindle axis with EGFP-CENP-C, and measurement of spindle volume and aspect ratio with EGFP-MAP4 were performed as described[31]. The time of prometaphase belt formation in Fig. 4 was defined as the time when the number of chromosomes that were located in the prometaphase belt region reached a maximum (S5B Fig.).

Time-lapse image acquisitions in Figs. 2, 6C, 7, S3 and S7 Figs. were performed using Leica TCS SP5 with an HCX PL Apo Lambda Blue 40x 1.25 oil objective. Image analysis was performed using Fiji software [74]. In Fig. 2, H2B-EGFP-expressing oocytes microinjected with 70-kDa-dextran-TAMRA were sequentially irradiated with 3% of the 488 nm and 561 nm laser and scanned. 3D+t image datasets of individual oocytes were registered using H2B-EGFP signal by the Correct 3D Drift plug-in in Fiji. Chromosome volume was measured from 3D reconstructed images when H2B signal was intensity-thresholded. Dextran in the area of the nucleus was measured from the single confocal section through the center of the nucleus. Identifications of the onset and end of AF, dextran influx, and chromosome condensation were done using defined thresholds (S2 Fig.).

Immunostaining

Immunostaining was conducted as previously described in Figs. 1 and 3 [75] and Fig. 4 and S1 Fig. [31]. pT210 PLK1 was detected by rabbit polyclonal (1: 100; Santa Cruz Biotechnology), kinetochores by human CREST serum (1:100; Europa Bioproducts), α-tubulin by mouse monoclonal (1:500; Sigma), BUBR1 by sheep polyclonal (1:100; Abcam), pT669 BUBR1 by rabbit polyclonal [76]at 1:500 with the peptide LIKKLSPIIEESREATHSSGF at 100 μg/ml, histone H3 by rabbit polyclonal (1:500; Abcam), and pS28 H3 by rat monoclonal (1:500; Abcam) antibodies. For stable KT-MT attachment detection, oocytes were cultured in ice-cold M2 medium for 10 minutes before fixation.

In vitro phosphorylation assay and Western blot

Recombinant proteins of GST-EMI1 (1–211 a.a., wild-type) and GST-EMI1–2A (S124A, S128A) were purified from BL21 (DE3) pLysS E. coli cells (Promega) with Glutathione-sepharose beads (GE). His-PLK1 was bound to Ni sepharose 6 Fast Flow (GE) and washed three times with wash buffer (20 mM Tris-HCl (pH 7.5), 10 mM $MgCl_2$), suspended in kinase buffer (20 mM Tris-HCl (pH 7.5), 10 mM $MgCl_2$, 100 μM ATP) supplemented with the phosphatase inhibitor cocktail EDTA free (Nacalai tesque). The His-PLK1-bound beads were mixed with the GST-fused proteins and incubated at 30°C for 30 minutes. After the kinase reaction the supernatant was collected by centrifugation, reactions were stopped by boiling in 2×Laemmli sample buffer supplemented with 10% β-mercaptoethanol. SDS-PAGE and transfer to PDVF membrane (Millipore) were performed by standard methods. To detect phosphorylations, the membrane was incubated for 1 hour with Phos-tagTM BLT-104 (NARD Institute) prepared according to the manufacturer's instructions and then probed with Streptavidin-conjugate HRP (Jackson). To detect the GST-fusion proteins, the membrane blocked with Blocking One (nacalai tesque) was incubated for 30 minutes with GST-tag HRP-DirecT (MBL) antibody. The HRP signals were detected using Luminata Forte Western HRP Substrate (Millipore) by LAS 3000 mini (GE).

Supporting Information

S1 Fig. PLK1 localizations in live oocytes. (A) Time-lapse imaging of meiosis I in oocytes expressing EGFP-PLK1 (green) and H2B-mCherry (chromosomes, red). Maximum intensity z-projection images at representative time points are shown. Time after NEBD (h:mm). Scale bar = 10 μm. (B) The mean intensities of EGFP-PLK1 at 10 kinetochores and 5 MTOCs selected on images shown in Fig. 1A at each timepoint (prometaphase, 2 hours after NEBD; metaphase, 5 hours after NEBD), and at the anaphase spindle midzone were measured. The data were normalized by the value of the prometaphase kinetochores. Average and s.d. are shown (n = 3 oocytes). (C) The mean intensities of BUBR1 pT669 (green) and BUBR1 (red) at 20 kinetochores selected from each BI2536 concentration were measured. The BUBR1 pT669 level relative to BUBR1 was calculated and normalized by the value of the 0 nM. Average and s.d. are shown (n = 5 oocytes at 3 hours after NEBD). $***p < 0.0001$. (D) The mean intensities of histone H3 pS28 and histone H3 at chromosomes were measured. The H3 pS28 level relative to H3 was calculated and normalized by the value of the 0 nM. Average and s.d. are shown (n = 5 oocytes at 3 hours after NEBD). (E) The mean intensities of EGFP-PLK1 at 10 kinetochores and 10 MTOCs were measured. The data were normalized by the value of the control kinetochores and control MTOCs. Average and s.d. are shown (n = 3 oocytes at 6 hours after NEBD). $*p < 0.05$, $** p < 0.01$. (TIF)

S2 Fig. Analysis of chromosome condensation and NEBD in BI2536- and flavopiridol-treated oocytes. Determination of the onset and end of 70 kDa dextran influx and the onset and end of chromosome condensation from curves from individual oocytes. Dextran signals were normalized by scaling between 0 and 1 according global minimum and maximum, and chromosome volume was normalized to 1 as described in Fig. 2C.
(TIF)

S3 Fig. PLK1 does not control lamin disassembly. (A) Time lapse imaging of lamin B1-EGFP and H2B-mCherry in oocytes after induction of meiotic resumption in control, 100 nM BI2536 and 1 μM flavopiridol medium. Pictures represent single section from bright field (BF), single confocal section of lamin B1-EGFP (green) and maximum intensity z-projection for H2B-mCherry (red). Scale bar = 20 μm. (B) Length of lamin B1-EGFP disassembly. Means with 95% confidence intervals are presented (n = 16, 21, 12; $***p < 0.0001$).
(TIF)

S4 Fig. Smaller spindles are formed in PLK1-inhibited oocytes. (A) Volume rendering of the signals of EGFP-MAP4 (microtubules, green) and H2B-mCherry (chromosomes, red) in the presence of DMSO (control) or 100 nM BI2536. (B) The volume of the spindle was measured throughout meiosis I. Time after NEBD (h). Average and s.d. are shown (n = 8, 17).
(TIF)

S5 Fig. PLK1 is required for chromosome alignment. (A) Kinetochore positions were determined from the time-lapse images of EGFP-CENP-C and H2B-mCherry in oocytes cultured in the presence of DMSO (control) or 100 nM BI2536. The kinetochore positions are shown in the 3D plot as green spheres. Red bars connect homologous kinetochores. The view perpendicular to the chromosome distribution equator (top view) is shown. Time after NEBD (h:mm). The unit of the grid is 5 μm. (B) Chromosome distribution was viewed perpendicular to the equator, and the distance between the center and the chromosome was measured. The values were normalized by the distance of the most distal chromosome. Chromosomes that show >0.707 normalized distances were categorized as located in the prometaphase belt region, and its fraction was plotted over time. The time of prometaphase belt formation was defined as the time when the number of chromosomes that were located in the prometaphase belt region reached a maximum. Data from three oocytes in each condition are shown. Time after NEBD (h). (C) Distance between the paired kinetochores of homologous chromosomes was measured. Average and s.d. are plotted (n = 60, 60 from three oocytes cultured in each condition. $***p < 0.001$).
(TIF)

S6 Fig. EMI1 is phosphorylated by PLK1 *in vitro*. Recombinant GST-EMI1 or GST–EMI1–2A (S124A and S128A) proteins were incubated with His-PLK1-bound beads and analyzed the phosphorylation level with Phos-tag. The signals were measured, and the phosphorylation level relative to the protein level was measured and normalized.
(TIF)

S7 Fig. Cyclin B is destroyed normally when BI2536 is added after MG132 release. The same experimental scheme as in Fig. 7A was applied, but cyclin B-EGFP was expressed.(A) Anaphase phenotypes after MG132 release in control and BI2536-treated oocytes expressing cyclin B-EGFP. PB = polar body. Note that the BI2536-treated oocytes did not exhibit DNA decondensation. Compare with Fig. 7B. (B) Time-lapse imaging of cyclin B-EGFP (green) and H2B-mCherry (red) after DMSO (control, top) or 100 nM BI2536 (bottom) was added at the time of the MG132 release (h:mm). Each phenotype from S7A Fig. is shown on a representative

image sequence. Scale bar = 20 μm. (C) Quantification of cyclin B-EGFP destruction. Values were normalized to 1 at the time when imaging was started. Time relative to MG132 washout. The "BI2536 with anaphase" curve represents BI2536-treated oocytes that underwent abnormal chromosome segregation (3rd row in S8B Fig.). The "BI2536 w/o anaphase" curve represents BI2536-treated oocytes that did not undergo chromosome segregation (2nd row in S8B Fig.). Average and s.d. are shown (n = 11, 12). (D) Degradation rate of cyclin B-EGFP was calculated from (C). Average and s.d. are shown.
(TIF)

S1 Movie. PLK1 localizes to MTOCs, kinetochores and the spindle midzone. Time-lapse imaging of meiosis I in oocytes expressing EGFP-PLK1 (green) and 3mCherry-CENP-C (kinetochores, red). Maximum intensity z-projection images are shown. Color-merged (left) and grayscale for EGFP-PLK1 (right). Time after induction of meiotic resumption (hh:mm:ss). Scale bar = 10 μm.
(MP4)

S2 Movie. Chromosome condensation and nuclear envelope permeabilization in BI2536- and flavopiridol-treated oocytes. The green channel represents the maximum intensity z-projection of H2B-EGFP signal, red channel represents single confocal section of 70-kDa-dextran-TAMRA signal. Time after induction of meiotic resumption (minutes).
(MP4)

S3 Movie. PLK1 is required for efficient formation of the acentriolar spindle. Time-lapse imaging of meiosis I in oocytes expressing EGFP-MAP4 (microtubules, green) and H2B-mCherry (chromosomes, red) in the presence of DMSO (control, left) or 100 nM BI2536 (right). Maximum intensity z-projection images are shown. Time after NEBD (hh:mm:ss). Scale bar = 10 μm.
(MP4)

S4 Movie. Complete kinetochore tracking during meiosis I in PLK1-inhibited oocytes. Time-lapse imaging of meiosis I in oocytes expressing EGFP-CENP-C (kinetochores, green) and H2B-mCherry (chromosomes, red) in the presence of DMSO (control, left) or 100 nM BI2536 (right). Maximum intensity z-projection images are shown. White lines indicate kinetochore tracks over 5 timepoints. Time after NEBD (hh:mm:ss). Scale bar = 10 μm.
(MP4)

S5 Movie. PLK1 activates the APC/C through multiple pathways. Time-lapse imaging of oocytes expressing securin-EGFP (green) and H2B-mCherry (chromosomes, red) in the presence of DMSO (control, top left), 100 nM BI2536 (top right), 1 μM reversine (bottom left), or both of BI2536 and reversine (bottom right). Maximum intensity z-projection images are shown. Time after NEBD (h). Scale bar = 10 μm.
(MP4)

S6 Movie. PLK1 is required for full activation of the APC/C. Time-lapse imaging of securin-EGFP (green) and H2B-mCherry (red) after DMSO (control, top) or 100 nM BI2536 (bottom) was added at the time of metaphase I (6.5 hours after the induction of meiotic resumption). Time after BI2536 addition (hh:mm). Scale bar = 20 μm.
(MP4)

S7 Movie. PLK1 is essential for chromosome segregation, first polar body extrusion, and maintenance of the condensed state of chromosomes. Time-lapse imaging of securin-EGFP (green) and H2B-mCherry (red) after DMSO (control, top left) or 100 nM BI2536 was added

at the time of the MG132 washout (h). The BI2536-treated oocytes that exhibited no chromosome segregation (top right), abnormal chromosome segregation (bottom left), and chromosome decondensation after abnormal segregation (bottom right) are shown. Time after MG132 washout (hh:mm). Scale bar = 20 μm.
(MP4)

Acknowledgments

We thank Dr. Martin Anger for providing the securin-EGFP construct, Dr. Keith T. Jones for the cyclin B1-EGFP construct, Dr. Yoshinori Watanabe for the His-PLK1 construct, Dr. Geert Kops for the anti-pT669 BubR1 antibody, and Dr. Peter Lénárt for critical reading of the manuscript and professor Richard M Schultz for discussion of this project.

Author Contributions

Conceived and designed the experiments: PS TSK JM JE. Performed the experiments: PS TSK SY MK AB VB AM PS. Analyzed the data: PS TSK AB. Contributed reagents/materials/analysis tools: PS TSK. Wrote the paper: PS TSK. Project supervision and manuscript revision: JM JE.

References

1. Petronczki M, Lenart P, Peters JM (2008) Polo on the Rise-from Mitotic Entry to Cytokinesis with Plk1. Dev Cell 14: 646–659. doi: 10.1016/j.devcel.2008.04.014 PMID: 18477449
2. Archambault V, Glover DM (2009) Polo-like kinases: conservation and divergence in their functions and regulation. Nat Rev Mol Cell Biol 10: 265–275. doi: 10.1038/nrm2653 PMID: 19305416
3. Barr FA, Sillje HH, Nigg EA (2004) Polo-like kinases and the orchestration of cell division. Nat Rev Mol Cell Biol 5: 429–440. PMID: 15173822
4. Sumara I, Gimenez-Abian JF, Gerlich D, Hirota T, Kraft C, et al. (2004) Roles of polo-like kinase 1 in the assembly of functional mitotic spindles. Curr Biol 14: 1712–1722. PMID: 15458642
5. Lane HA, Nigg EA (1996) Antibody microinjection reveals an essential role for human polo-like kinase 1 (Plk1) in the functional maturation of mitotic centrosomes. J Cell Biol 135: 1701–1713. PMID: 8991084
6. Hauf S, Roitinger E, Koch B, Dittrich CM, Mechtler K, et al. (2005) Dissociation of cohesin from chromosome arms and loss of arm cohesion during early mitosis depends on phosphorylation of SA2. PLoS Biol 3: e69. PMID: 15737063
7. van Vugt MA, van de Weerdt BC, Vader G, Janssen H, Calafat J, et al. (2004) Polo-like kinase-1 is required for bipolar spindle formation but is dispensable for anaphase promoting complex/Cdc20 activation and initiation of cytokinesis. J Biol Chem 279: 36841–36854. PMID: 15210710
8. Brennan IM, Peters U, Kapoor TM, Straight AF (2007) Polo-like kinase controls vertebrate spindle elongation and cytokinesis. PLoS One 2: e409. PMID: 17476331
9. Burkard ME, Randall CL, Larochelle S, Zhang C, Shokat KM, et al. (2007) Chemical genetics reveals the requirement for Polo-like kinase 1 activity in positioning RhoA and triggering cytokinesis in human cells. Proc Natl Acad Sci U S A 104: 4383–4388. PMID: 17360533
10. Petronczki M, Glotzer M, Kraut N, Peters JM (2007) Polo-like kinase 1 triggers the initiation of cytokinesis in human cells by promoting recruitment of the RhoGEF Ect2 to the central spindle. Dev Cell 12: 713–725. PMID: 17488623
11. Santamaria A, Neef R, Eberspacher U, Eis K, Husemann M, et al. (2007) Use of the novel Plk1 inhibitor ZK-thiazolidinone to elucidate functions of Plk1 in early and late stages of mitosis. Mol Biol Cell 18: 4024–4036. PMID: 17671160
12. Neef R, Preisinger C, Sutcliffe J, Kopajtich R, Nigg EA, et al. (2003) Phosphorylation of mitotic kinesin-like protein 2 by polo-like kinase 1 is required for cytokinesis. J Cell Biol 162: 863–875. PMID: 12939256
13. Ito J, Yoon SY, Lee B, Vanderheyden V, Vermassen E, et al. (2008) Inositol 1,4,5-trisphosphate receptor 1, a widespread Ca2+ channel, is a novel substrate of polo-like kinase 1 in eggs. Dev Biol 320: 402–413. doi: 10.1016/j.ydbio.2008.05.548 PMID: 18621368
14. Pahlavan G, Polanski Z, Kalab P, Golsteyn R, Nigg EA, et al. (2000) Characterization of polo-like kinase 1 during meiotic maturation of the mouse oocyte. Dev Biol 220: 392–400. PMID: 10753525

15. Tong C, Fan HY, Lian L, Li SW, Chen DY, et al. (2002) Polo-like kinase-1 is a pivotal regulator of microtubule assembly during mouse oocyte meiotic maturation, fertilization, and early embryonic mitosis. Biol Reprod 67: 546–554. PMID: 12135894

16. Xiong B, Sun SC, Lin SL, Li M, Xu BZ, et al. (2008) Involvement of Polo-like kinase 1 in MEK1/2-regulated spindle formation during mouse oocyte meiosis. Cell Cycle 7: 1804–1809. PMID: 18583944

17. Pomerantz Y, Elbaz J, Ben-Eliezer I, Reizel Y, David Y, et al. (2012) From ubiquitin-proteasomal degradation to CDK1 inactivation: requirements for the first polar body extrusion in mouse oocytes. FASEB J 26: 4495–4505. doi: 10.1096/fj.12-209866 PMID: 22859367

18. Lincoln AJ, Wickramasinghe D, Stein P, Schultz RM, Palko ME, et al. (2002) Cdc25b phosphatase is required for resumption of meiosis during oocyte maturation. Nat Genet 30: 446–449. PMID: 11912493

19. Solc P, Saskova A, Baran V, Kubelka M, Schultz RM, et al. (2008) CDC25A phosphatase controls meiosis I progression in mouse oocytes. Dev Biol 317: 260–269. doi: 10.1016/j.ydbio.2008.02.028 PMID: 18367163

20. Jackman M, Lindon C, Nigg EA, Pines J (2003) Active cyclin B1-Cdk1 first appears on centrosomes in prophase. Nat Cell Biol 5: 143–148. PMID: 12524548

21. Lobjois V, Jullien D, Bouche JP, Ducommun B (2009) The polo-like kinase 1 regulates CDC25B-dependent mitosis entry. Biochim Biophys Acta 1793: 462–468. doi: 10.1016/j.bbamcr.2008.12.015 PMID: 19185590

22. Elia AE, Cantley LC, Yaffe MB (2003) Proteomic screen finds pSer/pThr-binding domain localizing Plk1 to mitotic substrates. Science 299: 1228–1231. PMID: 12595692

23. Toyoshima-Morimoto F, Taniguchi E, Nishida E (2002) Plk1 promotes nuclear translocation of human Cdc25C during prophase. EMBO Rep 3: 341–348. PMID: 11897663

24. Watanabe N, Arai H, Nishihara Y, Taniguchi M, Watanabe N, et al. (2004) M-phase kinases induce phospho-dependent ubiquitination of somatic Wee1 by SCFbeta-TrCP. Proc Natl Acad Sci U S A 101: 4419–4424. PMID: 15070733

25. Lenart P, Petronczki M, Steegmaier M, Di Fiore B, Lipp JJ, et al. (2007) The small-molecule inhibitor BI 2536 reveals novel insights into mitotic roles of polo-like kinase 1. Curr Biol 17: 304–315. PMID: 17291761

26. Macurek L, Lindqvist A, Lim D, Lampson MA, Klompmaker R, et al. (2008) Polo-like kinase-1 is activated by aurora A to promote checkpoint recovery. Nature 455: 119–123. doi: 10.1038/nature07185 PMID: 18615013

27. van Vugt MA, Bras A, Medema RH (2004) Polo-like kinase-1 controls recovery from a G2 DNA damage-induced arrest in mammalian cells. Mol Cell 15: 799–811. PMID: 15350223

28. Solc P, Schultz RM, Motlik J (2010) Prophase I arrest and progression to metaphase I in mouse oocytes: comparison of resumption of meiosis and recovery from G2-arrest in somatic cells. Mol Hum Reprod 16: 654–664. doi: 10.1093/molehr/gaq034 PMID: 20453035

29. Schuh M, Ellenberg J (2007) Self-organization of MTOCs replaces centrosome function during acentrosomal spindle assembly in live mouse oocytes. Cell 130: 484–498. PMID: 17693257

30. Golsteyn RM, Mundt KE, Fry AM, Nigg EA (1995) Cell cycle regulation of the activity and subcellular localization of Plk1, a human protein kinase implicated in mitotic spindle function. J Cell Biol 129: 1617–1628. PMID: 7790358

31. Kitajima TS, Ohsugi M, Ellenberg J (2011) Complete kinetochore tracking reveals error-prone homologous chromosome biorientation in mammalian oocytes. Cell 146: 568–581. doi: 10.1016/j.cell.2011.07.031 PMID: 21854982

32. Brunet S, Maria AS, Guillaud P, Dujardin D, Kubiak JZ, et al. (1999) Kinetochore fibers are not involved in the formation of the first meiotic spindle in mouse oocytes, but control the exit from the first meiotic M phase. J Cell Biol 146: 1–12. PMID: 10402455

33. Arnaud L, Pines J, Nigg EA (1998) GFP tagging reveals human Polo-like kinase 1 at the kinetochore/centromere region of mitotic chromosomes. Chromosoma 107: 424–429. PMID: 9914374

34. Liu D, Davydenko O, Lampson MA (2012) Polo-like kinase-1 regulates kinetochore-microtubule dynamics and spindle checkpoint silencing. J Cell Biol 198: 491–499. doi: 10.1083/jcb.201205090 PMID: 22908307

35. Foley EA, Kapoor TM (2013) Microtubule attachment and spindle assembly checkpoint signalling at the kinetochore. Nat Rev Mol Cell Biol 14: 25–37. doi: 10.1038/nrm3494 PMID: 23258294

36. Hansen DV, Loktev AV, Ban KH, Jackson PK (2004) Plk1 regulates activation of the anaphase promoting complex by phosphorylating and triggering SCFbetaTrCP-dependent destruction of the APC Inhibitor Emi1. Mol Biol Cell 15: 5623–5634. PMID: 15469984

37. Moshe Y, Boulaire J, Pagano M, Hershko A (2004) Role of Polo-like kinase in the degradation of early mitotic inhibitor 1, a regulator of the anaphase promoting complex/cyclosome. Proc Natl Acad Sci U S A 101: 7937–7942. PMID: 15148369

38. Golan A, Yudkovsky Y, Hershko A (2002) The cyclin-ubiquitin ligase activity of cyclosome/APC is jointly activated by protein kinases Cdk1-cyclin B and Plk. J Biol Chem 277: 15552–15557. PMID: 11859075

39. Kotani S, Tugendreich S, Fujii M, Jorgensen PM, Watanabe N, et al. (1998) PKA and MPF-activated polo-like kinase regulate anaphase-promoting complex activity and mitosis progression. Mol Cell 1: 371–380. PMID: 9660921

40. Kraft C, Herzog F, Gieffers C, Mechtler K, Hagting A, et al. (2003) Mitotic regulation of the human anaphase-promoting complex by phosphorylation. EMBO J 22: 6598–6609. PMID: 14657031

41. Wianny F, Tavares A, Evans MJ, Glover DM, Zernicka-Goetz M (1998) Mouse polo-like kinase 1 associates with the acentriolar spindle poles, meiotic chromosomes and spindle midzone during oocyte maturation. Chromosoma 107: 430–439. PMID: 9914375

42. Vanderheyden V, Wakai T, Bultynck G, De Smedt H, Parys JB, et al. (2009) Regulation of inositol 1,4,5-trisphosphate receptor type 1 function during oocyte maturation by MPM-2 phosphorylation. Cell Calcium 46: 56–64. doi: 10.1016/j.ceca.2009.04.004 PMID: 19482353

43. Burkard ME, Santamaria A, Jallepalli PV (2012) Enabling and disabling polo-like kinase 1 inhibition through chemical genetics. ACS Chem Biol 7: 978–981. doi: 10.1021/cb200551p PMID: 22422077

44. Scutt PJ, Chu ML, Sloane DA, Cherry M, Bignell CR, et al. (2009) Discovery and exploitation of inhibitor-resistant aurora and polo kinase mutants for the analysis of mitotic networks. J Biol Chem 284: 15880–15893. doi: 10.1074/jbc.M109.005694 PMID: 19359241

45. Elowe S, Hummer S, Uldschmid A, Li X, Nigg EA (2007) Tension-sensitive Plk1 phosphorylation on BubR1 regulates the stability of kinetochore microtubule interactions. Genes Dev 21: 2205–2219. PMID: 17785528

46. Swain JE, Ding J, Wu J, Smith GD (2008) Regulation of spindle and chromatin dynamics during early and late stages of oocyte maturation by aurora kinases. Mol Hum Reprod 14: 291–299. doi: 10.1093/molehr/gan015 PMID: 18353803

47. Anger M, Klima J, Kubelka M, Prochazka R, Motlik J, et al. (2004) Timing of Plk1 and MPF activation during porcine oocyte maturation. Mol Reprod Dev 69: 11–16. PMID: 15278898

48. Potapova TA, Sivakumar S, Flynn JN, Li R, Gorbsky GJ (2011) Mitotic progression becomes irreversible in prometaphase and collapses when Wee1 and Cdc25 are inhibited. Mol Biol Cell 22: 1191–1206. doi: 10.1091/mbc.E10-07-0599 PMID: 21325631

49. Haren L, Stearns T, Luders J (2009) Plk1-dependent recruitment of gamma-tubulin complexes to mitotic centrosomes involves multiple PCM components. PLoS One 4: e5976. doi: 10.1371/journal.pone.0005976 PMID: 19543530

50. Sdelci S, Schutz M, Pinyol R, Bertran MT, Regue L, et al. (2012) Nek9 phosphorylation of NEDD1/GCP-WD contributes to Plk1 control of gamma-tubulin recruitment to the mitotic centrosome. Curr Biol 22: 1516–1523. doi: 10.1016/j.cub.2012.06.027 PMID: 22818914

51. Zhang X, Chen Q, Feng J, Hou J, Yang F, et al. (2009) Sequential phosphorylation of Nedd1 by Cdk1 and Plk1 is required for targeting of the gammaTuRC to the centrosome. J Cell Sci 122: 2240–2251. doi: 10.1242/jcs.042747 PMID: 19509060

52. Casenghi M, Meraldi P, Weinhart U, Duncan PI, Korner R, et al. (2003) Polo-like kinase 1 regulates Nlp, a centrosome protein involved in microtubule nucleation. Dev Cell 5: 113–125. PMID: 12852856

53. Herbert M, Levasseur M, Homer H, Yallop K, Murdoch A, et al. (2003) Homologue disjunction in mouse oocytes requires proteolysis of securin and cyclin B1. Nat Cell Biol 5: 1023–1025. PMID: 14593421

54. Santaguida S, Tighe A, D'Alise AM, Taylor SS, Musacchio A (2010) Dissecting the role of MPS1 in chromosome biorientation and the spindle checkpoint through the small molecule inhibitor reversine. J Cell Biol 190: 73–87. doi: 10.1083/jcb.201001036 PMID: 20624901

55. Hached K, Xie SZ, Buffin E, Cladiere D, Rachez C, et al. (2011) Mps1 at kinetochores is essential for female mouse meiosis I. Development 138: 2261–2271. doi: 10.1242/dev.061317 PMID: 21558374

56. Marangos P, Verschuren EW, Chen R, Jackson PK, Carroll J (2007) Prophase I arrest and progression to metaphase I in mouse oocytes are controlled by Emi1-dependent regulation of APC(Cdh1). J Cell Biol 176: 65–75. PMID: 17190794

57. Zhou L, Yang Y, Zhang J, Guo X, Bi Y, et al. (2013) The role of RING box protein 1 in mouse oocyte meiotic maturation. PLoS One 8: e68964. doi: 10.1371/journal.pone.0068964 PMID: 23874827

58. Hanisch A, Wehner A, Nigg EA, Sillje HH (2006) Different Plk1 functions show distinct dependencies on Polo-Box domain-mediated targeting. Mol Biol Cell 17: 448–459. PMID: 16267267

59. Kang YH, Park JE, Yu LR, Soung NK, Yun SM, et al. (2006) Self-regulated Plk1 recruitment to kinetochores by the Plk1-PBIP1 interaction is critical for proper chromosome segregation. Mol Cell 24: 409–422. PMID: 17081991

60. Lenart P, Ellenberg J (2003) Nuclear envelope dynamics in oocytes: from germinal vesicle breakdown to mitosis. Curr Opin Cell Biol 15: 88–95. PMID: 12517709

61. Beaudouin J, Gerlich D, Daigle N, Eils R, Ellenberg J (2002) Nuclear envelope breakdown proceeds by microtubule-induced tearing of the lamina. Cell 108: 83–96. PMID: 11792323

62. Laurell E, Beck K, Krupina K, Theerthagiri G, Bodenmiller B, et al. (2011) Phosphorylation of Nup98 by multiple kinases is crucial for NPC disassembly during mitotic entry. Cell 144: 539–550. doi: 10.1016/j.cell.2011.01.012 PMID: 21335236

63. Santamaria A, Wang B, Elowe S, Malik R, Zhang F, et al. (2011) The Plk1-dependent phosphoproteome of the early mitotic spindle. Mol Cell Proteomics 10: M110 004457. doi: 10.1074/mcp.M110.007302 PMID: 21988777

64. Salina D, Bodoor K, Eckley DM, Schroer TA, Rattner JB, et al. (2002) Cytoplasmic dynein as a facilitator of nuclear envelope breakdown. Cell 108: 97–107. PMID: 11792324

65. Li H, Liu XS, Yang X, Song B, Wang Y, et al. (2010) Polo-like kinase 1 phosphorylation of p150Glued facilitates nuclear envelope breakdown during prophase. Proc Natl Acad Sci U S A 107: 14633–14638. doi: 10.1073/pnas.1006615107 PMID: 20679239

66. Abe S, Nagasaka K, Hirayama Y, Kozuka-Hata H, Oyama M, et al. (2011) The initial phase of chromosome condensation requires Cdk1-mediated phosphorylation of the CAP-D3 subunit of condensin II. Genes Dev 25: 863–874. doi: 10.1101/gad.2016411 PMID: 21498573

67. Liu J, Lewellyn AL, Chen LG, Maller JL (2004) The polo box is required for multiple functions of Plx1 in mitosis. J Biol Chem 279: 21367–21373. PMID: 15016807

68. Kudo NR, Anger M, Peters AH, Stemmann O, Theussl HC, et al. (2009) Role of cleavage by separase of the Rec8 kleisin subunit of cohesin during mammalian meiosis I. J Cell Sci 122: 2686–2698. doi: 10.1242/jcs.035287 PMID: 19625504

69. Hadjantonakis AK, Papaioannou VE (2004) Dynamic in vivo imaging and cell tracking using a histone fluorescent protein fusion in mice. BMC Biotechnol 4: 33. PMID: 15619330

70. Jaffe LA, Terasaki M (2004) Quantitative microinjection of oocytes, eggs, and embryos. Methods Cell Biol 74: 219–242. PMID: 15575609

71. Kudo NR, Wassmann K, Anger M, Schuh M, Wirth KG, et al. (2006) Resolution of chiasmata in oocytes requires separase-mediated proteolysis. Cell 126: 135–146. PMID: 16839882

72. Reis A, Chang HY, Levasseur M, Jones KT (2006) APCcdh1 activity in mouse oocytes prevents entry into the first meiotic division. Nat Cell Biol 8: 539–540. PMID: 16715549

73. Rabut G, Ellenberg J (2004) Automatic real-time three-dimensional cell tracking by fluorescence microscopy. J Microsc 216: 131–137. PMID: 15516224

74. Schindelin J, Arganda-Carreras I, Frise E, Kaynig V, Longair M, et al. (2012) Fiji: an open-source platform for biological-image analysis. Nat Methods 9: 676–682. doi: 10.1038/nmeth.2019 PMID: 22743772

75. Solc P, Baran V, Mayer A, Bohmova T, Panenkova-Havlova G, et al. (2012) Aurora kinase A drives MTOC biogenesis but does not trigger resumption of meiosis in mouse oocytes matured in vivo. Biol Reprod 87: 85. doi: 10.1095/biolreprod.112.101014 PMID: 22837479

76. Suijkerbuijk SJ, Vleugel M, Teixeira A, Kops GJ (2012) Integration of kinase and phosphatase activities by BUBR1 ensures formation of stable kinetochore-microtubule attachments. Dev Cell 23: 745–755. doi: 10.1016/j.devcel.2012.09.005 PMID: 23079597

MRE11 is involved in H2AX phosphorylation and protects chromosome integrity during mouse oocyte maturation

Alexandra Mayer[1], Vladimir Baran[1, 2], Yogo Sakakibara[3], Adela Brzakova[1], Ivana Ferencova[1], Jan Motlik[1], Tomoya S Kitajima[3], Richard M Schultz[4], Petr Solc[1,5]

(1) Institute of Animal Physiology and Genetics AS CR, Libechov, Czech Republic
(2) Institute of Animal Physiology, Kosice, Slovakia
(3) Laboratory for Chromosome Segregation, RIKEN Center for Developmental Biology, Kobe, Japan
(4) Department of Biology, University of Pennsylvania, Philadelphia, U. S. A.
(5) Correspondence: e-mail: solc@iapg.cas.cz

Abstract

Because low levels of DNA double strand breaks (DSBs) appear not to activate ATM-mediated prophase I checkpoint in full-grown oocytes, there may exist mechanisms to protect chromosome integrity during meiotic maturation. Using live imaging we demonstrate that low levels of DSBs induced by the radiomimetic drug Neocarzinostatin (NCS) increase the incidence of chromosome fragments and lagging chromosomes but do not lead to APC/C activation and anaphase onset delay. The number of DSBs, represented by γH2AX foci, significantly decreases between prophase I and metaphase II in both control and NCS-treated oocytes. Transient treatment with NCS increases >2-fold the number of DSBs in prophase I oocytes, but less than 30% of these oocytes enter anaphase with segregation errors. MRE11, but not ATM, is essential for DSBs detection in prophase I and is involved in H2AX phosphorylation during metaphase I. Inhibiting MRE11 by mirin during meiotic maturation results in anaphase bridges and also increases the number of γH2AX foci in metaphase II. Compromised DNA integrity in mirin-treated oocytes indicates a role for MRE11 in the DNA repair during meiotic maturation.

Key words: double strand DNA breaks, DNA damage, MRE11, meiotic maturation, mouse oocytes

Introduction

Cells possess mechanisms that protect genome integrity. Double-strand DNA breaks (DSBs) are the most serious DNA lesions that can lead, if left unrepaired, to chromosome rearrangements or loss of genetic information. DSBs arise from cellular metabolism (e.g., oxygen radicals), DNA processes (replication, transcription), cell cycle deregulation or exogenous genotoxic stress (e.g., ionizing irradiation). To protect genome integrity cells have evolved DNA damage response (DDR) mechanisms that ensure DNA damage detection, arrest of cell cycle progression (by activating DNA damage checkpoints) and trigger the repair process. When the DNA damage cannot be efficiently repaired cells enter senescence or apoptosis(Altmeyer and Lukas, 2013).

The complex of MRE11, RAD50 and NBS1 (MRN) plays a central role in sensing and repairing DSBs (Stracker and Petrini, 2011). MRN exhibits several enzymatic activities including 3´-5´ exonuclease and endonuclease activity of MRE11, and ATPase and adenylate kinase activity of RAD50. Although NBS1 lacks enzymatic activity it provides regulatory functions through protein-protein interactions (Rein and Stracker, 2014). MRN is an early DSBs sensor that binds to DSBs and promotes Ataxia telangiectasia mutated (ATM) kinase activation (Carson et al., 2003; Uziel et al., 2003). ATM phosphorylates histone H2AX at serine 139 (γH2AX)(Burma et al., 2001). Consequently, MDC1 (mediator DNA damage checkpoint protein), a predominant γH2AX recognition factor in mammalian cells, interacts with γH2AX. MDC1 recruits further MRN complexes that stimulate ATM, thereby initiating a positive feedback loop that leads to γH2AX propagation around DSBs (Jungmichel and Stucki, 2010). MRN promotes repair of DSBs through homology recombination (HR), non-homologous end-joining (NHEJ) and alternative non-homologous end-joining (a-NHEJ) pathways. MRN also forms a bridge between broken DNA ends and stimulates a resection of DNA ends that is essential for DSBs repair (Stracker and Petrini, 2011). Single-strand DNA generated by DNA resection activates ataxia telangiectasia and RAD3-related (ATR) kinase. Locally active sensor kinases ATR and ATM phosphorylate and activate transducer checkpoint kinases 1 and 2 (CHK1 and CHK2, respectively). CHK1 and CHK2 then phosphorylate many effector proteins involved in cell cycle checkpoint and DNA repair (Ciccia and Elledge, 2010).

Natural formation of DSBs in zygotene stage by SPO11 endonuclease is essential for meiotic recombination of homologous chromosomes that results in chiasmata formation (Baudat et al., 2000). Ionizing irradiation causes loss of primordial follicles through TAp63-dependent expression of proapoptotic proteins PUMA and NOXA in oocytes. Interestingly,

the fertility of *Puma* $^{-/-}$ *Noxa* $^{-/-}$ mice exposed to ionizing radiation is the same as wild type non-irradiated controls(Kerr et al., 2012), which suggests that oocytes can repair DSBs during the long prophase I arrest(Carroll and Marangos, 2013).

Mouse oocytes from preovulatory follicles can detect DSBs as documented by γH2AX foci formation after exogenous DSBs induction (Marangos and Carroll, 2012; Yuen et al., 2012; Ma et al., 2013; Lin et al., 2014). Full-grown oocytes express a relatively low level of ATM when compared to growing oocytes or blastocysts, which likely accounts for the limited activation of the ATM-CHK1 pathway after inducing DSBs in full-grown oocytes (Marrangos and Carroll, 2012). Such limited ATM activation, however, does not prevent H2AX phosphorylation in these oocytes, suggesting that H2AX phosphorylation is independent of ATM, at least when DNA damage is low. Only a high level of DSBs triggers CHK1-dependent inhibitory phosphorylation of CDC25B on S323 and DNA damage checkpoint activation that results in a delay in resumption of meiosis(Marangos and Carroll, 2012). For example, severe DSBs induced by drugs of the bleomycin family delay meiotic resumption, anaphase promoting complex (APC/C) activation, and first polar body emission. Although the incidence of oocytes resuming meiosis is decreased when DSBs are numerous, those oocytes that successfully resume meiosis mature to and arrest at metaphase II. Nevertheless, unaligned chromosome fragments arise in metaphase I and the spindle assembly checkpoint (SAC) activity is prolonged as evidenced from the persistent localization of BUB3 to kinetochores and delayed cyclin B destruction (Ma et al., 2013; Lin et al., 2014). In addition, severe DSBs induced by neocarzinostatin (NCS) (≥300 ng/ml) prevent first polar body emission and cause chromosomal fragmentation (Yuen et al., 2012).

DNA integrity in oocytes is essential for reproduction (Ashwood-Smith and Edwards, 1996; Carroll and Marangos, 2013; Titus et al., 2013). Thus, it is unclear why the DNA damage threshold for checkpoint activation in full-grown prophase I oocytes seems elevated. A possible explanation is that there may be a selective advantage to repair the damage later during the cell cycle rather than activate the checkpoint during resumption of meiosis. Oocytes can repair previously induced minor DNA damage during the lengthy meiotic M phases (Marangos and Carroll, 2012; Carroll and Marangos, 2013); note that UV irradiation or treatment with mutagenic drugs induces unscheduled DNA synthesis in prophase I oocytes, and metaphase I and II eggs (Masui and Pedersen, 1975; Brazill and Masui, 1978). Similarly, although freshly isolated mouse metaphase II eggs exhibit substantial DNA damage most of the damage is repaired in RAD51-dependent manner following 6 h of in vitro culture (Kujjo et al., 2010). Furthermore, microinjection recombinant RAD51 or pharmacological RAD51

inhibition enhances or decreases DNA repair, respectively, after IR irradiation or doxorubicin treatment (Perez et al., 2007; Kujjo et al., 2010).

There is little, if any, knowledge about the activity of DDR signaling during meiotic maturation. Here, we use H2AX phosphorylation, together with MDC1 co-localization, as a marker of DSBs and DDR activity. By employing immunofluorescence and live confocal microscopy, we find that MRE11 is involved in H2AX phosphorylation in meiosis I not only under normal conditions but also after inducing exogenous DSBs. Moreover, we find that MRE11 is important for maintaining chromosome integrity during meiotic maturation.

Results

Double strand DNA breaks (DSBs) induced by Neocarzinostatin in GV-stage oocytes result in chromosome segregation problems in anaphase I

To study the response of oocytes following increased DNA damage during meiotic maturation we used the radiomimetic drug Neocarcinostatin (NCS), which effectively induces DSBs in mouse oocytes(Yuen et al., 2012). Oocytes arrested in GV-stage by milrinone were exposed to increasing concentrations of NCS (5-100 ng/ml) for 1 h and then analysed for γH2AX/MDC1 foci (Fig. 1 A, B), which are sensitive markers of DSBs (Burma et al., 2001). We identified a NCS concentration-dependent increase in DSBs as documented by the increased number of γH2AX/MDC1 foci (Fig. 1A, B).

To analyse the effects of increased DSBs on cell cycle progression and chromosome segregation we treated oocytes isolated from transgenic mice constitutively expressing H2B-EGFP(Hadjantonakis and Papaioannou, 2004) with NCS as described above and after transfer to milrinone-, NCS-free medium, the oocytes were examined for meiotic progression and chromosome segregation by live-cell confocal imaging (Fig. 1C and Movie 1). Increasing the number of DSBs led to a dose-dependent increase in chromosome segregation problems in anaphase I (Fig. 1D). NCS treatment had no effect on the incidence of resumption of meiosis and time to onset of anaphase (data not shown and Fig. 1E). The highest NCS concentration, however, significantly delayed anaphase onset (Fig. 1E) and caused resorption of the first polar body in ~40% of oocytes (Fig. 1F).

In summary, these data demonstrate that we can induce and readily quantify the number of new (extra) DSBs in GV-stage oocytes. At a low concentration of NCS (10 ng/ml) GV-stage oocytes showed ~2.5-fold increase in γH2AX foci but only about a quarter of these oocytes exhibited chromosome segregation problems (Fig. 1D). In principle, using this low NCS concentration would permit studying a physiologically relevant response to DSBs and

moreover, may be low enough to enable DSBs repair or other DNA processes that protect chromosome integrity.

Segregation problems in anaphase I following NCS treatment are predominantly due to chromosome fragmentation

Careful examination of segregation problems in NCS treated oocytes suggested the presence of lagging chromosomes at anaphase I and free diffusion of several chromosomes in the cytoplasm of metaphase II oocytes (Figure 1C). To understand how these abnormal chromosomes are generated, we monitored the dynamics of individual chromosomes throughout meiotic maturation in oocytes expressing the chromosome marker H2B-mCHERRY and the kinetochore marker 2mEGFP-CENPC(Sakakibara et al., 2015) after treatment of NCS at the GV-stage (Fig. 2A and Movie 2). No significant differences in chromosome congression and alignment were observed between control and NCS-treated oocytes. However, we found that in NCS-treated oocytes at metaphase, a substantial number of chromosomes were abnormally stretched as indicated by a significantly longer distance between homologous kinetochores (Fig. 2B). The hyperstretched chromosomes often had a region with undetectable H2B-mCHERRY, although the physical connection between homologous kinetochores was unlikely to be completely lost because the hyperstretched chromosomes remained aligned on the metaphase plate (Movie 2). At anaphase I, NCS-treated oocytes exhibited 1-6 lagging chromosomes, whereas no control oocytes did. The vast majority of the lagging chromosomes carried no kinetochores (Fig. 2C), indicating that they are chromosome fragments. These results suggest that a higher number of DSBs leads to the loss of chromosome integrity and results in chromosome fragmentation at anaphase I.

Low levels of DSBs cause chromosome segregation problems but do not delay APC/C activation and anaphase onset

Inducing DSBs in mouse oocytes by bleomycin or zeocin treatment leads to a substantial delay in emission of the first polar body, and a delayed and reduced activation of APC/C (Ma et al., 2013; Lin et al., 2014). Treating oocytes with a very high concentration of NCS (1μg/ml) inhibits emission of the first polar body (Yuen et al., 2012). Severe DSBs also indirectly activate the SAC by disrupting kinetochore-microtubule attachment(Lin et al., 2014). As shown above we found that a low NCS concentration (10 ng/ml) led to chromosome segregation problems in about 25% oocytes but a high NCS concentration (100 ng/ml) resulted in about 90% of the oocytes displaying problems with chromosome segregation (Fig. 1D).

In light of these findings we monitored APC/C activation by expressing securin-EGFP, which is a well-established marker of APC/C activation(Herbert et al., 2003), in oocytes treated with a low or high NCS concentration (Fig. S1A and Movie 3). The time of anaphase onset (Fig. S1B) and securin-EGFP destruction (Fig. S1C) was not altered either in control oocytes not exhibiting chromosome segregation problems or oocytes treated with the 10 ng/ml NCS that had or did not have such problems. We observed delayed securin-EGFP destruction and anaphase onset only in oocytes treated with 100 ng/ml of NCS in which all oocytes exhibited chromosome segregation problems (Fig. S1B, C). These data suggest that a low level of DSBs (close to a physiological level) does not delay APC/C activation and anaphase onset, although it generates errors in chromosome segregation.

H2AX phosphorylation changes during meiotic maturation and phosphorylated H2AX co-localizes with MDC1

To monitor DDR signaling during meiotic maturation we analysed H2AX phosphorylation on S139 (γH2AX) in control and oocytes treated with a low concentration of NCS (10 ng/ml) (Fig. 3A). In control prophase I arrested GV-stage oocytes γH2AX localized in small nuclear foci. After meiotic resumption γH2AX spread along the entire condensed chromosomes although some chromosome domains with a locally higher γH2AX signal intensity were distinguishable. The γH2AX signal associated with chromosomes reached maximum intensity at metaphase I and was distributed homogenously along the chromosome. The intensity of the γH2AX signal was reduced in MII eggs when compared to MI eggs (Fig. 3B).

As expected, NCS increased the staining intensity of chromosome-associated γH2AX in GV-stage oocytes, but once the oocytes entered meiosis I, similar amounts of chromosome-associated γH2AX were observed in control and NCS-treated oocytes at metaphase I and the same was noted for MII (Fig. 3B). As described above, the number of γH2AX foci in GV-stage oocytes was increased ~ 2.5 times after NCS treatment when compared to controls (Fig. 3C). The significant decrease in chromosome-associated γH2AX signal during the metaphase I – metaphase II transition allowed us to analyse γH2AX foci formation in MII eggs. The number of γH2AX foci significantly decreased both in control and NCS-treated oocytes during maturation from GV stage to MII. The small increase in the median number of γH2AX foci of NCS MII eggs when compared to controls was not significant (Fig. 3C). When we counted the number of MII oocytes with at least one γH2AX focus we found that about 30% of NCS-treated oocytes exhibited at least one γH2AX focus in MII compared to only about 5% of control oocytes, whereas 95% of the control oocytes did not have any γH2AX

foci (Fig. 3D). Interestingly, the number of oocytes entering anaphase I with segregation errors after NCS treatment was consistent with the number of oocytes exhibiting γH2AXfoci in MII (Fig, 1D).

The low number of γH2AX foci in MII eggs could reflect lower accessibility of the of γH2AX antibody to detect γH2AX foci on the highly condensed MII chromosomes. Accordingly we induced DSBs in MII eggs (control damage MII) (Fig. 3E) and observed an increase in the number of γH2AX foci when compared to MII control or MII NCS eggs (Fig. 3D); this treatment was sufficient to generate at least one γH2AX focus > 90% of the oocytes (Fig. 3D). The reduced number of γH2AX foci in control damage MII eggs compared to GV-stage NCS-treated oocytes (Fig. 3C) probably reflects lower NCS accessibility due to the condensed structure of metaphase chromosomes.

In both control and NCS-treated oocytes MDC1, which acts as γH2AX sensor, completely co-localized with γH2AX until MI. Nevertheless, we observed a reduced MDC1 association with γH2AX foci and no association with the weak chromosomal γH2AX signal on MII chromosomes (Fig. 3A). Interestingly, induction of new DSBs in MII eggs (control damage MII) led to formation of DSBs foci containing both γH2AX and MDC1 (Fig. 3E).

These data suggest that H2AX is constitutively phosphorylated during meiotic maturation and this phosphorylation is not affected by inducing DSBs. Importantly, the decrease in the number of both endogenous and NCS-induced γH2AX foci between GV-stage and MII implies that DNA repair or other DNA processes, such as DNA break tethering, occur during meiotic maturation.

ATM is not responsible for H2AX phosphorylation during meiotic maturation

We next explored what signalling pathway was responsible for H2AX phosphorylation during meiotic maturation. ATM is the principle kinase that phosphorylates H2AX in the region of DSBs in somatic cells (Burma et al., 2001). ATM is expressed in mouse oocytes but is activated only after extensive DSBs occur (Marangos and Carroll, 2012). As anticipated, pharmacological ATM inhibition by KU55933 had no effect on γH2AX/MDC1 foci number in GV-stage oocytes (Figure S2A, B) and also no significant effect on H2AX phosphorylation and MDC1 chromatin association in MI (Figure S2A, C). KU55933 treatment did not reduce the number of γH2AX foci induced by NCS in GV-stage oocytes (Figure S2A, B) nor did induce any chromosome segregation problems in anaphase I (Figure S2D). In contrast, KU55933 efficiently inhibited H2AX phosphorylation in NCS-treated mouse NIH3T3 fibroblasts, demonstrating that the drug was active (Figure S3 E, F). In summary, ATM has no impact on H2AX phosphorylation either during normal meiotic

maturation or after induction of a low number of DSBs, which is in agreement with a previous report(Marangos and Carroll, 2012). Therefore, ATM is dispensable for meiotic maturation.

MRE11 is essential for H2AX phosphorylation in MI but not MII and inhibiting MRE11 increases the number of DSBs in MII eggs

We next determined whether MRE11, which is involved in sensing of DSBs, DDR signal amplification, and DNA repair(Stracker and Petrini, 2011), is responsible for H2AX phosphorylation in oocytes. MRE11 localized in the nucleus of GV-stage oocytes (Fig. 4A) and MRE11 protein is expressed during meiotic maturation (Fig. 4B). To establish a role for MRE11 in H2AX phosphorylation in mouse oocytes, we used the small molecule inhibitor mirin, which inhibits nuclease activity of MRE11 and prevents MRN-dependent signal amplification in somatic cells(Dupre et al., 2008). Treatment of prophase I arrested GV-stage oocytes with 100 μM mirin for 1 h did not affect the number of γH2AX/MDC1 foci (Fig. 4C, D), whereas when DNA damage was induced by NCS in the presence of mirin the number of γH2AX/MDC1 foci was significantly reduced compared to NCS only (Fig. 4C, E). Inhibition of MRE11 during meiotic maturation by mirin substantially decreased the amount of chromatin-associated phosphorylated H2AX and MDC1 binding in MI oocytes (Fig. 4 C, F), followed by the increase in γH2AX foci number on metaphase II chromosomes (Figure 4 C, D). The number of MII eggs with at least one γH2AX focus was highly increased after mirin treatment during meiotic maturation (Fig. 4G).

The increased number of γH2AX foci in MII eggs after maturation in mirin-containing medium raised the question whether MRE11 is essential for regulation of H2AX phosphorylation in MII eggs. Accordingly, we isolated in vivo matured MII eggs that were then treated in vitro with NCS and cultured in the presence or absence of mirin (Fig. 5A). Treatment with mirin alone had no effect on the number of γH2AX foci, whereas NCS induced a significant increase in the number of γH2AX foci. Although treatment with both NCS and mirin decreased the number of γH2AX foci ($p=0.025$) this decrease was small when compared to dramatic effect of mirin on γH2AX foci induced by NCS in GV-stage oocytes ($p< 0.0001$, Fig. 4E). Moreover, mirin did not affect the number of MII eggs with at least 3 γH2AX foci (Fig. 5B), suggesting that H2AX phosphorylation is less dependent on MRE11 at MII. In contrast, when control oocytes or oocytes treated with NCS at GV stage and then matured in mirin-free or mirin-containing medium the number of γH2AX foci in MII eggs was significantly higher in the mirin or NCS+mirin groups when compared to controls (Fig. 5C,D). Thus, MRE11 is not essential for γH2AX foci formation in MII eggs when the oocytes were previously treated with NCS in the GV stage.

Collectively we found that MRE11 regulates H2AX phosphorylation in MI, but the increased number of γH2AX foci in MII eggs after maturation in mirin suggests an increase in the number of DSBs during maturation and that H2AX phosphorylation in MII eggs is partly independent of MRE11 activity.

MRE11 controls chromosome segregation and integrity

We have shown above that inducing new DSBs by NCS leads to chromosome segregation problems in anaphase I (Figs. 1C, D, 2A). Because we observed an increased number of DSBs in MII eggs after mirin treatment during meiotic maturation, we used live imaging to monitor meiotic maturation and chromosome segregation in H2B-EGFP expressing oocytes to gain better insight into the dynamics of these processes (Fig. S3A and Movie 4). Addition of mirin (100 μM) to culture medium caused a significant delay in both resumption of meiosis and anaphase onset (Fig. 6A, B). More importantly, chromosome segregation errors occurred in about 25% of oocytes whereas only 3% of control oocytes entered anaphase with chromosome segregation errors (Fig. 6C). In ~10% of oocytes mirin inhibited resumption of meiosis and also increased portion (from 10% in control to 30% in mirin) of oocytes arrested in MI (Fig.6D)

In somatic cells and mitotic *Xenopus* extracts MRE11 is involved in spindle formation and chromosome alignment in part by regulating RAN-GTP signalling (Rozier et al., 2013). We also used live imaging to monitor spindle formation in oocytes expressing MAP4-EGFP and H2B-CHERRY (Fig. S3B and Movie 5). Mirin-treated oocytes exhibited normal spindle formation including spindle volume and normal chromosome alignment (Fig. 3SB, C) demonstrating that MRE11 does not regulate spindle formation in mouse oocytes.

To characterize the types of segregation errors in mirin-treated oocytes in more detail we analysed chromosome segregation and integrity in oocytes expressing H2B-mCHERRY and the kinetochore marker CENPC-EGFP (Fig. 6E and Movie 6). Anaphase bridges represented almost all segregation problems. In contrast to NCS-treated oocytes (Fig. 2) we did not detect chromosome fragment formation during anaphase (Fig. 6D).

Taken together, these results provide compelling evidence that MRE1 is involved in correct chromosome segregation and preservation of chromosome integrity.

Discussion

Results of experiments reported here extend the previous finding that phosphorylation of H2AX in mouse prophase I oocytes increases in response to new DSBs induced exogenously by radiomimetic drugs (Yuen et al., 2012; Ma et al., 2013; Lin et al., 2014) by

using lower concentrations of NCS that generate a physiological number of DSBs and finding an increase in the number of chromosome segregation errors without activation of the APC/C and any delay in onset of anaphase I. These findings contrast with previous results that used high concentrations of NCS that induce a non-physiological increase in the number of DSBs and result in delayed resumption of meiosis and MI arrest with fragmented chromosomes (Yuen et al., 2012). In addition, such oocytes with high level of DSBs also exhibit a delay in the time of emission of the first polar body, lower APC/activation but greater SAC activation as a consequence of disrupted microtubule-kinetochore attachments (Ma et al., 2013; Lin et al., 2014).

High-resolution imaging of live oocytes treated with low concentrations of NCS reveal that chromosome structure is altered shortly after resumption of meiosis as evidenced by stretched homologs. Chromosome fragments, however, appear only after anaphase onset, which implies that mechanical forces during chromosome segregation and cohesion loss are the source of chromosome breakage for chromosomes that harboured a higher number of DSBs. Before chromosome segregation DSBs are already present on chromosomes but cohesion between sister chromatids may help support chromosome structure. We also observe instances in what appears to be intact lagging chromosomes, suggesting that microtubule-kinetochore attachment is affected by DSBs. In cancer cells when DNA damage is induced in mitosis, DDR selectively stabilizes microtubule-kinetochore attachments through AURKA and PLK1 kinases, which increases the frequency of lagging chromosomes in anaphase (Bakhoum et al., 2014). Thus, this phenomenon appears to operate in MI when homologous chromosomes segregate. An interesting question for future investigation is whether the increased level of DSBs in oocytes from older females (Titus et al., 2013) contributes to the higher incidence of aneuploidy associated with age; loss of cohesion is the primary source(Chiang et al., 2010).

H2AX is phosphorylated during DDR in interphase cells and forms typical γH2AX foci (Burma et al., 2001). In addition, H2AX phosphorylation increases during mitosis in an ATM-dependent manner in the absence of exogenous DNA damage. The γH2AX, however, does not form foci but rather spreads over the condensed chromosomes. Because both ATM and H2AX are important for genome integrity, phosphorylation of H2AX likely contributes to non-erroneous transmission of genetic information during mitosis even in the absence of DNA damage (Ichijima et al., 2005; McManus and Hendzel, 2005). Consistent with this proposal is our finding that H2AX phosphorylation increases after resumption of meiosis and reaches a maximum at MI and then decreases by MII. Moreover, H2AX phosphorylation in

MI is ATM-independent but MRE11-dependent. ATM- independent H2AX phosphorylation in MI is in agreement with low ATM expression and activation in mouse oocytes (Marangos and Carroll, 2012). MRE11-dependent H2AX phosphorylation in MI suggests that MRE11 plays a role in chromosome integrity.

Whereas γH2AX spreads over chromosomes in MI during maturation under normal conditions and after inducing DSBs, in prophase I and MII γH2AX forms separate foci. The increase in γH2AX foci formation enhanced by NCS treatment in prophase I arrested oocytes is prevented by MRE11 inhibition. In addition, when normal ovulated MII eggs are treated with NCS together with mirin, we observe only reduced number of γH2AX foci, i.e., there still is an increase in the number of γH2AX foci. These data suggest that DSBs recognition in prophase I arrested oocytes is MRE11-dependent, whereas in MII DSBs recognition is not or at least partly independent of MRE11 activity. DSBs repair in MII eggs depends on the homologous recombination factor RAD51 (Kujjo et al., 2010; Kujjo et al., 2012) and MRE11 is involved in homologous recombination in somatic cells (Stracker and Petrini, 2011). A question for future investigation is whether MRE11 is essential for DNA repair although it is not essential for DSBs recognition in MII.

MRE11 is active and involved in H2AX phosphorylation during meiotic maturation without exogenous DSBs. Inhibiting MRE11 during meiotic maturation increases the number of γH2AX foci in MII eggs and imaging live oocytes reveals more stretched homologous chromosomes in prometaphase and MI, which is similar to the effect of NCS treatment. Spindle formation and chromosome alignment is normal but DNA anaphase bridges are visible when MRE11 is inhibited. Anaphase bridges may be associated with incomplete or incorrect DSBs repair (Acilan et al., 2007). Our data suggest that MRE11 is essential to prevent structural instability but it is dispensable for spindle formation during meiotic maturation in mouse oocytes.

Somatic cells in mitosis can detect DSBs as evident from γH2AX/MDC1 and MRE11 foci formation. Downstream events, however, such as RNF8 and RNF16 binding and recruitment of repair factors 53BP and BRCA1, are suppressed by CDK1 and PLK1 that phosphorylate RNF8, 53BP1 and a regulatory subunit of the DNA ligase IV (XRCC4)(Terasawa et al., 2014b). Artificial restoration of 53BP binding to DSBs in mitotic cells by expressing a non-phorphorylatable 53BP1 mutant leads to sister telomere fusion due to NHEJ repair followed by chromosome segregation errors(Lee et al., 2014; Orthwein et al., 2014). Although the efficiency of DSB repair during mitosis is much lower than in interphase, a substantial proportion of the DSBs is repaired during mitosis and the repair

process is regulated by mechanisms other than those active in other cell-cycle phases. XRCC4 does not localize to mitotic chromosomes but DNA ligase IV associates with chromosomes(Terasawa et al., 2014a). CtIP facilitates DSB-end resection by MRN, which is involved in both HR and A-NHEJ repair pathways(Zhang and Jasin, 2011). Interestingly, down-regulation of CtIP in mitotic cells significantly increases incidence of anaphase bridges(Terasawa et al., 2014a), which are marker of genome instability(Montgomery et al., 2003).

Our findings indicate that DNA repair operates during meiotic maturation. In particular, we observe that the number of γH2AX foci significantly decreases between prophase I and MII during oocyte maturation. Oocytes transiently treated with NCS exhibit a 2.5-fold increase in DSBs number in prophase I, but following maturation to MII only about 30% of the MII eggs had > 1 DSB. Interestingly, this number is similar to the number of oocytes entering anaphase with chromosome segregation errors after transient NCS treatment in prophase I. Additionally, inhibiting MRE11 during meiotic maturation increases the number of γH2AX foci in MII eggs and also results in anaphase bridges. Because mirin inhibits nuclease activity (DSB-end resection), but not DNA tethering activity of MRE11(Dupre et al., 2008), compromised DNA integrity in mirin-treated oocytes implicates involvement of MRE11 in the DNA repair during meiotic maturation. Moreover, DNA damage induced by UV irradiation leads to detectable DNA synthesis in maturing oocytes(Masui and Pedersen, 1975; Brazill and Masui, 1978). Alternatively, the anaphase bridges observed in mirin-tgreated oocytes could be a consequence of telomere dysfunction; in primary human telomerase negative G2 cells, MRE11 and phosphorylated NBS1 are recruited to telomeres to ensure their protection (Verdun et al., 2005).

Collectively, our data suggest that DNA repair occurs after resumption of meiosis during the prolonged MI phase and that MRE11 is critical for such DNA repair. Future investigations will address the mechanisms of DNA repair, which appear to differ in interphase cells, mitosis or meiosis and which repair pathway(s) operate(s) in maturing oocytes, noting that MRE11 is involved in all types of repair (Stracker and Petrini, 2011) and RAD51 (HR factor) is involved in repair in MII eggs (Kujjo et al., 2010; Kujjo et al., 2012).

Materials and methods

Animal use ethical statement

The mice in this study were used in accordance with the Act No 246/1992 of the Czech Republic on the protection of animals against cruelty. The Projects of Experiments on

animals and animal welfare were approved by The Expert Committee of the Academy of Sciences of the Czech Republic and by The Animal Care and Use Committee of RIKEN CDB. Mice were housed in a temperature-controlled room with proper 12/12 darkness-light cycles, fed with a regular ad libitum diet.

Culture of oocytes and mRNA microinjection

The oocytes were obtained from 8–12-week-old CD1 or H2B-EGFP transgenic mice(Hadjantonakis and Papaioannou, 2004) on CD1 genetic background (CD1-Tg(HIST1H2BB/EGFP)) sacrificed by cervical dislocation 46 h after the injection of 5 IU equine serum gonadotropin (eCG). To obtain CD1-Tg(HIST1H2BB/EGFP) we repeatedly (>10 times) backcrossed transgenic and H2B-EGFP-expressing males with wild-type CD1 females. Oocytes were collected in M2 medium and cultured in MEM medium (Sigma-Aldrich) supplemented with 0.22 mM sodium pyruvate, 4 mg/ml BSA (Sigma-Aldrich) and 50 μg/ml Gentamicin (Sigma-Aldrich) in a 5% CO_2 atmosphere. The culture medium was supplemented with 2.5 μM milrinone (Sigma-Aldrich) or 200 nM 3-isobutyl-1-metyl-xanthine (IBMX, Sigma-Aldrich) to prevent meiotic maturation (Tsafriri et al., 1996). The MRE11 inhibitor mirin (Sigma-Aldrich) was used at concentration 100 μM, the radiomimetic drug NCS (Neocarzinostatin, Sigma-Aldrich) at 5 - 100 ng/ml, and the ATM inhibitor KU55933 (Sigma-Aldrich) at 10 μM.

To obtain in vivo matured MII eggs mice were stimulated by injection of 5 IU human chorionic gonadotropin (hCG) 44 h after eCG stimulation. MII eggs were isolated 12 h post-hCG administration in M2 medium and the expanded cumulus cells surrounding MII eggs were removed by hyaluronidase (Sigma Aldrich, H4272) treatment.

Oocytes were microinjected as previously described (Solc et al., 2008) in M2 medium with 5 pl of 80 ng/μl H2b-mCherry (Kitajima et al., 2011), 125 ng/μl Egfp-Cenp-C(Kitajima et al., 2011), 150 ng/μl 2mEGFP-CENP-C(Sakakibara et al., 2015), 50 ng/μl Securin-Egfp(Kudo et al., 2006) and 125 ng/μl Map4-Egfp(Schuh and Ellenberg, 2007) cRNAs. Oocytes were cultured for 2 h in MEM medium supplemented with milrinone or IBMX to allow protein expression after mRNAs microinjection.

Live confocal microscopy

Time-lapse image acquisitions in Fig. 1C, S1A and S3A, B were performed using Leica TCS SP5 with an HCX PL Apo Lambda Blue 40x 1.25 oil objective with 1x zoom; 12 confocal 7.5-μm optical sections were taken with a1024 x 1024 pixel image resolution using 10 min time intervals. For kinetochore imaging in EGFP-CENP-C expressing oocytes (Fig. 6E) we used the tracking function of the Matrix Screen module in LAS AF software (Leica

Microsystems). The area of the chromosomes of individual oocytes expressing H2B-mCHERRY and EGFP-CENP-C was irradiated with 6% of the 488 nm and 3% of the 561 nm lasers and 14 confocal 2-µm optical sections scanned by HyD detectors with 12x zoom in 256 x 256 or 512 x 512 pixel image resolution by 1000Hz speed bi-directional scan were acquired. Kinetochores imaging in live oocytes in Fig. 2A was done as described previously(Sakakibara et al., 2015).

Immunofluorescence Confocal Microscopy

After a brief wash in PBS the oocytes were fixed in 3.7% paraformaldehyde in PBS for 30 min at room temperature; the *zona pellucida* was not removed. After washing with PBS (3X for 10 min), the oocytes were permeabilized for 15 min with 0.5% Triton X-100 in PBS and incubated with 2% normal donkey serum (Jackson Immuno Research, 017-000-121) in PBS for 2h at room temperature. The oocytes were then incubated overnight at 4°C with primary antibodies diluted in PBS/0.2% normal donkey serum. After washing the oocytes in PBS (3X for 20 min), the cells we incubated for 1 h at room temperature with secondary antibodies. γH2AX was detected by rabbit monoclonal antibody (Cell Signaling Technology, 9718), MDC1 by mouse monoclonal antibody, clone P2B11 (Millipore, 05-1572), MRE11 by rabbit polyclonal antibody (Novus Biologicals, NB100-142). All primary antibodies were used at a dilution 1:200. Anti-mouse antibody conjugated with TRITC or anti-rabbit antibody conjugated with FITC (Jackson ImmunoResearch) were used at a dilution 1:100. After a final wash in PBS/BSA, the oocytes were mounted in Mowiol (with 0.25µg/ml DAPI for DNA staining) between a slide and cover glass using a spacer to preserve the three-dimensional (3D) structure of the oocytes.

Oocytes were scanned using Leica TCS SP5 with HCX Pl Apo Lambda Blue 63x 1.4 oil objective. A sequential scan was applied in the 16-bit image depth with 1024 x 1024 pixel image resolution for 4x zoom on the entire oocytes or 512 x 512 pixel image resolution for 8x zoom on the chromosome area. Three-dimensional scanning was performed using 1-µm optical sections through the oocyte volume.

Image analysis

Image analysis was performed using Fiji software (Schindelin et al., 2012). For γH2AX foci number analysis we segmented γH2AX signal by applying an intensity threshold on 3D images previously denoised using PureDenoise plugin (Luisier et al., 2010). γH2AX foci number was measured by 3D Object Counter(Bolte and Cordelieres, 2006) on the segmented 3D images. γH2AX fluorescence associated with chromatin was measured by redirection of 3D mask of intensity-thresholded DNA signal to γH2AX channel.

We denoised the original time-lapse images in Fig. S1A and S3B by applying Gaussian blur (r=1). Securin-EGFP intensity in Fig. S1C was measured on maximum intensity z-projection images of the oocytes. Spindle volume in Fig. S3B was measured from 3D+t reconstructed images when EGFP-MAP4 signal was intensity-thresholded.

Western blot

For immunoblotting, 200 oocytes per sample were collected at GV stage (0 h) or MII stage (7 h). Oocytes were lysed in 10 μl of 1 × Reducing SDS Loading Buffer (Cell Signaling) and heated at 100 °C for 3 min. Proteins were separated by gradient 4-12% SDS–PAGE and transferred to a nitrocellulose membrane using a dry blotting system iBlot (Life Technologies). The membrane was blocked in 5% milk in 0.05% Tris-buffer saline-Tween (TBST), pH 7.4 for 1 h. The membrane was then washed in TBST and incubated at 4 °C overnight in the presence of the MRE11 antibody (Cell Signaling Technology, 4895) at dilution 1:1000. To visualize the proteins an ECL kit (Amersham) was used and films were scanned with a GS-800 densitometer (Bio-Rad).

Statistical analysis

NCSS2007 software (NCSS, LLC., Kaysville Utah) was used for statistical analysis. Differences in foci number and immunofluorescence intensity were evaluated by the Student t-test. Differences in medians were measured by Mann-Whitney test when the data showed non-normal distribution. Samples with $P<0.05$ were considered as statistically significant.

Acknowledgment

This study was supported by grant LH12057 (Czech-US scientific program, Ministry of Education, Youth and Sports) to P.S. Work at IAPG was supported by Institutional Research Concept 67985904. This work benefited from European Regional Development Fund, project ExAM - CZ.1.05/2.1.00/03.0124 to. J.M. Y.S. was supported by a RIKEN Special Postdoctoral Fellowship. T.S.K. was supported by a grant for JSPS Bilateral Joint Research projects with P.S and by RIKEN CDB. V.B was supported by a grant from SRDA (APVV-0237-10). R.M.S. was supported by a grant from NIH (HD058730).

Author contribution

A.M. performed experiments, analysed the data and wrote the manuscript. V.B., Y.S., A.B. and I.F. performed experiments. J.M. supervised the project, T.S.K. analysed data, supervised the project and wrote the manuscript, R.M.S. supervised the project and wrote the manuscript,

P.S. designed the experiments, analysed data, supervised the project and wrote the manuscript.

References

Acilan, C., Potter, D. M. and Saunders, W. S. (2007). DNA repair pathways involved in anaphase bridge formation. *Genes Chromosomes Cancer* **46**, 522-531.

Altmeyer, M. and Lukas, J. (2013). To spread or not to spread--chromatin modifications in response to DNA damage. *Curr. Opin. Genet. Dev.* **23**, 156-165.

Ashwood-Smith, M. J. and Edwards, R. G. (1996). DNA repair by oocytes. *Mol Hum Reprod* **2**, 46-51.

Bakhoum, S. F., Kabeche, L., Murnane, J. P., Zaki, B. I. and Compton, D. A. (2014). DNA-damage response during mitosis induces whole-chromosome missegregation. *Cancer Discov* **4**, 1281-1289.

Baudat, F., Manova, K., Yuen, J. P., Jasin, M. and Keeney, S. (2000). Chromosome synapsis defects and sexually dimorphic meiotic progression in mice lacking Spo11. *Mol. Cell* **6**, 989-998.

Bolte, S. and Cordelieres, F. P. (2006). A guided tour into subcellular colocalization analysis in light microscopy. *J. Microsc.* **224**, 213-232.

Brazill, J. L. and Masui, Y. (1978). Changing levels of uv light and carcinogen-induced unscheduled DNA synthesis in mouse oocytes during meiotic maturation. *Exp. Cell Res.* **112**, 121-125.

Burma, S., Chen, B. P., Murphy, M., Kurimasa, A. and Chen, D. J. (2001). ATM phosphorylates histone H2AX in response to DNA double-strand breaks. *J. Biol. Chem.* **276**, 42462-42467.

Carroll, J. and Marangos, P. (2013). The DNA damage response in mammalian oocytes. *Front Genet* **4**, 117.

Carson, C. T., Schwartz, R. A., Stracker, T. H., Lilley, C. E., Lee, D. V. and Weitzman, M. D. (2003). The Mre11 complex is required for ATM activation and the G2/M checkpoint. *EMBO J.* **22**, 6610-6620.

Ciccia, A. and Elledge, S. J. (2010). The DNA damage response: making it safe to play with knives. *Mol. Cell* **40**, 179-204.

Dupre, A., Boyer-Chatenet, L., Sattler, R. M., Modi, A. P., Lee, J. H., Nicolette, M. L., Kopelovich, L., Jasin, M., Baer, R., Paull, T. T. et al. (2008). A forward chemical genetic screen reveals an inhibitor of the Mre11-Rad50-Nbs1 complex. *Nat Chem Biol* **4**, 119-125.

Hadjantonakis, A. K. and Papaioannou, V. E. (2004). Dynamic in vivo imaging and cell tracking using a histone fluorescent protein fusion in mice. *BMC Biotechnol* **4**, 33.

Herbert, M., Levasseur, M., Homer, H., Yallop, K., Murdoch, A. and McDougall, A. (2003). Homologue disjunction in mouse oocytes requires proteolysis of securin and cyclin B1. *Nat. Cell Biol.* **5**, 1023-1025.

Chiang, T., Duncan, F. E., Schindler, K., Schultz, R. M. and Lampson, M. A. (2010). Evidence that weakened centromere cohesion is a leading cause of age-related aneuploidy in oocytes. *Curr. Biol.* **20**, 1522-1528.

Ichijima, Y., Sakasai, R., Okita, N., Asahina, K., Mizutani, S. and Teraoka, H. (2005). Phosphorylation of histone H2AX at M phase in human cells without DNA damage response. *Biochem. Biophys. Res. Commun.* **336**, 807-812.

Jungmichel, S. and Stucki, M. (2010). MDC1: The art of keeping things in focus. *Chromosoma* **119**, 337-349.

Kerr, J. B., Hutt, K. J., Michalak, E. M., Cook, M., Vandenberg, C. J., Liew, S. H., Bouillet, P., Mills, A., Scott, C. L., Findlay, J. K. et al. (2012). DNA damage-induced primordial follicle oocyte apoptosis and loss of fertility require TAp63-mediated induction of Puma and Noxa. *Mol. Cell* **48**, 343-352.

Kitajima, T. S., Ohsugi, M. and Ellenberg, J. (2011). Complete kinetochore tracking reveals error-prone homologous chromosome biorientation in mammalian oocytes. *Cell* **146**, 568-581.

Kudo, N. R., Wassmann, K., Anger, M., Schuh, M., Wirth, K. G., Xu, H., Helmhart, W., Kudo, H., McKay, M., Maro, B. et al. (2006). Resolution of chiasmata in oocytes requires separase-mediated proteolysis. *Cell* **126**, 135-146.

Kujjo, L. L., Laine, T., Pereira, R. J., Kagawa, W., Kurumizaka, H., Yokoyama, S. and Perez, G. I. (2010). Enhancing survival of mouse oocytes following chemotherapy or aging by targeting Bax and Rad51. *PLoS One* **5**, e9204.

Kujjo, L. L., Ronningen, R., Ross, P., Pereira, R. J., Rodriguez, R., Beyhan, Z., Goissis, M. D., Baumann, T., Kagawa, W., Camsari, C. et al. (2012). RAD51 plays a crucial role in halting cell death program induced by ionizing radiation in bovine oocytes. *Biol. Reprod.* **86**, 76.

Lee, D. H., Acharya, S. S., Kwon, M., Drane, P., Guan, Y., Adelmant, G., Kalev, P., Shah, J., Pellman, D., Marto, J. A. et al. (2014). Dephosphorylation enables the recruitment of 53BP1 to double-strand DNA breaks. *Mol. Cell* **54**, 512-525.

Lin, F., Ma, X. S., Wang, Z. B., Wang, Z. W., Luo, Y. B., Huang, L., Jiang, Z. Z., Hu, M. W., Schatten, H. and Sun, Q. Y. (2014). Different fates of oocytes with DNA double-strand breaks in vitro and in vivo. *Cell Cycle* **13**, 2674-2680.

Luisier, F., Vonesch, C., Blu, T. and Unser, M. (2010). Fast interscale wavelet denoising of Poisson-corrupted images. *Signal Processing* **90**, 415-427.

Ma, J. Y., Ou Yang, Y. C., Wang, Z. W., Wang, Z. B., Jiang, Z. Z., Luo, S. M., Hou, Y., Liu, Z. H., Schatten, H. and Sun, Q. Y. (2013). The effects of DNA double-strand breaks on mouse oocyte meiotic maturation. *Cell Cycle* **12**, 1233-1241.

Marangos, P. and Carroll, J. (2012). Oocytes progress beyond prophase in the presence of DNA damage. *Curr. Biol.* **22**, 989-994.

Masui, Y. and Pedersen, R. A. (1975). Ultraviolet light-induced unscheduled DNA synthesis in mouse oocytes during meiotic maturation. *Nature* **257**, 705-706.

McManus, K. J. and Hendzel, M. J. (2005). ATM-dependent DNA damage-independent mitotic phosphorylation of H2AX in normally growing mammalian cells. *Mol. Biol. Cell* **16**, 5013-5025.

Montgomery, E., Wilentz, R. E., Argani, P., Fisher, C., Hruban, R. H., Kern, S. E. and Lengauer, C. (2003). Analysis of anaphase figures in routine histologic sections distinguishes chromosomally unstable from chromosomally stable malignancies. *Cancer Biol Ther* **2**, 248-252.

Orthwein, A., Fradet-Turcotte, A., Noordermeer, S. M., Canny, M. D., Brun, C. M., Strecker, J., Escribano-Diaz, C. and Durocher, D. (2014). Mitosis inhibits DNA double-strand break repair to guard against telomere fusions. *Science* **344**, 189-193.

Perez, G. I., Acton, B. M., Jurisicova, A., Perkins, G. A., White, A., Brown, J., Trbovich, A. M., Kim, M. R., Fissore, R., Xu, J. et al. (2007). Genetic variance modifies apoptosis susceptibility in mature oocytes via alterations in DNA repair capacity and mitochondrial ultrastructure. *Cell Death Differ* **14**, 524-533.

Rein, K. and Stracker, T. H. (2014). The MRE11 complex: an important source of stress relief. *Exp. Cell Res.* **329**, 162-169.

606 **Rozier, L., Guo, Y., Peterson, S., Sato, M., Baer, R., Gautier, J. and Mao, Y.** (2013). The
607 MRN-CtIP pathway is required for metaphase chromosome alignment. *Mol. Cell* **49**, 1097-
608 1107.
609 **Sakakibara, Y., Hashimoto, S., Nakaoka, Y., Kouznetsova, A., Hoog, C. and Kitajima, T.**
610 **S.** (2015). Bivalent separation into univalents precedes age-related meiosis I errors in oocytes.
611 *Nat Commun* **6**, 7550.
612 **Schindelin, J., Arganda-Carreras, I., Frise, E., Kaynig, V., Longair, M., Pietzsch, T.,**
613 **Preibisch, S., Rueden, C., Saalfeld, S., Schmid, B. et al.** (2012). Fiji: an open-source
614 platform for biological-image analysis. *Nat Methods* **9**, 676-682.
615 **Schuh, M. and Ellenberg, J.** (2007). Self-organization of MTOCs replaces centrosome
616 function during acentrosomal spindle assembly in live mouse oocytes. *Cell* **130**, 484-498.
617 **Solc, P., Saskova, A., Baran, V., Kubelka, M., Schultz, R. M. and Motlik, J.** (2008).
618 CDC25A phosphatase controls meiosis I progression in mouse oocytes. *Dev. Biol.* **317**, 260-
619 269.
620 **Stracker, T. H. and Petrini, J. H.** (2011). The MRE11 complex: starting from the ends. *Nat*
621 *Rev Mol Cell Biol* **12**, 90-103.
622 **Terasawa, M., Shinohara, A. and Shinohara, M.** (2014a). Canonical non-homologous end
623 joining in mitosis induces genome instability and is suppressed by M-phase-specific
624 phosphorylation of XRCC4. *PLoS Genet* **10**, e1004563.
625 **Terasawa, M., Shinohara, A. and Shinohara, M.** (2014b). Double-strand break repair-adox:
626 Restoration of suppressed double-strand break repair during mitosis induces genomic
627 instability. *Cancer Sci* **105**, 1519-1525.
628 **Titus, S., Li, F., Stobezki, R., Akula, K., Unsal, E., Jeong, K., Dickler, M., Robson, M.,**
629 **Moy, F., Goswami, S. et al.** (2013). Impairment of BRCA1-related DNA double-strand break
630 repair leads to ovarian aging in mice and humans. *Sci Transl Med* **5**, 172ra121.
631 **Tsafriri, A., Chun, S. Y., Zhang, R., Hsueh, A. J. and Conti, M.** (1996). Oocyte maturation
632 involves compartmentalization and opposing changes of cAMP levels in follicular somatic
633 and germ cells: studies using selective phosphodiesterase inhibitors. *Dev. Biol.* **178**, 393-402.
634 **Uziel, T., Lerenthal, Y., Moyal, L., Andegeko, Y., Mittelman, L. and Shiloh, Y.** (2003).
635 Requirement of the MRN complex for ATM activation by DNA damage. *EMBO J.* **22**, 5612-
636 5621.
637 **Verdun, R. E., Crabbe, L., Haggblom, C. and Karlseder, J.** (2005). Functional human
638 telomeres are recognized as DNA damage in G2 of the cell cycle. *Mol. Cell* **20**, 551-561.
639 **Yuen, W. S., Merriman, J. A., O'Bryan, M. K. and Jones, K. T.** (2012). DNA double
640 strand breaks but not interstrand crosslinks prevent progress through meiosis in fully grown
641 mouse oocytes. *PLoS One* **7**, e43875.
642 **Zhang, Y. and Jasin, M.** (2011). An essential role for CtIP in chromosomal translocation
643 formation through an alternative end-joining pathway. *Nat Struct Mol Biol* **18**, 80-84.
644
645

Figure legends

Figure 1: DSBs induced by Neocarzinostatin in GV-stage oocytes result in chromosome segregation problems in anaphase I.
A) Immunofluorescence of control and NCS treated GV-stage oocytes labeled with pS139 H2AX (γH2AX) and MDC1 antibodies. Maximum z-projection of confocal section across nucleus is shown. **B)** Number of γH2AX foci in control and NCS treated GV-stage oocytes (n=137, 22, 118, 29, 21). **C)** Selected time frames of live H2B-EGFP control and NCS treated oocytes imaged by confocal microscopy. Arrowheads show chromosome segregation errors in anaphase and arrow shows diffusing chromosome fragment in MII. Maximum z-projection of H2B-EGFP and single bright filed section is shown. Time in hh:mm. **D)** Percentage of segregation errors in anaphase I and **E)** timing of anaphase onset in control and NCS treated oocytes (for C and D n=98, 17, 20, 56, 47, 113). **F)** Percentage of 1st polar body resorption after anaphase onset in control, 10 and 100 ng/ML NCS treated oocytes (n=98,55,76). Data in D), E) and F) are from analysis of time lapse movies of control and NCS treated H2B-EGFP oocytes as shown in C).

Figure 2: Chromosomes are fragmented in NCS-treated oocytes.
A) Time-lapse imaging of NCS-treated oocytes. Oocytes expressing 2mEGFP-CENP-C (green) and H2B-mCherry (red) were treated with NCS at 100 ng/ml. Green arrowheads indicate the homologous kinetochores of a bivalent, which is magnified on the right. Red arrowheads indicate lagging chromosomes. Time after NEBD (h:mm). Scale bar, 10 μm. **B)** Chromosome hyperstretching in NCS-treated oocytes. The distance between homologous kinetochores was measured in 3D in oocytes 6 h after NEBD (n=252, 409 bivalents). ***p<0.0001. **C)** NCS-treated oocytes exhibit lagging chromosomes without kinetochores. The number of lagging chromosomes at anaphase was counted (n=11, 17 oocytes). The lagging chromosomes were categorized. Error bars, s.d.

Figure 3: H2AX phosphorylation changes during meiotic maturation.
A) Immunofluorescence of control and NCS treated GV-stage, prometaphase I (PMI), metaphase I (MI) and metaphase II (MII) oocytes labeled with γH2AX and MDC1 antibodies. Maximum z-projection of confocal section across chromatin region is shown. In the case of MII oocytes, maximum z-projection for DNA and γH2AX but single confocal sections for MDC1 are used. Insets show maximum z-projection of metaphase II plate area. **B)** Quantification of γH2AX during meiotic maturation in control and NCS treated oocytes (n = 26, 28, 26, 27, 43, 8, 28, 23). **C)** Quantification of γH2AX foci number in GV-stage and MII oocytes treated with NCS in GV stage before meiotic maturation. Acute NCS treatment of metaphase II eggs (control damage MII) is also shown (n = 137, 118, 98, 84, 24). **D)** Percentage of MII eggs with at least one γH2AX focus (n = 106, 55, 21). **E)** Immunofluorescence of MII eggs treated acutely with NCS and labeled with γH2AX and MDC1 antibodies. Maximum z-projection of confocal sections is shown.

Figure 4: MRE11 is essential for H2AX phosphorylation in meiosis I and its inhibition during meiotic maturation causes the increase in DSBs in metaphase II.
A) Imunofluorescence of GV-stage oocytes stained with MRE11 antibody. Maximum z-projection is shown. **B)** Expression of MRE11 in GV-stage and MII oocytes detected by western blot (n=200 oocytes/lane). **C)** Immunofluorescence of control, mirin and NCS treated GV-stage, metaphase I and metaphase II oocytes labeled with γH2AX and MDC1 antibodies. Maximum z-projection of confocal section across chromatin region is shown. GV-stage oocytes were treated with Mirin, NCS or both for 1 h in milrinone supplemented medium before fixation. Metaphase I and II oocytes matured in the presence of Mirin for 7 or

16 h before fixation. **D)** Quantification of γH2AX foci number in GV-stage and MII oocytes treated with mirin in GV stage before meiotic maturation (n=137, 33, 200, 109). **E)** Quantification of γH2AX foci number in GV-stage oocytes non-treated (control) or treated with mirin, NCS or both for 1 h in milrinone-supplemented medium before fixation (n=153, 48, 118, 24). **F)** Quantification of γH2AX during meiotic maturation in control and mirin-treated oocytes (n=26, 8, 15, 21, 14, 32). **G)** Percentage of oocytes with at least one γH2AX focus matured into the metaphase II in control or mirin-supplemented medium (n=31, 58).

Figure 5: MRE11 is not required for H2AX phosphorylation in meiosis II.
A) Quantification of γH2AX foci number in in vivo matured metaphase II oocytes non-treated (control) or treated with mirin, NCS or both for 1 h in in metaphase II (n = 7, 17, 23, 29). **B)** Percentage of oocytes (from A) with at least three γH2AX foci. **C)** Quantification of γH2AX foci number in metaphase II oocytes treated or not with NCS in GV stage for 1 h before meiotic maturation in control or Mirin supplemented medium (n=31, 58, 72, 51). **D)** Percentage of oocytes (from C) with at least one γH2AX focus.

Figure 6: MRE11 controls chromosome segregation and integrity
A) Timing of resumption of meiosis resumption in control oocytes and oocytes treated with Mirin (n = 41, 36). **B)** Anaphase onset normalized to onset of NEBD in control oocytes and oocytes matured in Mirin (n = 38, 28). **C)** Percentage of segregation errors in anaphase in control oocytes and oocytes matured in Mirin (n = 38, 28). **D)** Percentage of oocytes arrested in GV, MI or MII stage upon maturation in control medium or upon addition of mirin (n = 41, 36). Data in A) - D) are from live time-lapse imaging of control and mirin treated H2B-EGFP oocytes as shown in Fig. 3A). **E)** Imaging of chromosome dynamics and integrity in live oocytes expressing H2B-mCHERRY and CENPC-EGFP and maturing in control or Mirin supplemented medium. Maximum z-projection of confocal section of selected time intervals is shown. Arrowheads show DNA anaphase bridges.

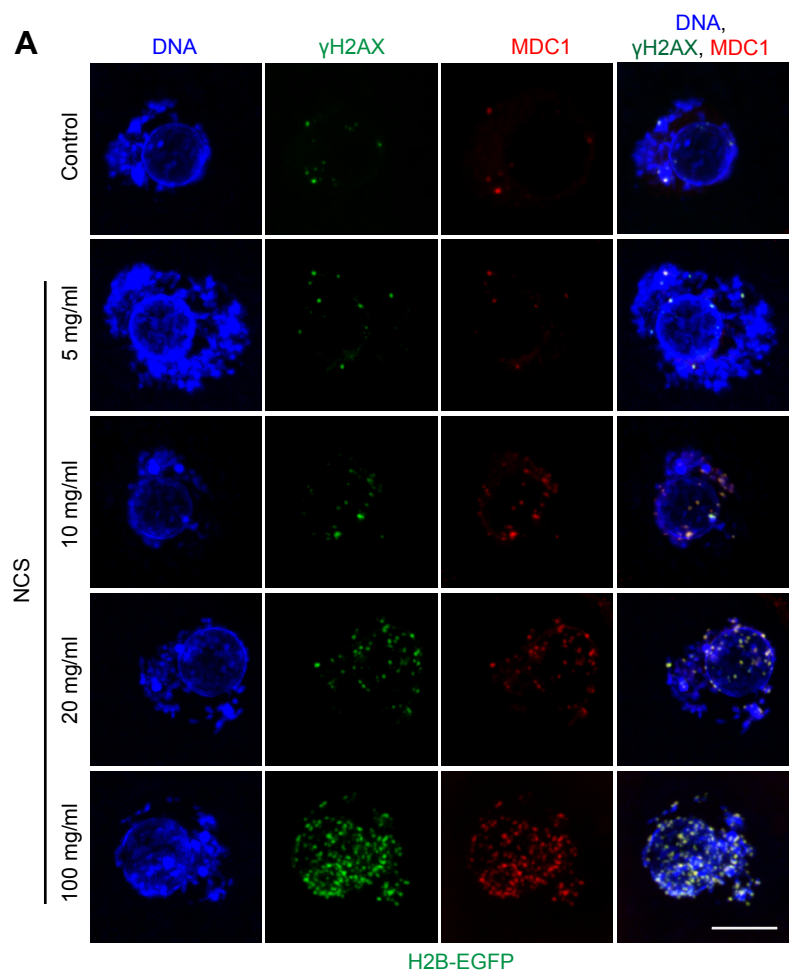
A
DNA
γH2AX
MDC1
DNA, γH2AX, MDC1
Control
5 mg/ml
10 mg/ml
20 mg/ml
100 mg/ml
NCS
H2B-EGFP

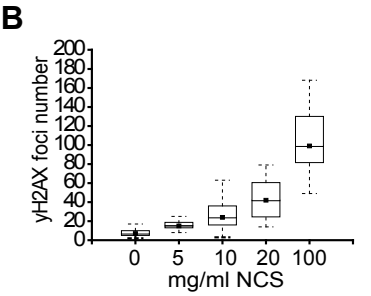
B
γH2AX foci number
0
20
40
60
80
100
120
140
160
180
200
0
5
10
20
100
mg/ml NCS

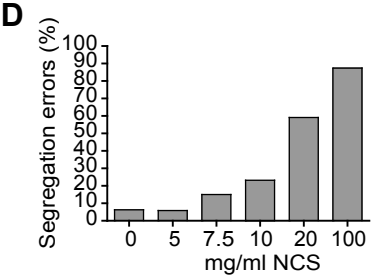
D
Segregation errors (%)
0
10
20
30
40
50
60
70
80
90
100
0
5
7.5
10
20
100
mg/ml NCS

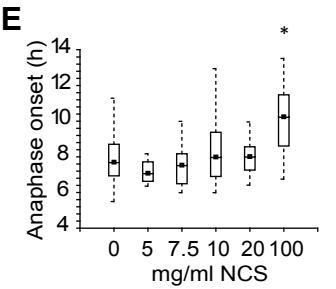
E
Anaphase onset (h)
4
6
8
10
12
14
*
0
5
7.5
10
20
100
mg/ml NCS

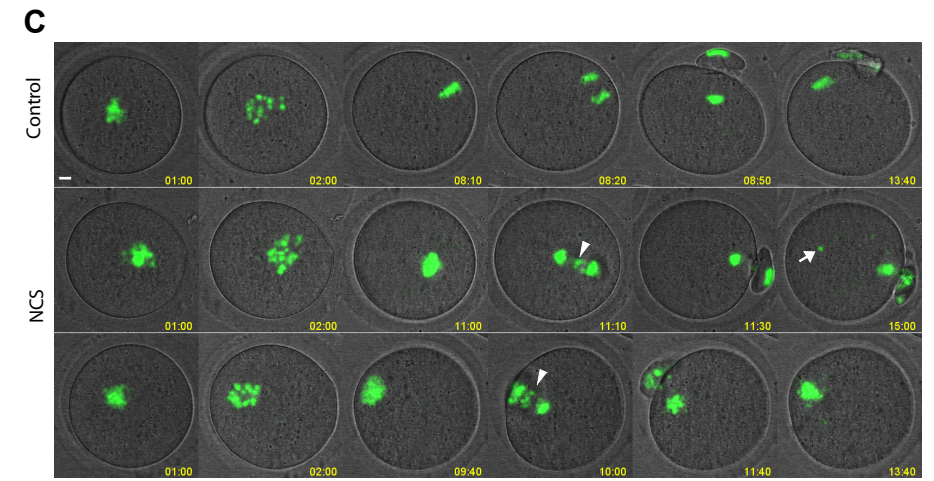
C
Control
NCS
01:00
02:00
08:10
08:20
08:50
13:40
01:00
02:00
11:00
11:10
11:30
16:00
01:00
02:00
09:40
10:00
11:40
13:40

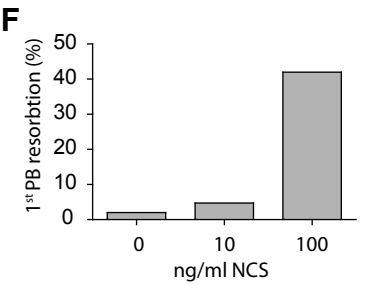
F
1st PB resorbtion (%)
0
10
20
30
40
50
0
10
100
ng/ml NCS

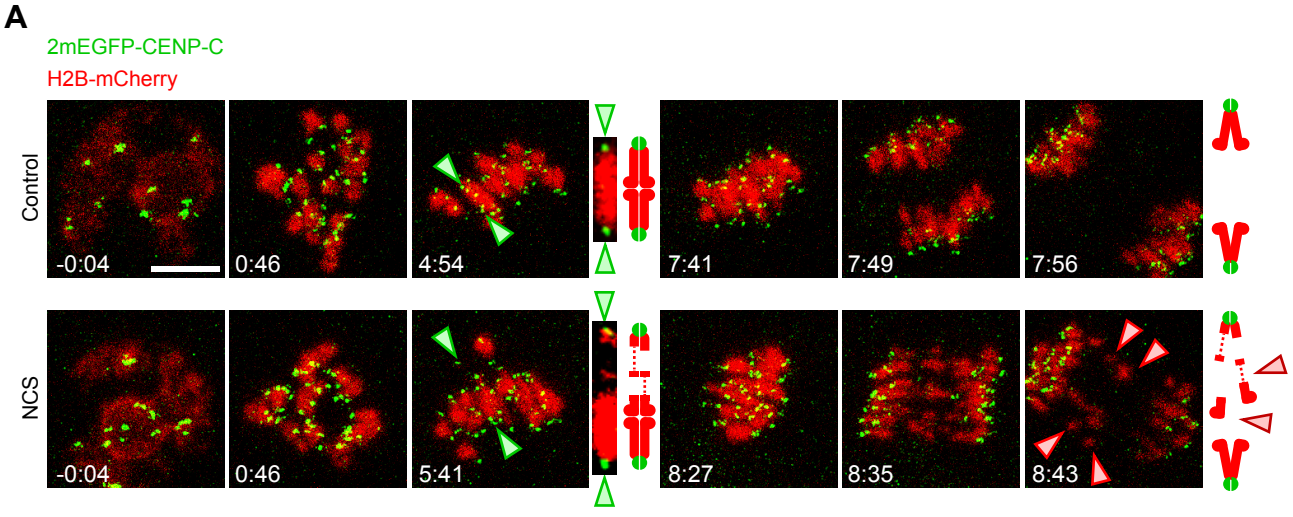
A
2mEGFP-CENP-C
H2B-mCherry
Control
NCS
-0:04
0:46
4:54
7:41
7:49
7:56
-0:04
0:46
5:41
8:27
8:35
8:43
B
Inter-kinetochore distance
(μm)
***
20
15
10
5
0
Control
NCS
C
Number of
lagging chromosomes
5
4
3
2
1
0
Control
NCS
w.o. kinetochore
w. kinetochore

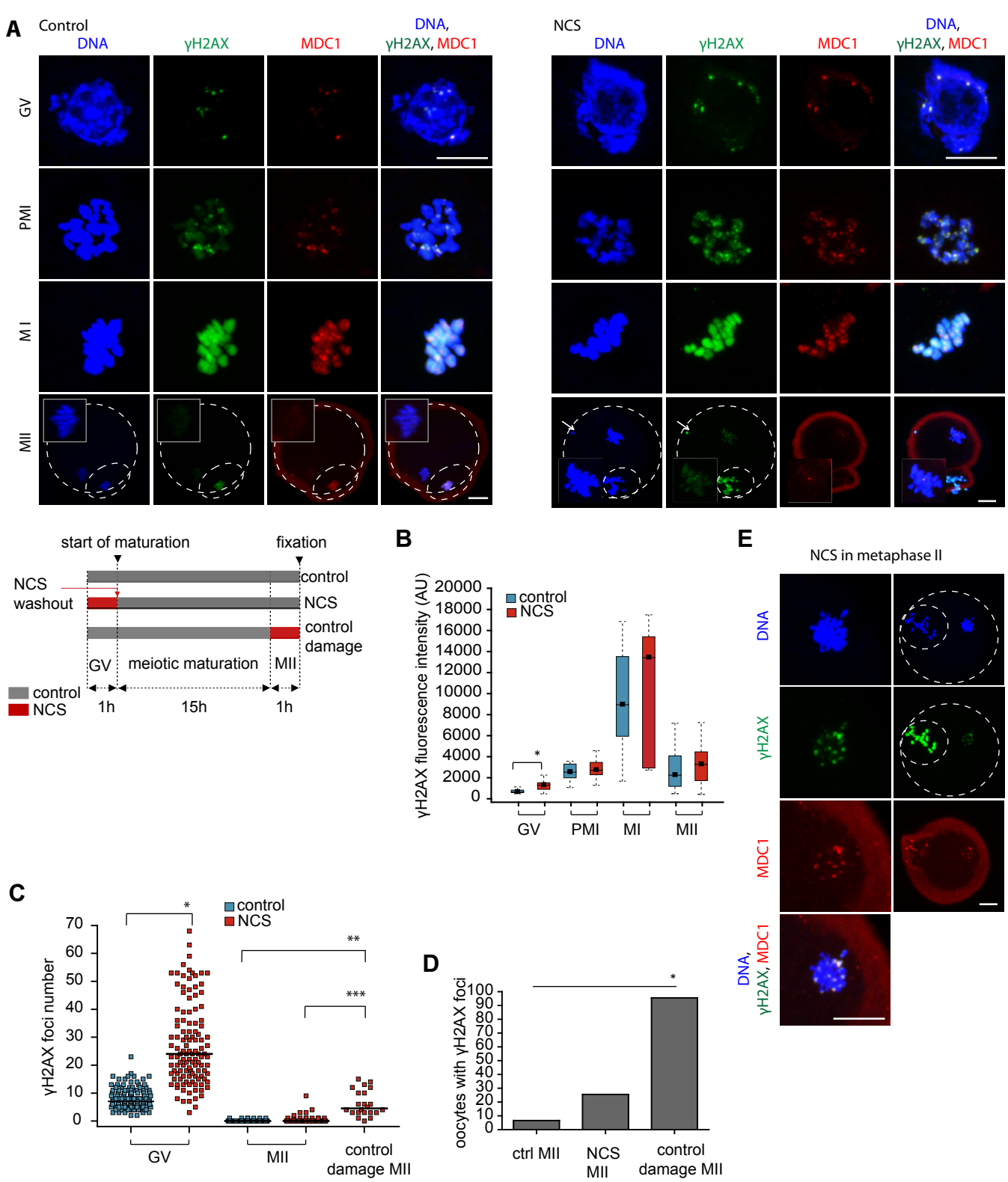
A
Control
DNA
γH2AX
MDC1
DNA, γH2AX, MDC1
NCS
GV
PMI
MI
MII
start of maturation
fixation
NCS washout
control
NCS
control damage
GV
meiotic maturation
MII
control
NCS
1h
15h
1h
B
γH2AX fluorescence intensity (AU)
20000
18000
16000
14000
12000
10000
8000
6000
4000
2000
0
control
NCS
GV
PMI
MI
MII
C
γH2AX foci number
70
60
50
40
30
20
10
0
control
NCS
GV
MII
control damage MII
D
oocytes with γH2AX foci
100
90
80
70
60
50
40
30
20
10
0
ctrl MII
NCS MII
control damage MII
E
NCS in metaphase II
DNA
γH2AX
MDC1
DNA, γH2AX, MDC1

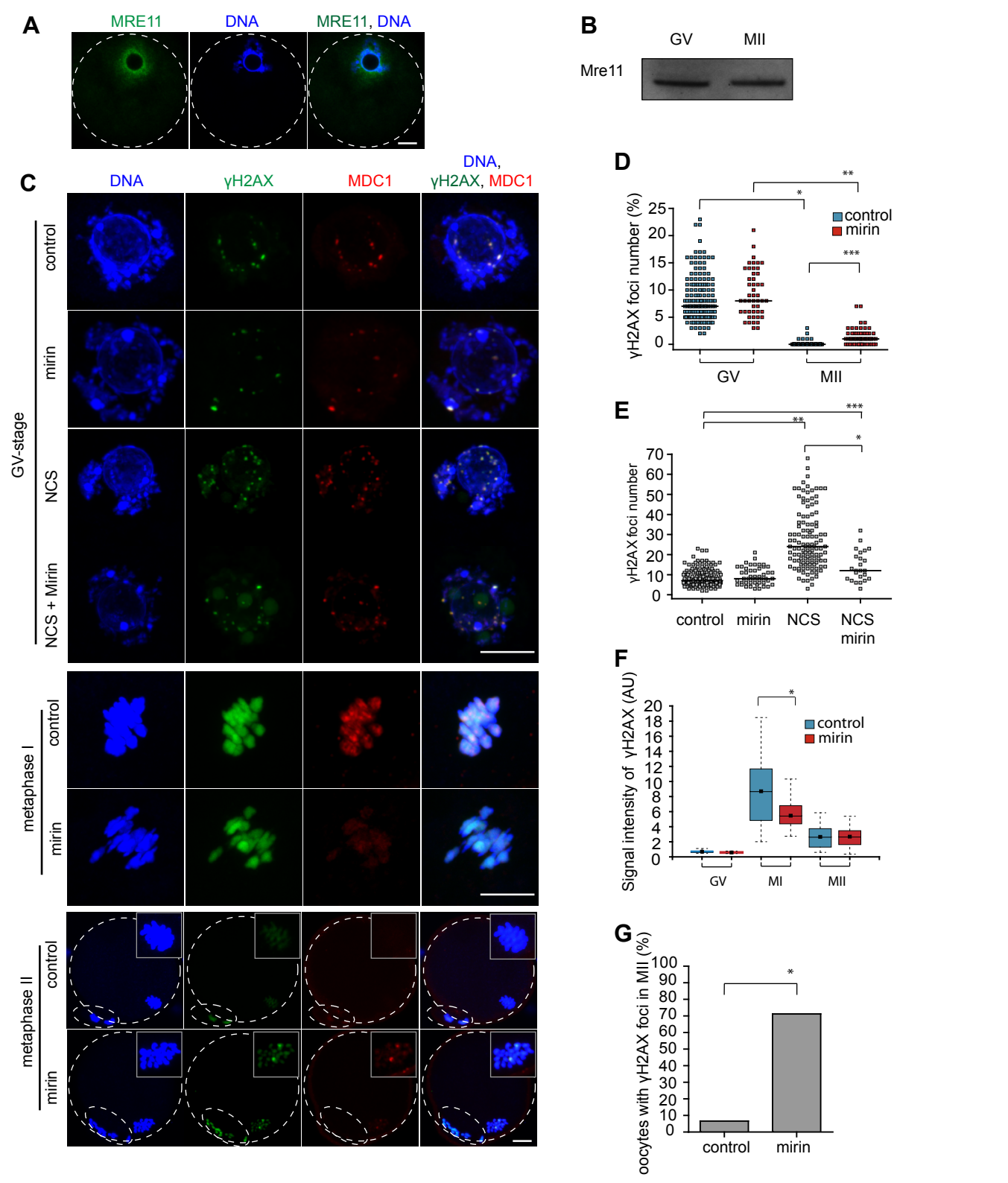
A
MRE11
DNA
MRE11, DNA
B
GV
MII
Mre11
C
DNA
γH2AX
MDC1
DNA, γH2AX, MDC1
GV-stage
control
mirin
NCS
NCS + Mirin
metaphase I
control
mirin
metaphase II
control
mirin
D
γH2AX foci number (%)
control
mirin
GV
MII
E
γH2AX foci number
control
mirin
NCS
NCS mirin
F
Signal intensity of γH2AX (AU)
control
mirin
GV
MI
MII
G
oocytes with γH2AX foci in MII (%)
control
mirin

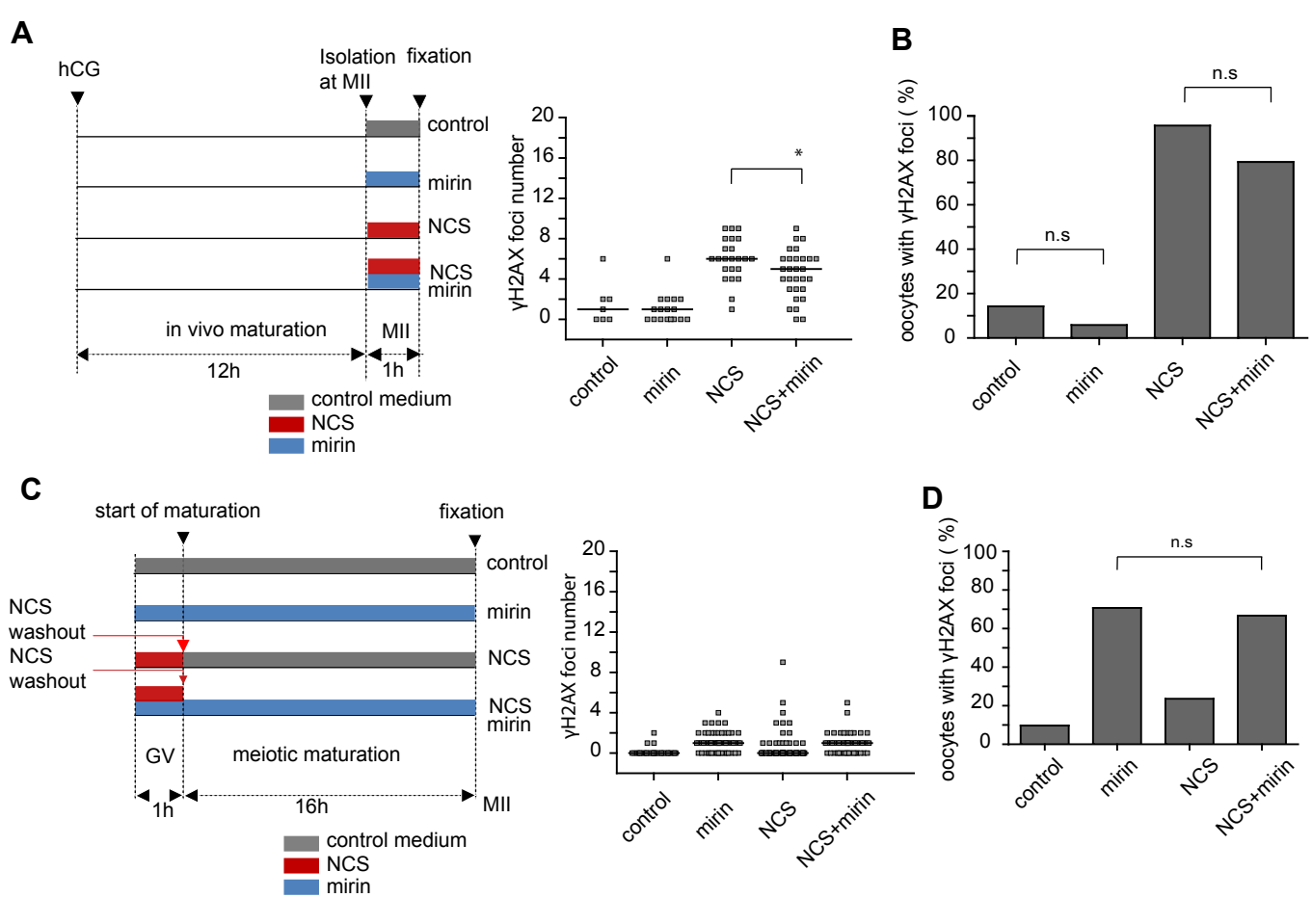
A
hCG
Isolation at MII
fixation
control
mirin
NCS
NCS
mirin
in vivo maturation
MII
12h
1h
control medium
NCS
mirin
γH2AX foci number
20
16
12
8
4
0
*
control
mirin
NCS
NCS+mirin
B
oocytes with γH2AX foci (%)
100
80
60
40
20
0
n.s
n.s
control
mirin
NCS
NCS+mirin
C
start of maturation
fixation
control
mirin
NCS
NCS
mirin
NCS
washout
NCS
washout
GV
meiotic maturation
1h
16h
MII
control medium
NCS
mirin
γH2AX foci number
20
16
12
8
4
0
control
mirin
NCS
NCS+mirin
D
oocytes with γH2AX foci (%)
100
80
60
40
20
0
n.s
control
mirin
NCS
NCS+mirin

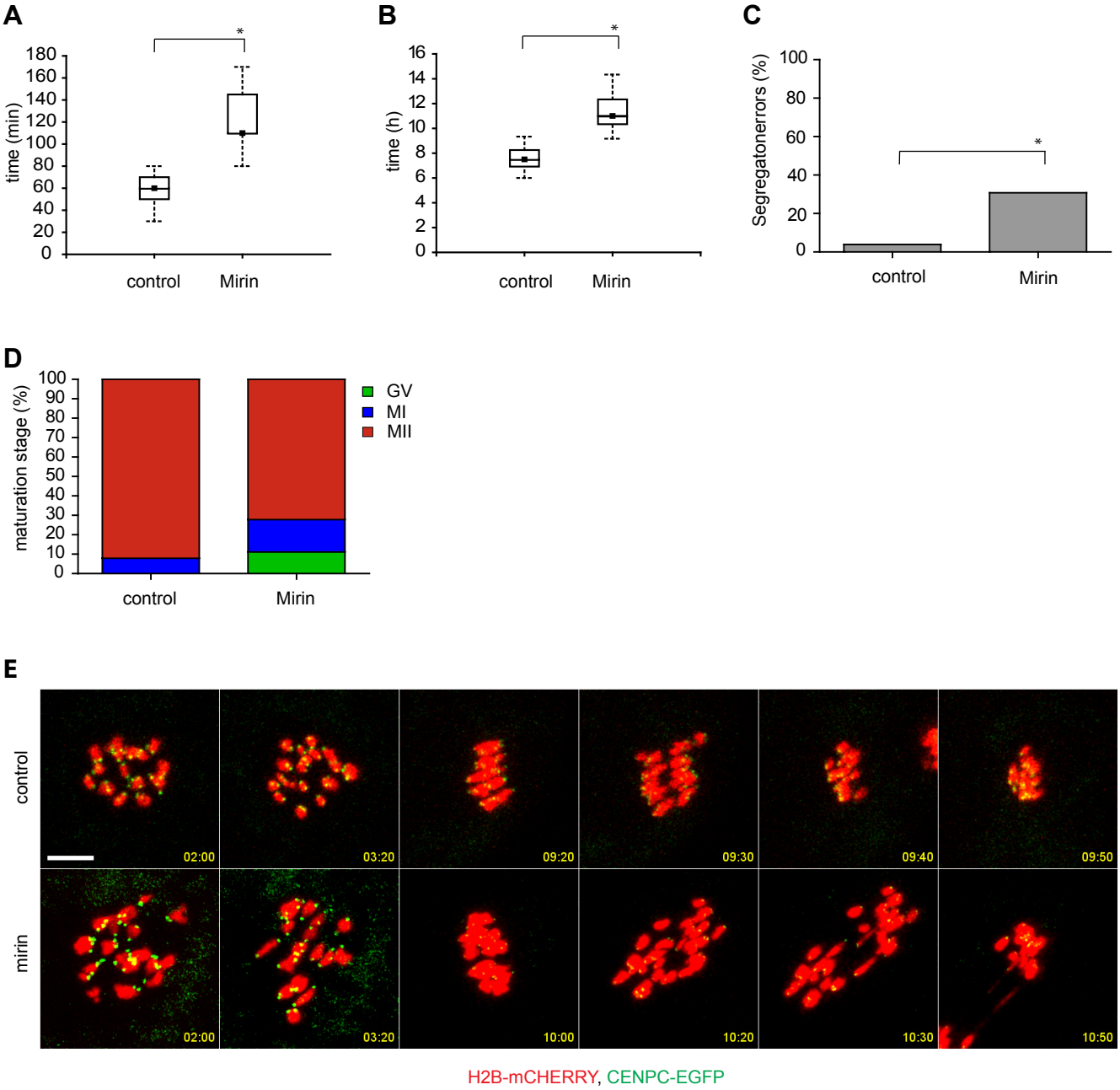
A
time (min)
180
160
140
120
100
80
60
40
20
0
*
control
Mirin
B
time (h)
16
14
12
10
8
6
4
2
0
*
control
Mirin
C
Segregatonerrors (%)
100
80
60
40
20
0
*
control
Mirin
D
maturation stage (%)
100
90
80
70
60
50
40
30
20
10
0
GV
MI
MII
control
Mirin
E
control
mirin
02:00
03:20
09:20
09:30
09:40
09:50
02:00
03:20
10:00
10:20
10:30
10:50
H2B-mCHERRY, CENPC-EGFP

Supplementary material

Figure S1: Low levels of DSBs cause segregation problems, but do not delay APC/C activation and anaphase onset.
A) Time-lapse imaging of oocytes expressing H2B-mCHERRY and securin-EGFP. Oocytes were untreated (control) or treated with 10 or 100 ng/ml NCS in GV stage and then matured in normal medium. Maximum z-projection of EGFP and mCHERRY channels and single bright field section is shown. Time in hh:mm. **B)** Anaphase onset in hours of oocytes expressing H2B-mCHERRY and securin-EGFP. Untreated (control), NCS treated (10 and 100 ng/ml) groups are subdivided into the subgroups with and without segregation errors (n=10, 9, 1, 6, 10). **C)** Quantification of securin-EGFP level during meiotic maturation. Securin-EGFP level was normalized to 1 in the time of resumption of meiosis. Means with SE are shown. Time is in hours. Note that only one control oocyte exhibited segregation error (n = 10, 9, 1, 6, 10).

Figure S2: ATM is not responsible for H2AX phosphorylation during meiotic maturation.
A) Immunofluorescence of control and KU55933 treated GV-stage and metaphase I oocytes labeled with γH2AX and MDC1 antibodies. Maximum z-projection of confocal sections across chromatin region is shown. KU55933 treated oocytes were pre-incubated with 10 μM KU55933 together with milrinone for 1 h in GV-stage and fixed or after milrinone washout they were cultured for 7 h in the presence of KU55933 before fixation. **B)** Quantification of γH2AX foci in GV-stage oocytes non-treated or treated with KU55933, NCS or both for 1 h in milrinone-supplemented medium before fixation (n= 23, 28, 10, 10). **C)** Quantification of γH2AX intensity in control and KU55933 treated oocytes in metaphase I (n = 10, 43). **D)** Quantification of chromosome segregation errors of H2B-EGFP control and KU55933 treated oocytes analysed by live confocal imaging (movies not shown) (n= 20, 11). **E)** Immunofluorescence of control, NCS and NCS+KU55933 treated NIH3T3 cells labelled with γH2AX antibody. **F)** Quantification of γH2AX fluorescence in control, NCS and NCS+KU55933 treated NIH3T3 cells (n= 27, 44, 33).

Figure S3: Spindle assembly is not affected by Mirin treatment
A) Time-lapse imaging of control and mirin treated H2B-EGFP oocytes. Maximum intensity z-projection of H2B-EGFP and single section of bright-field images in selected time frames are shown. **B)** Time lapse imaging of oocytes expressing MAP4-EGFP and H2B-mCHERRY in control or mirin-supplemented medium. Maximum intensity z-projection images are shown. Time is in hh:mm. Arrowheads in A) and B show chromosome segregation problems. **C)** The volume of the spindle (μm^3) during oocyte maturation quantified from 3D reconstructed data. Time t=0 corresponds to the time of NEBD (n=18, 31).

Fig. S1

A

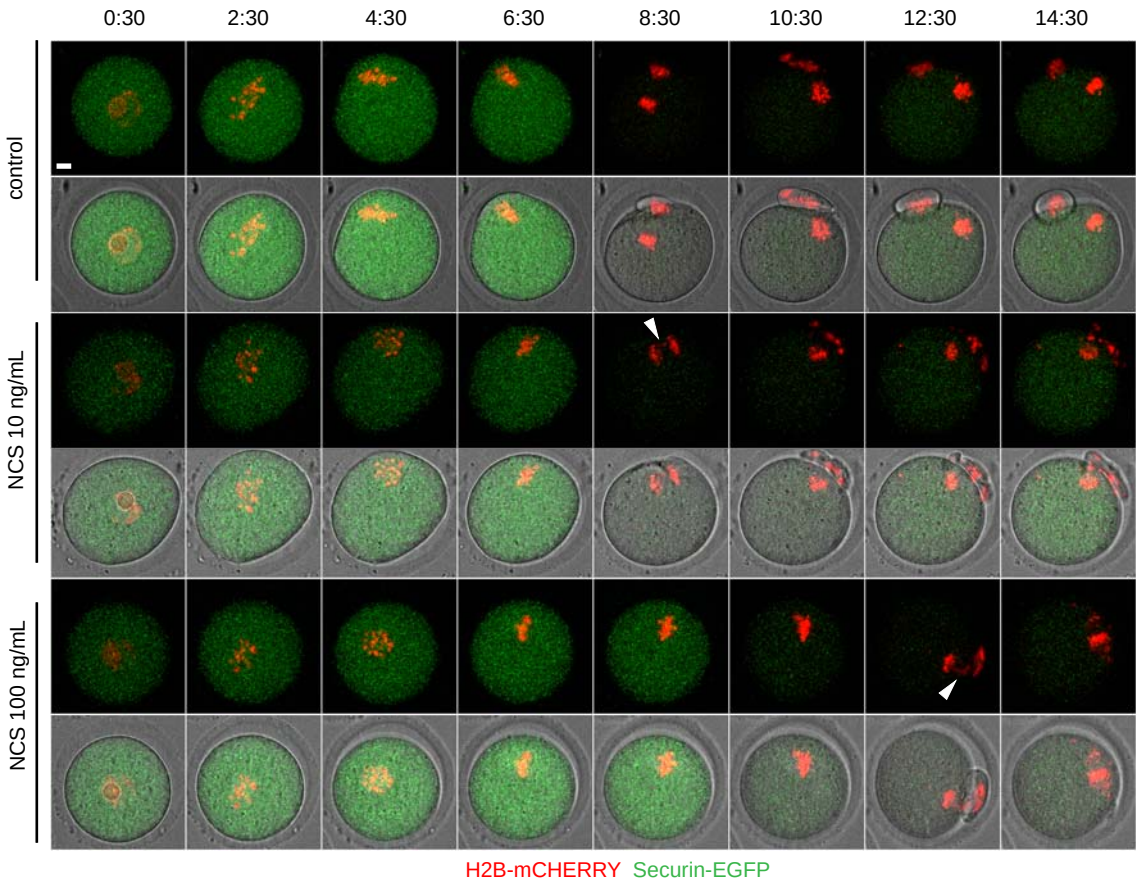
0:30
2:30
4:30
6:30
8:30
10:30
12:30
14:30
control
NCS 10 ng/mL
NCS 100 ng/mL
H2B-mCHERRY Securin-EGFP

B

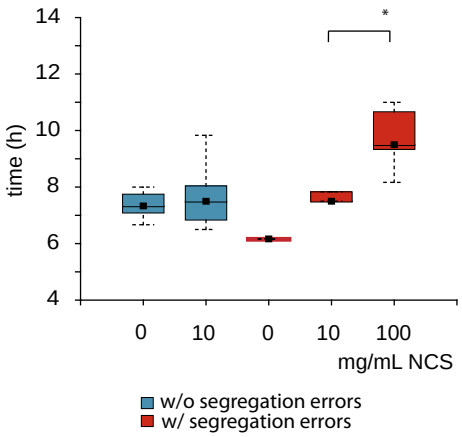
time (h)
14
12
10
8
6
4
*
0
10
0
10
100
mg/mL NCS
w/o segregation errors
w/ segregation errors

C

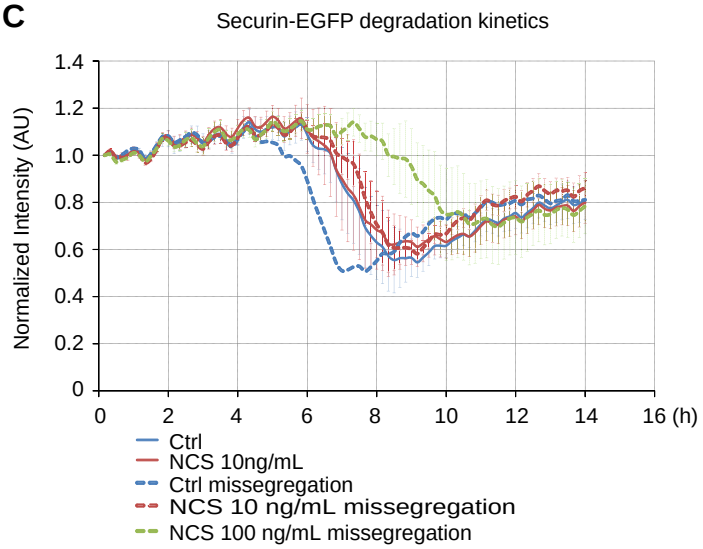
Securin-EGFP degradation kinetics
Normalized Intensity (AU)
1.4
1.2
1.0
0.8
0.6
0.4
0.2
0
0
2
4
6
8
10
12
14
16 (h)
Ctrl
NCS 10ng/mL
Ctrl missegregation
NCS 10 ng/mL missegregation
NCS 100 ng/mL missegregation

Fig. S2

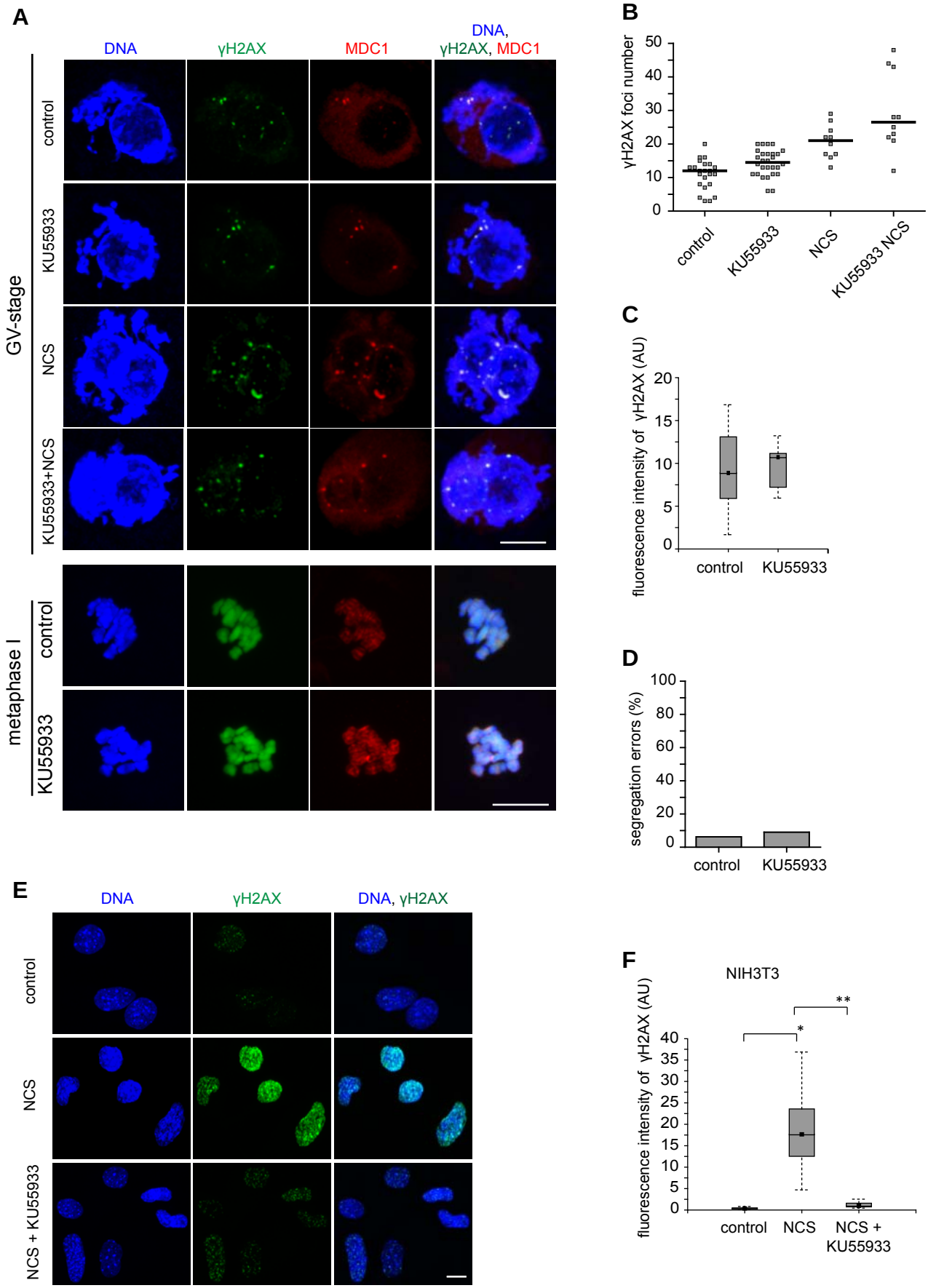
A
DNA
γH2AX
MDC1
DNA, γH2AX, MDC1
GV-stage
control
KU55933
NCS
KU55933+NCS
metaphase I
control
KU55933
B
γH2AX foci number
50
40
30
20
10
0
control
KU55933
NCS
KU55933 NCS
C
fluorescence intensity of γH2AX (AU)
20
15
10
5
0
control
KU55933
D
segregation errors (%)
100
80
60
40
20
0
control
KU55933
E
DNA
γH2AX
DNA, γH2AX
control
NCS
NCS + KU55933
F
NIH3T3
fluorescence intensity of γH2AX (AU)
40
35
30
25
20
15
10
5
0
*
**
control
NCS
NCS + KU55933

Fig. S3

A

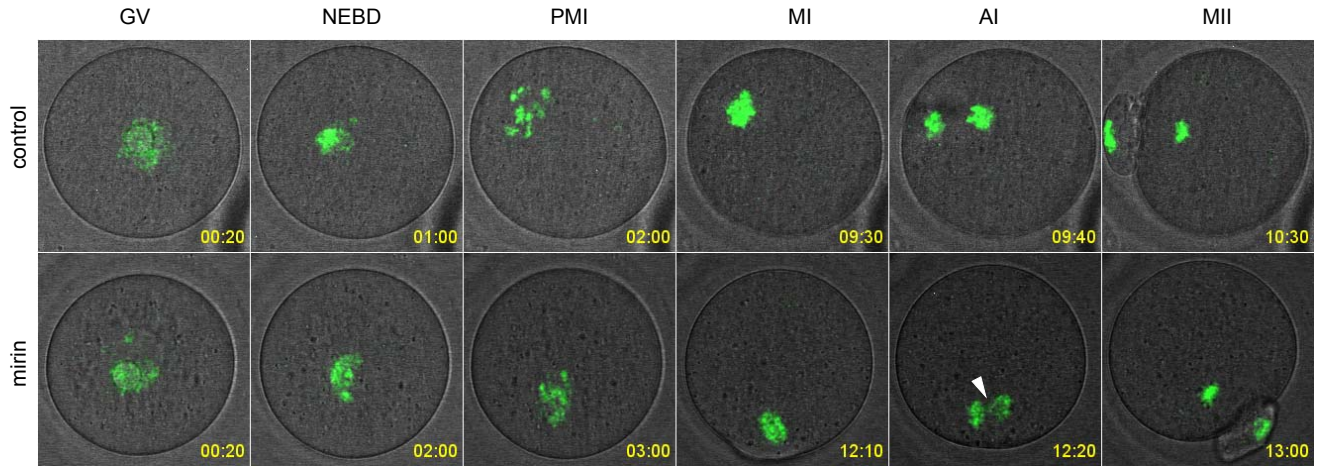

H2B-EGFP

B

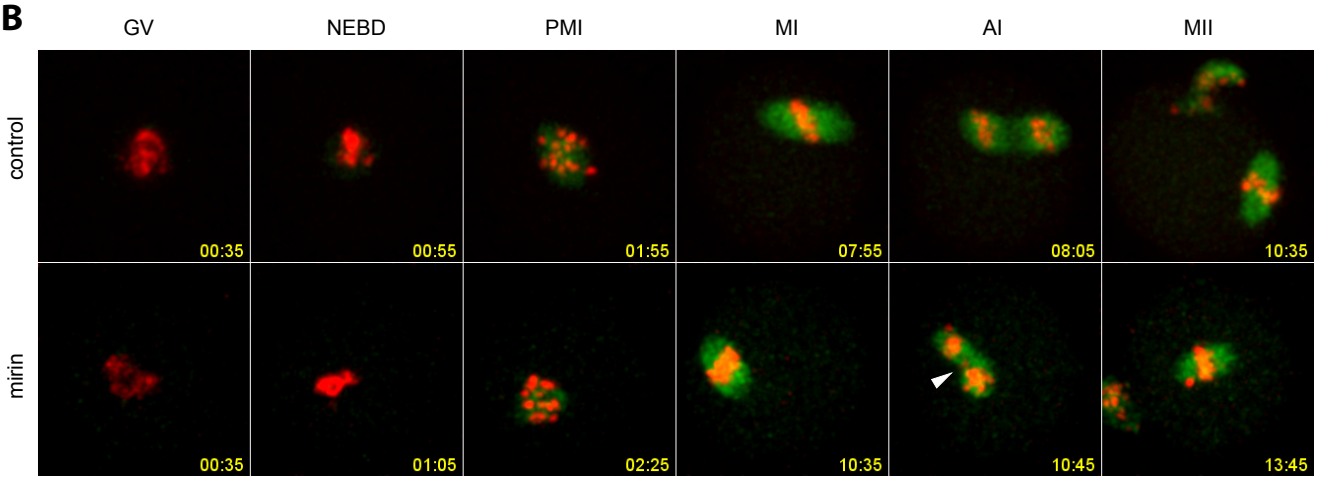

H2B-mCHERRY, MAP4-EGFP

C